N74-11714
NASA CR-132332

FINAL REPORT

on

ANALYSIS OF FATIGUE, FATIGUE-CRACK PROPAGATION, AND FRACTURE DATA

by

Carl E. Jaske, Charles E. Feddersen,

Kent B. Davies, and Richard C. Rice

November 1973

Prepared under Contract No. NAS1-11344

for

NATIONAL AERONAUTICS AND SPACE ADMINISTRATION

LANGLEY RESEARCH CENTER

BATTELLE

Columbus Laboratories

505 King Ave.

Columbus, Ohio 43201

NASA CR-132332

ANALYSIS OF FATIGUE, FATIGUE-CRACK PROPAGATION, AND FRACTURE DATA

By Carl E. Jaske, Charles E. Feddersen,
Kent B. Davies, and Richard C. Rice

Prepared under Contract No. NAS1-11344 by
BATTELLE'S COLUMBUS LABORATORIES
Columbus, Ohio

for

NATIONAL AERONAUTICS AND SPACE ADMINISTRATION

TABLE OF CONTENTS

TABLE OF CONTENTS (Continued)

ANALYSIS OF FATIGUE, FATIGUE-CRACK PROPAGATION, AND FRACTURE DATA

By Carl E. Jaske, Charles E. Feddersen, Kent B. Davies, and Richard C. Rice

Battelle's Columbus Laboratories

SUMMARY

Analytical methods have been developed for consolidation of fatigue, fatigue-crack propagation, and fracture data for use in design of metallic aerospace structural components. To evaluate these methods, a comprehensive file of data on 2024 and 7075 aluminums, Ti-6Al-4V, and 300M and D6AC steels was established. Data were obtained from both published literature and unpublished reports furnished by aerospace companies. Fatigue and fatigue-crack-propagation analyses were restricted to information obtained from constant-amplitude load or strain cycling of specimens in air at room temperature. Fracture toughness data were from tests of center-cracked tension panels, part-through crack specimens, and compact-tension specimens.

Both fatigue and fatigue-crack-propagation data were analyzed on a statistical basis using a least-squares regression approach. An arc-hyperbolic tangent function was used to relate the independent variable to the dependent variable. For fatigue, an equivalent strain parameter was used to account for stress ratio effects and was treated as the independent variable, and cyclic fatigue life was considered to be the dependent variable. An effective stress-intensity factor was used to account for the effect of load ratio on fatigue-crack propagation and was treated as the independent variable. In this latter case, crack-growth rate was considered to be the dependent variable.

Smooth-specimen and notched-specimen fatigue data were treated separately. Notched-specimen results were analyzed using a local stress-strain approach to account for fatigue damage at the notch root. Data for various types of notches and theoretical stress-concentration factors were consolidated by using a computed fatigue-strength reduction factor. Both the cyclic and monotonic stress-strain curves were employed in calculating the local stress-strain response from nominal loading information.

After computing mean fatigue and crack-growth curves by least-squares regression, tolerance-level curves were determined. Lower-level tolerance curves for 90 and 99 percent probability of survival with 95 percent level of confidence were determined for each fatigue curve. Two-sided tolerance bands for 90 and 99

percent probability with 95 percent confidence were determined for each mean crack-growth curve.

Fracture toughness data were tabulated for a particular material and specimen thickness in terms of average values at various temperatures and panel widths. Apparent, critical, and onset fracture toughness indexes were used in this tabulation.

INTRODUCTION

Recent experience with modern aerospace structures has emphasized the importance of considering both fatigue and fracture in the design and service performance of aircraft. A structural member may fracture at loads well below the nominal yield strength of the material if it contains a critical-size flaw. In some instances, such flaws may be introduced into the structural material by manufacturing processes. However, in most cases, flaws will become critical by growing from smaller flaws or from unflawed areas of stress concentration. This type of growth occurs by fatigue processes during cyclic loading of the structure.

Reaching total fracture under cyclic loading involves both fatigue-crack initiation and propagation. As shown in figure 1, crack-initiation life can vary considerably, depending upon the definition of a crack. The wide range of sizes (10^{-5} to 10^{-1} inch) considered to be cracks by various investigators causes an ill-defined area of overlap between initiation and propagation. In most fatigue tests of small specimens of virgin material, the initiation phase is generally considered to be a more significant portion of cyclic life than the propagation phase. Fatigue-crack-propagation data are usually obtained from precracked or flawed specimens.

In this program, fatigue data from uncracked smooth or notched specimens were treated separately from fatigue-crack-propagation data from precracked specimens. It was assumed that the total number of cycles to failure normally reported in fatigue tests of simple specimens was a reasonable approximation of the number of cycles required to initiate an engineering size flaw. Crack-propagation information was obtained from studies where cyclic crack growth was measured using a precracked sample. Fracture at a critical load level or flaw size also was treated separately.

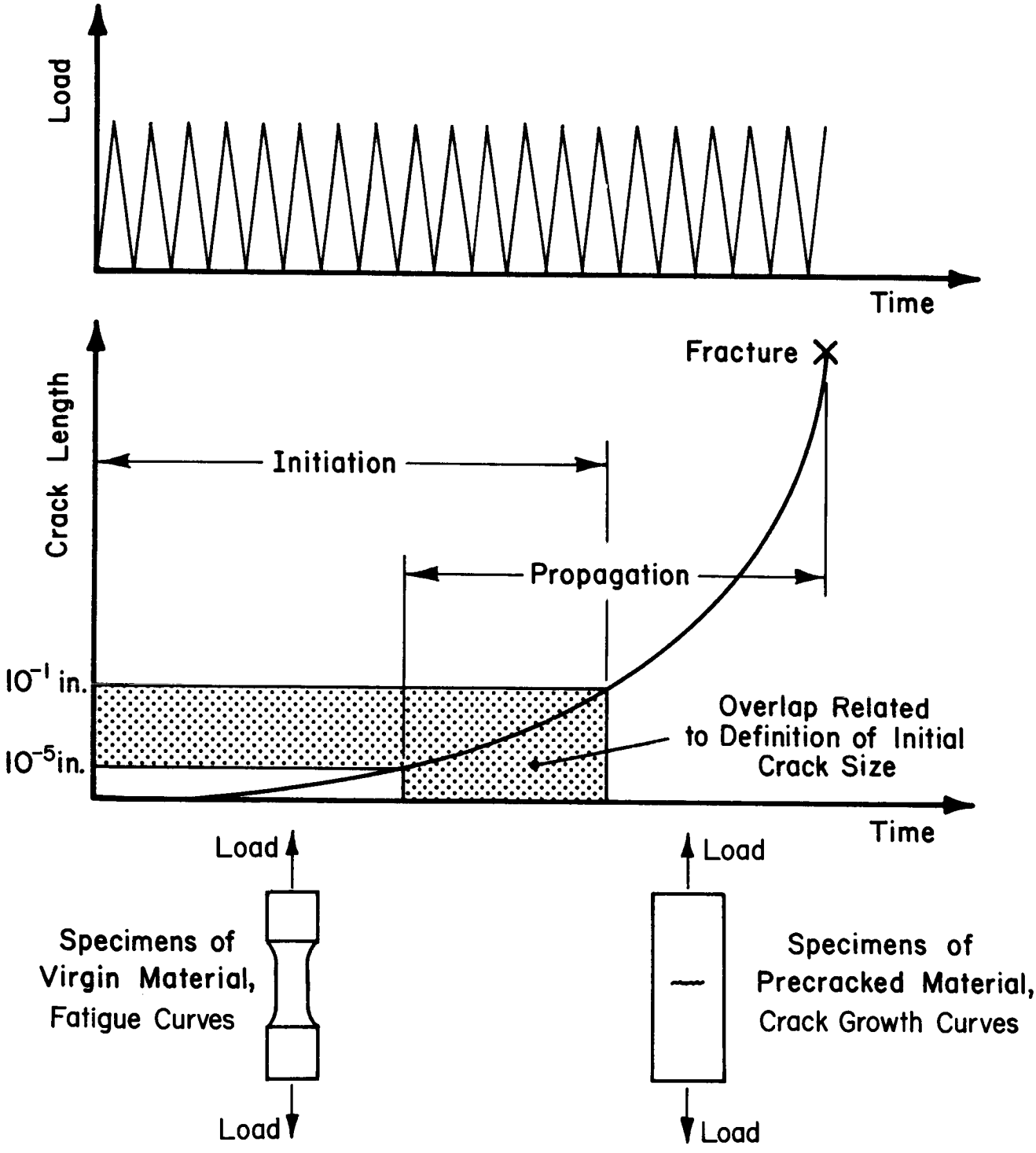

Figure 1. — Effect of definition of crack initiation on relation between fatigue-crack initiation and fatigue-crack propagation.

For conventional static properties of metals and alloys, extensive design allowables information is available in documents such as MIL-HDBK-5B (ref. 1). For fatigue, fatigue-crack propagation, and fracture data, however, design allowable values are usually not available and the data are presented in terms of typical or average values.

Part of the problem for fatigue and fatigue-crack propagation is that these behaviors are influenced by a wide range of parameters that include cyclic stress, mean stress, cyclic frequency, temperature, environment, product form and orientation with respect to loading, structural geometry (size, shape, and notch configuration), metallurgical and surface effects associated with heat treatment, microstructure, and machining practices. Most aerospace companies tend to generate data for a limited number of these many variables to fulfill specific local design needs. Much of this information is retained within each company, and that which becomes available in open literature is often digested in accordance with particular theoretical considerations and analytical procedures endemic to a given organization. Since these considerations and procedures vary among companies, it is difficult to affect a systematic consolidation of such data. Assessment of fatigue and fatigue-crack-propagation data is further complicated by the fact that there have been no standard methods for these types of testing. Recommended procedures for fatigue testing have been published recently (ref. 2).

Many of the aforementioned problems also influence fracture results. Standards for obtaining plane-strain fracture-toughness information have been developed recently (ref. 3). However, major differences in testing and analysis procedures still exist for plane-stress and transition-thickness conditions.

As a result of extensive visits and discussions with all major aerospace companies, it became evident to personnel at Battelle's Columbus Laboratories (BCL) who are responsible for maintaining MIL-HDBK-5B (ref. 1) that the major deficiencies in the Handbook were in the important areas of fatigue, fatigue-crack propagation, and fracture. This realization led to the initiation of a research program at BCL under the sponsorship of Langley Research Center. Work was directed toward systematizing and consolidating available fatigue, fatigue-crack propagation, and fracture information on 2024 and 7075 aluminum alloys, Ti-6Al-4V alloy, and 300M and D6AC steels. It was considered imperative that the analytical procedures be compatible with statistical methods of data presentation.

Similar approaches were used for both fatigue and fatigue-crack propagation, as illustrated in figure 2. The logarithm of fatigue life was the dependent variable in both cases. An equivalent strain parameter similar to that suggested by Walker (ref. 4) and Smith, et al. (ref. 5) was used to account for stress ratio effects and was treated as an independent variable in the fatigue analysis. A similar effective stress-intensity factor (ref. 4) was used to account for stress ratio effects and was treated as the independent variable in the fatigue-crack-propagation analysis.

Fatigue-crack propagation is more complicated than fatigue because different life curves (fig. 2) are obtained for each different state of initial damage. Thus, fatigue-crack-propagation results are usually presented in terms of crack-growth rate as shown schematically in figure 3. The layering of rate data as a function of stress ratio can be accounted for using the effective stress-intensity concept mentioned above.

Treatment of fracture data was limited to tabulation and graphical summary of information in terms of three indexes of fracture toughness.

Primary emphasis of the fatigue work was on data for 2024 and 7075 aluminum alloys, with a secondary effort directed toward annealed Ti-6Al-4V alloy and a high-strength steel. The fatigue-crack propagation and fracture work was limited to data for the 2024 and 7075 alloys and 300M and D6AC steels.

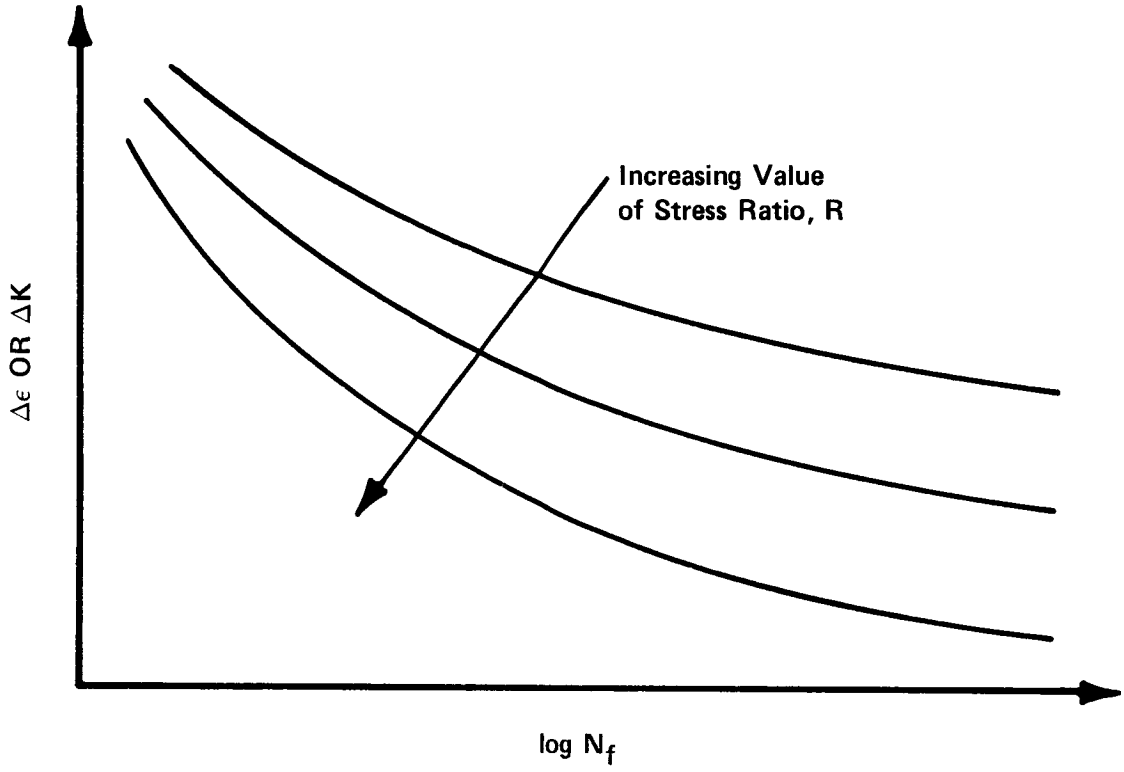

FATIGUE ANALYSIS, ϵ_{eq}	FATIGUE CRACK PROPAGATION ANALYSIS, K_{eff}
$\log N_f = f[\Delta\epsilon, R]$	$\log N_f = f[\Delta K, R]$
or specifically,	or specifically,
$\log N_f = f[\Delta\epsilon^m (S_{max}/E)^{1-m}]$	$\log N_f = f[\Delta K^m K_{max}^{1-m}]$

m may be treated as a material parameter

Figure 2. — Similarity between fatigue and fatigue-crack-propagation analysis.

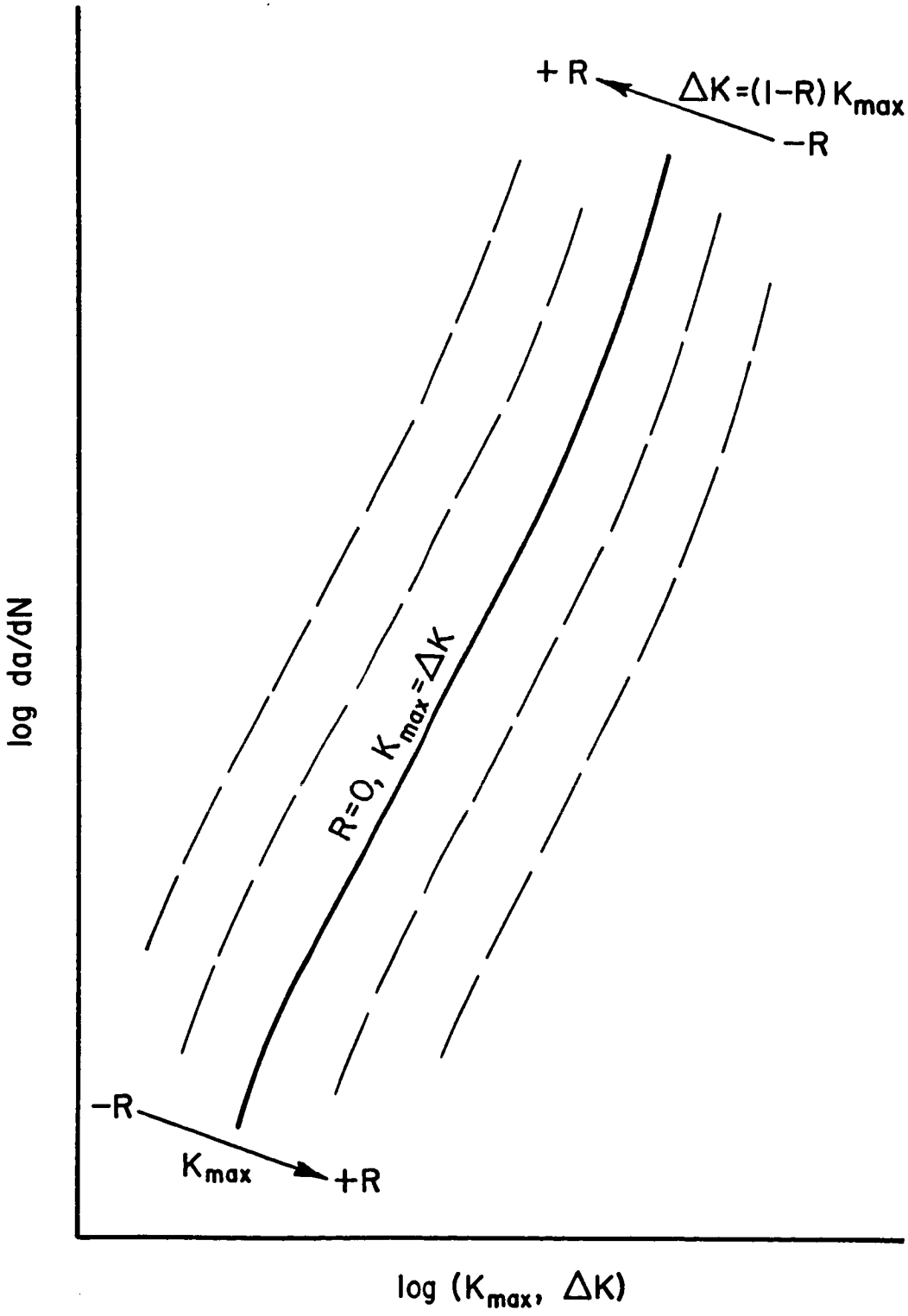

Figure 3. — Schematic illustration of layering in fatigue-crack-propagation rate data.

SYMBOLS

A	mean stress coefficient
A_i	ith regression coefficient
a	crack length, mm (in.)
da/dN	fatigue crack growth rate
$\Delta a/\Delta N$	approximate crack growth rate
a_i	ith value of crack length, mm (in.)
B	stress amplitude coefficient
C	Paris' coefficient
C_1, C_2	regression coefficient in arc-hyperbolic tangent relation
c	crack half length, mm (in.)
c_c	crack half length at unstable fracture, mm (in.)
c_o	initial crack half length, mm (in.)
D	multiplicative regression coefficient
$DD_{j(i)}$	the jth order divided difference at point i
E	elastic modulus, MN/m^2 (ksi)
e	nominal strain
Δe	nominal strain range
e_a	nominal strain amplitude
$e_a(1), e_a(2)$	specific values of e_a used to define stress-strain curve
e_{max}	maximum nominal strain
Δe_p	plastic nominal strain range
K	stress intensity factor, $MN/m^{3/2}$ ($ksi\sqrt{in.}$)
ΔK	range of stress intensity factor, $MN/m^{3/2}$ ($ksi\sqrt{in.}$)
K_{app}	apparent fracture toughness, $MN/m^{3/2}$ ($ksi\sqrt{in.}$)
K_c	critical fracture toughness, $MN/m^{3/2}$ ($ksi\sqrt{in.}$)
K_{eff}	effective stress intensity factor, $MN/m^{3/2}$ ($ksi\sqrt{in.}$)

K_f	fatigue strength reduction factor
K_{Ic}	mode I critical fracture toughness, MN/m^2 ($ksi\sqrt{in.}$)
K_i	ith value of stress-intensity factor, MN/m^2 ($ksi\sqrt{in.}$)
K_{max}	maximum stress-intensity factor, MN/m^2 ($ksi\sqrt{in.}$)
K_o	threshold stress-intensity factor, MN/m^2 ($ksi\sqrt{in.}$)
K_q	toughness at onset of crack extension, MN/m^2 ($ksi\sqrt{in.}$)
K_t	theoretical stress concentration factor
K_ϵ	strain concentration factor
K_σ	stress concentration factor
K_1, K_2	strength coefficients, MN/m^2 (ksi)
k	Stulen coefficient
L	regression coefficient
M	Elber optimization coefficient
M'	value of slope of function Φ
m	Walker exponent
N	number of cycles
N_f	number of cycles to failure
N_i	ith value of number of cycles
n	sample population
n'	Paris' exponent
n_1, n_2	strain hardening exponents
P_{max}	maximum load, KN (kip)
P_Q	5 percent secant offset load, KN (kip)
Q	plasticity corrected shape factor
q	degree of polynomial
R	stress ratio
R^2	proportion of variation explained by regression equation
R_m^2	modification of R^2 to account for degrees of freedom

r	notch root radius, mm (in.)
S	nominal stress, MN/m^2 (ksi)
ΔS	nominal stress range, MN/m^2 (ksi)
SSD	residual sum of squares
S_a	nominal stress amplitude, MN/m^2 (ksi)
$S_a(1), S_a(2)$	specific values of S_a used to define stress-strain curve
S_c	maximum nominal fracture stress, MN/m^2 (ksi)
S_{eq}	equivalent nominal stress, MN/m^2 (ksi)
S_m	mean nominal stress, MN/m^2 (ksi)
S_{max}	maximum nominal stress, MN/m^2 (ksi)
S_{min}	minimum nominal stress, MN/m^2 (ksi)
S_n	net stress or uncracked section
S_o	nominal stress at onset of crack extension, MN/m^2 (ksi)
S_{op}	crack closure nominal stress, MN/m^2 (ksi), $S_{op} > 0$
s	standard error of estimate
T	thickness, mm (in.)
TSS	regression (or total) sum of squares
TUS	tensile ultimate strength, MN/m^2 (ksi)
TYS	tensile yield strength, MN/m^2 (ksi)
t	Students' t multiplier
u	confidence level
V	variance
w	panel width, mm (in.)
X	independent variable - $\tanh^{-1} [\Phi(\epsilon_{eq})]$ or $\tanh^{-1} [\Phi(K_{eff})]$
X_i	ith value of independent variable
$\bar{X}$	mean value of X
Y	dependent variable - $\log N_f$ or $\log da/dN$
Y_i	ith value of dependent variable

$\bar{Y}$	mean value of Y
$Y_{u',\nu}$	tolerance limit at a level of confidence (u) for a given number of degrees of freedom (ν)
α	mean stress exponent
β	stress amplitude exponent
ϵ	local strain
$\Delta\epsilon$	local strain range
ϵ'	translated local strain
ϵ_a	local strain amplitude
ϵ_e	lower limit of inverse hyperbolic tangent function
ϵ_{eq}	equivalent local strain
ϵ_{max}	maximum local strain
$\Delta\epsilon_p$	plastic local strain range
ϵ_u	upper limit of inverse hyperbolic tangent function
ν	degrees of freedom
ρ	notch analysis material constant
σ	local stress, MN/m^2 (ksi)
$\Delta\sigma$	local stress range, MN/m^2 (ksi)
σ'	translated local stress, MN/m^2 (ksi)
σ_a	local stress amplitude, MN/m^2 (ksi)
σ_m	mean local stress, MN/m^2 (ksi)
σ_{max}	maximum local stress, MN/m^2 (ksi)
σ_{min}	minimum local stress, MN/m^2 (ksi)
Φ_I	value of intercept of function Φ

ACQUISITION, COMPILATION, STORAGE, AND RETRIEVAL OF DATA

To implement the evaluation of existing fatigue, fatigue-crack-propagation, and fracture data, it was necessary to make an extensive survey of the literature and of aerospace companies that might have unpublished internal reports. A computerized system was developed to compile and store data obtained from this survey. Data from more than 120 reports and documents were acquired, compiled, and stored.

Data Acquisition

Information was taken both from the open literature and from company reports. Applicable reports were obtained from the technical files of the Metals and Ceramics Information Center (MCIC) located at BCL. Throughout the program, new reports, acquired by MCIC, were screened and added to the data base when applicable. In order to obtain as much recent information as possible, additional literature searches were obtained from the National Aeronautics and Space Administration (NASA) (refs. 6 and 7) and the Defense Documentation Center (DDC) (refs. 8 and 9). In addition, pertinent reports obtained through the MIL-HDBK-5 (ref. 1) program were used.

Internal reports from aerospace companies and unpublished data were obtained from various laboratories that conduct fatigue, fatigue-crack-propagation, and fracture research. A letter was prepared and sent out to 89 selected members of the American Society for Testing and Materials (ASTM) Committee E09 on Fatigue. A similar letter was also sent to 18 members of the ASTM Committee E24 on Fracture Testing of Metals and to 46 members of the MIL-HDBK-5 Coordination Group. Positive responses were received from about 40 percent of those surveyed. Pertinent data from the responses were entered into the data storage files. The type of information that was requested in these letters is summarized in the following three sections.

Basic Fatigue Information.– For the alloys of interest (2024 and 7075 aluminum, Ti-6Al-4V, and high-strength steels), fatigue data were desired from axial-load tests of simple specimens that reflect basic material behavior. This requirement excluded joints or components but included both notched and unnotched data, where notch configuration and severity were variables. Data for cyclic

lives ranging from $>10^2$ to $<10^7$ cycles, both strain and load-controlled test data, and variable stress ratio (or mean stress) data were of interest.

Basic test data were desired; i.e., tables of stress or strain versus life-time. In cases where crack initiation was determined, this information (and the initiation criterion employed) was desired. For tests involving cyclic plasticity, cyclic stress-strain information in the form of stress and strain as a function of loading history were needed.

In addition to the fatigue data, correlative information concerning specimen geometry and fabrication, material product form, dimensions and processing, test techniques and controls, laboratory environment and mechanical properties were also desired. The latter information was required to aid in making decisions about pooling various samples of data.

Fatigue-Crack-Propagation Information. — Fatigue-crack-propagation data were desired for center-cracked panels (in a variety of widths), part-through-cracked or surface-flawed specimens, compact-tension specimens, and double-cantilever-beam specimens. It was useful to have data that delineated crack initiation cycles from a geometrically known starter flaw as well as initial propagation data from it, if such information was available. Delineation of the stress cycle employed for each test, as well as test frequency, was necessary. In some cases, multiple tests were conducted on a single specimen such that propagation occurred on successive crack-growth segments under different cyclic-stress conditions. Each of these conditions was considered as a single test in the analysis, and the conditions needed to be described.

Basic test data again were desired; i.e., tabular displays of crack size versus cycles. For each specimen, the associated test stress cycle description was given.

In addition to the basic crack-propagation data, correlative information as described for fatigue data were necessary.

Fracture Information. — The fracture data collection was more complex in that there was a thickness dependence on fracture toughness that was of greater significance than for fatigue and fatigue-crack propagation. This thickness dependence influenced the mode of fracture (such designations as slant, transition, and flat fracture descriptions were used) corresponding to plane stress, transitional stress, and plane-strain fracture toughness. A variety of tests have been

employed, only a few of which are standardized (ref. 3). Thus, test specimen description and test techniques had to be delineated carefully and completely. Specific tests for which data were desired included the center-cracked panel, part-through or surface-flawed specimens, compact-tension specimens, double-cantilever-beam specimens, and notched-bend specimens.

Basic test data were needed rather than fracture toughness values. These included original crack length, critical crack length, ultimate load or stress, and load or stress at which slow stable crack growth initiated (presented in tabular form). Load-compliance records were obtained when possible.

As stated before, correlative information was desired with particular emphasis on test methods and techniques.

Data Recording and Storage

Information used in this program was stored in a format for computerized analysis. Detailed data has been recorded on punched cards for use at BCL. These data were transferred to magnetic tapes and forwarded to NASA Langley Research Center. To help document the encoded data, a short abstract was prepared for each report from which information was taken. This abstract summarized briefly the type of data encoded along with correlative information not recorded in the data file. The check list shown in figure 4 was used in preparing these abstracts. Sample abstracts are presented in figures 5 and 6. A complete set of abstracts was sent to NASA Langley along with the magnetic tapes. Each source from which data were taken and an abstract prepared are listed in Appendix A. Each source was assigned a unique reference number when it was added to the data base.

The basic medium for recording the fatigue, fatigue-crack-propagation, and fracture data collected and compiled on this program is the standard 80 column computer punch card. Data card file sequences and formats which have been selected to provide a consistent procedure for encoding these data are described in the following subsections.

Each data file may contain up to four basic types of cards depending on the type of information being recorded. These card forms are

Card 1: Title or lead card, identifying test and material

Card 2: Subtitle card, containing supplementary testing, compositional, or processing information where desirable

Card 3: Data card describing specific test parameters and results

Card 4: Crack growth card listing cycle count and crack size.

DATA SOURCE ABSTRACT CHECKLIST

For Each Report From Which Data is Obtained
Check for, and Record, the Following Items.

General Report Information

(1) Reference Number.
(2) Materials.
(3) Authors, Title, Publisher/Source, Publication Date.

Test Information

(1) Type of Test (Fatigue, Fatigue-Crack Propagation, Fracture), Summary of Report Abstract.
(2) Type of Test Machines, Load or Strain Control?
(3) Number of Specimens.
(4) Stress Ratios.
(5) Test Temperature and Environment.
(6) Test Frequencies.
(7) If Fatigue-Crack Propagation —
    (a) Plane Strain or Plane Stress?
    (b) Basic Data or "Digested" Data?

Specimen Data

(1) Melting Practice/Heat Treatment of Specimens.
(2) Ductility.
(3) Fabrication Methods.
(4) Surface Finish.
(5) Specimen Dimensions.
(6) Chemical Composition.
(7) Tensile Properties (TYS, TUS, Reduction of Area, Elongation, Elastic Modulus).
(8) Are There Stress-Strain Curves or Data? Are They Monotonic or Cyclic?

Figure 4. — Checklist used for preparation of report abstracts.

REFERENCE NUMBER 3

Materials: 2024-T3, 7075-T6, 4130 Steel

Grover, H. J., Bishop, S. M., Jackson, L. R., "Axial-Load Fatigue Tests on Notched Sheet Specimens of 24S-T3 and 75S-T6 Aluminum Alloys and of SAE 4130 Steel with Stress-Concentration Factor of 5.0", NACA TN 2390, Battelle Memorial Institute, June (1951).

Test Information

(1) Fatigue Tests: Axial-load fatigue tests were conducted on notched specimens of three sheet materials with one stress concentration factor and four mean stress levels.

(2) Type of Test Machine: Krouse direct repeated-stress test machine.

(3) Number of Specimens: 49/2024-T3, 47/7075-T6, and 42/4130.

(4) Stress Ratio: R = -1.0 to 0.70.

(5) Test Temperature and Environment: Tests were conducted at room temperature in air.

(6) Test Frequency: 1100 - 1500 cpm.

Specimen Data

(1) Melting Practice/Heat Treatment: Not specified.

(2) Ductility: Not specified.

(3) Fabrication Methods: Specimens were machined from 0.09 inch thick 2024-T3 and 7075-T6 aluminum and from 0.075 inch thick 4130 steel. Notches were cut in a series of machining cuts.

(4) Surface Finish: Specimens were electropolished.

(5) Specimen Dimensions: Gross length = 15.5 inches, gross width = 2.25 inches, net width = 1.5 inches, root radius = 0.03125 inch (K_t = 5).

(6) Chemical Composition: Not specified.

(7) Tensile Properties:

Material	TYS, ksi	TUS, ksi	Elong., %
2024-T3	54.0	73.0	18.2
7075-T6	76.0	82.5	11.4
4130	98.5	117.0	14.3

(8) Stress-Strain Curves: Not given.

Figure 5. — Sample abstract for report containing fatigue data.

REFERENCE NUMBER 15 (MCIC 73988)

Materials: 300 M

Pendleberry, S. L., Simenz, R. F., and Walker, E. K., "Fracture Toughness and Crack Propagation of 300 M Steel", Technical Report No. DS-68-18, Lockheed-California Company, August (1968).

Test Information

(1) Fracture and Crack Propagation Tests: Tests were conducted on one material in three product forms to study the effects of material thickness and strength level.

(2) Type of Test Machine: Lockheed-designed closed-hoop servohydraulic fatigue machine (150,000 lb. capacity), Lockheed-designed axial load resonant fatigue machine (250,000 lb. capacity), and a universal hydraulic testing machine (60,000-400,000 lb. capacity).

(3) Number of Specimens: 132 specimens were used to obtain both crack propagation and fracture data.

(4) Stress Ratio: R = 0.1 or 0.5.

(5) Test Temperature and Environment: Tests were conducted at room temperature in a moist air or salt spray environment.

(6) Test Frequency: 20 cps to precrack specimens.

(7) FCP Data: Presented in basic form.

Specimen Data

(1) Melting Practice/Heat Treatment: Specimens were normalized at 1700°F/1-1/2 hours, air cooled, austinitized at 1600°F/1-1/2 hours, oil quenched, and double-tempered at 500°F to 1050°F depending upon strength level desired.

(2) Ductility: Not given.

(3) Fabrication Methods: Specimens were machined from 0.125 inch sheet, 0.5 or 0.75 inch plate or forgings. Precracking was done by axial tension-tension fatigue generated from an EDM slot.

(4) Surface Finish: Specimens were left as machined.

(5) Specimen Dimensions:

Specimen Type	Thick-ness, inch	Gross Length, inch	Net Length, inch	Gross Width, inch	Net Width, inch	Slot Length, inch	Slot Width, inch
Surface Crack	.125	14	3.5	4	2.25	.08	.006
Surface Crack	.375	16	3.5	5	2.25	.08	.006
Surface Crack	.75	28	9.0	12	4.5	.08	.010
Through Crack	.125	15	---	5	---	.5	---
Through Crack	.375	28	9.0	12	5.0	.5	.010

(6) Chemical Composition: See report for analysis of each heat of material.

(7) Tensile Properties: See report for original materials' properties, results of heat treatment study and properties of control specimens after heat treatment.

(8) Stress-Strain Curves: Not given.

Figure 6. — Sample abstract for report containing fatigue-crack propagation and fracture data.

Each data file always contains at least Cards 1 and 3. Card 2 is an optional card which may be necessary to supplement, clarify or expand Card 1 information in particular situations. Card 4 is a particular addenda of crack-growth information (i.e., cycle count and crack size) necessary only for fatigue-crack-propagation analysis.

Title or Lead Card (Card 1) Format. – The format of Card 1 is illustrated in figure 7. Eleven fields of general descriptive information are presented. Their contents are as follows:

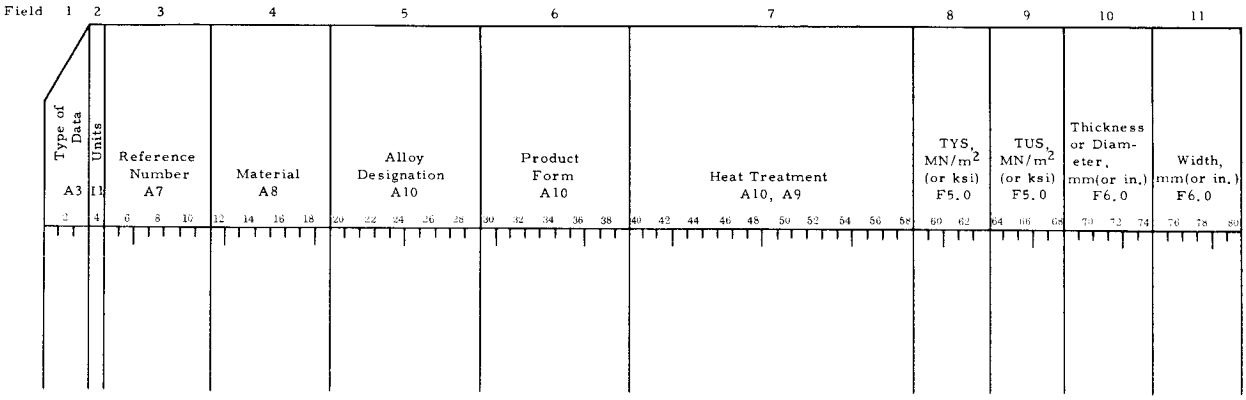

Figure 7. – Format for encoding of title or lead card (card 1).

(1) The type of data contained in the associated data file is indicated in columns 1 through 3 by using an alphanumeric format with three coding abbreviations:

FAT – data from constant-amplitude-fatigue tests where the controlled variable is stress or strain and the dependent variable is the total number of cycles to complete failure of the specimen (i.e., the fatigue life).

FCP – fatigue-crack-propagation data from a constant-amplitude stress or strain-cycling test where the size of a fatigue crack is monitored as a function of the number of loading cycles.

FT – data from a monotonic loading (load or displacement controlled) test to fracture of a specimen with an initial fatigue precrack.

(2) The dimensional units of the recorded data in the file are identified in column 4. A blank denotes International System (SI) of Units; a value of 1 indicates English units; and a value of 2 indicates CGS units.

(3) The source reference number is listed in columns 5 through 11 in an alphanumeric code of the following format:

"NNNNNNL",

where N is a numeric character (0 to 9) and L is an alphabet character (A to Z). The numeric code corresponds to the references numbers in Appendix A. The suffix letter refers to a specific batch of data from the referenced document. This reference number is the same as that listed on the succeeding data cards.

(4) The type of material (e.g., aluminum, steel, and titanium) is described in columns 11 through 19 using an alphanumeric format.

(5) The alloy designation (e.g., SAE 4340, 7075-T651, Ti-6Al-4V) is given in columns 20 through 29 in an alphanumeric format.

(6) The product form (e.g., plate, sheet, bar, forging, and casting) is listed in columns 30 through 39 in an alphanumeric format.

(7) The heat treatment (e.g., Q and T, STA, annealed, normalized) is described in columns 40 through 58 in an alphanumeric format.

(8) The TYS, MN/m^2 (or ksi), is given in columns 59 through 63 in a fixed point numeric format.

(9) The TUS MN/m^2 (or ksi), is given in columns 64 through 68 in a fixed point numeric format.

(10) Thickness or diameter, mm (or in.), of the specimen is listed in columns 69 through 74 in a fixed point numeric format. For a round specimen where this value represents the diameter, columns 75 through 80 (item 11 below) will be blank.

(11) Width, mm (or in.), of the specimen is given in columns 75 through 80 in a fixed point numeric format. For a round specimen these columns are blank and the diameter is given in item 10 above.

Subtitle Card (Card 2) Format. — The subtitle card is an optional card provided for particular instances where supplementary information is necessary or desirable. This is an open-field card whose format is coded alphanumerically and read directly as a subtitle to Card 1 in data listings or tabulations.

Data Card (Card 3) Format. — This card contains the principal test parameters and results of each test on which data are collected and compiled. Since the types of data may represent either fatigue, fatigue-crack propagation, or fracture tests, three formats are necessary for this card as detailed in the following subsections. Where similar test parameters are encountered among the types of data, common fields have been assigned to the formats.

Fatigue (FAT) Data Card Format. — The fatigue data card contains 13 fields of information listed in the following formats (see fig. 8):

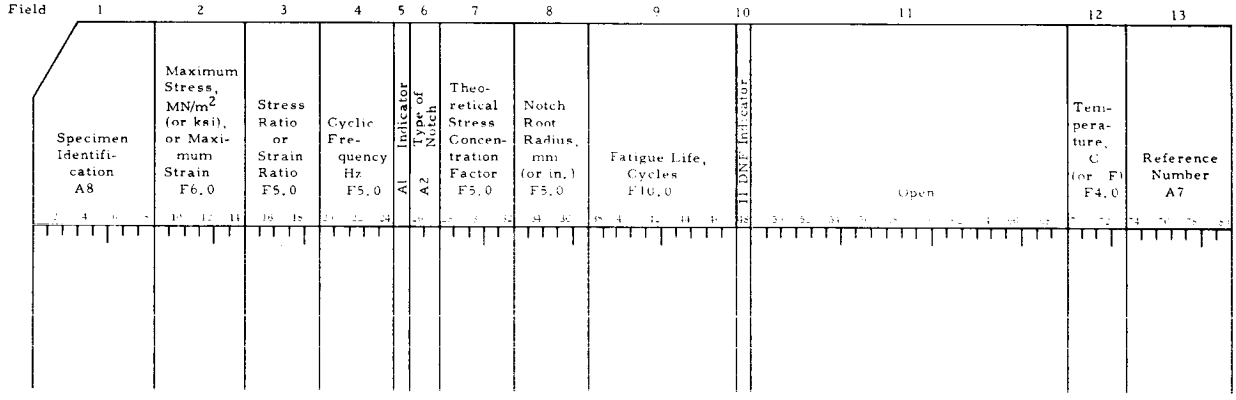

Figure 8. — Format for encoding fatigue data card (card 3).

(1) Specimen identification is listed in columns 1 through 8 using an alphanumeric format.

(2) Maximum stress, MN/m^2 (or ksi), or maximum strain is listed in columns 9 through 14 in a fixed point numeric format. The stress or strain option is designated by the Field 5 indicator.

(3) Stress ratio or strain ratio (ratio of minimum to maximum value) is listed in columns 15 through 19 in a fixed point numeric format. The stress or strain option is designated by the Field 5 indicator.

(4) Cyclic frequency, Hz, is listed in columns 20 through 24 in a fixed point numeric format.

(5) An indicator is given in column 25 to show whether items 2 or 3 above are in terms of stress or strain. If this column is blank, stress is indicated; and if this column contains an "E", strain is indicated.

(6) The type of notch configuration is listed in columns 26 and 27 by the following abbreviations:

CN – center-notched sheet or plate

EN – edge-notched sheet or plate

FN – fillet-notched sheet or plate

CR – circumferentially notched round bar.

These columns are blank for an unnotched specimen.

(7) The theoretical stress-concentration factor of the notch geometry is given in columns 28 through 32 in a fixed point numeric format. These columns are blank for an unnotched specimen.

(8) The notch root radius, mm (or in.), is given in columns 33 through 37 in a fixed point numeric format. These columns are blank for an unnotched specimen.

(9) The fatigue life, cycles, is given in columns 38 through 47 in a fixed point numeric format.

(10) An indicator is given in column 48 to show whether or not the specimen was a runout. A "1" in column 48 indicates that the specimen did not fail (DNF).

(11) This is an open field and columns 48 through 69 are left blank.

(12) Test temperature, $^{\circ}C$ (or $^{\circ}F$), is listed in columns 70 through 73 in a fixed point numeric format.

(13) The source reference number is given in columns 74 through 80 in an alphanumeric format of the following type:

"NNNNNNL",

where N is a numeric character (0 to 9) and L is an alphabet character (A to Z). The numeric code corresponds to the source reference numbers in Appendix A. The suffix letter refers to a specific batch of data from the referenced document. This source reference number is the same as that listed on the corresponding Number 1 Lead Data Card.

Fatigue-Crack Propagation (FCP) Data Card Format. – The complete recording of fatigue-crack-propagation data requires two different card formats. Card 3,

described herein, contains the basic test information; Card 4, described later, contains the cycle counts and crack size measurements as determined from the test. Thus, the data file from a single fatigue-crack-propagation test is made up of one Card 3 and one or more Card 4's.

The layout of Card 3 for the fatigue-crack-propagation test parameters is shown in figure 9.

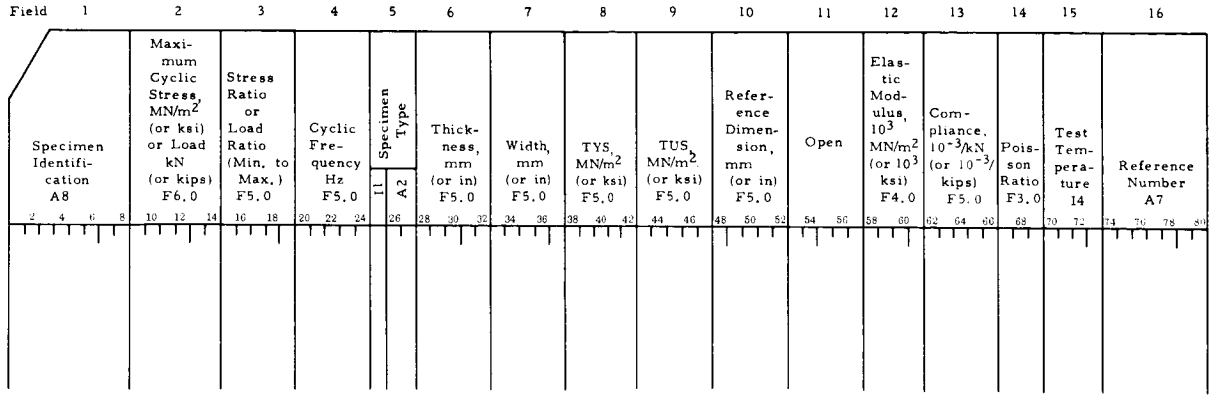

Figure 9. — Format for encoding fatigue-crack-propagation data card (card 3).

A total of 16 fields are indicated. The field contents are as follows:

(1) Specimen identification is listed in columns 1 through 8 using an alphanumeric format.

(2) Maximum cyclic stress, MN/m^2 (or ksi), or maximum cyclic load, kN (or kips) is listed in columns 9 through 14 in a fixed point numeric format. The stress or load option is designated by the Field 5 indicator.

(3) Stress ratio or load ratio (ratio of minimum to maximum values) is listed in columns 15 through 19 in a fixed point numeric format. The stress or load option is designated by the Field 5 indicator.

(4) Cyclic frequency, Hz, is listed in columns 20 through 24 in a fixed point numeric format.

(5) The specimen type is indicated in column 25 as a numeric code and supplemented in columns 26 and 27 by an acronymonic code for easier identification. Since the specimen type also determines the usual convention for selecting either stress or load in the analysis, it is

this field that designates the stress or load option for Fields 2 and 3. The following convention is used in fatigue-crack propagation:

Code	Specimen Type	Option
1CT	Compact Tension	Load
2CC	Center Crack	Stress
3SF	Surface Flaw or Part-through Crack	Stress
5DC	Double Cantilever Beam	Load
6NB	Notch Bend	Load

(6) Specimen thickness, mm (or in.), is listed in columns 28 through 32 in a fixed point numeric format.

(7) Specimen width, mm (or in.), is listed in columns 33 through 37 in a fixed point numeric format.

(8) Tensile yield strength, MN/m^2 (or ksi), representative of that specimen material is listed in columns 38 through 42 in a fixed point numeric format.

(9) Tensile ultimate strength, MN/m^2 (or ksi), representative of that specimen material is listed in columns 43 through 47 in a fixed point numeric format.

(10) A reference dimension, mm (or in.), is listed in columns 48 through 52 in a fixed point numeric format. This dimension is utilized when experimental measurements are recorded relative to a point other than the crack origin prescribed by the analysis.

(11) This is an open field and columns 53 through 57 are left blank.

(12) Elastic modulus, 10^3 MN/m^2 (or 10^3 ksi), is listed in columns 58 through 61 in a fixed point numeric format.

(13) Specimen compliance, $10^{-6}N^{-1}$ (or $10^{-6}lb^{-1}$), used specifically for the double cantilever specimen is listed in columns 62 through 66 in a fixed point numeric format.

(14) Poisson's ratio for elastic deformation is listed in columns 67 through 69 in a fixed point numeric format.

(15) Test temperature, °C (or °F), is listed in columns 70 through 73 in a fixed point numeric format.

(16) The source reference number is given in columns 74 through 80 in an alphanumeric format of the following type:

"NNNNNNL",

where N is a numeric character (0 to 9) and L is an alphabet character (A to Z). The numeric code corresponds to the source reference numbers in Appendix A. The suffix letter refers to a specific batch of data from the referenced document. This source reference number is the same as that listed on the corresponding Number 1 Lead Data Card.

Fracture (FT) Data Card Format. — Fracture data for a variety of test specimen configurations is accommodated on the card format shown in figure 10. The detail presented is dictated to a large degree by the number of important crack lengths and stresses which are associated with and reported for thin sheet (plane stress) fracture studies.

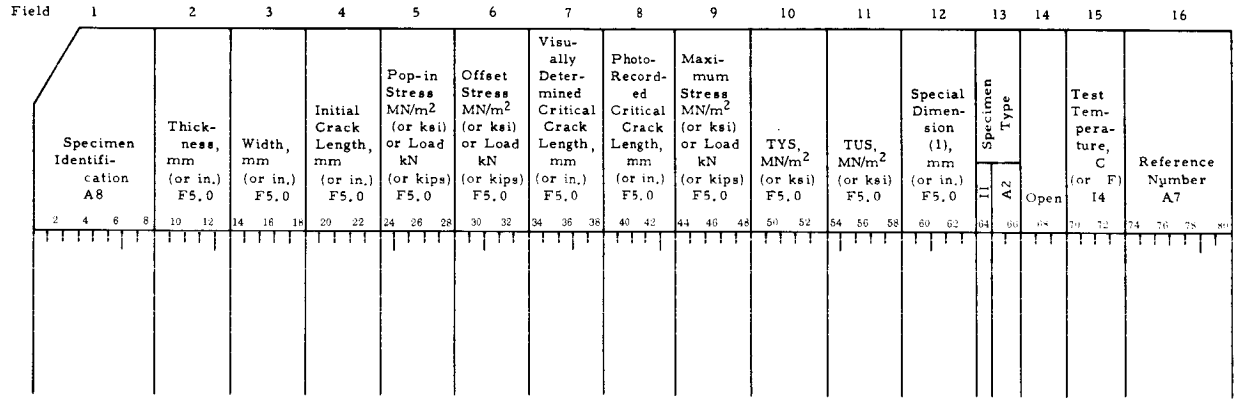

Figure 10. — Format for encoding fracture data card (card 3).

A total of 16 fields of data are contained on the card. Their contents are as follows:

(1) Specimen identification is listed in columns 1 through 8 using an alphanumeric format.

(2) Specimen thickness, mm (or in.), is listed in columns 11 through 13 using a fixed point numeric format.

(3) Specimen width, mm (or in.), is listed in columns 14 through 18 using a fixed point numeric format.

(4) Initial crack length, mm (or in.), as measured for the fatigue precrack is listed in columns 19 through 23 using a fixed point numeric format.

(5) "Pop-in" stress, MN/m^2 (or ksi), or "pop-in" load, kN (or kips), is listed in columns 24 through 28 using a fixed point numeric format. The stress or load option is designated by the Field 13 indicator.

(6) Offset stress, MN/m^2 (or ksi), or offset load, kN (or kips), is listed in columns 29 through 33 using a fixed point numeric format. The stress or load option is designated by the Field 13 indicator.

(7) Visually determined critical crack length, mm (or in.), is listed in columns 34 through 38 using a fixed point numeric format.

(8) Photo-recorded critical crack length, mm (or in.), is listed in columns 39 through 43 in a fixed point numeric format.

(9) Maximum stress, MN/m^2 (or ksi), or maximum load, kN (or kips), is listed in columns 44 through 48 in fixed point numeric format. The stress or load option is designated by the Field 13 indicator.

(10) Tensile yield strength, MN/m^2 (or ksi), representative of that specimen material is listed in columns 49 through 53 in a fixed point numeric format.

(11) Tensile ultimate strength, MN/m^2 (or ksi), representative of that specimen material is listed in columns 54 through 58 in a fixed point numeric format.

(12) A special dimension, mm (or in.), characteristic of that specimen type is listed in columns 59 through 63 in a fixed point numeric format.

(13) The specimen type is indicated in column 64 as a numeric code and supplemented in columns 65 and 66 by an acronymonic code for easier identification. Since the specimen type also determines the usual convention for selecting either stress or load in the analysis, it is this field that designates the option for Fields 5, 6, and 9. The following conventions that were used in fatigue-crack propagation are also used for fracture:

Code	Specimen Type	Option
1CT	Compact Tension	Load
2CC	Center Crack	Stress
3SF	Surface Flaw or Part-through Crack	Stress
5DC	Double Cantilever Beam	Load
6NB	Notch Bend	Load

(14) An open field is in columns 67 through 69.

(15) Test temperature, °C (or °F), is listed in columns 70 through 73 in an integer format.

(16) The source reference number is given in columns 74 through 80 in an alphanumeric format of the following type:

"NNNNNNL",

where N is a numeric character (0 to 9) and L is an alphabet character (A to Z). The numeric code corresponds to the source reference numbers in Appendix A. The suffix letter will refer to a specific batch of data from the referenced document. This source reference number is the same as that listed on the corresponding Number 1 Lead Data Card.

Crack-Growth Card (Card 4) Format.- The crack-growth card is used for recording the crack-size measurements and cycle counts associated with a given fatigue-crack-propagation test or test specimen. Each card contains one set of data points. The format of Card 4 for crack-growth measurements is illustrated in figure 11.

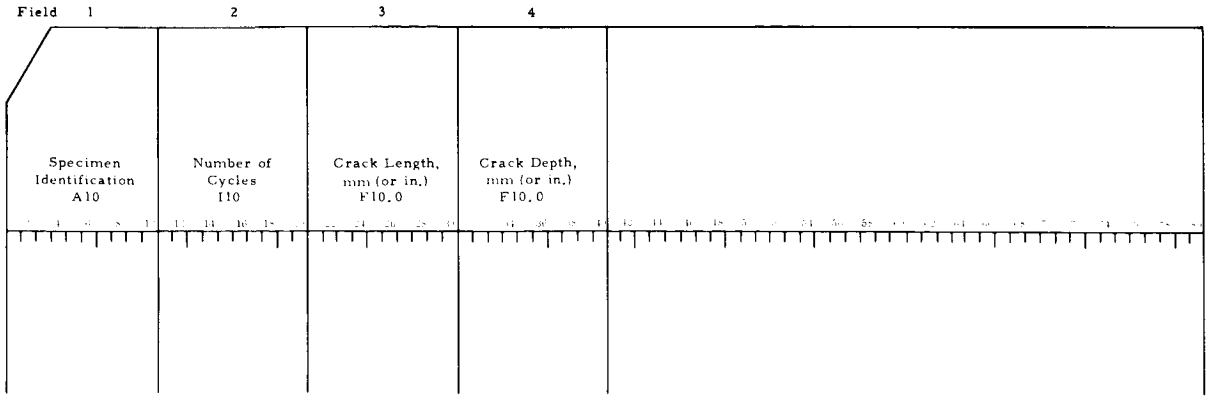

Figure 11. - Format for encoding crack-growth data card (card 4).

A total of 4 fields are indicated. Their contents are as follows:

(1) Specimen identification is listed in columns 1 through 8 using an alphanumeric format.

(2) Number of cycles associated with the first data point on the card is listed in columns 11 through 20 in an integer format.

(3) Crack length, mm (or in.), associated with the first data point on the card as measured in the width dimension of the specimen is listed in columns 21 through 30 in a fixed point numeric format.

(4) Crack depth, mm (or in.), as measured into the thickness of the specimen is listed in columns 31 through 40 in a fixed point numeric format.

Data Retrieval and Sorting

The data handling system consists of two sets of programs. The first set implements the storage of fatigue, fatigue-crack propagation, and fracture data on magnetic tape. The second set implements the retrieval of data on the basis of certain specified parameters.

The storage program writes the data in card-image format on seven-track magnetic tape at a density of 800 bits per inch. Materials are separated from each other by end-of-file cards. There is a different tape for each type of data.

Data retrieval is implemented through a set of programs that sorts the data by a number of parameters including stress ratio, stress, frequency, environment, and test temperature. These parameters must be specified on a separate control card. Specified data then may be transferred from the magnetic tape to any of a number of output devices. Information may be obtained in the form of magnetic tape, punched cards, or printed output. Either SI or English units may be used.

Additional analytical subprograms are added to the sorting program to obtain graphical output and to perform curve fitting and statistical analysis. Figure 12 presents a flow chart outlining the data storage and retrieval system.

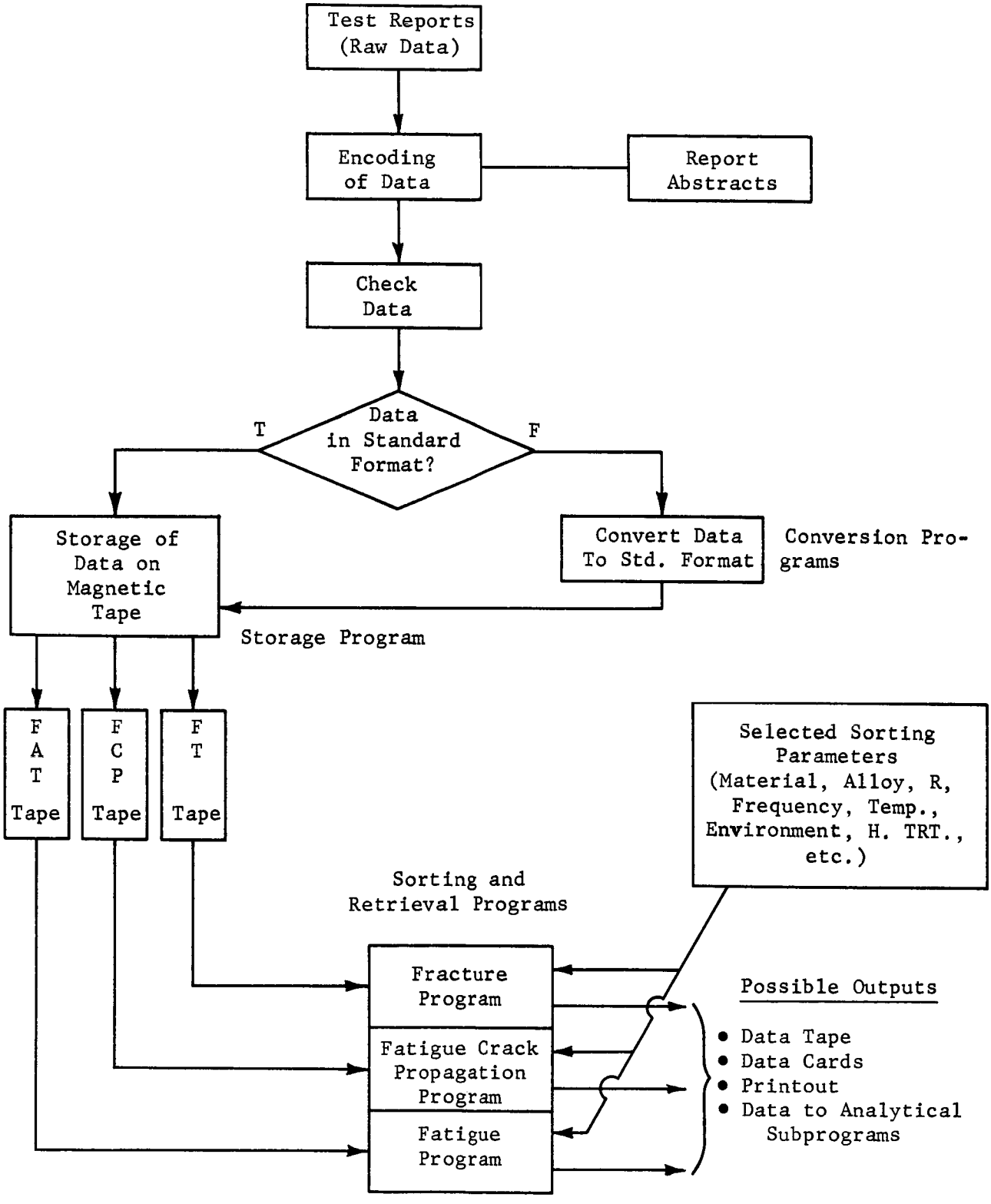

Figure 12. – Data storage, retrieval, and sorting system flow chart.

STATISTICAL METHODS OF ANALYSIS

The phenomenological approach to the study of fatigue and fatigue-crack propagation is usually concerned with formulating a model of material behavior. In the present program, this model took the form of a regression equation that was fitted to empirical data. Statistical analysis provided a method by which the performance of the various empirical models could be compared and evaluated.

The method which was developed for the analysis of fatigue data is outlined in Appendix C. The formulations which were used in the analysis are discussed in the following section.

In the fatigue analysis, a third-order polynomial proved to be useful for many of the initial comparative studies. The equation was written in the following form:

$$\log N_f = A_0 + A_1 \varepsilon_{eq} + A_2 \varepsilon_{eq}^2 + A_3 \varepsilon_{eq}^3 \quad . \tag{1}$$

Further investigations revealed that equation (1) could be simplified to a linear regression equation involving a single independent variable,

$$Y = A_0 + A_1 X \quad , \tag{2}$$

where X represented a mapping function linearly related to the dependent variable Y. This same simple functional form was also found to be useful in the fatigue-crack-propagation analyses.* A least-squares regression procedure was used to establish optimum coefficients for equations (1) and (2). The optimization procedure was based on a minimization of the standard error of estimate,

$$s = \sqrt{\frac{\Sigma(Y-\bar{Y})^2}{n-2}} \quad . \tag{3}$$

Different formulations for the independent variables were compared through calculation of the statistical parameter, R^2. This factor, which provided a quantitative estimate of goodness of fit, was used to describe the fraction of the sum of squares of deviations of the dependent variable from its mean associated with the regression. It was defined by the relationship

$$R^2 = 1 - SSD/TSS = 1 - \frac{\Sigma(Y_i-Y)^2}{\Sigma Y^2} \quad . \tag{4}$$

---

* The exact definition of this mapping function was omitted here for simplicity, it is detailed in the later sections on fatigue and fatigue-crack propagation. Briefly, however, for the fatigue analysis $X = f(\varepsilon_{eq})$ and $Y = \log N_f$, and for the fatigue-crack-propagation analysis, $X = {}_f(K_{eff})$ and $Y = \log da/dN$.

Values of R^2 approaching 100 percent were considered most desirable, since that tendency indicated a large percentage of the variance of the dependent variable was attributable to the regression. In the case of fatigue, such values of R^2 indicated a good correlation between equivalent strain and fatigue life. In the case of fatigue-crack propagation, they indicated a well-defined relationship between the effective stress-intensity factor and crack-growth rate. The R^2 parameter was used extensively in the two sections of this report on fatigue and fatigue-crack propagation.

In parts of the fatigue analysis where the degree of fit for one material was compared with that for another material, a modified value of R^2, designated as R_m^2, was used. Such a statistic was necessary when the sample population was fairly small in comparison with the number of degrees of freedom. For example, R_m^2 was used to compare a small sample of fatigue data on Ti-6Al-4V alloy with a large sample of data on 300M steel. (See Table 2 on page 38.) This term provided a more realistic estimate of fit than R^2, since it accounted for the number of degrees of freedom and the sample population. It provided a sample estimate of the fraction of the variance of the dependent variable attributable to regression (ref. 10) and was expressed as follows:

$$R_m^2 = 1 - \frac{(1-R^2)(n-1)}{(n-\nu-1)} \quad . \tag{5}$$

In cases where n was only slightly larger than ν, the R_m^2 statistic was appreciably smaller than the R^2 statistic. However, when $n \gg \nu$, the value of R_m^2 approached that of R^2. Thus, only values of R^2 were computed for comparison of results from large data sample populations.

After screening the formulations of interest, it was considered desirable to establish tolerance limits on the best empirical models. These tolerance limits are calculated to define an interval which can be claimed to contain a specified proportion of the data population with a specific degree of confidence. Before tolerance limits could be calculated, it was necessary to determine whether the data satisfied the appropriate statistical conditions. Primarily, the data had to be independent and be normally distributed about the regression line and had to have zero mean deviations from that line and have a constant variance (ref. 11).

When the residuals (or deviations from the mean curve) were plotted as a function of actual values of the dependent variable, it was possible to determine, by inspection, whether the data were independent and had an essentially uniform variance throughout their range. Actual values for the dependent variable were used since it was then possible to compare different fitting functions without

changing the fatigue life values of individual data points on the residual plot. If only one fitting function had been studied, it would have been reasonable to use predicted values of the dependent variable as is customary in most statistical analyses. The additional criterion of log-normality was tested in several cases through construction and examination of frequency distribution plots of the residuals. Although log-normality of the data was not proved, the frequency distribution plots indicated that the data were not skewed appreciably and were reasonably approximated by a log-normal distribution.

After statistical conditions were satisfied, it was possible to calculate the estimated variance of a specific value of Y about the regression line. For a first order equation [eq. (2)], the point estimate of variance was defined according to the following expression:

$$V = s^2 \left[\frac{1}{n} + \frac{(X-\bar{X})^2}{\Sigma(X_i \bar{X}_i)^2} \right] \quad , \tag{6}$$

To solve equation (6), it was necessary to determine values of X_i for each data value based on values of ϵ_{eq}. Then $\bar{X}$ was calculated as a simple average of the X_i's. The same process was used in order to calculate s^2, based on values of Y_i. After these calculations were completed, the variance was calculated for a selected value of X. Knowing the estimates of variance at X, it was then possible to determine tolerance limits of level (u) at a desired confidence (ν), according to the following formulation (ref. 12)

$$Y_{u,\nu} = Y \pm t \sqrt{s^2+V} \quad . \tag{7}$$

Equation (7) was only valid, however, for data sets which were essentially of uniform variance throughout the range of Y.

In cases where the variance was nonuniform, it was necessary to modify the residuals through the use of a weighting function, W(X), so that the transformed residuals were approximately uniform. A discussion of this process is included in the Fatigue Analysis section of this report.

In defining all of the above equations, it was assumed that the data under analysis were constituents of a single population, presumably from a single source, where factors such as between laboratory and between test machine variability were of no importance. In a practical situation, however, a large data accumulation for a given material is often the result of work at numerous laboratories. In such a case, it is inevitable that some portion of the observed data variance is really caused by between-system variations. It is desirable to isolate these two factors so that the material scatter can be considered apart from the laboratory-introduced

scatter. If, for example, it is found that the between-laboratory variance of two combined data sets is much larger than the within-laboratory variance of either subpopulation, it is reasonable to analyze the data separately since the ratio of variances indicates that there is a strong possibility the two materials are different or the procedure used to test them was not the same. The following paragraphs discuss this problem as it pertains to populations of fatigue data. Basic aspects of the discussion are also applicable to fatigue-crack-propagation data.

A method proposed by Mandel and Paule (ref. 13), involving the interlaboratory evaluation of a material with an uneven number of specimens from different sources, was considered as a means of properly accounting for within-laboratory and between-laboratory variance factors. This method was found to be useful in certain cases where fatigue data for a given material, although generated at different laboratories, were obtained from tests run at consistent values of stress ratio and notch concentration. It was questionable whether the approach had application for most of the accumulated data file, however, since the majority of data from different sources were nonuniform in values of stress ratio and notch concentration. To use the method for data such as these, it would necessarily have followed that the means of consolidation on R and K_t was sufficiently good that individual sets of data could not be statistically isolated. This then implied that data from different sources, even though possibly of nonequal stress ratio or notch concentration, could have been compared, after consolidation, as identical data.

Investigations did not provide sufficient evidence to support this conclusion. Most sources contained data at only a few values of R. In some cases, a particular stress ratio was represented by only a few nonreplicate tests. The same was true for much of the data generated with K_t as a variable. This lack of uniform and consistent data made it difficult to conclude with confidence that consolidated data run at different R and K_t values were completely homogeneous.

Despite this problem, it was considered appropriate to calculate tolerance limits on the combined data sets according to equation (7), since all requirements involving randomness, normality, and uniformity of variance appeared to be met satisfactorily. Since it was concluded that subpopulations could not be accepted or rejected on the basis of an examination of variances, particular data sets were included or excluded on the basis of their overall effect on the quality of fit (R^2) which was obtainable. In some instances, a visual examination of the plotted data was sufficient to exclude a particular data subset.

FATIGUE ANALYSIS

Designers of aircraft structural components usually base their fatigue analysis on data from stress versus number of cycles to failure (S-N) curves. Data for these S-N curves are obtained from constant-amplitude fatigue tests of simple notched or unnotched specimens. The stress value in the S-N curve is usually either S_{max} or S_a and the S-N relationship is defined for a constant value of S_m or R. Curves are generated at several values of S_m or R to determine the effect of mean stress or stress ratio. To obtain estimates of fatigue life for other values of mean stress, interpolations between existing data must be made. Average S-N curves are often used to construct modified Goodman diagrams to aid in making these interpolations. A set of S-N curves is normally required for both smooth specimens and several sets of notched specimens with different notch concentrations.

Determination of a meaningful set of average S-N curves for a material may require 100 or more specimens. If a statistically based S-N curve is required for each condition, this number could easily increase to 500 or more specimens. Since such large amounts of fatigue data are not available, even for well-characterized materials, it is desirable to have an analytical method for combining data from different S-N curves to obtain a single curve containing sufficient data to allow the development of a statistically based S-N type relationship for each material.

The following sections describe the analytical formulations and approximations which were used in the development of the final analytical model. The problem of consolidation of data generated at different mean stresses is considered first. Three different formulations of equivalent strain are reviewed and compared. Next, the consolidation of notched data is considered. Various methods of estimating local alternating, mean and maximum stress levels are described and critically analyzed. The final step relates to the establishment of a functional relationship between equivalent strain and fatigue life. The overall results conclude the section.

Equivalent Strain Concept in Unnotched Specimens

It has been found in work done at BCL that the effect of mean stress on fatigue life can be reasonably accounted for through the use of an equivalent stress (or strain). Equivalent stress is defined by an equation relating two

terms that uniquely define constant-amplitude loading conditions. One term represents the cyclic stress amplitude in terms of either ΔS or S_a, while the other term defines the mean stress, either directly as S_m or indirectly as S_{max} in conjunction with S_a. If equivalent strain rather than stress is used, ΔS and S_a are replaced by Δe and e_a.

The following section includes a derivation of the equivalent strain equations which were evaluated as a part of this program. The determination of strain amplitudes through usage of the cyclic stress-strain curve is also described. Factors influencing the final choice of an equivalent strain formulation are discussed at the close of the section.

Formulations of Interest. – Two general formulations of equivalent stress have been reviewed. The first involves an additive combination of two stress parameters,

$$S_{eq} = A\, S_m^{\alpha} + B\, S_a^{\beta} \quad . \tag{8}$$

Equation (8) reduces to a form suggested by Stulen (ref. 14) when B, α, and β are set equal to unity,

$$S_{eq} = k\, S_m + S_a \quad . \tag{8a}$$

When both coefficients, A and B, and the exponent β are assumed equal to one, equation (8) simplifies to another form originally proposed by Topper and Sandor (ref. 15),

$$S_{eq} = S_m^{\alpha} + S_a \quad . \tag{8b}$$

Since equations (8a) and (8b) are applicable only in cases where stress levels are nominally elastic, it was necessary to consider a more general formulation. To account for inelastic stress-strain behavior, equations (8a) and (8b) were modified to define an equivalent strain* so that equation (8a) was transformed to

$$\epsilon_{eq} = e_a + k\, S_m/E \quad , \tag{8c}$$

and equation (8b) was rewritten as

$$\epsilon_{eq} = e_a + S_m^{\alpha}/E \quad . \tag{8d}$$

---

* For unnotched specimens, local equivalent strain was considered to be the same as nominal equivalent strain. For notched specimens, the determination of a local equivalent strain was of prime interest.

The second general formulation of equivalent stress involves a multiplicative combination of stress factors,

$$S_{eq} = D\ \Delta S^{\alpha}\ S_{max}^{\beta} \quad . \tag{9}$$

When the parameters $D = 1$, $\alpha + \beta = 1$, and $m = \alpha$, equation (9) describes a form proposed by Walker (ref. 4)

$$S_{eq} = (\Delta S)^{m}\ (S_{max})^{1-m} \quad . \tag{9a}$$

For inelastic stress-strain response, equation (9a) was modified to the following form:

$$\epsilon_{eq} = (2e_a)^{m}\ (S_{max}/E)^{1-m} \quad . \tag{9b}$$

Since e_a was required to define each equivalent strain, it became necessary to calculate the strain amplitude in cases where it was not measured during the test. The following section briefly outlines this calculation procedure.

Strain-Amplitude Determination by Use of the Cyclic Stress-Strain Curve. – In tests performed under strain control, values for e_a and S_m (or S_{max}) were known. However, in load control tests, only values of S_m (or S_{max}) and S_a were known and e_a had to be calculated. Use of the cyclically stable stress-strain curve provided a good estimate of e_a from known values of S_a. A logarithmic trilinear approximation of the cyclic stress-strain curve was defined as follows:

$$\begin{aligned} S_a &= E\ e_a, \quad 0 \le S_a(1) \quad , \\ S_a &= K_1\ e_a^{n_2}, \quad S_a(1) < S_a \le S_a(2) \quad , \\ S_a &= K_2\ e_a^{n_2}, \quad S_a(2) < S_a \quad . \end{aligned} \tag{10}$$

Appropriate values of the equation parameters for the investigated materials are presented in table 1. Experimental cyclic stress-strain data from the present study are detailed in Appendix B.

A number of different parameter values are indicated for Ti-6Al-4V because cyclic as well as monotonic properties for the material vary greatly, depending on processing and product form. When the titanium data were analyzed, the set of cyclic and monotonic values which appeared to most reasonably represent the cyclic and monotonic stress-strain behavior of the material were used.

Selection of a Method. – Initial investigations showed that all three equivalent strain formulations [eqs. (8c), (8d), and (9b)] provided good mean

TABLE 1

CONSTANTS USED TO DEFINE TRI-LINEAR CYCLIC STRESS-STRAIN CURVES

Material	E, MN/m^2 (ksi)	K_1, MN/m^2 (ksi)	K_2, MN/m^2 (ksi)	$S_a(1)$, MN/m^2 (ksi)	$S_a(2)$, MN/m^2 (ksi)	$e_a(1)$	$e_a(2)$	n_1	n_2
2024-T4 Bar[a]	70 300 (10 200)	1 165 (169)	676 (98)	414 (60)	572 (83)	0.0059	0.0275	0.200	0.048
2024-T3 Sheet[b]	73 100 (10 600)	5 135 (745)	917 (133)	358 (52)	435 (63)	0.0049	0.0071	0.499	0.150
7075-T6 Bar[a]	71 000 (10 300)	1 406 (204)	896 (130)	483 (70)	662 (96)	0.0068	0.0285	0.213	0.087
7075-T6 Sheet[b]	72 400 (10 500)	22 260 (3 230)	2 550 (370)	326 (47)	465 (67)	0.0045	0.0071	0.782	0.346
300M Billet[b]	199 900 (29 000)	17 370 (2 520)	7 240 (1 050)	1 140 (165)	1 520 (220)	0.0057	0.0098	0.529	0.339
Ti-6Al-4V Plate[c]	110 300 (16 000)	6 650 (965)	2 400 (348)	618 (90)	765 (111)	0.0056	0.0089	0.458	0.240
Ti-6Al-4V Cylindrical Forging[d]	115 100 (16 700)	8 890 (1 290)	2 140 (310)	702 (102)	828 (120)	0.0061	0.0081	0.493	0.198
Ti-6Al-4V Hot Rolled Bar[e]	108 900 (15 800)	3 915 (568)	1 340 (194)	741 (107)	828 (120)	0.0068	0.0105	0.341	0.104
Ti-6Al-4V Bar[f]	110 300 (16 000)	7 440 (1 080)	1 870 (272)	794 (115)	978 (142)	0.0072	0.0110	0.450	0.144

[a]Values based on data of Endo and Morrow (ref. 16) and Landgraf, et al. (ref. 17).

[b]Values based on data generated at BCL.

[c]Annealed condition, based on unpublished BCL data.

[d]Annealed condition, coarse microstructure, from Gamble (data source ref. 90).

[e]Annealed condition, fine microstructure, from Gamble (data source ref. 90).

[f]STA condition, from Smith, et al. (ref. 18).

stress data consolidations. Subsequently, the three methods were analyzed in detail to determine which method gave the best overall results.

As stated previously, the major objective in selecting an equivalent strain formulation was to consolidate fatigue test data generated at different stress ratios so that all data for a particular material might be treated as one set and be represented by a single curve. Examination of the Stulen and Topper-Sandor equivalent strain relations [eqs. (8c) and (8d)] reveals that data generated at nonzero mean stress values are adjusted by a factor related to the magnitude of the equation parameters k or α, so that the data more closely represent zero mean stress data trends. The best value of k or α is determined by the relative influence on fatigue life of mean stress as compared to alternating stress. A high value of k or α indicates a large mean stress effect.

An analogous situation exists for the Walker formulation [eq. (9b)]. Mean stress is not present directly in the formulation but it can be easily introduced because $S_m = S_{max} - S_a$. In this case, lower values of m imply greater effect of mean stress, since lowering the m value increases the exponent on S_{max}, making a change in S_{max} (and therefore S_m) more important relative to e_a.

To determine the best values of k, α, and m, a third order polynomial equation [eq. (1)] was fit to selected data sets for each definition of equivalent strain. Which of these three constants was optimized, depended upon which definition of equivalent strain was used. The constant k was used for the Stulen method [eq. (8c)], α was used for the Topper-Sandor method [eq. (8d)], and m was used for the Walker method [eq. (9b)]. The polynomial was used because it fit the results quite well in the region of available data and because it provided a convenient tool for comparison of the degree of data collapse obtainable for each equivalent strain equation. It was found, however, that the polynomial behaved unrealistically outside the range of data. This did not inhibit its use as a comparative tool, but did create some doubt as to the polynomial's usefulness in providing a functional relationship between equivalent strain and fatigue life. This problem will be discussed further in a later section.

In using equation (1), equivalent strain was treated as the dependent variable (i.e., $Y = \epsilon_{eq}$), and the logarithm of fatigue life was treated as the independent variable (i.e., $X = \log N_f$). The equation coefficients (A_0, A_1, A_2, and A_3) were determined by least squares regression. Depending upon which of the three methods was used, an optimum value of the material constant (k, α, or m) was determined by iteratively conducting the regression analysis until a minimum value of the standard error of estimate was obtained. Results for five different sets of smooth-specimen data are summarized in table 2. All data points

TABLE 2

COMPARISON OF EQUIVALENT STRAIN FORMULATIONS FOR UNNOTCHED 2024-T4 ALUMINUM BAR, 2024-T3 and 7075-T6 ALUMINUM SHEET, Ti-6Al-4V BAR, AND 300 M STEEL BILLET

Method	Number of Data Points	R^2, percent	R_m^2, Percent	Material[a] Constant	Regression Coefficients for 3rd Degree Polynomial			
					B_1	B_2	B_3	B_4
2024-T4 Bar[b]								
Stulen	18	97	96	0.444	-1.55×10^{-2}	2.05×10^{-2}	-5.76×10^{-3}	4.82×10^{-4}
Walker	18	96	95	0.324	-8.67×10^{-3}	1.92×10^{-2}	-5.89×10^{-3}	5.13×10^{-4}
Topper-Sandor	18	97	96	0.798	-1.51×10^{-2}	2.02×10^{-2}	-5.68×10^{-3}	4.74×10^{-4}
2024-T3 Sheet[c]								
Stulen	64	92	91	0.426	1.49×10^{-2}	-3.87×10^{-3}	4.00×10^{-4}	-1.74×10^{-5}
Walker	64	93	92	0.402	1.39×10^{-2}	-1.35×10^{-3}	-2.37×10^{-4}	-2.70×10^{-5}
Topper-Sandor	64	92	91	0.786	1.87×10^{-2}	-6.29×10^{-3}	9.20×10^{-4}	-5.41×10^{-5}
7075-T6 Sheet[c]								
Stulen	51	92	91	0.450	6.28×10^{-2}	-2.87×10^{-2}	4.59×10^{-3}	-2.46×10^{-4}
Walker	51	93	92	0.384	8.45×10^{-2}	-3.85×10^{-2}	6.16×10^{-3}	-3.30×10^{-4}
Topper-Sandor	51	91	90	0.810	6.38×10^{-2}	-2.91×10^{-2}	4.65×10^{-3}	-2.49×10^{-4}
Ti-6Al-4V Bar[d]								
Stulen	18	87	84	0.564	1.11×10^{-1}	-5.48×10^{-2}	9.46×10^{-3}	-5.41×10^{-4}
Walker	18	95	93	0.354	9.04×10^{-2}	-4.35×10^{-2}	7.55×10^{-3}	-4.35×10^{-4}
Topper-Sandor	18	88	85	0.870	1.13×10^{-1}	-5.63×10^{-2}	9.74×10^{-3}	-5.57×10^{-4}
300 M Billet[e]								
Stulen	69	85	84	0.480	2.67×10^{-2}	-8.91×10^{-3}	1.12×10^{-3}	-3.09×10^{-5}
Walker	69	85	84	0.366	2.32×10^{-2}	-4.62×10^{-3}	-4.18×10^{-5}	4.69×10^{-5}
Topper-Sandor	69	85	84	0.852	2.60×10^{-2}	-8.59×10^{-3}	9.87×10^{-4}	-3.11×10^{-5}

[a]Value of k for Stulen method; value of m for Walker method; and value of α for Topper-Sandor method.

[b]Data reported by Topper and Morrow (data source ref. 13), negative mean stresses excluded.

[c]Data reported by Grover, et al. (data source ref. 1).

[d]Data reported by Titanium Metals Corporation of America (data source ref. 70), bar stock was in the annealed condition.

[e]Data reported by Bateh, et al. (data source ref. 14).

were equally weighted in the analysis, and results for specimens that did not fail (i.e., runouts) were excluded.

After performing the regression analysis for each material with each formulation, a review of the results did not provide sufficient evidence for the selection of one method of defining equivalent strain in preference to the other two. In four out of five data sets, the Walker method was as good or better in terms of R^2 than the Stulen and Topper-Sandor equations. In the one instance, where the regression fit was poorer, the R^2 value was still a very high 96 percent.

The Walker method was attractive for one other major reason — the formulation used for stress-ratio compensation in the consolidation of fatigue data was exactly analogous to the equation found useful in the consolidation of fatigue-crack-propagation data obtained from tests at different stress ratios. In a real structure, where flaw initiation and propagation both may represent a significant percentage of the useful service life, it is expedient to treat both phases as two interrelated parts of a single damage process rather than as separate phenomena. Therefore, an equation such as the Walker equivalent-strain equation, which compensates for stress-ratio effects in the same manner for both initiation and propagation, appeared to be the most useful method of the three investigated.

Further investigations were then conducted using the Walker formulation to determine the importance of specifying an exact value for m. Since the m value provided a compensation on stress ratio, it seemed likely that the optimum value of m determined by regression for a given data set was related to the stress-ratio values for which it was optimized. This was found to be true in a regression analysis performed on 2024-T3 sheet data, in which R = -1.0 data were excluded. This screening of the data reduced the m value from 0.41 to 0.39. Although the difference was only slight, it did indicate that an exact specification of m for a particular material was somewhat unrealistic. To choose a reasonable approximate value, however, it was necessary to determine how much deviation from optimum was allowable in the specification of m before drastic reductions in R^2 would occur. Figure 13 illustrates the results of a study performed on unnotched 2024-T3 sheet data. The percentage reduction in R^2 is plotted as a function of the deviation from the optimum value of m. The R^2 value was reduced less than one percent for all values of m within 0.07 of the optimum value. Deviations in m greater than 0.07 from the optimum caused substanital R^2 reductions, with large deviations in m (> 0.20) causing reductions in R^2 of over 10 percent.

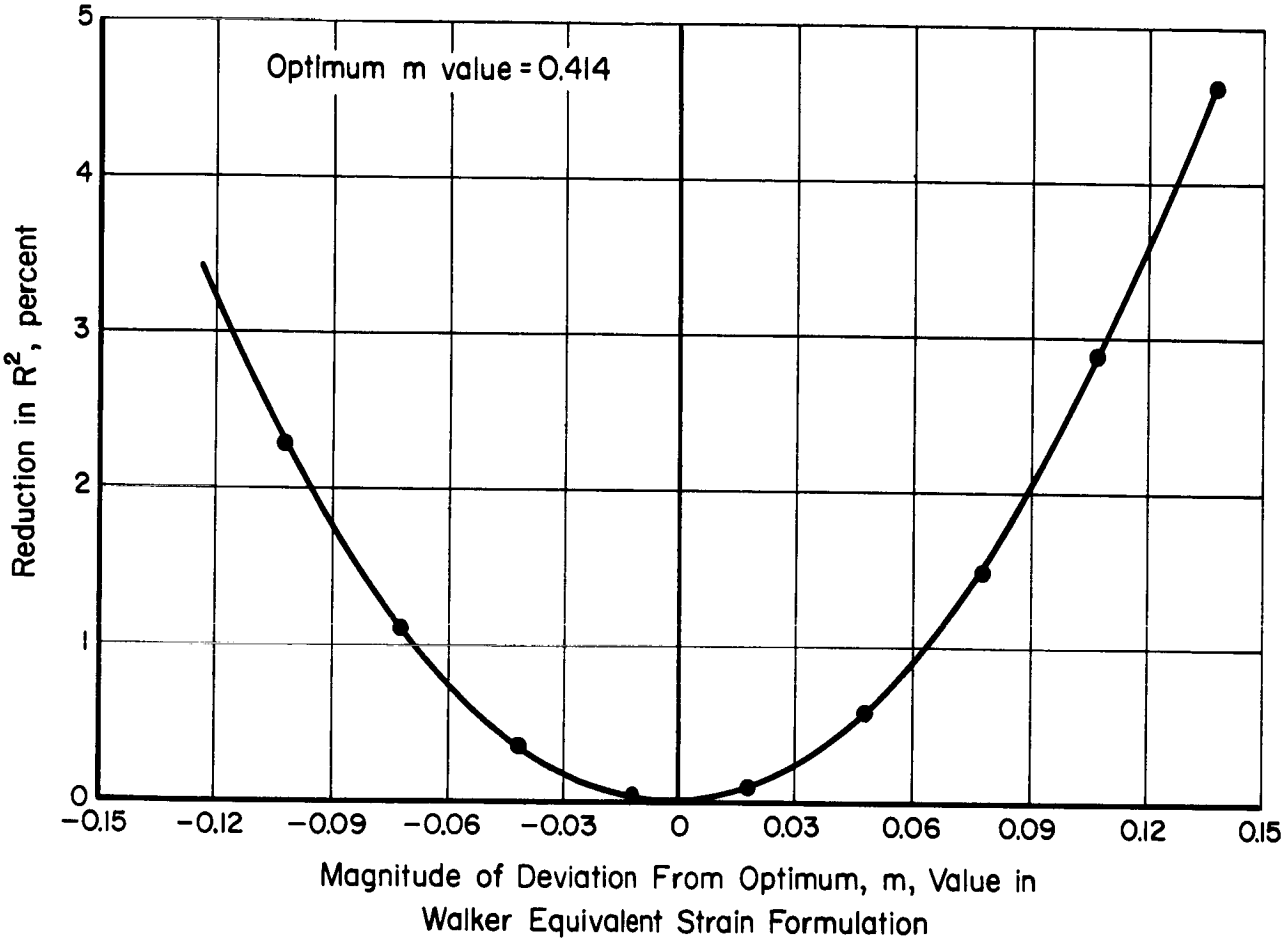

Figure 13. — Sensitivity of data consolidation to variation in m value.

After reviewing the data for all the investigated materials, it appeared reasonable to attempt usage of a single optimum m value for all the data. Table 3 indicates the resultant decrease in R^2 for each material when an R^2 value of 0.40 was chosen. The greatest R^2 reduction occurred with a titanium data sample in which an approximately 0.60 percent reduction was observed. Since even this reduction was comparatively small, an m value of 0.40 was used in all later analyses.

TABLE 3

REDUCTION IN R^2 RESULTING FROM SPECIFICATION OF m

Material	Optimum m Value	Optimum R^2, percent	TSS	SSD for m = 0.40	Reduction in R^2, for m = 0.40, percent
2024-T3 Sheet[a]	0.414	91.55	167.9	14.24	0.03
7075-T6 Sheet[a]	0.403	86.29	28.43	3.894	0.00
300M Billet[b]	0.366	77.02	33.02	7.725	0.41
Ti-6Al-4V Bar[c]	0.426	86.09	13.87	2.012	0.59

[a]Data reported by Grover, et al (data source ref. 1).

[b]Data reported by Bateh, et al (data source ref. 14).

[c]Data reported by Titanium Metals Corporation of America (data source ref. 70), bar stock was in the annealed condition.

Local Stress and Strain Approximations in Notched Specimens

Beyond the consolidation of smooth-specimen data through mean-stress compensation, it was also of interest to combine notched-specimen data in a similar fashion by appropriately accounting for notch effects. Since values of e_a and S_{max} were used to calculate equivalent strain values for unnotched specimens, it

also seemed reasonable to calculate equivalent strain values for notched specimens in exactly the same way by using adjusted values of e_a and S_{max}, which would be representative of local strain amplitudes and maximum-stress levels.

Estimation of Local Alternating Stresses and Strains. — Smooth-specimen simulations of local stress-strain behavior in notched specimens (ref. 19) indicate that combined strain hardening and stress relaxation often occur at the notch tip during constant-amplitude nominal-stress cycling. To estimate stable local values of alternating stress and strain from nominal values, it is necessary to compensate for this combined hardening and relaxation. Research (ref. 20) has shown that the effects of strain hardening or softening can be accounted for by using a cyclic stress-strain curve in combination with nominal alternating strain values modified by an appropriate notch-concentration factor, such as K_t, K_f, or K_ε.

All three modifying factors were investigated to determine which one gave the most reasonable indication of the local strain concentration. Consolidation of notched-specimen fatigue data was considered to be a measure of how well local strain was estimated.

K_t as a Strain-Concentration Factor. — The theoretical stress-concentration factor was used extensively in initial investigations as an estimate of the effective strain magnification at the notch root. In this way, local strain amplitude was estimated as follows:

$$\varepsilon_a = K_t S_a / E \quad , \tag{11a}$$

which is equivalent to the more general form

$$\varepsilon_a = K_t e_a \quad , \tag{11b}$$

when nominal strains are elastic. This method was found undesirable in further investigations because estimated strains were unrealistically high and conservative in cases where conditions of high nominal stress amplitude and high K_t existed.

The Neuber Rule and K_ε. — As an alternative, the strain-concentration factor was next investigated. This factor can be calculated by several different methods, but the most commonly used method employs a relationship developed by Neuber (ref. 21) which states that

$$K_t = (K_\sigma K_\varepsilon)^{\frac{1}{2}} \quad . \tag{12}$$

The value of K_σ can be written as

$$K_\sigma = \frac{\sigma_a}{S_a} \quad , \tag{13}$$

and K_ϵ can be written similarly as

$$K_\epsilon = \frac{\epsilon_a}{e_a} \quad . \tag{14}$$

Thus, equation (12) can be rewritten as

$$K_t = \left(\frac{\sigma_a}{S_a} \frac{\epsilon_a}{e_a} \right)^{\frac{1}{2}} \quad . \tag{15}$$

If equation (11) is used to define ϵ_a and the stress-strain function of equation (10) is used to define σ_a, it is possible to rewrite equation (15) so that ϵ_a is given in terms of known values of K_t, S_a, and e_a, and appropriate values of K_1, K_2, n_1, and n_2.* Three different equation forms may result, depending on whether the nominal and local strains are elastic or plastic.

Case 1.— If both local and nominal stress and strain are elastic, equation (15) reduces to equation (11a).

Case 2.— If local stress and strain are plastic and nominal stress and strain are elastic, the insertion of the elastic modulus and the stress-strain function of equation (10) into equation (15) gives

$$K_1 \text{ (or } K_2) \; \epsilon_a^{\,n_1 \text{ (or } n_2)+1} = (S_a K_t)^2 / E \quad . \tag{16}$$

Solving equation (16) in terms of local strain yields

$$\epsilon_a = \exp\left[\ln(S_a^{\,2} K_t^{\,2} / E K_1 (\text{or } K_2)) / (n_1 \text{ (or } n_2)+1) \right] \quad . \tag{17}$$

Case 3.— If both local and nominal stresses are plastic, equation (10) must be used for both nominal and local stress-strain behavior, so that equation (15), in general form, is rewritten as

$$K_1 \text{ (or } K_2) \; \epsilon_a^{\,n_1 \text{ (or } n_2)+1} = K_1 \text{ (or } K_2) \; \epsilon_a^{\,n_1 \text{ (or } n_2)+1} K_t^{\,2} \quad . \tag{18}$$

---

* When equation (10) is used to compute local stress-strain response, S_a and e_a are replaced by σ_a and ϵ_a, respectively.

Simplification of equation (18) reveals that local strain amplitude for the fully plastic condition is given by

$$\epsilon_a = \exp[\ln(K_1 (\text{or } K_2)e_a^{n_1 (\text{or } n_2)}K_t^2/K_1 (\text{or } K_2))/(n_1 (\text{or } n_2) + 1)] \quad . \quad (19)$$

In general, the constant terms, K_1, K_2, n_1, and n_2, on the left and right sides of equation (19) may have different values and must be treated separately.

A computerized solution of these equations then yields a means of local strain (or stress) determination through application of the Neuber Rule. It should be pointed out that Case 3 is rarely encountered in most practical applications. It is included in the discussion for the sake of completeness.

To determine the degree of data consolidation possible using the Neuber method of local strain determination, local stresses and strains for notched fatigue data were calculated from equations (11a), (17), and (19). Comparison of calculated equivalent strains for test data at different K_t values and zero mean stress revealed that unrealistically high strain amplitude estimates were calculated in cases involving high levels of nominal strain and K_t. Since no method was found to reasonably account for data at these extreme conditions, this method was also considered undesirable, at least when used in the manner outlined herein.

K_f as a Stress and Strain Concentration Factor. – As a third possibility, use of K_f was subsequently tested as a means of local strain estimation. This factor can also be written in several different forms; values of K_f calculated in this investigation were based on a method proposed by Peterson (ref. 22),

$$K_f = 1 + \frac{K_t - 1}{1 + \rho/r} \quad . \quad (20)$$

This expression was selected for use because it is simple and has been shown (ref. 23) to work reasonably well in comparison to a number of other methods of calculating K_f. Also, it offered a possible solution to the problems observed when using K_t or K_ϵ as a strain multiplier, where data fell further above the unnotched equivalent strain curve as the value of K_t increased.

Analysis of various notched-specimen data sets helped support this idea. Using a computer procedure to optimize the value of ρ for a given material, it was possible to account for even the highest values of K_t. Results were good enough to warrant the use of this method for determination of local cyclic strain amplitudes in all further notched-specimen analyses.

Table 4 indicates optimum values of ρ for the four investigated materials. Optimum values for the two aluminum alloys were very similar and it was possible to approximate these values at ρ = 0.18 mm (0.007 in.) with a reduction in the optimum value of R^2 of less than 0.10 percent. The value of 0.18 mm (0.007 in.) is considerably below that recommended by Peterson (ref. 22). His value of 0.63 mm (0.025 in.) gave R^2 values almost 2 percent lower than the optimized value. This difference was explained in part by the fact that the notched data were analyzed independently from the unnotched data. If the unnotched data had been included, a higher optimum ρ value would have resulted, because an increase in ρ would have lowered the overall notched curve, bringing it closer to the unnotched curve. It was considered desirable, however, to separate notched and unnotched data, since higher ρ values caused layering of the notched data for different K_t.

TABLE 4

OPTIMUM ρ VALUES FOR TWO ALUMINUM ALLOYS, A HIGH-STRENGTH STEEL, AND A TITANIUM ALLOY[a]

Material	SSD	TSS	R^2, percent	Optimum ρ, mm (in.)
2024-T3 Sheet[b]	5.37	110.10	95.13	0.21 (0.0083)
7075-T6 Sheet[b]	4.73	146.30	96.77	0.17 (0.0067)
300M Forging[c]	16.81	153.40	89.04	0.046 (0.0018)
Ti-6Al-4V Bar[d]	5.10	21.94	76.76	0.020 (0.0008)

[a]Data were adjusted according to the weighting function W(X), defined in the next part of the Fatigue Analysis section.

[b]Data reported by Grover et al (data source refs. 2 through 4).

[c]Data reported by Bateh et al (data source ref. 14).

[d]Data reported by Titanium Metals Corp. of America (data source ref. 70).

The optimum ρ value for the 300M forging data was 0.046 mm (0.0018 in.). This compares with a ρ value of 0.028 mm (0.0011 in.) which was developed from

Peterson's empirical formula (ref. 22) based upon an ultimate tensile strength of 2000 MN/m^2 (290 ksi). Although Peterson's value resulted in only a 0.5 percent reduction in R^2, the optimized value of 0.046 mm (0.0018 in.) was used in all 300M data consolidation. Since there was substantial scatter in most of the titanium data, a reasonable ρ value was difficult to define. The optimized value of 0.02 mm (0.0008 in.) obtained from a sample of Ti-6Al-4V bar data did appear to provide reasonable consolidation on K_t for most data sets, so this value was used in all subsequent analyses.

Estimation of Mean and Maximum Stress Levels. – Even after appropriately determining a local cyclic strain amplitude, it was necessary to develop a method for prediction of the effects of stress relaxation on stable local mean-stress values. Smooth specimen, strain-controlled tests performed at BCL (see Appendix B) indicated that the stable local mean stress under constant-amplitude cycling could be approximated by considering a hypothetical mean stress which would develop after an initial loading cycle, if no hardening or softening occurred during that cycle. The development of this method and experimental results to determine its validity are presented in the following discussion.

Two simple methods of predicting local mean stresses were evaluated using results from strain-controlled tests in which positive mean strains were maintained. As table 5 indicates, especially for the 7075-T6 sheet, the cyclically stable mean stresses were low when $\Delta\epsilon$ was large, but they were higher when $\Delta\epsilon$ was small. This reduction of mean stress is related to the amount of plastic deformation that occurs in each cycle.

An understanding of this phenomenon can be found through an examination of the material stress-strain behavior under these conditions. Upon initial loading in tension, deformation will follow the monotonic stress-strain curve (Curve A in fig. 14) and σ is related to ϵ by some function

$$\sigma = f_m(\epsilon) \quad . \tag{21}$$

Deformation upon reversal of the loading direction (Curve B in fig. 14) will be influenced by the prior loading. If the influence of previous loading is small, Curve B can probably be related to the monotonic stress-strain response. However, if this influence is large, Curve B would be more closely approximated by the stable cyclic stress-strain curve. For intermediate cases, use of a transient cyclic stress-strain curve would be more appropriate.

TABLE 5

COMPARISON OF ACTUAL WITH PREDICTED
VALUES OF STABLE MEAN STRESS

Specimen	Strain Ratio	Total Strain Range	Actual Mean Stress, MN/m^2 (ksi)	Predicted Mean Stress	
				By equation (27a) MN/m^2 (ksi)	By equation (27b) MN/m^2 (ksi)
2024-T3 Aluminum Sheet					
7	0	0.0206	25 (3.6)	8.3 (1.2)	-81.3 (-11.8)
8	0	0.0153	7.6 (1.1)	8.3 (1.2)	-65 (-9.4)
6	0	0.0101	15 (2.2)	20 (2.9)	5.0 (0.73)
10	0.5	0.0100	36 (5.2)	29 (4.2)	15 (2.2)
7075-T6 Aluminum Sheet					
8	0	0.0204	49 (7.1)	41 (5.9)	73.8 (10.7)
9	0	0.0152	43 (6.3)	58 (8.4)	106 (15.4)
7	0	0.0101	160 (23.2)	188 (27.3)	198 (28.7)
11	0.5	0.0096	198 (28.8)	247 (35.9)	253 (36.7)

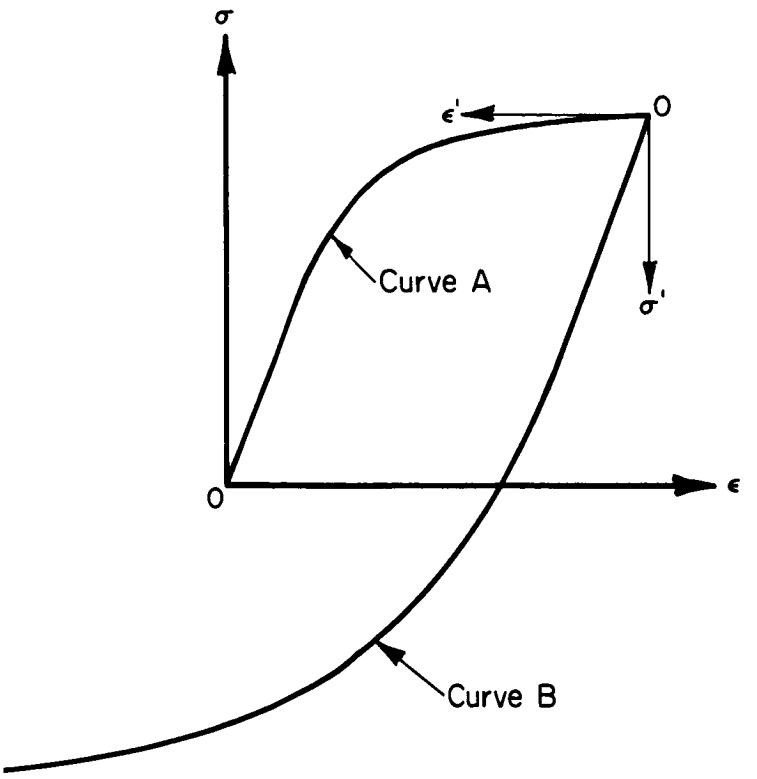

Figure 14. – Schematic illustration of stress-strain response during first reversal of loading history.

Morrow (ref. 24) has pointed out that stable stress-strain behavior after a reversal in loading can be approximated by multiplying the cyclic stress-strain curve by a factor of 2. Using this observation, the translated stress-strain values of Curve B, could be approximated by the monotonic or cyclic stress-strain funetion,

$$\sigma'/2 = f_m\ (\epsilon'/2) \tag{22a}$$

or

$$\sigma'/2 = f_c\ (\epsilon'/2) \quad . \tag{22b}$$

It follows from equation (21) that

$$\sigma_{max} = f_m\ (\epsilon_{max}) \quad . \tag{23}$$

From equation (23), it can be shown that

$$\sigma'_{max} = 2f_m\ (\epsilon'_{max}/2) \tag{24a}$$

or

$$\sigma'_{max} = 2f_c\ (\epsilon'_{max}/2) \quad . \tag{24b}$$

Then, it follows that

$$\sigma_{min} = \sigma_{max} - \sigma'_{max} \quad , \tag{25}$$

and

$$\sigma_m = (\sigma_{max} + \sigma_{min})/2 \quad . \tag{26}$$

By combining equations (24), (25), and (26) one finds that

$$\sigma_m = \sigma_{max} - f_m \, (\epsilon'_{max}/2) \tag{27a}$$

or

$$\sigma_m = \sigma_{max} - f_c \, (\epsilon'_{max}/2) \quad . \tag{27b}$$

Using equation (10) as the cyclic function (f_c) and equation (10) again with monotonic parameters as listed in table 6 as the monotonic function (f_m), two predicted values [eqs. (27a) and (27b)] of mean stress were computed for each of the tests with a mean strain. Results of these calculations are compared with the actual stable mean stresses in table 5. Examination of the data shows that use of equation (27a) gave the most reasonable predictions for both alloys. Equation (27b) gave lower predicted values for 2024-T3 aluminum than did equation (27a) because this alloy cyclically hardened. This trend was oppostie for 7075-T6 aluminum because it cyclically softened. It is interesting to note that compressive-mean stresses would be obtained with initial loading in compression. Also, it is important to realize that this procedure will not apply to variable-amplitude loading because each loading cycle is influenced by the prior cyclic history. Thus, a more detailed and complete stress-strain analysis as a function of loading history would be required for variable-amplitude conditions.

Establishment of a Relationship Between Equivalent Strain and Fatigue Life

One of the major goals at the outset of this program was to develop the capability to estimate, within a desired confidence, the expected fatigue life of a particular alloy, given information on maximum stress, stress ratio, and (if notched) notch condition. Toward this end, initial work was centered on maximum consolidation of notched and unnotched fatigue data for various combinations of stress concentration and/or mean stress. The Walker equivalent-strain formulation, discussed in earlier sections of this report, was found to be useful in the consolidation process, and good correlations were established between ϵ_{eq} and log N_f through the use of a polynomial expression,

$$\epsilon_{eq} = A_0 + A_1 \log N_f + A_2(\log N_f)^2 + A_3(\log N_f)^3 \quad . \tag{28}$$

TABLE 6

CONSTANTS USED TO DEFINE TRI-LINEAR MONOTONIC STRESS-STRAIN CURVES

Material[a]	E, MN/m^2 (ksi)	K_1, MN/m^2 (ksi)	K_2, MN/m^2 (ksi)	$S_a(1)$, MN/m^2 (ksi)	$S_a(2)$, MN/m^2 (ksi)	$e_a(1)$	$e_a(2)$	n_1	n_2
2024-T4 Bar	70 300 (10 200)	841 (122)	462 (67)	274 (40)	379 (55)	0.0039	0.0185	0.200	0.048
2024-T3 Sheet	73 100 (10 600)	1 013 (147)	431 (62.5)	344 (50)	364 (53)	0.0047	0.0060	0.200	0.032
7075-T6 Bar	74 000 (10 300)	1 303 (189)	827 (120)	444 (62)	601 (87)	0.0060	0.0265	0.213	0.087
7075-T6 Sheet	72 400 (10 500)	3 240 (470)	889 (129)	493 (72)	544 (79)	0.0069	0.0086	0.375	0.103
300M Billet	199 900 (29 000)	24 950 (3 620)	7 860 (1 140)	1 280 (186)	1 590 (231)	0.0064	0.0093	0.588	0.342
Ti-6Al-4V Plate	110 300 (16 000)	4 450 (645)	1 050 (153)	750 (109)	875 (127)	0.0068	0.0101	0.354	0.032
Ti-6Al-4V Cylindrical Forging	115 100 (16 700)	5 100 (740)	1 075 (156)	760 (110)	886 (129)	0.0066	0.0100	0.380	0.047
Ti-6Al-4V Hot Rolled Bar	108 900 (15 800)	4 120 (598)	1 330 (193)	937 (136)	1 010 (147)	0.0086	0.0120	0.318	0.056
Ti-6Al-4V Bar	110 300 (16 000)	2 860 (415)	1 340 (194)	1 100 (160)	1 170 (170)	0.0100	0.0119	0.202	0.030

[a]All data are from references as cited in table 1.

A major difficulty arose, however, when an attempt was made to establish a measure of confidence in the calculated fatigue lives. Since log N_f was the independent variable in this equation, it was appropriate to establish limits on ϵ_{eq}, given log N_f, rather than the desired result which would have established confidence limits on log N_f, given ϵ_{eq}.

Fatigue Life as a Dependent Variable.--In order to eliminate the problem discussed above, a variety of new formulations were studied employing log N_f as a dependent variable. The desirability of a given formulation was based on essentially three factors: (1) predictive capability, (2) simplicity, and (3) physical significance.

The first important aspect, predictive capability, was defined solely on the basis of the R^2 statistic, which was discussed in the earlier section on statistical analysis. Simplicity in a formulation was also an important factor since the addition of extra terms in an expression often reduces the significance of the coefficients of original terms. Lastly, the physical significance of a particular equation was considered important since a physically meaningful equation, in contrast to an empirically derived one, was more likely to be useful in a general application. This, of course, was true only as long as the initial insight was correct and was properly applied.

The following sections outline a variety of attempted formulations involving log N_f as a dependent variable. They briefly summarize the relative merit of the various equations as applied to notched and unnotched data used in previous evaluations.

Polynomial Data Fitting.--The first method investigated for establishing fatigue life as a dependent variable simply involved an interchange of variables in equation (28), making ϵ_{eq} an independent variable so that

$$\log N_f = A_0 + A_1\epsilon_{eq} + A_2\epsilon_{eq}^2 + A_3\epsilon_{eq}^3 \quad , \tag{29}$$

where ϵ_{eq} represented the Walker formulation as expressed in equation (9b) Using equation (29), a regression analysis of selected data sets showed that R^2 values were almost equal to those obtained with equation (28). The problem of polynomial uncontrollability outside the range of data still existed, however. To partially eliminate this problem, it was thought useful to define

an intercept value for the polynomial at ¼ cycle of fatigue life in terms of the true fracture ductility, in a manner comparable to that suggested by Morrow (ref. 24).

This operation eliminated one degree of freedom in the polynomial and resulted in slightly better curve definition, but it did not sufficiently improve the overall usefulness of the polynomial as a functional relationship between ε_{eq} and log N_f to warrant its implementation.

Multivariable Stepwise Regression Analysis.—Much of the analytical work performed in the early phases of this program was centered on usage of the three formulations for equivalent strain, but there was also some interest in and some effort devoted towards the development of alternate functional forms which could give comparable or superior data consolidations. Multivariable stepwise regression was used to test and compare a variety of factors in regard to their usefulness as components of a fatigue life prediction equation.

Two basic equation forms were reviewed, the first of which involved combinations of e_a and S_m, as follows:

$$\log N_f = f(e_a, S_m) \quad . \tag{30}$$

Stepwise multiple regression of equation (30) provided an optimum solution of the form

$$\log N_f = A_0 + A_1 e_a^2 S_m/E + A_2 e_a + A_3 e_a S_m/E \quad . \tag{31}$$

The independent variables are listed in order of significance, with the combination $e_a^2 S_m/E$ providing the most significant increase in R^2 and the terms e_a and $e_a S_m/E$ providing lesser, yet significant, improvements in R^2. Including all three variables, the accumulated R^2 for the equation using unnotched 7075-T6 data was 82.0 percent. This was a much poorer consolidation than that obtained using equation (29).

The second general equation was defined so that combinations of maximum stress and stress ratio or total strain range could be examined,

$$\log N_f = f(S_{max}, R \text{ or } \Delta e) \quad . \tag{32}$$

The optimum solution for this combination of variables was found to be an inverse relationship, written as follows:

$$\log N_f = \frac{1}{A_0 + A_1 \log S_{max} + A_2(1+R)} \quad . \tag{33}$$

The R^2 value for this functional form using unnotched 7075-T6 data was 90.9 percent which was only slightly less than the value obtained for the third order polynomial using the Walker equivalent strain term. However, this formulation did not appear to be entirely satisfactory either, since it was observed that the regression fit for certain stress ratios was much better than that at others. Also, the data could not be displayed as well graphically since it was necessary to consider two variables (S_{max} and R) in each plot, as compared to a single variable (ε_{eq}) in the polynomial equation. So, investigations were continued in an attempt to discover a simpler formulation which would accurately model the consolidated fatigue data trends.

The Inverse Hyperbolic Tangent Function. — A variety of functions were reviewed in the search for a functional relationship which would provide a useful empirical model for consolidated fatigue data. Hyperbolic, exponential, and power functions were all investigated and found to be unsatisfactory for fitting the complete range of available data. However, the inverse hyperbolic tangent function provided a reasonable model of fatigue data trends throughout the life range of interest, 10 to 10^8 cycles to failure.

This function, which was chosen and modified specifically to model the sigmoidal shape of the fatigue-crack-propagation (da/dN versus K_{eff}) curve, was also found to provide a useful model of consolidated fatigue data trends. Since this relation is derived in detail in the Fatigue-Crack-Propagation Analysis Section, it is outlined only briefly here in terms of its application to fatigue data.

To implement its usage, the following functional form was established:

$$\log N_f = A_0 + A_1 \tanh^{-1}[\Phi(\varepsilon_{eq})] \quad . \tag{34}$$

The scaling function, $\Phi(\varepsilon_{eq})$, was appropriately defined as

$$\Phi(\varepsilon_{eq}) = \frac{\log(\varepsilon_u \varepsilon_e / \varepsilon_{eq}^2)}{\log(\varepsilon_u / \varepsilon_e)} \quad , \tag{35}$$

where values of ε_u and ε_e were selected to appropriately bound the complete range of data, as illustrated in figure 15. The upper limit, ε_u, was found to be reasonably represented in most cases by the following approximation:

$$\varepsilon_u = \varepsilon_{eq} \Big|_{N_f = 10} + 0.0025 \quad . \tag{36}$$

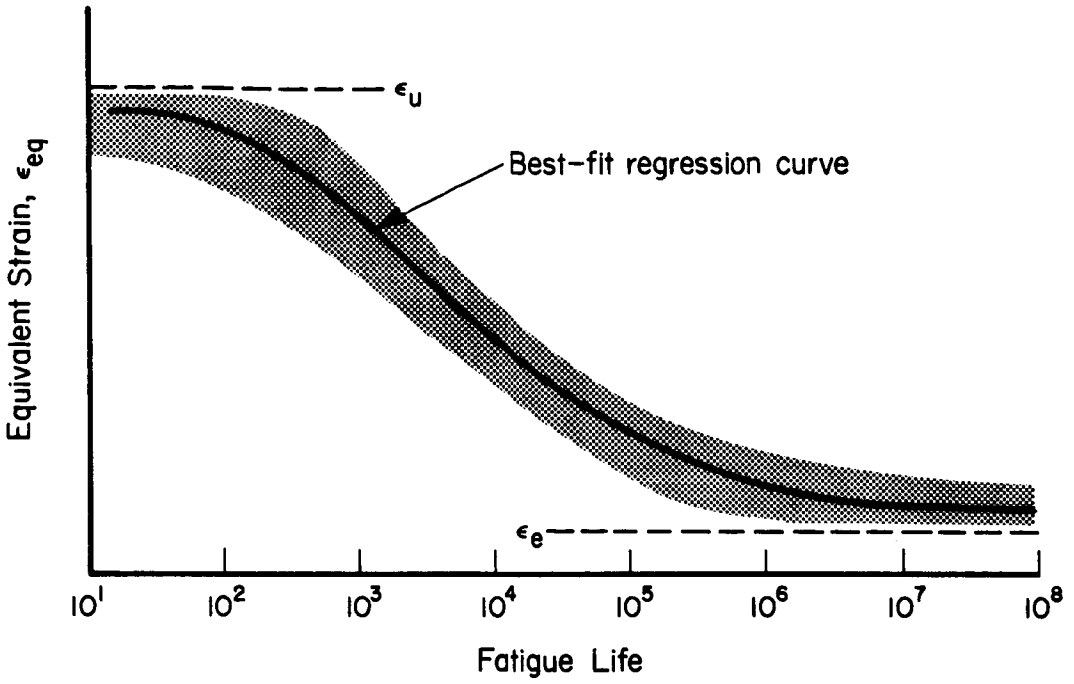

Figure 15. – Schematic illustration of regressed inverse hyperbolic tangent curve and appropriate functional limits.

In cases where representative data did not exist at a fatigue life of 10 cycles, it was necessary to estimate a value of ϵ_u. Attempts to define a value for ϵ_u in terms of true fracture ductility and true fracture strengths resulted in values of ϵ_u which were unacceptably high. Values for the lower limit, ϵ_e, were well represented by an equivalent strain value approximately corresponding to a fatigue limit. It was determined accordingly as

$$\epsilon_e = \epsilon_{eq}\Big|_{N_f = 10^8} - 0.0005 \quad . \tag{37}$$

Once again, in cases where representative data did not exist, a reasonable value of ϵ_e was chosen.

To avoid error in calculation of the inverse hyperbolic tangent function, it was necessary to specify values of ϵ_u and ϵ_e which were higher and lower, respectively, than any calculated value of equivalent strain.

The Weighting Function, W(X). – To calculate point estimates of variance for establishing tolerance limits on the inverse hyperbolic tangent function, it was necessary (in the case of fatigue) to apply a weighting function to the data in order to satisfy the statistical requirement of uniform variance.

Before this step could be taken, it was important to identify the pattern of changing variance. Examination of plotted residuals revealed that the data scatter often increased substantially at either extreme of the fatigue life range. The increased variance was most evident in long-life fatigue data. It was also in this life range that the slope of the fitted curve was greatest (i. e., a small change in the independent variable, ϵ_{eq}, corresponded to a large change in the dependent variable, log N_f).* Since the variance seemed to be related in some fashion to the slope of the curve, it appeared desirable to establish a weighting function which would modify the residuals (and, therefore, the observed data variance) according to the "steepness" of the fitting function.

Several functions of this type were reviewed. One suggested formulation**, involving a weight factor proportional to the square of the slope of the fitted curve, proved to be useful with some modifications. The weighting function was expressable as

$$1/W(X) \propto \left[\frac{d(Y)}{d(X)}\right]^2 = \left[\frac{d(\log N_f)}{d(\epsilon_{eq})}\right]^2 \quad , \tag{38}$$

where the derivative for the inverse hyperbolic tangent expression [eq. (34)] was found to be

$$\frac{d(\log N_f)}{d(\epsilon_{eq})} = \frac{-2.0\, A_1\, [\log(\epsilon_u/\epsilon_e)](\log e)}{\epsilon_{eq}\, \{[\log(\epsilon_u/\epsilon_e)]^2 - [\log(\epsilon_u \epsilon_e/\epsilon_{eq}^2)]^2\}} \quad . \tag{39}$$

To make the weighting function [eq. (38)] independent of the absolute slope of the curve and dependent only on a ratio of slopes at two points along the curve, the derivative [eq. (39)] was normalized through division by a minimum value of that derivative. For the inverse hyperbolic tangent function, the minimum derivative always occurred at the inflection point of the curve which was located midway between the function limits. Therefore, at an equivalent strain given by

$$\epsilon_{eq} = \frac{\epsilon_u + \epsilon_e}{2} \quad , \tag{40}$$

---

* With log N_f plotted in the customary fashion, along the abscissa, it appears that the slope is actually least in the long-life region. It is useful to consider, however, that log $N_f = f(\epsilon_{eq})$, rather than the visually implied relationship, $\epsilon_{eq} = f(\log N_f)$.

** Based on communication with Lars Sjodahl, General Electric Company, Cincinnati, Ohio, May 8, 1973.

the minimum derivative was defined as*

$$\left(\frac{d(\log N_f)}{d(\varepsilon_{eq})}\right)\Bigg|_{\frac{\varepsilon_u + \varepsilon_e}{2}} = \frac{-4.0\, A_1\, [\log(\varepsilon_u/\varepsilon_e)](\log \ell)}{(\varepsilon_u+\varepsilon_e)\{[\log(\varepsilon_u/\varepsilon_e)]^2 - [\log(\varepsilon_u\varepsilon_e/\varepsilon_{eq}^2)]^2\}} \quad . \quad (41)$$

Then a combination of equations (38), (39), and (41) resulted in a normalized weighting function, expressable as

$$W(\varepsilon_{eq}) = \left[\frac{\left(\frac{d(\log N_f)}{d(\varepsilon_{eq})}\right)\Big|_{\frac{\varepsilon_u + \varepsilon_e}{2}}}{\left(\frac{d(\log N_f)}{d(\varepsilon_{eq})}\right)\Big|_{\varepsilon_{eq}}}\right]^2 . \quad (42)$$

The value of $W(\varepsilon_{eq})$ was then bounded between 0.0 and 1.0 with values near 1.0 at midrange of the fitted curve and values decreasing (according to the square of the ratio of slopes) toward 0.0 at the limits of the curve.

This function was then applied directly to the residuals in the manner shown in Appendix H. Characteristically, the function had almost no effect on data falling in the midrange portion of the curve. It did, however, substantially reduce the relative magnitudes of the residuals near the extremes of the function. The overall effect of this weighting operation was an approximately uniform data variance.

Results of Fatigue Analysis

Up to this point, the discussion has dealt with the various considerations which were involved in the development of the overall fatigue data consolidation and modelling process. The following paragraphs describe the results of those considerations.

A fatigue data consolidation and modelling process was developed through which a conglomerate set of fatigue test data at various mean stresses and notch concentrations could be consolidated into a single curve and be reasonably described by a simple analytical expression. Also, statistical considerations were applied, incorporating weight factors, so that probability of survival curves

---

* In equations (41) and (42) the vertical slash adjacent to the derivative designates an evaluation of the derivative at the indicated point.

could be constructed about this consolidated data band from which an estimate of simple specimen fatigue life for a given material could be obtained from a single plot, once the controlling parameters (S_{max}, Δe, K_t, and r) were specified. An outline in Appendix C provides a step-by-step illustration of this procedure.

This process was successfully applied to 2024 and 7075 aluminum alloys in several different product forms and tempers and to 300M steel in the forged condition. It was also used with marginal success on a Ti-6Al-4V alloy, consisting of numerous product forms and heat-treatment conditions.

In these analyses, notched and unnotched specimen data were treated separately because there was a sufficient amount of each type of data to consider them on a statistical basis. When the two types were combined, the R^2 values were decreased by amounts up to about 10 percent. Thus, it would be acceptable to combine notched and unnotched results when there are not enough data to analyze them separately on a statistical basis. A better correlation of notched and unnotched data would have been obtained if a more realistic analysis of notch root stress-strain behavior had been available.

Table 7 summarizes the results of the analyses that were made for each material using the final model incorporating the hyperbolic tangent function. Weighted R^2 values are presented for each combined data set. Also, optimum equation coefficients are listed, along with the function limits which were employed in each consolidation process. The data source references for each material are included in the final column. Graphical displays of the consolidated fatigue data are presented in Appendix D. The best-fit regression curve is drawn through the data and 90 and 99 percent tolerance curves (95 percent confidence) are drawn below that line. Comments concerning individual plots are presented in the introductory comments of Appendix D.

FATIGUE-CRACK-PROPAGATION ANALYSIS

The determination of the safe life of an aerospace structure must be based on a detailed knowledge of the entire continuum of damage mechanisms. This begins with an understanding of the process of fatigue and its role in leading to the initiation of macrocracks, and continues as these macrocracks grow to a size which may be critical for the complete fracture of a structure or structural component. Once a macrocrack has been initiated, crack growth from the initiation site, due to continuing fatigue damage, must be predicted in a rational

TABLE 7.

RESULTS OF NOTCHED AND UNNOTCHED FATIGUE DATA CONSOLIDATION USING THE INVERSE HYPERBOLIC TANGENT FUNCTION WITH WEIGHTED EQUIVALENT STRAIN DATA

Material	Type of Data	Number of Data Points	Weighted R^2, percent	Regression Coefficients		Limits Employed		Data Source Reference Numbers
				A_0	A_1	ϵ_u	ϵ_e	
2024-T3 Sheet	Unnotched	121	98.9	4.644	2.914	0.0152	0.0018	1, 7
	Notched	887	96.8	4.867	3.417	0.0150	0.0021	2 through 9
2024-T4 Bar and Rod	Unnotched	62	97.8	4.170	2.705	0.0150	0.0020	13, 82
	Notched	114	94.9	4.635	2.892	0.0150	0.0020	82
7075-T6 Sheet	Unnotched	220	97.3	4.899	2.809	0.0150	0.0016	1, 7, 10
	Notched	695	96.3	4.969	3.313	0.0170	0.0020	2 through 10
7075-T6 Clad Sheet	Unnotched	369	99.6	4.408	1.760	0.0160	0.0015	91
7075-T6, -T651 Bar	Unnotched	137	87.3	4.587	2.658	0.0160	0.0015	82, 87
	Notched	471	93.4	4.818	2.618	0.0160	0.0015	82, 87
300M Billet and Forging	Unnotched	289	90.4	4.796	2.565	0.0154	0.0026	11,12,14,88,89
	Notched	218	89.2	5.259	3.073	0.0161	0.0023	11, 12, 14
Annealed Ti-6Al-4V Sheet[a]	Unnotched	76	81.9	6.033	6.402	0.0160	0.0020	75, 81
Bar and Extrusion (125 ksi TYS)[b]		60	68.1	5.756	3.218	0.0160	0.0020	69, 70, 86
Bar, Extrusion, and Forging (140 ksi TYS)[a]		367	73.3	5.415	3.577	0.0160	0.0020	12,73,76,79,86
Casting[c]		50	76.6	5.033	1.044	0.0160	0.0020	71
Annealed Ti-6Al-4V Sheet[b]	Notched	28	43.3	6.625	2.789	0.0160	0.0020	75
Bar and Extrusion (125 ksi TYS)[b]		53	80.8	7.149	4.140	0.0160	0.0020	69, 70
Bar, Extrusion, and Forging (140 ksi TYS)[a]		171	73.2	6.164	3.591	0.0160	0.0020	12, 73, 76, 79
Casting[c]		78	86.1	5.862	3.354	0.0160	0.0020	71, 72, 80
STA Ti-6Al-4V Sheet[d]	Unnotched	98	95.1	4.565	1.967	0.0160	0.0020	84
Forging, Casting, and Plate[d]		50	79.0	5.897	4.100	0.0160	0.0020	78, 79
STA Ti-6Al-4V Sheet[d]	Notched	96	85.0	6.905	3.909	0.0170	0.0020	84
Casting and Plate[d]		28	88.6	5.848	2.177	0.0160	0.0020	78, 80

[a] Monotonic and cyclic stress-strain calculations were based on data from Ti-6Al-4V Hot Rolled Bar (see tables 1 and 6).

[b] Monotonic and cyclic stress-strain calculations were based on data from Ti-6Al-4V Plate (see tables 1 and 6).

[c] Monotonic and cyclic stress-strain calculations were based on data from Ti-6Al-4V Cylindrical Forging (see tables 1 and 6).

[d] Monotonic and cyclic stress-strain calculations were based on data from Ti-6Al-4V Bar (see tables 1 and 6).

manner. Since an accurate physical model of crack-tip damage accumulation does not exist, a fatigue-crack-propagation model that accurately characterizes the mechanical behavior of the material is generally used. Then the model, which summarizes or characterizes experimental results, must be inverted to yield predictions of structure life under given loading conditions.

This section of the report describes the formulation of a phenomenological, fatigue-crack-propagation model. The initial subsection on mechanical behavior, which describes the basic characteristics of the crack-growth process, is followed by a discussion of the problem of modelling this process. This latter subsection is broken down into descriptions of formulating the dependent variable, independent variable, and analytical model. Methods of evaluating crack-growth rate as the dependent variable are discussed in detail. The independent variable portion explains various functions used to account for the effects of stress ratio. Based on the results of the above work, various analytical models, including a nonlinear analytical expression, are examined in Formulation of an Analytical Model. The final subsection details the application of the analytical model to five sets of data.

Observed Mechanical Behavior

Studies have been conducted in numerous laboratories to obtain fatigue-crack-propagation data for various materials. Extensive tests have been performed by various investigators utilizing center-cracked, compact-tension, and surface-flaw specimens. Data have been generated on high-strength steel, aluminum, and titanium alloys under both constant- and variable-amplitude loading conditions. The present investigation, however, is concerned only with constant-amplitude results. Fatigue-crack-propagation data, recorded in the form of crack-length measurements and cycle counts (a_i, N_i) are not directly useful for design purposes since a variety of stress levels, stress ratios, initial crack conditions, and environmental conditions are encountered. To make use of these data, a fatigue-crack-propagation model must account for the effects of these parameters on crack growth and, hence, on specimen life.

In general, the relationship between crack size and number of applied cycles can be represented as a crack-growth curve drawn through the raw data points as shown in figure 16. The resulting monotonic curve is described in terms of two intervals connected by a transition region.

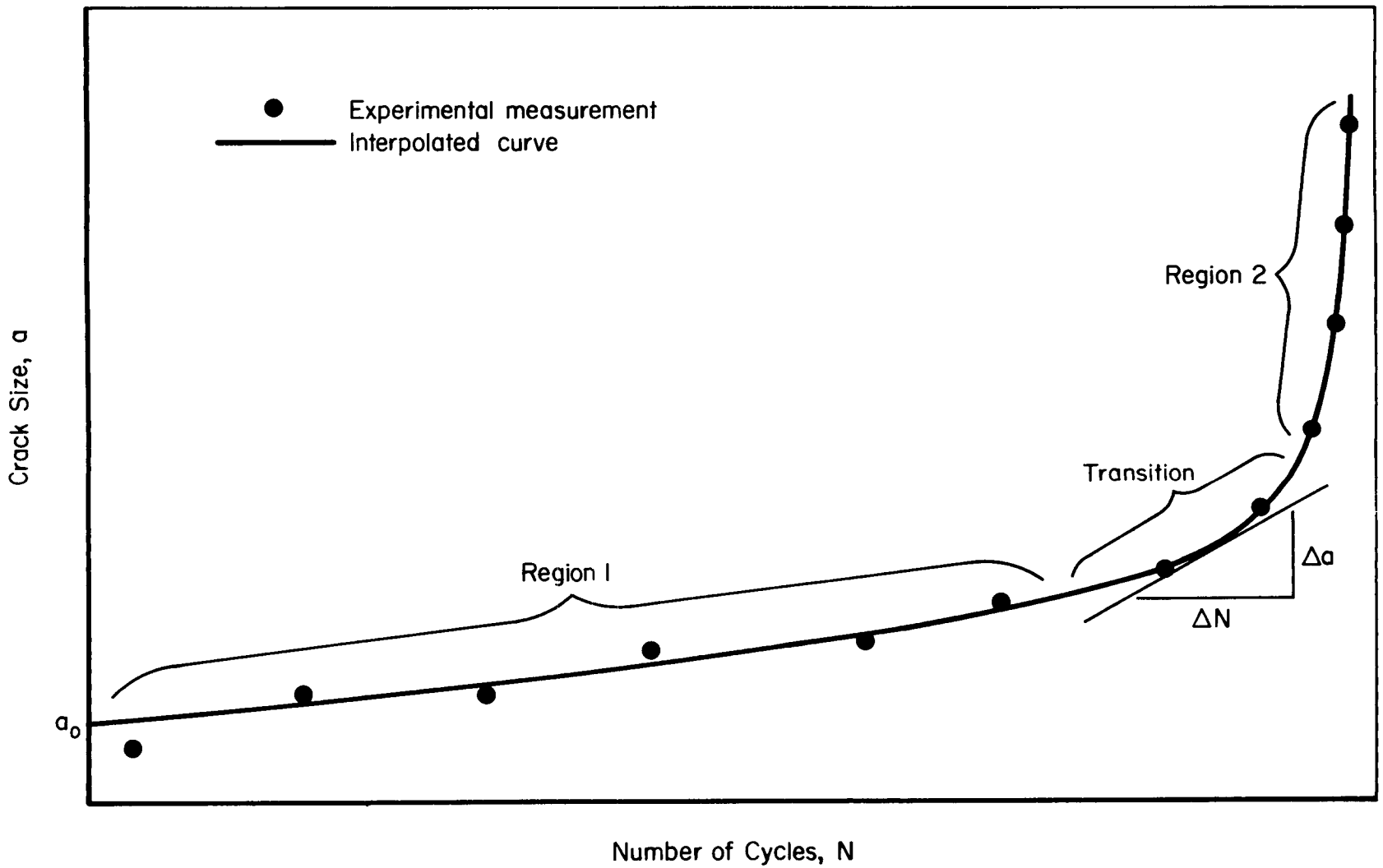

Figure 16. – Schematic example of typical crack-growth curve.

(1) A region (Region 1) of slow growth over a wide range of cycles where the slope is relatively small

(2) A region (Region 2) of exceedingly rapid growth until failure or test termination.

Families of curves for a given material are generated when the maximum stress, stress ratio, or environmental conditions are varied.

Historically, it has been found convenient to model this crack-damage behavior as a rate process and to formulate a dependent variable based on the slope of the growth curve. The instantaneous rate of change of crack length, or an approximation to it,

$$Y = \frac{da}{dN} \simeq \frac{\Delta a}{\Delta N} \quad , \tag{43}$$

was chosen as the dependent variable for the formulation of a fatigue-crack-propagation model. The independent variable for the process was selected to account for the more basic mechanical variables of cyclic stress, stress ratio, and crack size.

An appeal to the theory of linear elasticity has suggested that the damage severity at the crack tip might be represented by a stress-intensity factor which, in general form, may be written as

$$K = S\sqrt{a}\, g(a,w) \quad , \tag{44}$$

where g(a,w) is a geometric scaling function dependent on crack and specimen geometry. As a result, the independent variable is usually considered as some function of K and stress ratio, or as originally suggested by Paris et al (ref. 25), some function of

$$\Delta K = (1-R)K \quad . \tag{45}$$

If the slope of the crack-growth curve is calculated at the various data points, and if the stress-intensity factor is calculated at these same points, then the locus of points $\left(\frac{da}{dN}, K\right)_i$ can be plotted. These variables are generally plotted on log-log scales to obtain a crack-growth-rate curve such as that shown in figure 17. Examination of this curve suggests several factors of importance that will have to be accounted for in the formulation of a crack-growth model.

In most materials, there is an upper limit to the crack severity and associated critical stress-intensity factor which a material can sustain. At this critical value, the crack will propagate unstably. For the rate diagram of da/dN versus ΔK or K_{max}, the K_c value is the terminal (or upper) limit on the abscissa as illustrated schematically in figure 17. On a K_{max} basis, the rate of crack growth becomes very large as K_{max} approaches K_c, such that the growth-rate curve

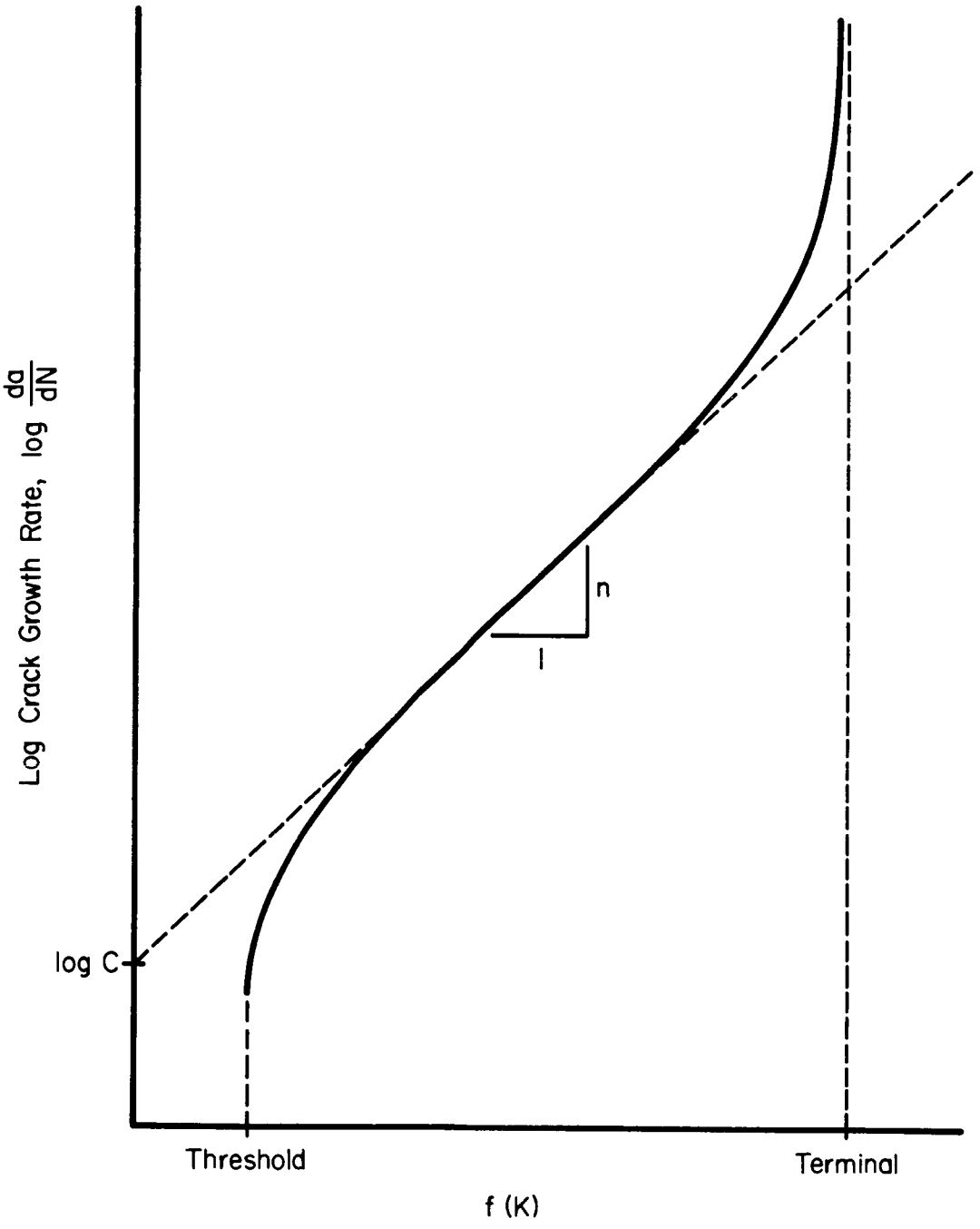

Figure 17. – Typical crack-growth-rate behavior.

becomes asymptotic to this limit. On a ΔK basis, this limit is $(1-R)K_c$. At the other extreme, a minimum crack-growth rate of zero is anticipated at a zero value of ΔK or K_{max} value. However, this assumption appears to be conservative because of evidence that there actually exists a threshold below which there is no fatigue-crack propagation. (See fig. 17.)

The doubly logarithmic plot of da/dN versus K reveals a curve having sigmoidal shape. As an approximation, the curve might be represented by three linear segments. The first segment, beginning with crack initiation at K_o, is steeply sloped and indicates rapid rate of change of crack-growth rate. The second segment represents a longer interval of slower rate of change of crack-growth rate. The third segment also has a high slope and represents rapid, terminal crack growth near K_c. Most of the available test data lies in the second interval.

Within the general curve shape, described above, systematic variations in the data point locations are observed. When data from tests conducted at several different stress ratios are present, the plot of crack-growth rate versus stress-intensity factor will be layered into distinct bands about the locus of points having zero stress ratio. (Refer to fig. 3 on page 7.) Layering of data points also occurs as a result of variation in such parameters as test frequency, environment, and specimen grain direction. It is desirable to predict the characteristic effects of each parameter; thus, many researchers have formulated mathematical models accounting for these parametric effects. Assuming the variables K, R, and da/dN, the general form for the fatigue-crack-propagation model was established as

$$\frac{da}{dN} = f(K, R) \quad . \tag{46}$$

The following discussion describes efforts to obtain a useful functional form for f(K, R).

Structure of the Modelling Problem

The basic concepts discussed in the previous section suggest that the modelling procedure can be thought of as consisting of three distinct steps.

(1) Formulation of a dependent variable. — How can the crack-growth rates be best calculated from the discrete (a_i, N_i) data points?

(2) Formulation of an independent variable. — What combination of R and K can best be used to formulate an independent variable that will consolidate the crack-growth-rate data?

(3) Formulation of an analytical model. — What functional form containing the dependent and independent variables should be chosen to best approximate the sigmoidal character of the crack-growth-rate curve?

An approach to the solution of these three modelling problems is described in the following subsections.

Particular effort was devoted to obtaining an expression in which compensations for the effects of stress ratio were uncoupled from the factors influencing general curve shape. Such a feature permits a greater flexibility in the analysis of fatigue-crack-propagation data. Although several parameters affect the distribution of data points, stress ratio is the most significant of these. Accounting for other important parameters, such as frequency, was beyond the scope of the present work.

Formulation of a Dependent Variable. — It is necessary to obtain values for the dependent variable, the crack-growth rate, from the (a_i, N_i) data. Two basic methods of deriving the crack-growth rate have been used in the past; curve fitting and incremental-slope approximation. Curve fitting implies that an analytical expression is fitted to all of the crack-growth data by least-squares regression. Incremental-slope calculation implies the use of a divided differences scheme to find the slope at any given point along the crack-growth curve.

From the analyses conducted, it is apparent that the determination of such a derivative by means of some analytical expressions is far less desirable than the use of a local or segmental fit to the data. Since this observation has been made in all of the data sets analyzed, a formalized illustration of the inadequacies of the fitting of a single analytical expression is presented.

Of the general analytical expressions which are available for curve fitting, the most popular choice of functions with respect to numerical considerations are polynomials. To explore the application of polynomials in fitting the crack-growth curve, one must consider the characteristics of the crack-growth curve. Typically, two regions of the curve from crack initiation to specimen failure may be described as done earlier and shown in figure 16. These curve segments are connected by a transition region having a considerably smaller radius of curvature. It is observed that over the entire range of cyclic values, the curve is monotonically increasing.

Some general observations can be made about polynomials that are relevant to this situation. Consider a polynomial of degree q,

$$a(N) = A_0 + A_1N + A_2N^2 \ldots + A_qN^q \quad . \tag{47}$$

The first derivative of equation (47) is expressed by the following relation:

$$da/dN = A_1 + 2A_2N + \ldots + (q-1)A_qN^{q-1} \quad . \tag{48}$$

Equation (48) possesses q roots implying a finite number, q - 1, of extrema over the range of the function. Since the polynomial is not a strictly monotone function over its range, it is necessary to utilize the function on regions where it does display monotone behavior. The existence of extrema in a candidate curve-fitting function presents very real difficulties. Sections of the curve having negative slope due to extrema would represent the physically impossible situation of negative crack growth. Such a result is unacceptable. Furthermore, since it is generally desirable to obtain the logarithms of the crack-growth rates, log (da/dN), also will be undefined at points having negative slope.

Figure 18 represents attempts to fit second through seventh degree polynomials to a typical crack-growth curve. These particular data were obtained from a 9.6-inch-wide, centrally cracked panel of 0.29-inch-thick, mill-annealed Ti-6Al-4V plate tested at a maximum cyclic stress of 5 ksi and a stress ratio of 0.1. No terms greater than degree seven were added because of computational difficulties encountered in dealing with the coefficients. Successive addition of higher order terms improved the fit of the polynomial to the data as indicated by the sum of squares of deviation listed in table 8. Although the higher order terms improved the fit, they introduced extrema with their resulting negative slopes. Because of these extrema, the fitted functions obtained are unsatisfactory models of crack growth.

TABLE 8.

COMPARISON OF CURVE FITTING RESULTS FOR POLYNOMIALS OF DEGREE q = 2 TO q = 7

Degree of Polynomial	SSD
2	7.4038
3	3.8250
4	2.1020
5	1.2387
6	0.7809
7	0.5254

Examination of figure 18 reveals a very close fit of data in the region of high crack-growth rate for q = 6 and q = 7. In this situation, where only

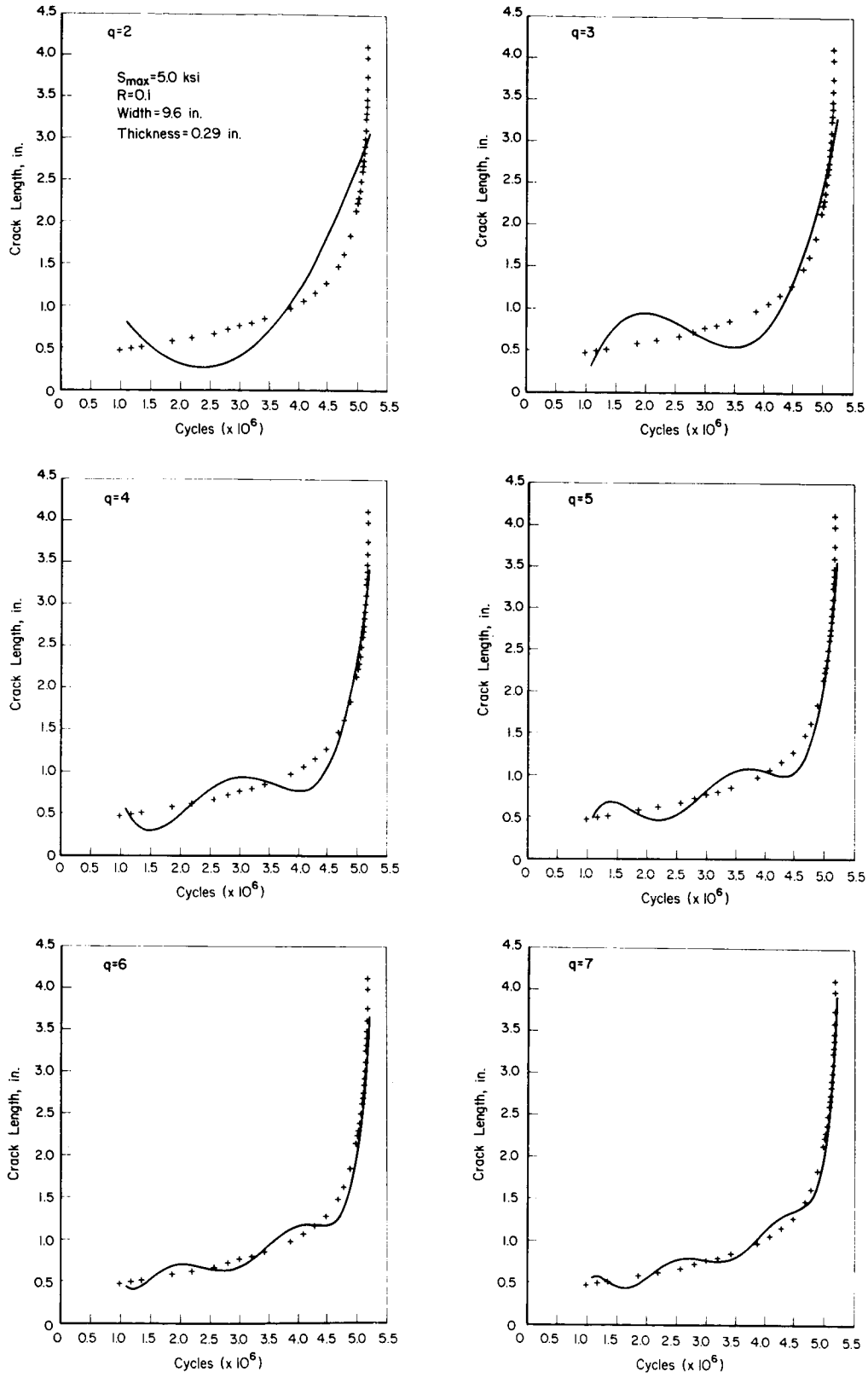

Figure 18. – Crack-growth data with best fit polynomial for Ti-6Al-4V plate.

isolated segments of the crack-growth curve are to be dealt with, the polynomials gave good results. However, this type of function seems to be unsuited to application to the whole cyclic range. Thus, either the selection of another class of candidate functions for curve fitting or an appeal to point-to-point methods of slope evaluation was necessary.

Several other curve-fitting functions were examined. Among these was an exponential series,

$$a(N) = \sum_{i=o}^{q} A_i e^{iN} \quad . \tag{49}$$

Cases of q = 1 and q = 3 were tried, but no improvement was found.

The point-to-point method of slope evaluation involved use of the various divided difference schemes. The first divided difference was merely the slope between two adjacent points; thus

$$DD_{1(i)} = \frac{\Delta a}{\Delta N} = \frac{a_{i+1} - a_i}{N_{i+1} - N_i} \quad . \tag{50}$$

Since the crack growth achieved between two data points was usually small, observational errors, measurement errors, and subtle material variations influenced the rate evaluation. With this technique, each rate or slope determination was defined entirely by the local conditions. An averaging of these variations was achieved by using higher order divided-difference schemes. In the next level of refinement, the three-point divided-difference technique, a selection of successive subsets of three data points was used to specify the derivative at the central point. By using Newton's interpolation formula to define a second-degree polynomial through the three data points, we may express the derivatives at the intermediate point i as

$$da/dN\Big|_i = f[N_{i-1}, N_i] + (N_i - N_{i-1}) \frac{f[N_i, N_{i+1}] - f[N_{i-1}, N_i]}{N_{i+1} - N_{i-1}} \quad , \tag{51}$$

where

$$f[N_{i-1}, N_i] = \frac{a_i - a_{i-1}}{N_i - N_{i-1}}$$

and

$$f[N_i, N_{i+1}] = \frac{a_i+1 - a_i}{N_{i+1} - N_i}$$

are the first divided differences. From a physical perspective, this can also be viewed as a slope-averaging technique since the first divided differences are

merely the slopes between data points. The mechanics of selecting subsets of data are shown in figure 19a. Figure 19b presents an array of divided differences in which the progression to higher order approximation can be seen.

A comparison of regression results for 2-, 3-, and 5-point subsets showed the superiority of the five-point divided-difference method in evaluating fatigue-crack-growth rates. Some researchers have utilized a seven-point divided-difference technique. Even though this method may result in a slightly better evaluation of crack-growth rates, it is questionable as to whether the magnitude of improvement would justify the added computational complexity. Use of a divided-difference technique implied that a certain number of data points had to both proceed and follow the data point at which the slope was being evaluated. Consequently, q - 1 data points had to be discarded when a qth order divided difference was used. In data sets where a small number of readings was taken, this feature often caused rejection of the entire set.

Most of the analyses performed in this study, involved use of the five-point divided-difference method.

Formulation of the Independent Variable. — It was previously suggested that the independent variable be some function of K and R. As a general form for the independent variable, assume

$$K_{eff}\ (K,\ R) = U(R)K_{max} \quad , \tag{52}$$

where U(R) is a functional relation that accounts for the effect of stress ratio.

A number of different forms for U(R) have been proposed. The simplest of these is U(R) = 1.0. In this way, it is asserted that no stress ratio effects are present; then,

$$K_{eff} = K_{max} \quad . \tag{53}$$

This relation is appropriate if no variation in stress ratio is contained in the data, or if the material is insensitive to changes in stress ratio.

The stress-intensity range also may be used as an independent variable. Letting U(R) = (1-R), the expression

$$K_{eff} = (1\text{-}R)K_{max} = \Delta K \tag{54}$$

results. This relation has been widely used in the past.

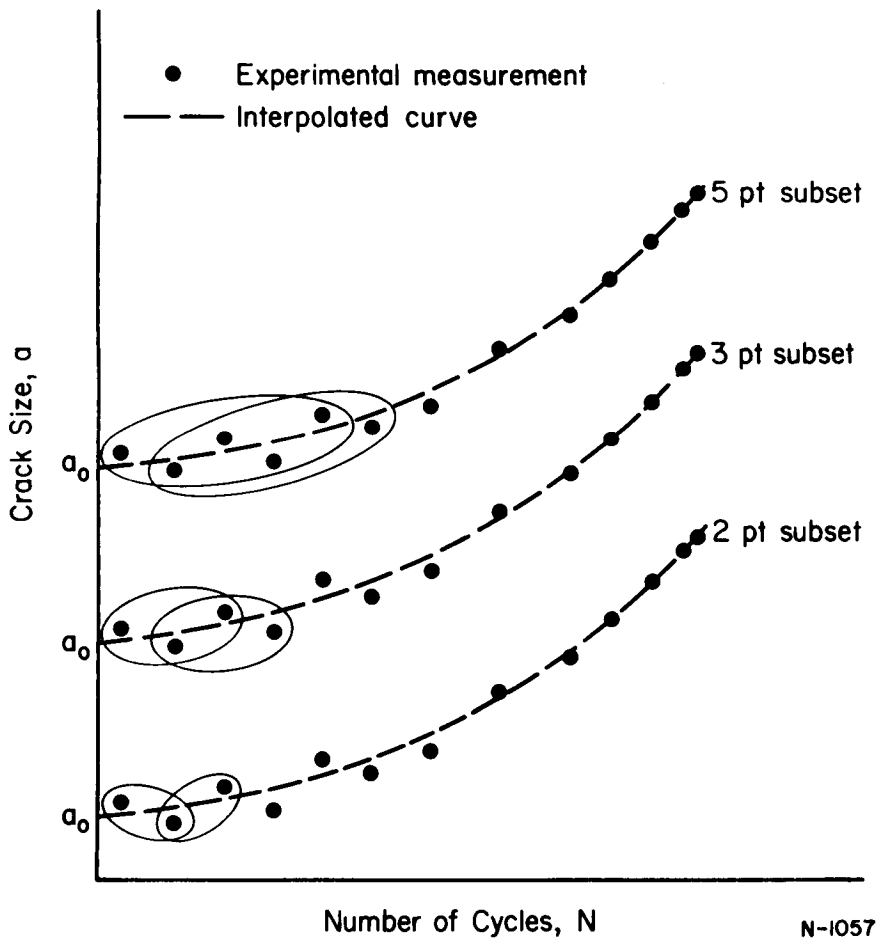

a. Sequential grouping of data subsets.

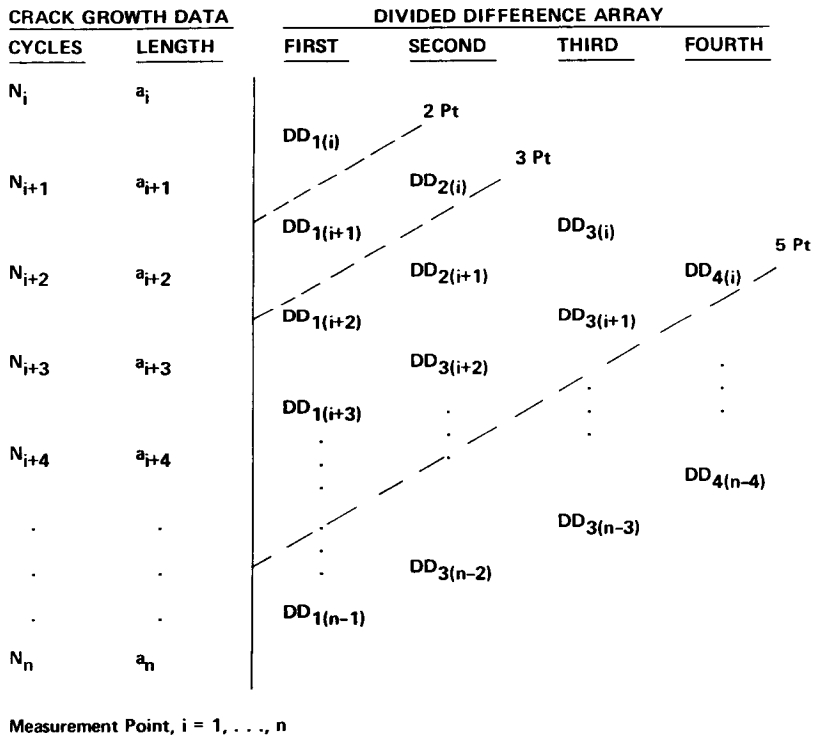

b. Divided difference array of basic crack growth data.

Figure 19. – Schematic illustration of point-to-point method of determining the slope of crack-growth curves.

Walker (ref. 4) proposed that the independent variable should represent a combination of maximum stress intensity and stress-intensity range. Letting $U(R) = (1-R)^m$, K_{eff} has the form

$$K_{eff} = (1-R)^m K_{max} \quad . \tag{55}$$

Mukherjee and Burns (ref. 26), and Roberts and Erdogan (ref. 27) have proposed similar relations in their respective studies.

More recently, Elber (ref. 28) proposed a fatigue-crack-propagation model that is based on crack-closure concepts. Elber observed that a crack in a center-cracked panel tended to close before the tensile load was removed. As a result, he defined a crack-closure stress below which the crack would be totally closed. A general form for the crack-propagation independent variable, based on these considerations, may be obtained. Elber proposed that $U(R) = (1-R)(1+MR)$, so that

$$K_{eff} = K_{max}(1-R)(1+MR) \quad , \tag{56}$$

where M is determined by optimization or by an experimental procedure.

The four candidates for U(R) may be compared graphically. Since U(R) represents a shifting factor accounting for the effect of stress ratio, it is reasonable to plot U(R) versus R for the four candidate functions (fig. 20).

Nominal coefficient values have been chosen in both the Walker and Elber relations to represent application to 7075-T6 aluminum alloy data. When $U(R) = 1.0$, no shifting for stress ratio occurs. If $U(R) = (1-R)$, then a linearly varying shifting factor from $U(R) = 2.0$ to $U(R) = 0$ is generated. Setting $U(R) = (1-R)^m$ produces much greater variation in U(R) for positive stress ratio than for negative stress ratios. A similar observation is made when $U(R) = (1+MR)(1-R)$.

The selection of a form for the independent variable should be based on physical insights as well as on statistical performance. Although physical arguments are not completely formulated at this time, some general considerations are possible. Since it has been observed that most materials exhibit stress-ratio dependent behavior, it is reasonable to assume that the choice of $U(R) = 1.0$ would seldom be satisfactory. It is also not reasonable to assume that $U(R) = (1-R)$, i.e., that the behavior is governed only by the stress-intensity range. The Walker formulation, which is a combination of these two effects, is a more physically justifiable selection. Taking a rather different approach, Elber based his expression directly on the observed physical behavior

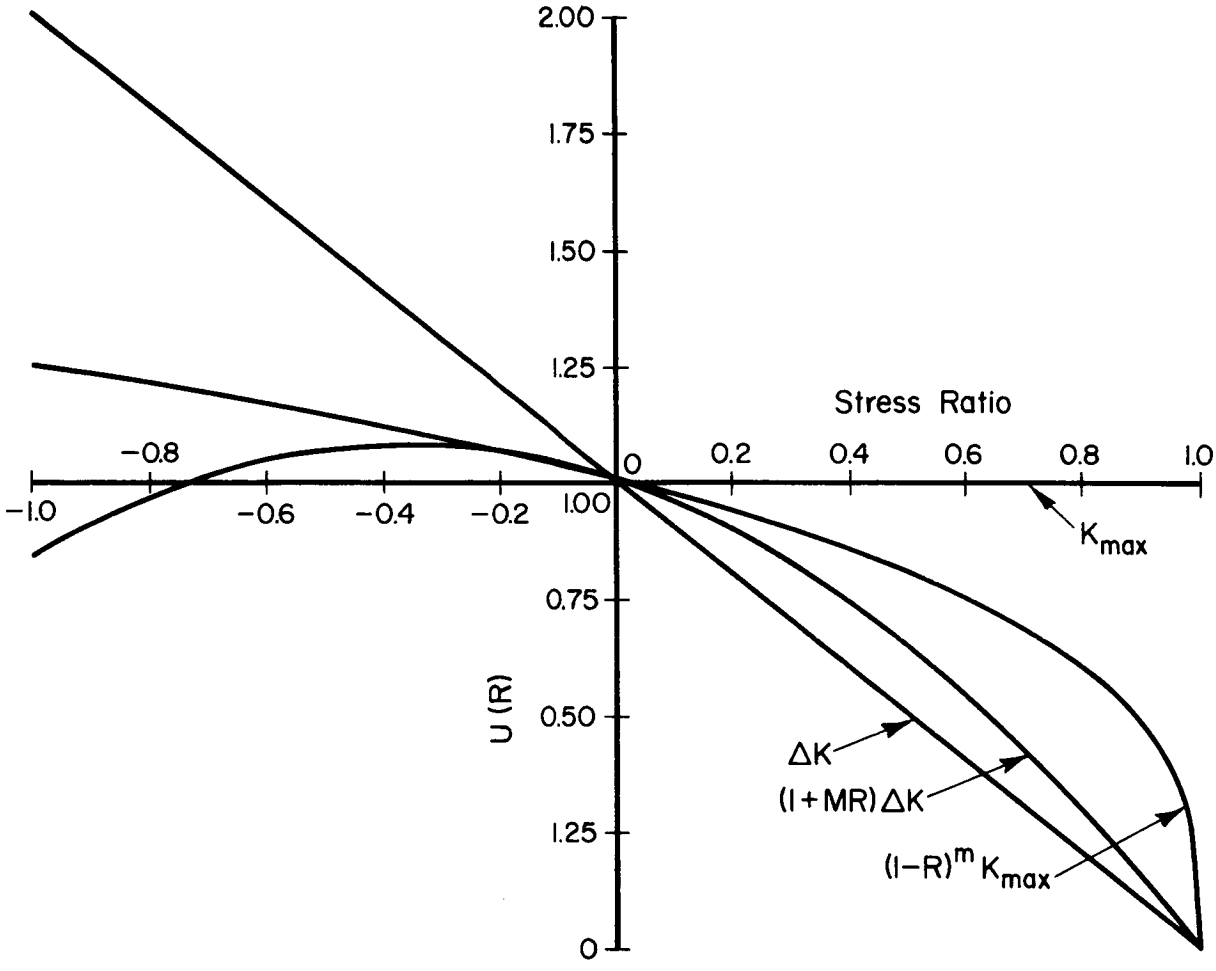

Figure 20. — Comparison of four candidate effective stress-intensity functions.

of crack closure. Table 9 contains a statistical comparison of the formulations. A three-point divided-difference scheme was used to evaluate the crack-growth rates. The four independent variable forms were used in a linear fatigue-crack-growth model. It was found on the basis of R^2, that the Walker expression, followed by the Elber expression, provided the best consolidation of data. The Walker formulation was chosen for use as an independent variable in the fatigue-crack-propagation model.

TABLE 9

COMPARISON OF INDEPENDENT VARIABLE FORMULATIONS FOR REGRESSION ANALYSIS OF DATA ON 2024-T3 ALUMINUM ALLOY

Formulation	SSD	R^2
$K_{eff} = K_{max}$	257.40	0.793
$= (1-R)\ K_{max}$	205.99	0.769
$= (1-R)^m\ K_{max}$	104.29	0.915
$= (1-R)(1+MR)\ K_{max}$	186.80	0.890

Since the Walker formulation of the independent variable was chosen for use in the following analyses, it is of interest to examine the nature of the coefficient m. Investigation of crack-growth-rate curves indicate the formation of bands of data with respect to stress ratio as indicated in figure 3 on page 7. From a graphical point of view, the coefficient m, which affects the coupling between K_{max} and ΔK, caused a shift of the data bands, i.e., a collapse of data towards the mean curve. In the case of a set of data having both positive and negative stress ratios, the points collapsed toward the R = 0 data since these data are not affected by coupling through m. When the subset consisted of two positive stress ratios, the coefficient m was selected to produce the best collapse of the two stress ratios towards a central line between them.

The value of the parameter m was obtained for various sets of data by minimizing the SSD value. A series of investigations was undertaken to determine the variations of m with respect to stress ratio within a set of data for a particular material. The data sets used previously (7075-T6 and 2024-T3 aluminum) were partitioned in various ways for analysis. The results are presented in table 10.

These correlations indicated that the coefficient m was highly dependent on the stress ratio distribution and the number of data points. In other words,

different m values were obtained when different subsets of data of a given material were regressed. Generally,

- The formulations $da/dN = C(K_{max})^{n'}$ and $da/dN = C(\Delta K)^{n'}$ were equally satisfactory when R = constant.
- When the subset of data consisted of specimens for which $R > 0$, m tended to be greater than 0.50.
- When the subset of data consisted of specimens for which $R < 0$, m tended to be less than 0.50.

A dependence of m on the material properties probably also exists. To uncover this relation, it would be necessary to compare test results for different materials. The comparison sets would have to consist of an identical number of data points run at the same stress ratio. Unfortunately, data meeting these requirements were not available.

TABLE 10

VARIATION OF COEFFICIENT m WITH RESPECT TO DISTRIBUTION OF STRESS RATIOS

Material	Stress Ratio	m	SSD	R^2
7075-T6[a]	-1.0 to 0.80	0.37	38.90	0.908
7075-T6	0.0 to 0.80	0.53	23.70	0.914
7075-T6	-1.0 to 0.0	0.04	4.10	0.972
7075-T6	0.0 to 0.33	0.50	7.30	0.922
7075-T6	0.50 to 0.80	0.70	12.20	0.912
7075-T6	-1.0 to -0.80	0.32	1.77	0.974
2024-T3[a]	-1.0 to 0.70	0.42	97.00	0.920
2024-T3	0.0 to 0.70	0.44	104.00	0.915

[a]Data from Hudson (data source ref. 48), and Dubensky (data source ref. 32).

Formulation of an Analytical Model. – Numerous models of the type illustrated by equation (46) have been formulated by researchers during the last decade. Excellent reviews of the literature have been presented in papers by Erdogan (ref. 29), Hoskin (ref. 30), and Coffin (ref. 31). Several fatigue-crack-propagation laws that have been widely used are described below. All of these are empirical equations relying upon regression analysis to calculate empirical coefficients. These relations can be quite logically divided into classes of linear and nonlinear functions.

Linear models, of necessity, neglect initial and terminal behavior. The general form for the linear model is

$$\frac{da}{dN} = C(K_{eff})^{n'} \quad . \tag{57}$$

Best known of these models is the linear law of Paris (ref. 32),

$$\frac{da}{dN} = C[(1-R)K]^{n'} = C(\Delta K)^{n'} \quad . \tag{58}$$

This equation is commonly fitted to the data in log-log form to yield the Paris regression coefficients C and n'. The Paris model is a linear approximation to the rate curve that incorporates a term to account for the effect of stress ratio. Although the law generally fits only the central segment of the data accurately, it has been used extensively in the literature.

Other linear models are possible, and several have been proposed. These relations, which must be considered elaborations on the Paris model, are due to Elber (ref. 28), Walker (ref. 4), and Roberts and Erdogan (ref. 27). The primary differences in these expressions lie in the choice of the independent variable as discussed in the previous section.

Modifications of the linear Paris model have been made to create a nonlinearity at the terminal end of the curve. To approximate the sigmoidal character of the rate curve, and to better account for the effects of stress ratio, Forman (ref. 33) proposed the relation,

$$\frac{da}{dN} = \frac{C[(1-R)K]^{n'}}{(1-R)(K_c-K)} \quad . \tag{59}$$

Forman's equation contains a singular term in the denominator to model the terminal region of crack growth. As K approaches the critical stress intensity, the denominator goes to zero. Manipulation of the Forman equation leads to

$$\frac{da}{dN} = \frac{(1-R)^{n'}}{(1-R)}\left[\frac{C\,K^{n'}}{(K_c-K)}\right] = \left(\frac{C(1-R)^{n'-1}K^{n'}}{K_c-K}\right) \quad . \tag{60}$$

The term, $(1-R)^{n'-1}$, is clearly similar to the Walker formulation for the independent variable and as such helps to account for the effect of stress ratio. Forman's equation has no provision for modelling the interval of crack initiation and, hence, generates only half of the sigmoidal curve. Variations on the form of the singularity are possible.

A computer program was written to evaluate various fatigue-crack-propagation laws. This program computed K values and calculated crack-growth rates by three-point divided differences. The models were fitted to these results by

linear regression. Sets of data for 7075-T6 and 2024-T3 aluminum alloys and Ti-6Al-4V titanium alloy were used for comparison purposes. Results of these regression analyses, in terms of R^2 values, are compared in table 11.

Variations on the form of the singularity in the Forman equation proved to be ineffective. The linear model with the Walker formulation for the independent variable and the Forman model showed the most promising results.

The other approach to the modelling of the crack-propagation process is to assume a nonlinear function. Recently, Collipriest (ref. 34) suggested a fatigue-crack-propagation law to model the entire rate curve. This nonlinear equation is based on the inverse hyperbolic-tangent function. The model may be written as

$$\frac{da}{dN} = \exp\left[n \cdot \frac{\ln K_c - \ln \Delta K_o}{2} \cdot \operatorname{arc\,tanh} \left\{ \frac{\ln \Delta K - \frac{\ln K_c(1-R) + \ln \Delta K}{2}}{\frac{\ln K_c(1-R) - \ln \Delta K_o}{2}} \right\} + \ln \left\{ C \cdot \exp\left(\frac{\ln K_c - \ln \Delta K_o}{2} \cdot n \right) \right\} \right] . \tag{61}$$

In Collipriest's equation, the independent variable takes the form of $K_{eff} = \Delta K$. This nonlinear approach was investigated further because it seemed to provide a realistic method for analysis of fatigue-crack-propagation data. Rather than utilizing Collipriest's equation, it was decided to derive a fatigue-crack-propagation model that would allow the implementation of the most effective of the independent variable formulations described earlier. The goal of this derivation was also to obtain a more compact analytical form for the fatigue-crack-propagation model.

The model was based on the inverse hyperbolic tangent suggested by Collipriest. The shape of the inverse hyperbolic-tangent function is shown in figure 21. The functional form assumed was

$$\log \frac{da}{dN} = C_1 + C_2 \tanh^{-1}\left[\Phi(K_{eff}) \right] . \tag{62}$$

The coefficients, C_1 and C_2, were to be determined by least squares regression. Examination of the $\tanh^{-1}$ curve suggested the proper form for $\Phi(K_{eff})$. The function, $\Phi(K_{eff})$, was chosen to scale values of the effective stress-intensity factor into values of the argument, thus positioning the $\tanh^{-1}$ curve relative to the rate curve. Figure 21 shows that the $\tanh^{-1}$ function goes to infinity at the values of $\Phi = -1$ and $\Phi = +1$. The initial and final conditions of the

TABLE 11

COMPARISON OF FATIGUE-CRACK PROPAGATION MODELS

	Material	m	log C	n′	L	SSD	R^2
Paris $da/dN = C(\Delta K)^{n'}$	Ti-6Al-4V		-8.830	3.223		55.16	0.949
	2024-T3		-9.298	3.937		285.99	0.769
	7075-T6		-6.770	2.214		168.80	0.600
Coupled $da/dN = C[(1-R)^m K_{max}]^{n'}$	Ti-6Al-4V	0.66	-9.670	3.600		18.29	0.983
	2024-T3	0.42	-10.280	4.470		104.29	0.915
	7075-T6	0.37	-9.310	3.890		38.90	0.908
Forman $da/dN = \frac{C(\Delta K)^{n'}}{[(1-R)(K_c-K_{max})]}$	Ti-6Al-4V		-6.970	3.340		20.30	0.981
	2024-T3		-7.130	3.650		112.71	0.881
	7075-T6		-6.000	2.700		48.09	0.887
Forman (Modification #1) $da/dN = \frac{C[(1-R)^m K_{max}]^{n'}}{[(1-R)^m(K_c-K_{max})]^L}$	Ti-6Al-4V	0.66	-9.638	3.600	-0.012	18.64	0.984
	2024-T3	0.68	-7.621	3.870	-0.959	94.50	0.924
	7075-T6	0.61	-7.090	3.290	-0.869	36.30	0.914
Forman (Modification #2) $da/dN = \frac{C(\Delta K)^{n'}}{[(1-R)(K_c-K_{max})]^L}$	Ti-6Al-4V		--	--	--	--	--
	2024-T3		-6.510	3.690	-1.390	100.50	0.918
	7075-T3		-5.830	2.940	-1.140	41.10	0.903
Forman (Modification #3) $\frac{C[(1-R)^m K_{max}]^{n'}}{(1-\frac{K_{max}}{K_c})}$	Ti-6Al-4V	0.72	-9.330	3.370		20.20	0.979
	2024-T3	0.54	-9.560	3.860		93.50	0.899
	7075-T6	0.46	-8.600	3.210		36.40	0.883
Elber $da/dN = C[(0.5+0.4R)(1-R)K_{max}]^{n'}$	2024-T3		-8.500	4.150		186.80	0.890

physical problem implied that the rate of change of da/dN should go to infinity at both the terminal and threshold values of K. Clearly, the regions of rapid rate of change of da/dN should correspond to arguments in the neighborhood of $\pm$ 1. To establish this correspondence, a function was assumed to scale the K_{eff} values into the interval Φ = -1 to Φ = +1.

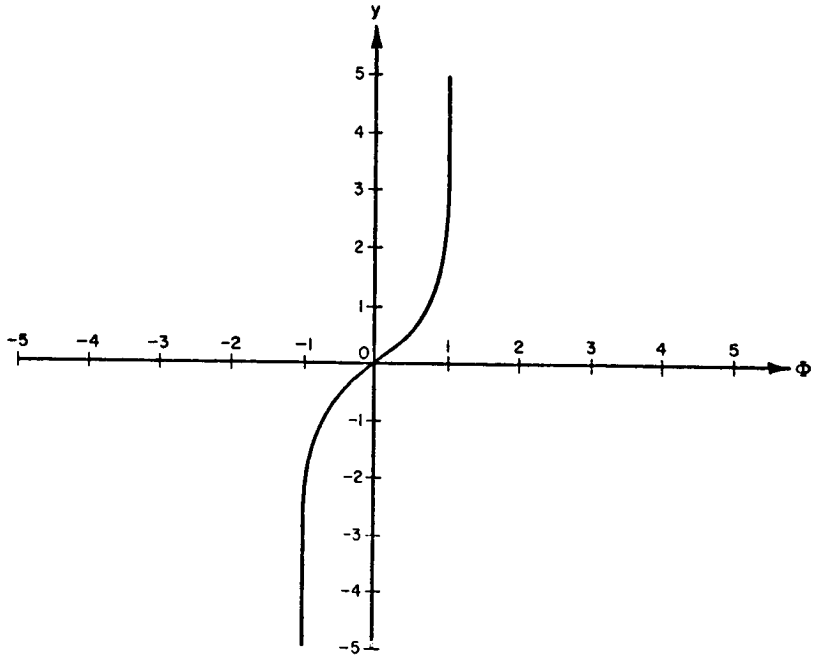

Figure 21. — Inverse hyperbolic tangent function.

The physical initial and final conditions were assigned to the points (log K_o, -1) and (log K_c, +1) on the Φ - log K plane as illustrated in figure 22.

Assuming a linear scaling function,

$$\Phi = M' \log K + \Phi_I \quad , \tag{63}$$

the slope and the intercept were determined by applying the conditions

$$\Phi = 1 \text{ when } K = \log K_c$$

$$\Phi = -1 \text{ when } K = \log K_o \quad . \tag{64}$$

These conditions yielded a system of simultaneous, linear, algebraic equations,

$$1 = M'(\log K_c) + \Phi_I$$

$$-1 = M'(\log K_o) + \Phi_I \quad . \tag{65}$$

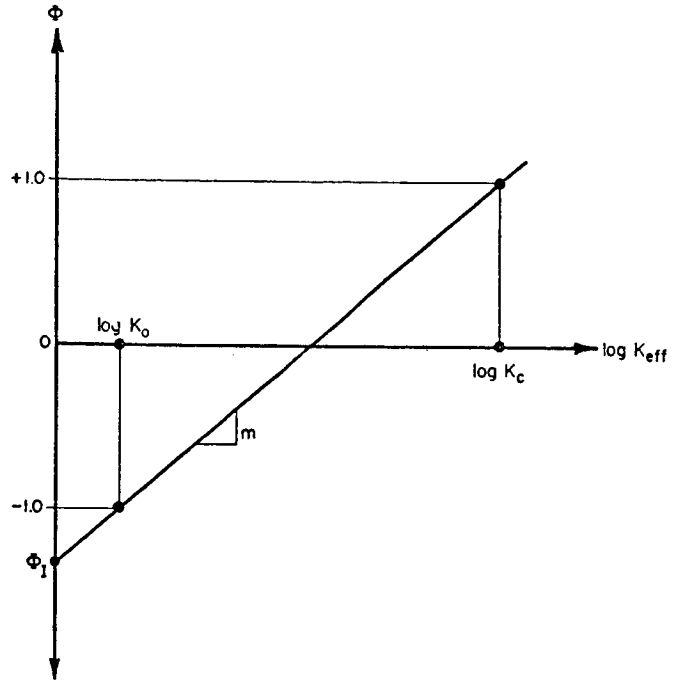

Figure 22. — Plot of $\Phi(K_{eff})$.

The slope and intercept were found by substitution to be

$$\Phi_I = \frac{\log K_c K_o}{\log K_o/K_c} \text{ and } M' = \frac{-2}{\log K_o/K_c} \quad .$$

Thus, it followed that

$$\Phi(K_{eff}) = \frac{-2 \log K_{eff}}{\log K_o/K_c} + \frac{\log K_c K_o}{\log K_o/K_c} = \frac{\log(K_c K_o/K_{eff}^2)}{\log (K_o/K_c)} \quad , \qquad (66)$$

and the basic form of the fatigue-crack-propagation model became

$$\log \frac{da}{dN} = C_1 + C_2 \tanh^{-1} \left(\frac{\log(K_c K_o/K_{eff}^2)}{\log(K_o/K_c)} \right) \quad . \qquad (67)$$

Completion of the fatigue-crack-propagation model required that a form for K_{eff} be chosen. Based on the previous comparison of the four possible candidates, the Walker formulation for K_{eff} was chosen. Thus, the complete fatigue-crack-propagation model was

$$\log \frac{da}{dN} = C_1 + C_2 \tanh^{-1} \left[\frac{\log [K_c K_o / (K_{max}(1-R)^m)^2]}{\log (K_o/K_c)} \right] \quad . \qquad (68)$$

It should be noted that when data containing only one stress ratio are regressed, the K_{max} formulation provided equally satisfactory results. In this case, the model was

$$\log \frac{da}{dN} = C_1 + C_2 \tanh^{-1} \left[\frac{\log [K_c K_o / K_{max}^2]}{\log [K_o K_c]} \right] . \qquad (69)$$

Analyses of Data: Application of the Inverse Hyperbolic Tangent Model

A fatigue-crack-propagation model that successfully accounted for the effects of stress ratio made possible the combination of sets of data from different sources. This was particularly desirable since the ultimate goal of the modelling effort was the characterization of the crack-propagation behavior of specific materials. Accordingly, it was necessary to obtain data over as wide a range of stress-intensity factors as was available. This collection effort included not only data from different specimen types but also from different heats of material. Data from various sources were combined on the basis of visual inspection although statistical techniques for combining data sets were available. Statistical methods (standard deviation and tolerance limits) were applied to regression equations for the combined data sets to complete the material characterization.

A computer program was developed to apply equation (68) to large sets of fatigue-crack-propagation data. Starting with encoded (a_i, N_i) data, this program fitted the inverse hyperbolic-tangent model to $\left[K_i, \frac{da}{dN} \Big|_i \right]$ values in the following steps:

(1) Crack-propagation rates were evaluated by a five-point divided-difference scheme.

(2) Maximum stress-intensity-factor values were calculated using the appropriate formula for the given specimen type.

(3) Values of the argument $\Phi(K_{eff})$ were calculated from the K_{max} results.

(4) Equation (67) was fitted to the $(\Phi(K_{eff}), \frac{da}{dN} \Big|_i)$ values by least squares regression. The coefficient m was optimized by minimizing the SSD value through iterative regression.

(5) Statistical parameters, including SSD, R^2, and S, were generated. Tolerance limits were computed from equation (7).

(6) The data, regression mean curve, and 90 and 99 percent tolerance-limit curves were plotted.

Analysis of the data necessitated that a selection be made for the values of K_o and K_c. An excellent summary of threshold values is presented in the paper by Donahue et al (ref. 35). Data are included in this source on a large number of materials. Values of K_c can be found in such publications as the Damage Tolerant Design Handbook (ref. 36). These two sources yielded average values for the K_o and K_c limits on the crack-growth rate curve. The data sets analyzed also contained upper and lower bounds on K_{max}.

Nominal values for K_o were selected from the paper by Donahue et al (ref. 35). Nominal values for K_c were established by inspection of the K_{max} values for the data sets. Data on five materials were analyzed: 7075-T6, 7075-T7351, and 2024-T3 aluminum; 300M steel; and Ti-6Al-4V alloy. The composition of these five data sets are listed below.

7075-T6 Aluminum Alloy. — Data on center-cracked bare and clad specimens were compiled from reports authored by Hudson (data source ref. 48), Hudson and Hardrath (data source ref. 92), McEvily and Illg (data source ref. 93), Broek (data source ref. 118), and Dubensky (data source ref. 32).

7075-T7351 Aluminum Alloy. — Data for center-cracked bare specimens including wide panels were obtained from unpublished BCL work and from Feddersen (data source ref. 41).

2024-T3 Aluminum Alloy. — A large amount of data on center-cracked bare and clad specimens was taken from reports published by Broek (data source refs. 118 and 119), Hudson and Hardrath (data source ref. 92), McEvily and Illg (data source ref. 93), Schijve et al (data source refs. 68, 120, and 121), Dubensky (data source ref. 32), and Carter (data source ref. 128).

Ti-6Al-4V Alloy. — Data on both center-cracked and compact-tension specimens were extracted from reports by Feddersen (data source ref. 125) and Bucci et al (data source ref. 115).

300M Steel Alloy. — Data on center-cracked specimens tested in humid air and saltwater spray environments, which covered a limited range of stress-intensity factors, comes from a report by Pendleberry et al (data source ref. 15).

Detailed results of the regression analyais performed on the five materials are presented in Appendix F and summarized in table 12. Number of data points, regression and optimization coefficients, K_o and K_c values, and statistical parameters are presented. Appendix figures F1 through F10 show the consolidated fatigue-crack-propagation data, the fitted curve and tolerance limits, and the plotted residuals.

TABLE 12

RESULTS OF REGRESSION ANALYSIS, COEFFICIENTS FOR EQUATIONS (68) AND (7)

Material	n, Number of Data Points	C_1	C_2	m	K_{O_3} $MN/m^{3/2}$ (ksi-in.$^{1/2}$)	K_{C_3} $MN/m^{3/2}$ (ksi-in.$^{1/2}$)	R^2	SSD	σ	$\bar{X}$	$\Sigma(X-\bar{X})^2$
2024-T3	3,407	-4.490	3.465	0.420	2.20 (2.00)	142.74 (130.00)	0.923	221.6	0.255	0.105	182.07
7075-T6	746	-4.207	2.241	0.320	3.29 (3.00)	85.64 (78.00)	0.912	47.28	0.252	0.178	79.34
7075-T7351	1,082	-4.043	2.574	0.350	4.36 (4.00)	109.90 (100.00)	0.952	33.81	0.177	0.221	79.38
300M	513	-5.186	1.296	0.335	8.78 (8.00)	65.88 (60.00)	0.661	28.56	0.236	0.00024	27.21
Ti-6Al-4V	782	-4.046	2.825	0.580	4.39 (4.00)	274.50 (250.00)	0.982	36.14	0.215	-0.161	161.20

Good characterizations of the data were obtained in most cases. Particularly satisfactory results were achieved for the titanium alloy (fig. F9). The sigmoidal character of this crack-growth-rate curve is clearly displayed. Rather poor results were obtained for the 300M steel (fig. F7). These data included only a limited range of stress-intensity factors and contained a large amount of scatter. This scatter probably represents the inherent behavior of the material because similar observations were made earlier for fatigue data on 300M steel.

A final comparison between three methods of fatigue-crack-propagation analysis was made. The five data sets were regressed in three different ways; with the inverse hyperbolic-tangent model, with the Paris model [eq. (58)], and with the Forman model [eq. (59)]. The results of the comparison are presented in table 13. From this table it is observed that the inverse hyperbolic-tangent model provided significant improvement in representation of the data, compared with the other two methods.

TABLE 13

COMPARISON OF FATIGUE-CRACK-PROPAGATION MODELS WITH COMPLETE DATA SETS

	Values of R^2		
Material	$\log\frac{da}{dN} = C + N \log K(1-R)$	$C + N \log\left(\frac{(1-R)K}{(1-R)(K_o-K)}\right)$	$C_1 + C_2 \tanh^{-1} \Phi$
7075-T6	0.669	0.875	0.912
2024-T3	0.829	0.877	0.923
Ti-6Al-4V	0.939	0.970	0.982
300M	0.415	0.585	0.661
7075-T7351	0.880	0.926	0.952

FRACTURE ANALYSIS

The accumulation of damage in a structural material terminates at fracture instability. In a chronological sense, this event concludes a chain of crack-damage processes such as have been portrayed in the previous sections. Fracture toughness and residual strength provide the quantitative characterizations of

fracture instability which are necessary to determine both the load carrying capacity of the material at a given stage of crack damage and the life remaining for subcritical damage processes.

Fracture Toughness and Residual Strength

Although fracture toughness and residual strength are related descriptors of fracture instability, they do imply different subtleties in the fracture event as well as different perspectives on the occurrence of crack extension prior to fracture. Generally, fracture toughness refers to a distinct material characteristic associated with abrupt fracture instability, under a rising load, after only minimal amounts of crack extension. In contrast, residual strength refers to fracture behavior which is accompanied by much larger amounts of crack extension prior to the critical instability. The former term is usually associated with relatively brittle fracture under quasi-plane-strain conditions of stress state in the material, while the latter is associated with quasi-plane-stress or transitional-stress-state behavior.

In name, the term residual strength infers that useful strength remains in the structural material even after some stable extension of the crack. As will be seen later in the discussion, residual strength is also quantified in dimensions of toughness and is frequently identified as "apparent" fracture toughness.

Factors Influencing Fracture Behavior

There are a large number of material, metallurgical, and mechanical variables which influence fracture behavior. These include alloy composition, process details (i.e., mechanical reduction and/or heat treatment) associated with a product form, the stress-state effects related to product size, and temperature.

While such an itemization of primary factors may suggest that a characterization of fracture behavior can be achieved through a simple categorization of these details, such is not the case generally. These factors are highly interdependent, and a discrete segregation of effects is frequently impossible or, at least, not economically feasible.

For example, for a given alloy composition and product form, a specific section size (and, hence, stress-state characteristic) may be associated with a particular degree of mechanical reduction, such that another section size may

have a distinctly different level of mechanical reduction. In other words, two different size product forms of common alloy composition may, in reality, be two different materials from the perspective of fracture behavior due to differing degrees of contained mechanical work. Similarly, in quench-rate sensitive materials, the degree and uniformity of heat treatment can vary dramatically with the geometric size of the product.

As a result of these considerations, it is reasonable to expect a close quantitative correlation of fracture behavior where details of alloy, process, size, and temperature are closely aligned. Where any one of these factors is allowed to vary, anomalous fracture behavior can be expected. Although the differences may be rationalized in a qualitative manner, they cannot be assessed with much quantitative satisfaction.

It appears that further insight to fracture behavior is still dependent on a continuing compilation of fracture data, until a broad enough reservoir of data is available to enlarge the analysis.

Characterization of Fracture Behavior by Stress-Intensity-Factor Concepts

The severity of the crack-tip elastic-stress field can be defined by the stress-intensity-factor concepts of linear elastic fracture mechanics. The general analytical formulation of the stress-intensity factor is

$$K = S\sqrt{a}\, f(a,c,w) \quad , \tag{70}$$

where f(a,c,w) is a geometric scaling function dependent on crack and specimen geometry. For the specimen configurations considered in this program, the specific formulations are, for the compact-type (CT) specimen,

$$K = (P/Tw)\sqrt{a}\,[29.6-185.5(a/w) + 655.7(a/w)^2 - 1017.0(a/w)^3 + 638.9(a/w)^4] \quad ; \tag{71}$$

for the center-cracked (CC) tension panel,

$$K = S\sqrt{c}\,[\pi \sec(\pi c/w)]^{\frac{1}{2}} \quad ; \tag{72}$$

and for the part-through crack (PTC) or surface-flaw specimen,

$$K = S\sqrt{a}\,[1.21\ \pi/Q]^{\frac{1}{2}} \quad , \tag{73}$$

where

$$Q = [E(a/c)]^2 - 0.212\ (S/TYS)^2 \quad , \tag{74}$$

and E(a/c) is the complete elliptic integral of the second kind. These are the basic formulations which were used for evaluating fracture data in this program.

As will be seen in the ensuing discussion, fracture instability is not a discrete event for most structural materials. Thus, the characterization of different stages of the fracture process will be identified by different subscripts on the stress and crack dimensions contained in the above expressions.

Crack Behavior Associated With Fracture

As a basis for comparing of the fracture behavior of various specimen and crack configurations, a brief description of the crack extension associated with the fracture process is presented in the following discussion. As will be seen, there are a number of important bench marks associated with crack extension prior to fracture. Any or all of these may be noted in a particular specimen and crack configuration. In order to make a rational correlation of the characteristic fracture parameters which are derived, it is necessary to relate the important bench marks in a comparable and equivalent manner.

Crack Extension and Specimen Response. – Under a rising load, a fatigue-precracked fracture specimen deforms initially in the linear and elastic manner shown in figure 23. During this initial stage of loading, the crack extension and plasticity associated with specimen deformation are nonexistent or, at least, negligible. At some point of loading, a nonlinearity in the specimen load-deflection curve is noted and may be attributed to a combination of crack extension and plasticity. The degree to which each process prevails could be characterized by unloading and marking these specimens; however, this is usually not done in the general characterization of fracture. It is only important to note that the two processes can and do interact to develop the nonlinearity. Finally, after sufficient loading and crack extension, a strain or energy instability will develop to fracture the specimen.

Parameters of Fracture Characterization. – From the previous descriptions, there are at least three bench marks to which fracture characterization parameters can be referenced. These are

- The onset of crack extension
- Apparent fracture instability
- Critical fracture instability.

These points are indicated on figure 23 as the points Q, A, and C, respectively.

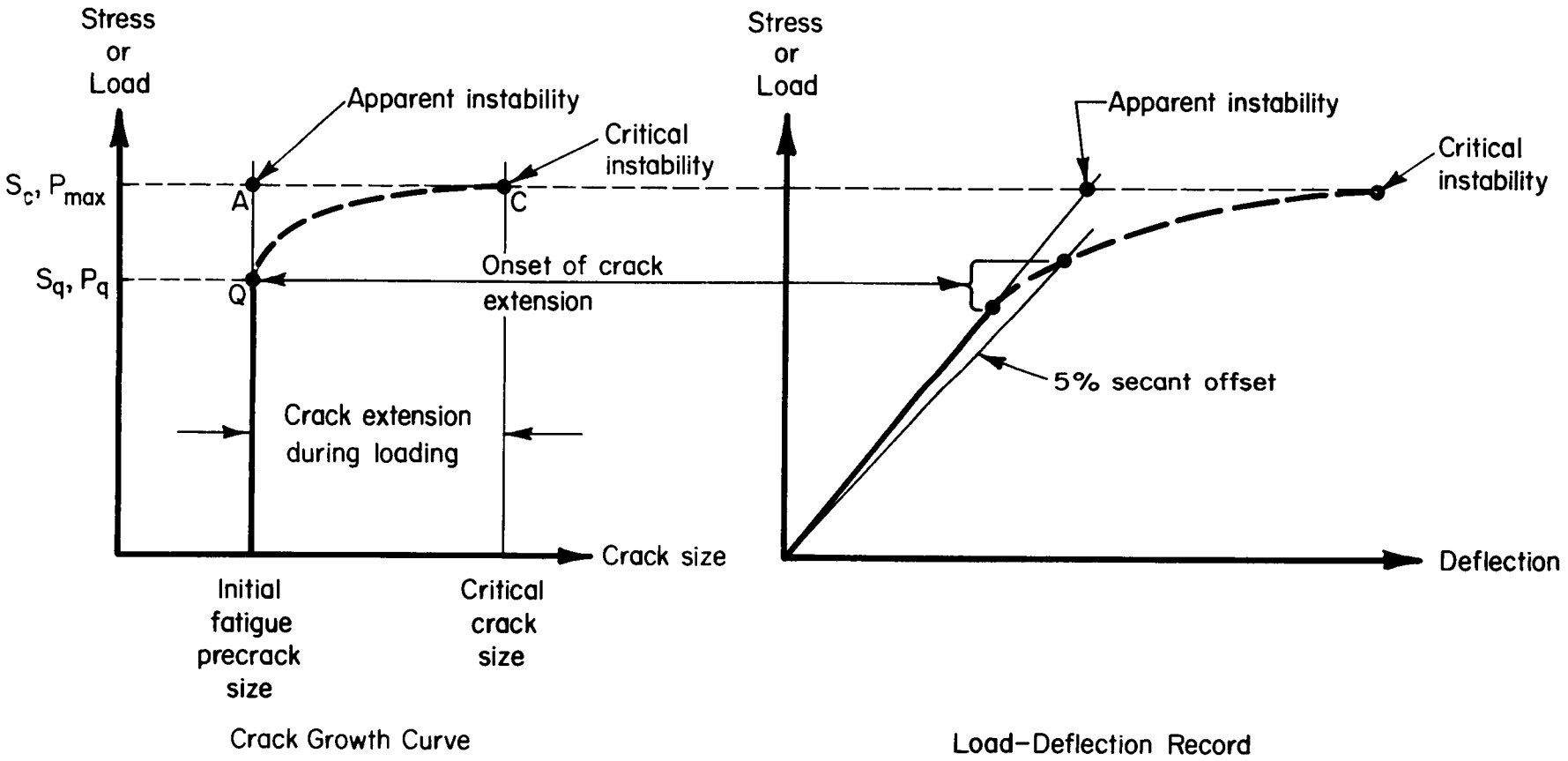

Figure 23. Relation of crack extension and specimen response during fracture test.

At this point, it is appropriate to point out and repeat the distinction between the general concepts of fracture toughness and residual strength. If fracture occurs in an abrupt fashion after only minimal amounts of crack extension, Point C will occur very close to Points Q and A, such that the fracture event is essentially a discrete and unique point. The resultant characterization parameter would be a "fracture toughness" value for the material. However, if Point C is removed from Points Q and A, all points, as well as the intervening curve, are important descriptors of the fracture behavior. This latter behavior is generally referred to as residual strength for which one partial, but incomplete measure is the "apparent" fracture toughness at Point A.

The fracture parameters which are associated with these points for various specimens are indicated in table 14.

TABLE 14.

FRACTURE PARAMETERS ASSOCIATED WITH BENCHMARKS OF STRESS AND CRACK EXTENSION

Stress State	Plane-Strain	Plane-Stress and Transitional	
Specimen Type	CT	CC	PTC
Onset of Crack Extension	K_{Ic}	K_q, K_{Ic}[a]	K_q, K_{Ic}[a]
Apparent Fracture Instability	K_{app}	K_{app}	K_{app}
Critical Fracture Instability[b]	--	K_c	--

[a]Provided that plane-strain criteria are satisfied.

[b]Generally not monitored in compact specimen and part-through crack specimen tests.

Data Evaluation

As a characterization of terminal crack behavior, the compilation of fracture toughness and residual strength data on the subject materials has been limited to those stress state and specimen configurations which are most relevant to the fatigue-crack-propagation studies. These are the quasi-plane-strain fracture toughness as determined by compact specimens in accordance with ASTM Designation: E-399-72 (ref. 3), quasi-plane stress and transitional fracture

toughness, as determined by center-cracked tension panels, and part-through crack (or surface flaw) fracture toughness, which simulates natural crack conditions. While each of these has a distinct role in the analysis of damage tolerant structures, their interfaces are not completely clear because of the interdependent complexities of geometric configuration, stress state and basic material properties.

The evaluation of experimental data of any nature involves two basic steps, namely screening and analysis. The data are screened in order to assure satisfaction of the basic criteria on the characteristics being evaluated. The analysis, of course, is concerned with computation of the characteristic parameters.

Screening Criteria. – Within the concepts of linear elastic fracture mechanics, there are two basic constraints imposed on fracture data to assure the characterization of elastic fracture instability. These are frequently referred to as the net section stress criterion and the size requirement. The former assures that the stress on the gross structural section is dominantly elastic at failure; the latter reflects the degree of local plasticity which may be manifested adjacent to the crack tip. Together, these constraints determine the validity* of the test as a representation of elastic fracture.

Net Section Stress Criterion. – The criterion which is imposed on fracture toughness and residual strength data to assure elastic fracture conditions has evolved from experience and, to a large degree, is approximate for each specimen type.

The net section stress is the nominal stress on the uncracked section determined in accordance with elementary concepts of strength of materials. It does not include the stress concentrating effect of the notch or crack and is used only as a simple measure of the nominal stress conditions on the load bearing area of the specimen. The net section stress formulations and ratios are defined in table 15. For the compact fracture specimen, the net section stress includes both a bending and tension stress component due to the load eccentricity. For the center-cracked and part-through crack specimen, the net section stress is simply a tension stress on the uncracked area due to axial loading.

---

* It is important to recognize that in this context the terms "valid" and "invalid" refer to the adequacy of the elastic-stress condition and do not question the authenticity of the test per se.

TABLE 15.

NET SECTION STRESS CRITERIA FOR VARIOUS SPECIMEN-CRACK CONFIGURATIONS

Specimen Type	Net Section Stress, S_n	Net Section Stress Criterion, S_n/TYS
Compact	$\frac{P}{T \cdot w} \frac{2(2+\frac{a}{w})}{(1-\frac{a}{w})^2}$	0.8
Center-Cracked	$\frac{S}{(1-\frac{2c}{w})}$	0.8
Part-Through Crack	$\frac{S}{(1-\frac{\pi}{4}\frac{a}{T}\frac{2c}{w})}$	0.9

Size Requirement. – Although the size requirement is not totally independent of the net section stress criterion, its consideration arises from slightly different concepts. In this context, it is used primarily as a thickness requirement on the compact specimen to assure plane-strain constraint of the plastic zone. In accordance with ASTM Designation: E-399-72 (ref. 3), this requirement is stated as

$$T \leq 2.5 \, (K_{Ic}/TYS)^2 \quad . \tag{75}$$

It should be noted that while this criterion is also imposed on the crack length within the above standard, the previous net section stress criterion is even more restrictive on crack length, such that it need not be included here.

Data Analysis. – The basic fracture data in the form of specimen and crack dimensions, loads and stress levels have been analyzed in accordance with equations (71), (72), and (73) subject to the above screening criteria. Specifically, the combinations of load or stress levels, and crack size dimensions used with these equations for the parameters listed in table 14 are, for the compact specimen,

$$K_{Ic} = g(P_q, a_o) \tag{76}$$

$$K_{app} = g(P_{max}, a_o) \quad , \tag{77}$$

for the center-cracked specimen,

$$K_q = g(S_q, c_o) \tag{78}$$

$$K_{app} = g(S_c, c_o) \tag{79}$$

$$K_c = g(S_c, c_c) \quad , \tag{80}$$

and for the part-through crack specimen,

$$K_q = g(S_q, a_o) \tag{81}$$

$$K_{app} = g(S_c, a_o) \quad . \tag{82}$$

The analyses have been performed by digital computer using the program listed in Appendix G. The output of such analyses are available as a tabular format of basic fracture data and associated fracture parameters. For each specimen type, the data are categorized by material alloy, product form, thickness, grain direction, and buckling restraint of the crack edge (if appropriate to the thickness). Within this grouping, tabulations are presented by subcategories of test temperature and specimen size or width.

Results

The tabulations of data which have been compiled and evaluated in accordance with the previous procedures are described in the following subsections. Although the formats have been developed to consolidate the data on a common basis, there are variations which reflect the different quantities and measurements involved in each type of test.

Compact Specimen. — The compact specimen is used primarily to determine the plane-strain fracture toughness of relatively thick materials. A sample tabular format for the output of this type of fracture data is presented in figure 24. Since, at the present time, the initial fatigue precrack length, the 5 percent secant offset load and the maximum load are the principal quantities derived from such a test, these quantities are presented along with the specimen dimensions as basic data. The analysis results are presented as toughness values associated with the offset and maximum load calculated in accordance with equation (71), using the combination of equations (76) and (77), respectively. The effective net section stress ratio and size requirements are presented as validity checks. Finally, the data source reference is listed.

TABLE FRACTURE TOUGHNESS VALUES FOR COMPACT TYPE SPECIMENS OF 15.24 MILLIMETER THICK ALUMINUM 7075 ALLOY EXTRUSION

CRACK ORIENTATION IS L-T

SPECIMEN IDENT	TEST TEMP	TENSILE PROPERTIES		SPECIMEN DIMENSIONS			LOAD		MATERIAL OFFSET	TOUGHNESS APPRNT	SIZE DEF-SET	REMT APP-RNT	LOAD RATIO	STRESS RATIO	REF
				THICK-NESS	WIDTH	CRACK LENGTH	P(Q)	P(MAX)							
	C	TYS	TUS	(T)	(W)	(A)			K(IC)	K(APP)			PQ/PMAX	SN/TYS	
		MN/SQ(M)		MILLIMETER			KILONEWTONS		MN/(M)3/2		MILLIMETER				
L#101	21	465.4	527.5	15.240	25.400	12.827	8.01	8.677	32.15*	34.33*	11.9	14.0	1.083	0.907	94A
L#102	21	465.4	527.5	15.240	25.400	12.725	7.997	8.958	31.71*	35.52*	11.6	14.6	1.120	0.892	94A
L#103	21	465.4	527.5	15.240	25.400	12.497	8.157	8.586	31.50*	33.58*	11.5	12.6	1.050	0.876	94A
L#104	21	465.4	527.5	15.240	25.400	12.878	8.29[illegible]	8.824	33.48*	34.32*	12.9	14.0	1.040	0.949	94A
L#301	21	479.9	537.8	25.400	50.800	26.695	16.714	16.910	30.33	30.58	10.0	10.2	1.012	0.905	94A
L#302	21	479.9	537.8	25.400	50.800	25.324	19.[illegible]5	19.[illegible]08	31.84	31.84	11.0	11.0	1.000	0.612	94A
L#303	21	479.9	537.8	25.400	50.800	26.310	17.577	17.822	30.58	31.00	10.1	10.4	1.014	0.599	94A
L#304	21	479.9	537.8	25.400	50.800	24.943	18.35[illegible]	19.491	29.99	31.84	9.8	11.0	1.062	0.570	94A
L#305	21	479.9	537.8	25.400	50.800	25.222	18.[illegible]83	18.467	30.03	30.56	9.8	10.2	1.021	0.575	94A
R#812	21	490.6	535.7	25.400	50.800	25.298	20.954	23.[illegible]55	34.95	38.45	13.2	15.0	1.100	0.570	94A
R#813	21	490.6	535.7	25.400	50.800	25.222	21.[illegible]52	23.[illegible]55	36.11	38.28	14.1	15.9	1.060	0.691	94A
R#814	21	490.6	535.7	25.400	50.800	25.273	20.[illegible]04	21.218	34.64	35.33	13.0	13.5	1.020	0.664	94A
R#821	21	490.6	535.7	25.400	50.800	24.[illegible]59	20.[illegible]13	20.928	33.57	34.24	12.2	12.7	1.020	0.638	94A
R#822	21	490.6	535.7	25.400	50.800	24.467	20.[illegible]92	21.716	33.00	35.32	11.8	13.5	1.070	0.625	94A
R#823	21	490.6	535.7	25.400	50.800	25.171	20.56[illegible]	21.773	34.65	34.38	12.5	12.8	1.010	0.550	94A
R#824	21	490.6	535.7	25.400	50.800	24.638	19.562	21.129	31.40	33.92	10.7	12.5	1.080	0.591	94A
R#825	21	490.6	535.7	25.400	50.800	25.425	20.813	21.645	34.97	36.36	13.2	14.3	1.040	0.673	94A
R#831	21	490.6	535.7	25.400	50.800	26.187	21.031	22.495	34.04	37.55	13.7	16.9	1.040	0.748	94A
R#832	21	490.6	535.7	25.400	50.800	26.116	21.387	22.027	37.20	38.32	15.0	15.9	1.030	0.728	94A
L#601	21	479.2	541.3	25.400	50.800	25.451	20.[illegible]7	20.817	34.00	35.02	12.6	13.4	1.030	0.557	94A
L#602	21	479.2	541.3	25.400	50.800	26.213	19.85[illegible]	20.661	34.98	36.39	13.3	14.4	1.040	0.590	94A
L#603	21	479.2	541.3	25.400	50.800	25.959	20.03[illegible]	20.256	34.78	35.13	13.2	13.4	1.010	0.581	94A
L#604	21	479.2	541.3	25.400	50.800	25.451	20.67[illegible]	21.712	35.12	36.53	13.4	14.5	1.040	0.678	94A
L#605	21	479.2	541.3	25.400	50.800	25.908	19.913	20.101	33.74	34.75	12.4	13.1	1.030	0.560	94A
L#606	21	479.2	541.3	25.400	50.800	25.959	20.647	21.202	35.11	36.87	13.4	14.8	1.050	0.588	94A
L#701	21	476.1	541.3	25.400	50.800	25.781	19.714	20.706	33.83	35.53	12.1	13.4	1.050	0.650	94A
L#711	21	476.1	533.7	25.400	50.800	25.451	21.231	22.717	35.72	38.22	14.1	15.2	1.070	0.595	94A
L#712	21	476.1	533.7	25.400	50.800	25.273	22.053	22.944	35.74	38.20	14.9	15.2	1.040	0.712	94A
L#713	21	476.1	533.7	25.400	50.800	25.502	21.213	22.272	35.80	37.59	14.2	15.6	1.050	0.598	94A
L#721	21	476.1	533.7	25.400	50.800	25.730	21.35[illegible]	23.278	36.53	39.32	14.8	17.6	1.090	0.717	94A
L#722	21	476.1	533.7	25.400	50.800	25.933	20.09[illegible]	22.617	35.75*	37.34*	14.2	17.1	1.100	0.705	94A
L#723	21	476.1	533.7	25.400	50.800	25.857	22.277	23.389	34.49	40.31	15.3	18.0	1.050	0.755	94A
L#724	21	476.1	533.7	25.400	50.800	25.425	20.99[illegible]	22.877	35.26	38.43	13.8	15.4	1.090	0.585	94A
							AVERAGE VALUE		34.31	35.82					
							STANDARD DEV.		2.32	2.80					

*NOTE- INVALID DATA VALUES NOT INCLUDED IN AVG. VALUE OR STD. DEV.

Basic Fracture Data → ← Toughness Evaluation

Figure 24. – Sample of tabular output for compact specimen fracture analysis results.

Center-Crack Specimen. – In that the center-crack specimen is used primarily to determine plane stress and transitional fracture toughness of relatively thin materials, more experimental quantities are usually recorded. A more expansive tabular format for this specimen type is shown in figure 25. The initial fatigue precrack length, the critical crack length as reported by the investigator, the 5 percent secant offset load, and maximum load are tabulated along with the specimen dimensions as basic fracture data. From these items, the offset, apparent and critical toughness are computed in accordance with equation (72) and the dimensional combinations of equations (78), (79), and (80), respectively. The associated net section stress ratios are also presented as validity checks. Finally, the data source reference is noted.

Within the field of each table, the data are categorized and grouped by test temperature and specimen width. Following each grouping, where more then one valid value exists, an average value and standard deviation are presented.

Part-Through Crack Specimen. – The part-through crack or surface flaw specimen is used primarily as a direct representative of naturally occurring cracks in structural materials in a wide range of thicknesses. As a result, these specimens and their data can reflect a full range of stress states. A sample illustration of the tabular format for these data is presented in figure 26. Because this crack shape is generally semielliptical in shape, two dimensions, length and depth, are required for its description. The initial precrack size, 5 percent secant offset stress, and maximum stress are presented along with specimen dimensions as basic data. The toughness values are computed in accordance with equation (73) and the dimensional combinations of equations (81) and (82). The net section stress ratio is presented as a validity check. The shape ratio is included as an indication of the ellipticity of the shape. Finally, the data source reference is noted.

CONCLUSIONS

As a result of this study, it was found that large amounts of fatigue, fatigue-crack propagation, and fracture data can be consolidated for use in design applications. Each of these three areas of material behavior were treated separately, using large files of pertinent data that were gathered on 2024 and 7075

TABLE PLANE-STRESS AND TRANSITIONAL FRACTURE TOUGHNESS OF 1.02 MILLIMETER THICK ALUMINUM 2024-T3ALLOYCLAD SHEET

CRACK ORIENTATION IS L-T, BUCKLING OF CRACK EDGES NOT RESTRAINED

SPECIMEN IDENT	TEST TEMP C	TENSILE PROPERTIES YIELD ULT STR MN/SQ(M)	THICK-NESS (T)	WIDTH (W)	INITIAL 2C(O)	FINAL 2C(C)	OFFSET S(Q)	MAXI-MUM S(C)	OFFSET K(Q)	APPRNT K(APP))	CRITCL K(C)	OFFSET	APPRNT	CRITCL	REF
			++++++++++MILLIMETER++++++++++				++++MN/SQ(M)++++		++++++++MN/M3/2++++++++						
56	21	351.6 406.8	1.013	228.60	65.02	71.12	191.68	219.95	64.51	74.02*	78.24*	0.762	0.874	0.908	35A
55	21	351.6 406.8	1.016	228.60	63.25	71.12	195.13	219.95	64.58	72.79*	78.24*	0.767	0.865	0.908	35A
67	21	351.6 406.8	1.016	228.60	113.79	126.49	125.49	142.73	62.98	71.63*	79.19*	0.711	0.808	0.909	35A
68	21	351.6 406.8	1.016	228.60	112.27	123.95	126.80	141.35	61.90	70.10	76.85*	0.697	0.790	0.878	35A
75	21	351.6 406.8	1.016	228.60	159.51	166.10	66.19	68.26	49.01	50.54	53.47	0.623	0.642	0.699	35A
76	21	351.6 406.8	1.016	228.60	157.99	168.15	67.43	75.16	46.27	54.42	59.80*	0.584	0.692	0.808	35A
							AVERAGE VALUE		58.21	58.49	0.00				
							STANDARD DEV.		8.29	10.20	0.00				
101	21	351.6 406.8	1.016	508.00	57.41	187.20	186.16	276.49	56.36	83.69*	163.87*	0.597	0.886	1.245	35A
102	21	351.6 406.8	1.016	508.00	57.40	174.46	189.61	276.49	57.39	83.69*	126.98*	0.608	0.886	1.041	35A
							AVERAGE VALUE		56.87	0.00	0.00				
							STANDARD DEV.		0.74	0.00	0.00				
R10011	21	359.2 427.1	1.016	762.00	76.20	76.20	0.00	248.91	0.00	96.65	96.65	0.000	0.770	0.770	124C
R10012	21	351.0 427.1	1.016	762.00	152.40	152.40	0.00	131.68	0.00	96.17	96.17	0.000	0.683	0.683	124C
R10013	21	356.8 427.8	1.016	762.00	304.80	304.80	0.00	139.04	0.00	92.35	92.35	0.000	0.562	0.562	124C
R10017	21	347.5 426.4	1.016	762.00	304.80	304.80	0.00	104.74	0.00	90.73	90.73	0.000	0.503	0.503	124C
R10E111	21	353.7 429.2	1.015	762.00	304.80	304.80	0.00	139.64	0.00	92.82	92.82	0.000	0.569	0.569	124C
7078	21	348.9 426.7	1.021	762.00	381.00	520.38	0.00	122.06	0.00	112.28	150.98*	0.000	0.700	1.019	124C
7079	21	348.9 426.7	1.021	762.00	381.00	640.58	0.00	126.48	0.00	116.08	136.84*	0.000	0.723	0.882	124C
							AVERAGE VALUE		0.00	96.73	99.74				
							STANDARD DEV.		0.00	12.97	6.09				
R10E113	21	356.4 427.8	1.016	190.50	76.20	76.20	0.00	150.55	0.00	61.79	61.79	0.000	0.754	0.754	124C
R10E129	21	353.0 426.0	1.016	190.50	76.20	76.20	0.00	151.69	0.00	59.35	59.35	0.000	0.716	0.716	124C
R10E24*	21	356.1 427.5	1.016	190.50	76.20	76.20	0.00	173.31	0.00	65.51	65.51	0.000	0.799	0.799	124C
R10M144	-65	358.5 443.9	1.016	190.50	127.10	127.00	0.00	58.95	0.00	47.55	47.55	0.000	0.577	0.577	124C
825	21	356.9 427.5	1.016	190.50	12.70	12.70	0.00	312.03	0.00	44.33*	44.33*	0.000	1.026	1.026	124C
826	21	356.9 427.5	1.016	190.50	12.70	12.70	0.00	333.59	0.00	43.85*	43.85*	0.000	1.015	1.015	124C
827	21	356.9 427.5	1.016	190.50	12.70	12.70	0.00	334.43	0.00	43.66*	43.66*	0.000	1.006	1.006	124C
828	21	356.8 427.5	1.016	190.50	12.70	12.70	0.00	333.24	0.00	49.36*	52.08*	0.000	0.981	1.017	124C
829	21	356.4 427.5	1.016	190.50	12.70	26.67	0.00	248.00	0.00	40.92*	52.86*	0.000	0.947	1.028	124C
830	21	356.4 427.5	1.016	190.50	12.70	26.13	0.00	232.35	0.00	41.41*	52.43*	0.000	0.958	1.024	124C
831	21	356.4 427.5	1.016	190.50	12.70	50.40	0.00	226.85	0.00	37.17	47.04*	0.000	0.744	0.946	124C
832	21	356.4 427.5	1.016	190.50	12.70	66.04	0.00	211.64	0.00	29.96	46.26*	0.000	0.694	0.917	124C
833	21	356.3 427.5	1.016	190.50	12.70	110.49	0.00	113.60	0.00	16.92	38.36	0.000	0.392	0.793	124C
834	21	356.5 427.5	1.016	190.50	12.70	106.16	0.00	111.70	0.00	15.93	36.83	0.000	0.366	0.754	124C
835	21	356.9 427.5	1.016	190.50	12.70	110.29	0.00	89.63	0.00	12.75	32.18	0.000	0.294	0.735	124C
836	21	356.4 426.5	1.016	190.50	12.70	106.68	0.00	103.04	0.00	15.67	37.36	0.000	0.362	0.758	124C
							AVERAGE VALUE		0.00	35.22	56.44				
							STANDARD DEV.		0.00	20.75	6.59				

*NOTE- NET SECTION AT OR EXCEEDS 90 PERCENT OF YIELD STRENGTH, VALUE NOT INCLUDED IN AVG. VALUE OR STD. DEV.

Figure 25. — Sample of tabular output for center-cracked specimen fracture analysis results.

TABLE SURFACE-FLAW FRACTURE TOUGHNESS OF 9.40 MILLIMETER THICK TITANIUM TI-6AL-4VALLOY PLATE

CRACK ORIENTATION IS L-T

SPECIMEN IDENT	TEST TEST C	TENSILE PROPERTIES YIELD STR MN/SQ(M)	TENSILE PROPERTIES ULT STR MN/SQ(M)	SPECIMEN DIMENSIONS THICKNESS (T) MILLIMETER	SPECIMEN DIMENSIONS WIDTH (W) MILLIMETER	CRACK SIZE LENGTH 2(C) MILLIMETER	CRACK SIZE DEPTH A(D) MILLIMETER	STRESS OFFSET S(Q) MN/SQ(M)	STRESS MAXIMUM S(C) MN/SQ(M)	MATERIAL TOUGHNESS OFFSET K(Q) MN/(M)3/2	MATERIAL TOUGHNESS APPRNT K(APP) MN/(M)3/2	NET STRESS RATIO OFFSET	NET STRESS RATIO APPRNT	A/2C	REF
SHT3	-252	1602.4	1638.9	9.398	27.94	7.87	3.17	0.00	698.46	0.00	54.43	0.000	0.471	0.403	548
SHT4	-252	1602.4	1638.9	9.500	27.94	5.84	1.45	0.00	913.59	0.00	57.46	0.000	0.585	0.248	548
SHT5	-252	1602.4	1638.9	9.500	27.94	5.84	1.45	0.00	968.75	0.00	61.12	0.000	0.628	0.248	548
								AVERAGE VALUE		0.00	57.67				
								STANDARD DEV.		0.00	3.35				
SHT2	-195	1321.1	1362.5	9.423	50.80	7.11	2.54	0.00	1048.73	0.00	78.86	0.000	0.818	0.357	548
SHT3	-195	1321.1	1362.5	9.398	50.80	8.13	3.30	0.00	879.80	0.00	70.65	0.000	0.697	0.406	548
SHT1	-195	1321.1	1362.5	9.627	76.20	14.99	3.25	0.00	936.36	0.00	82.04	0.000	0.668	0.217	548
								AVERAGE VALUE		0.00	77.18				
								STANDARD DEV.		0.00	5.87				
SRT1	21	834.3	858.4	9.601	76.20	18.80	4.70	0.00	786.72	0.00	92.99*	0.000	1.042	0.250	548
SRT2	21	834.3	858.4	9.449	76.20	18.80	4.93	0.00	730.87	0.00	85.99*	0.000	0.972	0.257	548

*NOTE- NET SECTION STRESS EXCEEDS 90 PERCENT OF YIELD STRENGTH. VALUE NOT INCLUDED IN AVG. VALUE OR STD. DEV.

Figure 26. — Sample of tabular output for part-through crack or surface flaw fracture analysis results.

aluminum alloys, Ti-6Al-4V alloy, and 300M steel. Fatigue and fatigue-crack-propagation analyses were limited to constant-amplitude cycling conditions.

From studies of fatigue data, it was concluded that

(1) The Walker equivalent strain parameter can be used to account for effects of stress ratio.

(2) A local stress-strain analysis, which uses a computed K_f value and a technique to approximately account for relaxation of mean stress, can be used to account for notch effects.

(3) The inverse hyperbolic tangent function can be employed to model fatigue curves in terms of ε_{eq} versus log N_f for both unnotched and notched specimens.

(4) Using the $\tanh^{-1}$ function, it is possible to compute mean fatigue curves and tolerance limit curves for 90 and 99 percent probability of survival with 95 percent level of confidence.

From studies of fatigue-crack-propagation data, it was concluded that

(1) Crack growth curves can be simply and effectively approximated using a five-point, divided-difference scheme.

(2) The Walker effective stress-intensity formulation can be used to account for stress ratio effects.

(3) The inverse hyperbolic-tangent function can be used to model crack-growth rate curves.

(4) Using the $\tanh^{-1}$ function, mean growth rate curves and 90 and 99 percent probability two-sided tolerance bands with 95 percent confidence level can be developed.

From studies of fracture toughness and residual strength data, it was concluded that

(1) Consistent fracture characterization can be achieved with stress-intensity-factor concepts within a common categorization of the details of alloy, process, size, and temperature.

(2) Correlation of fracture behavior for various specimen types and stress-state conditions must be based on equivalent degrees of crack extension.

(3) A broader characterization of fracture data reflecting the influence of thickness effects, processing variable grain direction, and specimen configuration requires a continued expansion of the data reservoir.

APPENDIX A

DATA SOURCE REFERENCES

1. Grover, H. J.; Bishop, S. M.; and Jackson, L. R.: Fatigue Strengths of Aircraft Materials Axial-Load Fatigue Tests on Unnotched Sheet Specimens of 24S-T3 and 75S-T6 Aluminum Alloys and of SAE 4130 Steel. NACA TN 2324, 1951.

2. Grover, H. J.; Bishop, S. M.; and Jackson, L. R.: Fatigue Strengths of Aircraft Materials Axial-Load Fatigue Tests on Notched Sheet Specimens of 24S-T3 and 75S-T6 Aluminum Alloys and of SAE 4130 Steel with Stress-Concentration Factors of 2.0 and 4.0. NACA TN 2389, 1951.

3. Grover, H. J.; Bishop, S. M.; and Jackson, L. R.: Fatigue Strengths of Aircraft Materials Axial-Load Fatigue Tests on Notched Sheet Specimens of 24S-T3 and 75S-T6 Aluminum Alloys and of SAE 4130 Steel with Stress-Concentration Factor of 5.0. NACA TN 2390, 1951.

4. Grover, H. J.; Hyler, W. S.; and Jackson, L. R.: Fatigue Strengths of Aircraft Materials Axial-Load Fatigue Tests on Notched Sheet Specimens of 24S-T3 and 75S-T6 Aluminum Alloys and SAE 4130 Steel with Stress-Concentration Factor of 1.5. NACA TN 2639, 1952.

5. Hardrath, H. F.; and Illg, W.: Fatigue Tests at Stresses Producing Failure in 2 to 10,000 cycles, 24S-T3 and 75S-T6 Aluminum Alloy Sheet Specimens with a Theoretical Stress-Concentration Factor of 4.0 Subjected to Completely Reversed Axial Load. NACA TN 3132, 1954.

6. Landers, C. B.; and Hardrath, H. F.: Results of Axial-Load Fatigue Tests on Electropolished 2024-T3 and 7075-T6 Aluminum Alloy Sheet Specimens with Central Holes. NACA TN 3631, 1956.

7. Illg, W.: Fatigue Tests on Notched and Unnotched Sheet Specimens of 2024-T3 and 7075-T6 Aluminum Alloys and of SAE 4130 Steel with Special Consideration of the Life Range from 2 to 10,000 Cycles. NACA TN 3866, 1959.

8. Grover, H. J.; Hyler, W. S.; and Jackson, L. R.: Fatigue Strengths of Aircraft Materials Axial-Load Fatigue Tests in Edge-Notched Sheet Specimens of 2024-T3 and 7075-T6 Aluminum Alloys and of SAE 4130 Steel with Notch Radii of 0.004 and 0.070 Inch. NASA TN D-111, 1959.

9. Naumann, E. C.; Hardrath, H. F.; and Guthrie, D. E.: Axial-Load Fatigue Tests of 2024-T3 and 7075-T6 Aluminum-Alloy Sheet Specimens Under Constant-and-Variable-Amplitude Loads. NASA TN D-212, 1959.

10. Smith, C. R.: S-N Characteristics of Notched Specimens. NASA CR-54503, 1966.

11. Harmsworth, C. L.: Low-Cycle Fatigue Evaluation of Titanium 6Al-4V-2Sn and 300-M Steel for Landing Gear Applications. AFML-TR-69-48, 1969.

12. Deel, O. L.; and Mindlin, H.: Engineering Data cn New and Emerging Structural Materials. AFML-TR-70-252, 1970.

13. Topper, T. H.; and Morrow, JoDean, eds.: Simulation of the Fatigue Behavior of the Notch Root in Spectrum Loaded Notched Members (U). T & AM Report No. 333, Dept. of Theoretical and Appl. Mech., Univ. of Ill., Jan. 1970.

14. Bateh, E. J.; and McGee, W.: Axial Load Fatigue and Tensile Properties of 300 VAR Steel Heat Treated to 280-300 ksi. ER-10202 (MCIC 74342), Lockheed-Georgia Co., 1969.

15. Pendelberry, S. L.; Simenz, R. F.; and Walker, E. K.: Fracture Toughness and Crack Propagation of 300 M Steel. FAA Tech. Report No. DS-68-18 (DMIC 73988), 1968.

16. Newcomer, Robert E.: Improved Aluminum Alloys-Final Report. Report MDC A1666, McDonnell Douglas Corp., 1972.

17. Anon.: Fracture Toughness and Tear Tests. ML-TDR-64-238, Air Force Materials Laboratory, Research and Tech. Division, 1964.

18. Lindh, D. V.; and Eichenberger, T. W.: The Behavior of Several Materials With and Without Notches Under the Influence of Biaxial Stresses of Various Ratios. The Boeing Co., 1963.

19. Nordmark, G. E.; Lifka, B. W.; and Kaufman, J. G.: Fracture Toughness, Fatigue-Crack Propagation and Corrosion Characteristics of Aluminum Alloy Plates for Wing Skins. Quarterly Report (MCIC 57210), Aluminum Co. of America, 1964.

20. Anderson, W. E.: Fracture Toughness Data Summary. Report D6-9068 (MCIC 62308), The Boeing Co., 1962.

21. Eichenberger, T. W.: Fracture Resistance Data Summary. Report DA-20947 (MCIC 62306), The Boeing Co., 1962.

22. Masters, J. N.; Haese, W. P.; and Finger, R. W.: Investigation of Deep Flaws in Thin Walled Tanks. NASA CR-72606, 1970.

23. Allen, F. C.: Effect of Thickness on the Fracture Toughness of 7075 Aluminum in the T6 and T73 Conditions. Damage Tolerance in Aircraft Structures, ASTM STP 486, 1971, pp. 16-38.

24. Eitman, D. A.; and Rawe, R. A.: Plane Stress Cyclic Flaw Growth of 2219-T87 Aluminum and 5Al-2.5Sn ELI Titanium Alloys at Room and Cryogenic Temperatures. NASA CR-54956, 1966.

25. Ferguson, C. W.: Hypervelocity Impact Effects on Liquid Hydrogen Tanks. NASA CR-54852, 1966.

26. Orange, T. W.: Fracture Toughness of Wide 2014-T6 Aluminum Sheet at -320 F. NASA TN D-4017, 1967.

27. Figge, I. E.: Residual Static Strength of Several Titanium and Stainless-Steel Alloys and One Superalloy at -109 F, 70 F, and 550 F. NASA TN D-2045, 1963.

28. Orange, T. W.; Sullivan, T. L.; and Calfo, F. D.: Fracture of Thin Sections Containing Through and Part-Through Cracks. NASA TN D-6305 (MCIC 80104), 1971.

29. Feddersen, C. E.; Simonen, F. A.; Hulbert, L. E.; and Hyler, W. S.: An Experimental and Theoretical Investigation of Plane-Stress Fracture of 2024-T351 Aluminum Alloy. NASA CR-1678 (MCIC 78982), 1970.

30. Christian, J. L.; and Hurlich, A.: Physical and Mechanical Properties of Pressure Vessel Materials for Application in a Cryogenic Environment. ASD-TDR-62-258, Part II (MCIC 51527), General Dynamics/Astronautics, 1963.

31. Bonesteel, R. M.: Fracture Behavior of 1/4-in.-Thick 7075-T651 Al Containing Semielliptical Surface Flaws. 6-83-71-1 (MCIC 80572), Lockheed Missiles and Space Co., 1971.

32. Dubensky, R. G.: Fatigue Crack Propagation in 2024-T3 and 7075-T6 Aluminum Alloys at High Stresses. NASA CR-1732 (MCIC 79804), 1971.

33. Christian, J. L.; Yang, C. T.; and Witzell, W. E.: Physical and Mechanical Properties of Pressure Vessel Materials for Application in a Cryogenic Environment. ASD-TDR-62-258, Part III (MCIC 60578), General Dynamics/Astronautics, 1964.

34. Walker, E. K.: A Study of the Influence of Geometry on the Strength of Fatigue Cracked Panels. AFFDL-TR-66-92, Northrop Norair, 1966.

35. Gurin, P. J.: Crack Propagation Tests for Some Aluminum Alloy Materials. LR 10498, Lockheed Aircraft Corp., 1955.

36. McEvily, A. J.; Illg, W.; and Hardrath, H. F.: Static Strength of Aluminum-Alloy Specimens Containing Fatigue Cracks. NACA TN 3816, 1956.

37. Broek, D.: The Residual Strength of Aluminum Alloy Sheet Specimens Containing Fatigue Cracks or Saw Cuts. NLR-TR M.2143, National Aerospace Laboratory, Amsterdam, 1966.

38. Broek, D.: The Effect of Finite Specimen Width on the Residual Strength of Light Alloy Sheet. TR M.2152 (MCIC 70485), National Aero-and Astronautical Research Inst., Amsterdam, 1965.

39. Broek, D.: The Effect of the Sheet Thickness on the Fracture Toughness of Cracked Sheet. NLR-TR M.2160 (MCIC 70519), National Aerospace Laboratory, Amsterdam, 1966.

40. Broek, D.: Static Tests on Cracked Panels of 2024-T3 Alclad Sheet Materials from Different Manufacturers. NLR-TN M.2164, National Aerospace Laboratory, The Netherlands, 1966.

41. Feddersen, C. E.; and Hyler, W. S.: Fracture and Fatigue-Crack Propagation Characteristics of 7075-T7351 Aluminum Alloy Sheet and Plate. Report No. G-8902 (MCIC 79089), Battelle Memorial Institute, Columbus Laboratories, 1970.

42. Anon.: Fracture Toughness Data Summary of 2000 and 7000 Series Aluminum Alloys. The Boeing Co., 1965.

43. Babilon, C. F.; Wygonik, R. H.; Nordmark, G. E.; and Lifka, B. W.: Mechanical Properties, Fracture Toughness, Fatigue, Environmental Fatigue Crack Growth Rates and Corrosion Characteristics of High-Toughness Aluminum Alloy Forgings, Sheet and Plate. Fifth Technical Management Report, ALCOA, 1972.

44. Anon.: Thick Section Fracture Toughness. ML-TDR-64-236, Boeing-North American, 1964.

45. Sullivan, T. L.: Uniaxial and Biaxial Fracture Toughness of Extra-Low-Interstitial 5Al-2.5Sn Titanium Alloy Sheet at 20 K. NASA TN D-4016, 1967.

46. Figge, I. E.: Residual-Static-Strength and Slow-Crack-Growth Behavior of Duplex-Annealed Ti-8Al-1Mo-1V Sheet. NASA TN D-4358 (MCIC 71709), 1968.

47. Tiffany, C. F.; Lorenz, P. M.; and Hall, L. R.: Investigation of Plane-Strain Flaw Growth in Thick-Walled Tanks. NASA CR-54837 (MCIC 66218), 1966.

48. Hudson, C. M.: Effect of Stress Ratios on Fatigue-Crack Growth in 7075-T6 and 2024-T3 Aluminum-Alloy Specimens. NASA TN D-5390 (MCIC 75599), 1969.

49. Bateh, E. J.; and Edwards, W. T.: Evaluation of Tear Resistance of 7079 Aluminum Alloys (Sheet, Extrusions, and Forging). SMN 86 (MCIC 62309), Lockheed Aircraft Corp., 1962.

50. DeSaw, F. A.; Mishler, H. W.; Monroe, R. E.; and Lindh, D. V.: Development of a Manufacturing Method for the Production of Aircraft Structural Components of Titanium by High-Frequency Resistance Welding. AFML-TR-71-222, Battelle's Columbus Laboratories, 1971.

51. Bjeletich, J. G.: Development of Engineering Data on Thick-Section Electron-Beam-Welded Titanium. Interim Technical Report Nos. 1, 2, 3, 4, 5, and 7, LMSC-D177632 (MCIC 80505, 80945,81856, 82834), Lockheed Missiles and Space Co., June 1971-July 1972.

52. Orange, T. W.: A Semiempirical Fracture Analysis for Small Surface Cracks. NASA TN D-5340, 1969.

53. Pierce, W. S.: Effects of Surface and Through Cracks on Failure of Pressurized Thin-Walled Cylinders of 2014-T6 Aluminum. NASA TN D-6099, 1970.

54. Hall, L. R.: Plane-Strain Cyclic Flaw Growth in 2014-T62 Aluminum and 6Al-4V (ELI) Titanium. NASA CR-72396, 1968.

55. Packman, P. F.; Pearson, H. S.; Owens, J. S.; and Marchese, G. B.: The Applicability of a Fracture Mechanics-Nondestructive Testing Design Criterion. AFML-TR-68-32, Lockheed-Georgia Co., 1968.

56. Maynor, H. W., Jr.; and Waldrop, R. S.: Crack Toleration Ability of a High-Strength Biaxially Stressed Cylindrical Pressure Vessel Containing a Surface Crack. Final Report No. 9, Auburn Univ., 1971.

57. Kerlins, V.; and Pendleberry, S. L.: The Effect of Crack Type and Material Thickness on the Fracture Strength of 4340 Steel. SM-43113, Douglas Aircraft Co., 1963

58. Bockrath, G. E.; Wysocki, E. V.; and McGovern, D. J.: Design Criteria for Pressure Vessels. MDC-G0934, McDonnell Douglas Astronautics Co., 1971.

59. Tiffany, C. F.; and Lorenz, P. M.: An Investigation of Low-Cycle Fatigue Failures Using Applied Fracture Mechanics. ML-TDR-64-53 (MCIC 55916), The Boeing Co., 1964.

60. Randall, P. N.: Severity of Natural Flaws as Fracture Origins and a Study of the Surface Cracked Specimen. AFML-TR-66-204, TRW Systems, 1966.

61. Corn, D. L.; and Mixon, W. V.: Interim Report on the Effects of Crack Shape on Fracture Toughness. SM-44671, Douglas Aircraft Co., 1964.

62. Collipriest, J. E.: Part-Through-Crack Fracture Mechanics Testing. IR & D Summary Report SD71-319, North American Rockwell Corp., 1971.

63. Schwartzberg, F. R.; Gibb, R. H.; and Beck, E. J.: Experimental Study of Pop-In Behavior of Surface Flaw-Type Cracks. Final Report, NASA CR-108457, 1970.

64. Hoeppner, D. W.; Pettit, D. E.; Feddersen, C. E.; and Hyler, W. S.: Determination of Flaw Growth Characteristics of Ti-6Al-4V Sheet in the Solution-Treated and Aged Condition. NASA CR-65811, 1968.

65. Hall, L. R.; and Finger, R. W.: Investigation of Flaw Geometry and Loading Effects on Plane Strain Fracture in Metallic Structures. NASA CR-72659, 1971.

66. Dunsby, J. A.: Fatigue Tests on Notched Specimens of 2024-T351 Aluminum Alloy Under a Low Altitude Aircraft Load Spectrum. Aeronautical Report LR-504, NRC No. 13029 (MCIC 74000), National Aeronautical Establishment, National Research Council of Canada, 1968.

67. Feddersen, C. E.; Moon, D. P.; and Hyler, W. S.: Crack Behavior in D6AC Sheet -- An Evaluation of Fracture Mechanics Data for the F-111 Aircraft. MCIC Report 72-04, Battelle's Columbus Laboratories, 1972.

68. Schijve, J.; and DeRijk, P.: The Fatigue Crack Propagation in 2024-T3 Alclad Sheet Materials From Seven Different Manufacturers. NLR-TR M.2162, Reports and Transactions, National Aerospace Laboratory NLR, The Netherlands, vol. XXXIII, 1968.

69. Brockett, R. M.; and Gottbrath, J. A.: Development of Engineering Data on Titanium Extrusion for Use in Aerospace Design. AFML-TR-67-189 (MCIC 69807), Lockheed-California Co., 1967.

70. Anon.: Room and Elevated Temperature Fatigue Characteristics of Ti-6Al-4V. Titanium Metals Corp. of America, 1957.

71. McClaren, S. W.; Cook, O. H.; and Pascador, G.: Processing, Evaluation, and Standardization of Titanium Alloy Castings. AFML-TR-68-264 (MCIC 77121), Vought Aeronautics Division, LTV Aerospace Corp., 1969.

72. Jones, R. L.; and Pratt, W. M.: The Mechanical and Stress Corrosion Properties of Premium Quality Cast Aerospace Alloys. FGT-5742 (M-140), General Dynamics, Fort Worth Division, 1972.

73. VanOrden, J. M.; and Soffa, L. L.: Ti-6Al-4V Beta Forging Fatigue Tests--Model AH56A. LR 22236 (M-105), Lockheed-California Co., 1969.

74. Marrocco, A.: Evaluation of Annealed Ti-6Al-4V and Ti-6Al-6V-2Sn Extrusions. M & P-1-TR-70-1 (M-130), Grumman Aircraft Engineering Corp., 1970.

75. Illg, W.; and Castle, C. B.: Fatigue of Four Stainless Steels and Three Titanium Alloys Before and After Exposure to 550°F (561°K) Up to 8800 Hours. NASA TN D-2899 (MCIC 61319), 1965.

76. Simenz, R. F.; and Macoritto, W. L.: Evaluation of Large Ti-6Al-4V and IMI 679 Forgings. AFML-TR-66-57 (MCIC 64192), Lockheed-California Co., 1966.

77. Harrigan, M. J.: B-1 Fracture Mechanics Data for Air Force Handbook Usage. TFD-72-501, Los Angeles Division, North American Rockwell, Corp., 1972.

78. Sommer, A. W.; and Martin, G. R.: Design Allowables for Titanium Alloys. AFML-TR-69-161 (MCIC 75727), North American Rockwell Corp., 1969.

79. Beck, E.: Effect of Beta Processing and Fabrication on Axial Loading Fatigue Behavior of Titanium. AFML-TR-69-108 (MCIC 75472), Martin-Marietta Corp., 1969.

80. Bass, Colin D.: Evaluation of Ti-6Al-4V Castings. AFML-TR-69-116, WPAFB, 1969.

81. McClaren, S. W.; and Best, J. H.: Low Cycle Fatigue Design Data on Materials in a Multi-Axial Stress Field. RTD-TDR-63-4094 (DMIC 53998), LTV Vought Aeronautics, 1963.

82. Lazan, B. J.; and Blatherwick, A. A.: Fatigue Properties of Aluminum Alloys at Various Direct Stress Ratios. Part I - Rolled Alloys, WADC Technical Report 52-307, Part I, Univ. of Minnesota, 1952.

83. Lazan, B. J.; and Blatherwick, A. A.: Fatigue Properties of Aluminum Alloys at Various Direct Stress Ratios. Part II - Extruded Alloys, WADC Technical Report 52-307, Part II, Univ. of Minnesota, 1952.

84. Anon.: Determination of Design Data for Heat Treated Titanium Alloy Sheet. vol. 3 - Tables of Data Collected, ASD-TDR-335 vol. 3, Lockheed-Georgia Co., 1962.

85. Jones, R. L.: Mechanical Properties of D6AC Steel Forging, Billet and Plate. FGT 3075, General Dynamics, Fort Worth Division, 1964.

86. Anon.: Unpublished fatigue data on Ti-6Al-4V bar stock from Sikorsky Aircraft, SE-1521.

87. Anon.: Unpublished fatigue data on 7075-T651 aluminum bar from Beckman Instruments, Inc., October 13, 1972.

88. Jaske, C. E.: The Influence of Chemical Milling on Fatigue Behavior of 300 M VAR Steel. Final Report, Battelle Memorial Institute, Columbus Laboratories, April 1969.

89. Jaske, C. E.: The Influence of Variation in Decarburization Level Upon Fatigue Life of 300 M VAR Steel. Letter Report to the Bendix Corp., Battelle Memorial Institute, Columbus Laboratories, Sept. 30, 1968.

90. Gamble, R. M.: The Effect of Microstructure on the Tensile Properties, Low Cycle Fatigue Life, and Endurance Limit of Annealed Titanium Alloy 6Al-4V. M.S. Thesis, Univ. of Fla., 1972.

91. Smith, I.; Howard, D. M.; and Smith, F. C.: Cumulative Fatigue Damage of Axially Loaded Alclad 75S-T6 and Alclad 24S-T3 Aluminum Alloy Sheet. NACA TN 3293, 1955.

92. Hudson, C. M.; and Hardrath, H. F.: Effects of Changing Stress Amplitude on the Rate of Fatigue-Crack Propagation in Two Aluminum Alloys. NASA TN D-960, 1961.

93. McEvily, A. J.; and Illg, W.: The Rate of Fatigue-Crack Propagation in Two Aluminum Alloys. NACA TN 4394, 1958.

94. Anon.: Unpublished fracture toughness data on 7075-T76511, 7075-T73511, 2024-T8511, 2219-T851, and Ti-6Al-4V from Martin Marietta Aluminum, Dec. 1972 and Jan 1973.

95. Miller, James: Low Cycle Fatigue Under Biaxial Strain Controlled Conditions. J. Materials, JMLSA, vol. 7, no. 3, Sept. 1972, pp. 307-314.

96. Pearson, H. S.: Tear Resistance Properties of Types 420 and 422 Corrosion Resistant Steel, 7075-T6 and 2024-T3 Aluminum Alloy. ER 2332, Lockheed Aircraft Corp., 1957.

97. Schwartz, R. D.: Crack Propagation of a Number of High Strength Materials. Report No. 13961, Lockheed Aircraft Corp., 1961.

98. Pierce, William S.: Crack Growth in 2014-T6 Aluminum Tensile and Tank Specimens Cyclically Loaded at Cryogenic Temperatures. NASA TN D-4541, 1968.

99. Pierce, William S.; and Sullivan, Timothy L.: Factors Influencing Low-Cycle Crack Growth in 2014-T6 Aluminum Sheet at -320°F(77°K). NASA TN D-5140, 1969.

100. Anon.: Unpublished fatigue-crack-propagation and fracture toughness data on 7075 and 7175 aluminum from Kaiser Aluminum and Chem. Corp. Center for Technology, Jan. 22, 1973.

101. Illg, W.; and Imig, L. A.: Fatigue of Four Stainless Steels, Four Titanium Alloys, and Two Aluminum Alloys Before and After Exposure to Elevated Temperatures For Up to Three Years. NASA TN D-6145 (MCIC 80060), 1971.

102. Schijve, J.: The Fatigue Life of Unnotched and Notched 2024-T3 Alclad Sheet Materials From Different Manufacturers. NLR TR 68093C (MCIC 78665), National Aerospace Laboratory, The Netherlands, 1968.

103. VanOrden, J. M.: Evaluation of Alloy Spark-Sintered Ti-6Al-4V Ingot and Forged Bar. Report No. 24376 (MCIC 84380), Lockheed-California Co., 1971.

104. Wilks, I. E.; and Howard, D. M.: Effect of Mean Stress on the Fatigue Life of Alclad 24S-T3 and Alclad 75S-T6 Aluminum Alloy. WADC-TR-53-40, National Bureau of Standards, 1953.

105. Heitzmann, R. J.: Effect of Decarburization and Surface Defects on the Notched Fatigue Strength of Steel. ADR 02-09-67.1, Grumman Aircraft Engineering Corp., 1967.

106. Marrocco, A. G.: Evaluation of Ti-6Al-4V 'Pancake' Forgings, Effect of Surface Condition. EMG-87, Grumman Aircraft Engineering Corp., 1969.

107. Marrocco, A. G.: Evaluation of 'Mill Polished' Titanium Sheet (Effect of Surface Belt Grinding). EMG-86, Grumman Aircraft Engineering Corp., 1969.

108. Marrocco, A. G.: Evaluation of Ti-6Al-4V and Ti-6Al-6V-2Sn Forgings. EMG-82, Grumman Aircraft Engineering Corp., 1968.

109. Schijve, J.; and Jacobs, F. A.: Fatigue Tests on Unnotched and Notched Specimens of 2024-T3 Alclad, 2024-T8 Alclad and 7178-T6 Extruded Material. NLR TR 68017U, National Aerospace Laboratory, The Netherlands, 1968.

110. Anon.: Unpublished low cycle fatigue, crack propagation, and fracture mechanics data on Ti-6Al-4V from Pratt and Whitney Aircraft, March 26, 1973.

111. Ostermann, F.: Improved Fatigue Resistance of Al-Zn-Mg-Cu(7075) Alloys Through Thermomechanical Processing. AFML-TR-71-121 (MCIC 81240), Air Force Materials Laboratory, 1971.

112. Nordmark, G. E.; Lifka, B. W.; Hunter, M. S.; and Kaufman, J. G.: Stress-Corrosion and Corrosion-Fatigue Susceptibility of High-Strength Aluminum Alloys. AFML-TR-70-259 (MCIC 79945), ALCOA Research Laboratories, 1970.

113. VanOrden, J. M.: The Effects of Macrograin Size Control on Fatigue Properties of Titanium Alloy Forged Billet. LR-24375, Lockheed-California Co., 1971.

114. Wells, C. H.; and Sullivan, C. P.: Low-Cycle Fatigue Crack Initiation in Ti-6Al-4V. Transactions of the ASM, vol. 62, 1969, pp. 263-270 (MCIC 74479).

115. Bucci, R. J.; Paris, P. C.; Hertzberg, R. W.; Schmidt, R. A.; and Anderson, A. F.: Fatigue Threshold Crack Propagation in Air and Dry Argon for a Ti-6Al-4V Alloy. Stress Analysis and Growth of Cracks, Proceedings of the 1971 National Symposium on Fracture Mech., Part I, ASTM STP 513, 1972, pp. 125-140. Original data received from the G. E. Co., April, 1973.

116. Anon.: Fracture toughness data on aluminum and titanium alloys, MDC A0913 (MCIC 84360), McDonnell Douglas Corp., 1971.

117. Binning, M. S.: Direct Stress Fatigue Tests on DTD 5070A, BS L73 and Alclad 2024-T81 Sheets. TR 70221, Royal Aircraft Establishment, 1970.

118. Broek, D.; and Schijve, J.: The Influence of the Mean Stress on the Propagation of Fatigue Cracks in Aluminum Alloy Sheet. NLR-TR M.2111, Reports and Transactions, National Aero- and Astronautical Research Institute, 1965, pp. 41-61.

119. Broek, D.; and Schijve, J.: The Effect of Sheet Thickness on the Fatigue-Crack Propagation in 2024-T3 Alclad Sheet Material. NLR-TR M.2129, Reports and Transactions, National Aero- and Astronautical Research Institute, 1965, pp. 63-73.

120. Schijve, J.; and DeRijk, P.: The Effect of Temperature and Frequency on the Fatigue Crack Propagation in 2024-T3 Alclad Sheet Material. NLR-TR M.2138, Reports and Transactions, National Aero- and Astronautical Research Institute, 1965, pp. 87-98.

121. Schijve, J.; Nederveen, A.; and Jacobs, F. A.: The Effect of the Sheet Width on the Fatigue Crack Propagation in 2024-T3 Alclad Material. NLR-TR M.2142, Reports and Transactions, National Aero- and Astronautical Research Institute, 1965, pp. 99-112.

122. Hudson, C. M.: Fatigue-Crack Propagation in Several Titanium and Stainless-Steel Alloys and One Superalloy. NASA TN D-2331, 1964.

123. Cassatt, G.: Fracture Mechanics--K_{IC} Testing of 2024-T351 Aerial Mines Beam Cover Plate Material. Test Report 75410-71-12, The Boeing Co., 1971.

124. Smith, S. H.; and Liu, A. F.: Fracture Mechanics Application to Materials Evaluation and Selection for Aircraft Structure and Fracture Analysis. D6-17756.

125. Feddersen, C. E.; and Hyler, W. S.: Fracture and Fatigue-Crack-Propagation Characteristics of 1/4-in. Mill-Annealed Ti-6Al-4V Titanium Alloy Plate. Report No. G-9706, Battelle's Columbus Laboratories, 1971.

126. Feddersen, C. E.; Porfilio, T. L.; Rice, R. C.; and Hyler, W. S.: Part-Through-Crack Behavior in Three Thicknesses of Mill-Annealed Ti-6Al-4V. Report No. G-1384, Battelle's Columbus Laboratories, 1972.

127. Hudson, C. M.; and Newman, J. C., Jr.: Effect of Specimen Thickness on Fatigue-Crack Growth Behavior and Fracture Toughness of 7075-T6 and 7178-T6 Aluminum Alloys. NASA TN D7173, Langley Research Center, 1973.

128. Carter, T. J.: Crack Propagation Tests on 2024-T3 Unstiffened Aluminum Alloy Panels of Various Length-Width Ratios. C. P. No. 952, Aeronautical Research Council, British Ministry of Technology, 1967.

APPENDIX B

CYCLIC STRESS-STRAIN DATA

The method of fatigue analysis developed in this program required the use of both cyclic and monotonic stress-strain curves. Using the data source references of Appendix A and information from MIL-HDBK-5B (ref. 1), it was possible to characterize the monotonic stress-strain response for the materials of interest. However, outside of the data reported by Endo and Morrow (ref. 16), Landgraf et al (ref. 17), Smith et al (ref. 18), and Gamble (data source ref. 90), there was no appropriate information available on the cyclic stress-strain response of these same materials. To fill this void of information, a limited amount of complementary tests were conducted on 2.29 mm (0.09 in.) thick 2024-T3 and 7075-T6 aluminum sheet. Specimens were from the same lot of material used in a number of previous experimental programs (data source refs. 1 through 9).

All tests were performed using an electrohydrualic test system operated in closed-loop strain control at a constant strain rate of 4×10^{-3} sec^{-1}. Experimental procedures were similar to those reported by Jaske et al (ref. 37). Loading was axial and special lateral guides were used to prevent buckling. These guides were clamped about the specimen with a force light enough to avoid significantly influencing loading of the specimen. Strain was measured over a 1.27 mm (0.500 in.) gage length using a special extensometer with a linear variable displacement transformer (LVDT) as the transducer. Load was measured by a standard load cell in series with the specimen and continuously recorded on a time-based chart. Load-strain records were made periodically using an X-Y recorder.

Results of these experiments are summarized in table B1. For each alloy, three incremental step tests (ref. 17) were used to develop continuous monotonic and cyclic stress-strain curves up to 0.01 maximum strain (see figs. B1 and B2). To see if the cyclic stress-strain curves from the step tests could be used to predict cyclic stress-strain response under constant-amplitude strain cycling, seven specimens of each alloy were tested under constant-amplitude loading. For three tests the strain ratio (algebraic ratio of minimum to maximum strain) was equal to -1.0 (i.e., the mean strain was zero). A positive value of mean strain

was used in the other four tests — three were with a strain ratio of 0.0 and one was at a strain ratio of 0.5.

In all cases, results from the constant-amplitude tests were close to those predicted by the cyclic stress-strain curve from the step tests (figs. B1 and B2). Thus, it was concluded that these cyclic stress-strain curves could be used to describe the stable stress-strain response of these two materials.

Unpublished cyclic stress-strain data have been generated on 300M steel and annealed Ti-6Al-4V alloy during in-house studies conducted at BCL. Experimental procedures were the same as those described earlier, except that a 0.635 mm (0.250 in.) diameter, 1.27 mm (0.500 in.) gage length specimen was used. Cyclic stress-strain curves for these two alloys are presented in figures B3 and B4. Samples of the titanium alloy from the transverse (T) direction and from electron-beam (EB) welded plate cyclically hardened. Whereas, samples from the longitudinal (L) direction cyclically softened. The cyclic curve shown in figure B4 is for the L direction and the monotonic curve was estimated from published data (data source ref. 70). To show the wide variation in cyclic stress-strain behavior of this alloy, data from Smith et al (ref. 18) are presented in figure B5 and data from Gamble (data source ref. 90) are presented in figures B6 and B7.

TABLE B1.

RESULTS OF CYCLIC STRESS-STRAIN TESTS AT A STRAIN RATE OF 4×10^{-3} SEC^{-1}

Specimen	Type of Test[a]	Strain Ratio[b]	Stable Strain Range		Stable Stress Range, MN/m^2 (ksi)	Stable Mean Stress, MN/m^2 (ksi)	Fatigue Life N_f, cycles[c] (or blocks)
			Total	Plastic			
2024-T3 Sheet							
2	STEP	-1.0	0.0204 max		--	--	23-1/40
3	STEP	-1.0	0.0204 max		--	--	17-2/40
4	STEP	-1.0	0.0200 max		--	--	19-39/40
1	CA	-1.0	0.0233	0.0105	938 (136)	--	324
9	CA	-1.0	0.0152	0.0029	917 (133)	--	756
5	CA	-1.0	0.0098	0.0005	745 (108)	--	6 140
7	CA	0	0.0206	0.0075	917 (133)	23 (3.4)	178
8	CA	0	0.0153	0.0029	917 (133)	7.6 (1.1)	1 137
6	CA	0	0.0101	0.0001	710 (103)	15 (2.2)	6 270
10	CA	0.5	0.0100	0.0002	717 (104)	36 (5.2)	4 260
7075-T6 Sheet							
1	STEP	-1.0	0.0208 max		--	--	28-5/40
2	STEP	-1.0	0.0204 max		--	--	34
3	STEP	-1.0	0.0206 max		--	--	30-37/40
6	CA	-1.0	0.0201	0.0056	1 050 (152)	--	292
10	CA	-1.0	0.0150	0.0011	944 (137)	--	1 209

TABLE B1. – RESULTS OF CYCLIC STRESS-STRAIN TESTS AT A STRAIN RATE OF 4×10^{-3} sec^{-1} – Concluded

Specimen	Type of Test[a]	Strain Ratio[b]	Stable Strain Range		Stable Stress Range, MN/m^2 (ksi)	Stable Mean Stress, MN/m^2 (ksi)	Fatigue Life N_f, cycles[c] (or blocks)
			Total	Plastic			
4	CA	-1.0	0.0097	0.0001	710 (103)	--	6 173
8	CA	0	0.0204	0.0050	1 000 (145)	49 (7.1)	270
9	CA	0	0.0152	0.0007	979 (142)	43 (6.3)	511
7	CA	0	0.0101	--	703 (102)	160 (23.2)	4 611
11	CA	0.5	0.0096	--	684 (99.2)	198 (28.2)	3 270

[a]STEP indicates an incremental step test and CA indicates a constant amplitude test.

[b]Ratio of minimum to maximum strain.

[c]Cycles for constant-amplitude tests and blocks for incremental-step tests.

APPENDIX B

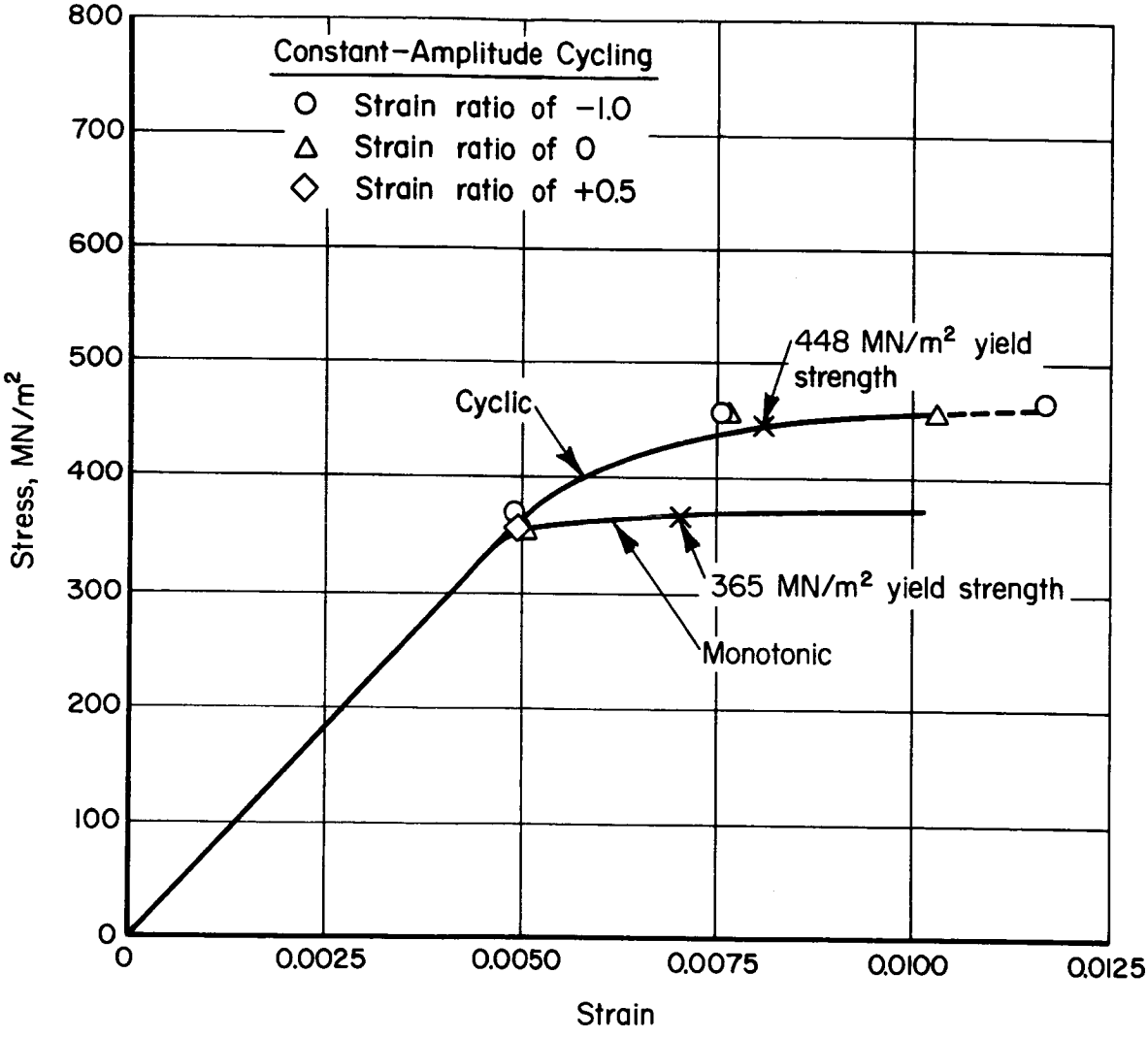

Figure B1. — Cyclic stress-strain behavior of 2024-T3 aluminum sheet.

APPENDIX B

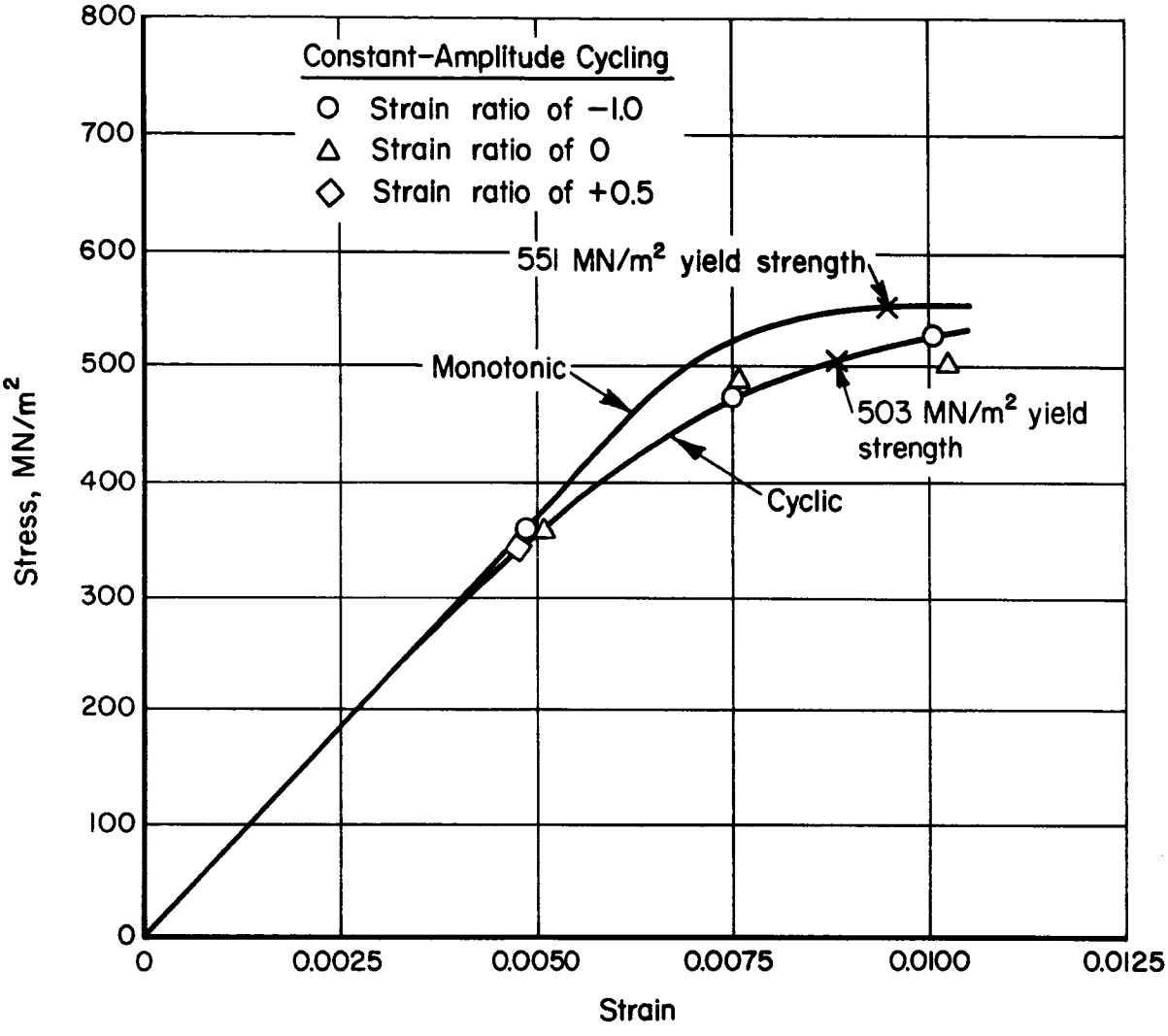

Figure B2. – Cyclic stress-strain behavior of 7075-T6 aluminum sheet.

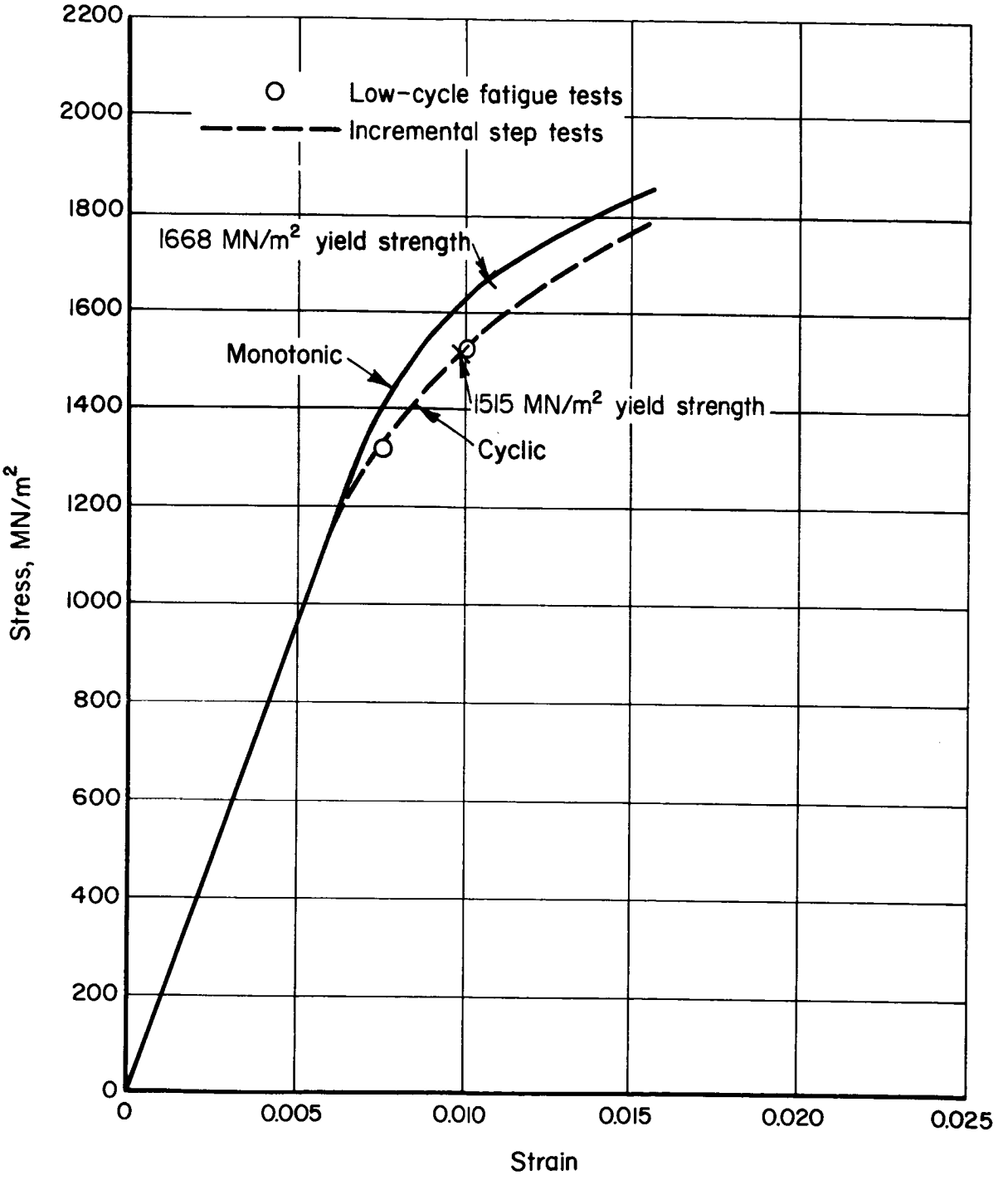

Figure B3. — Cyclic stress-strain behavior of 300M steel forging.

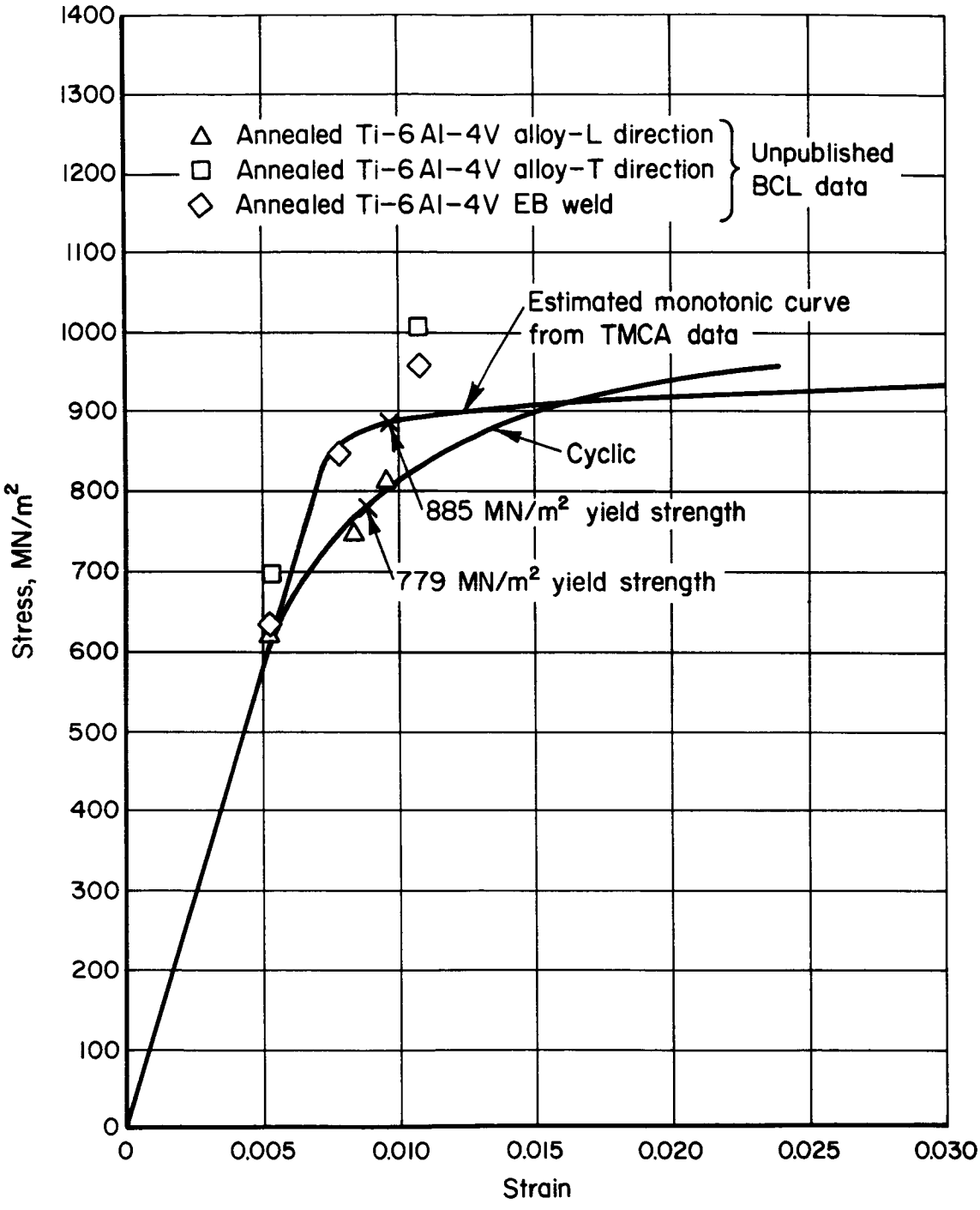

Figure B4. – Cyclic stress-strain behavior of annealed Ti-6Al-4V plate.

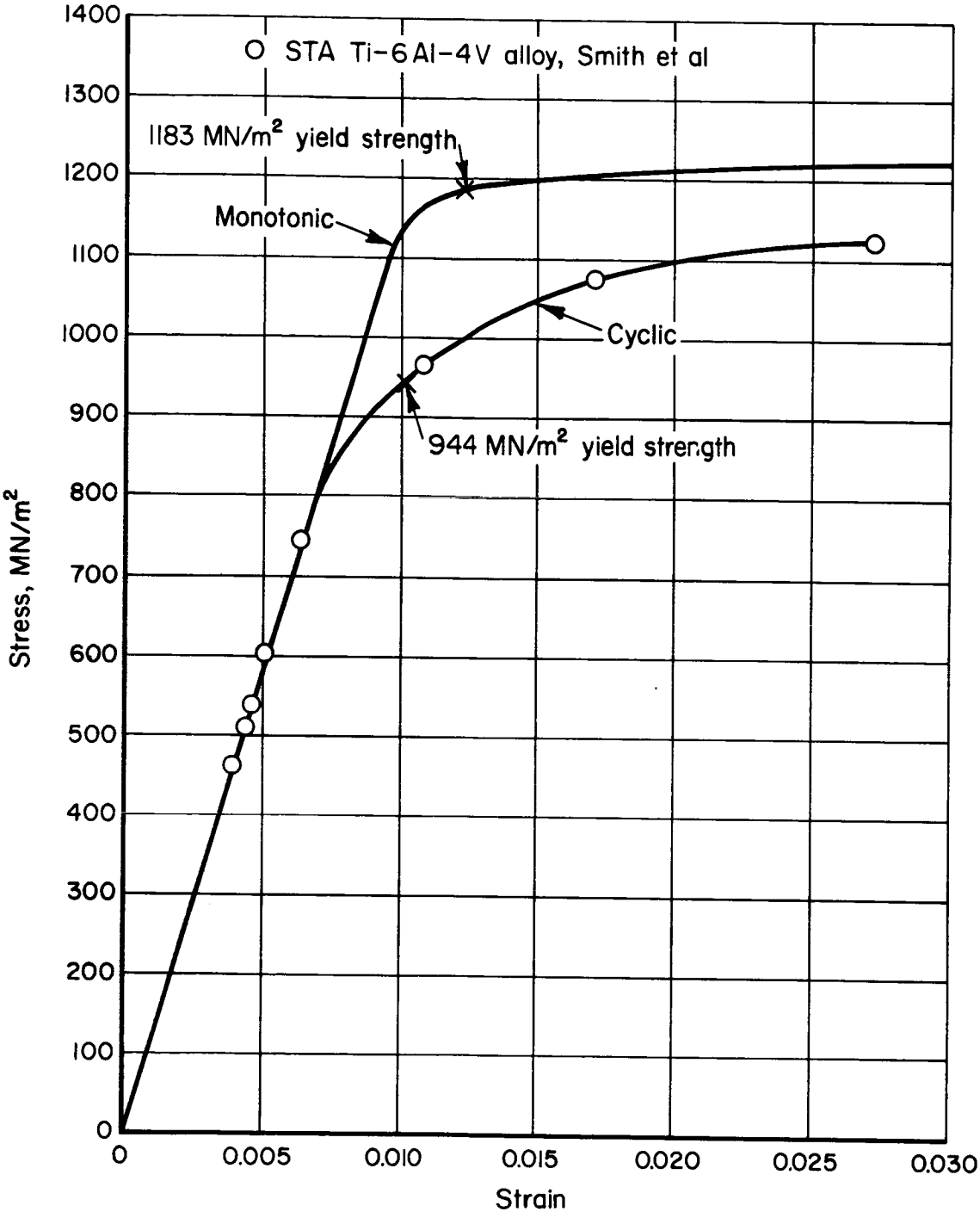

Figure B5. — Cyclic stress-strain behavior of solution-treated and aged (STA) Ti-6Al-4V bar, data from Smith et al (ref. 18).

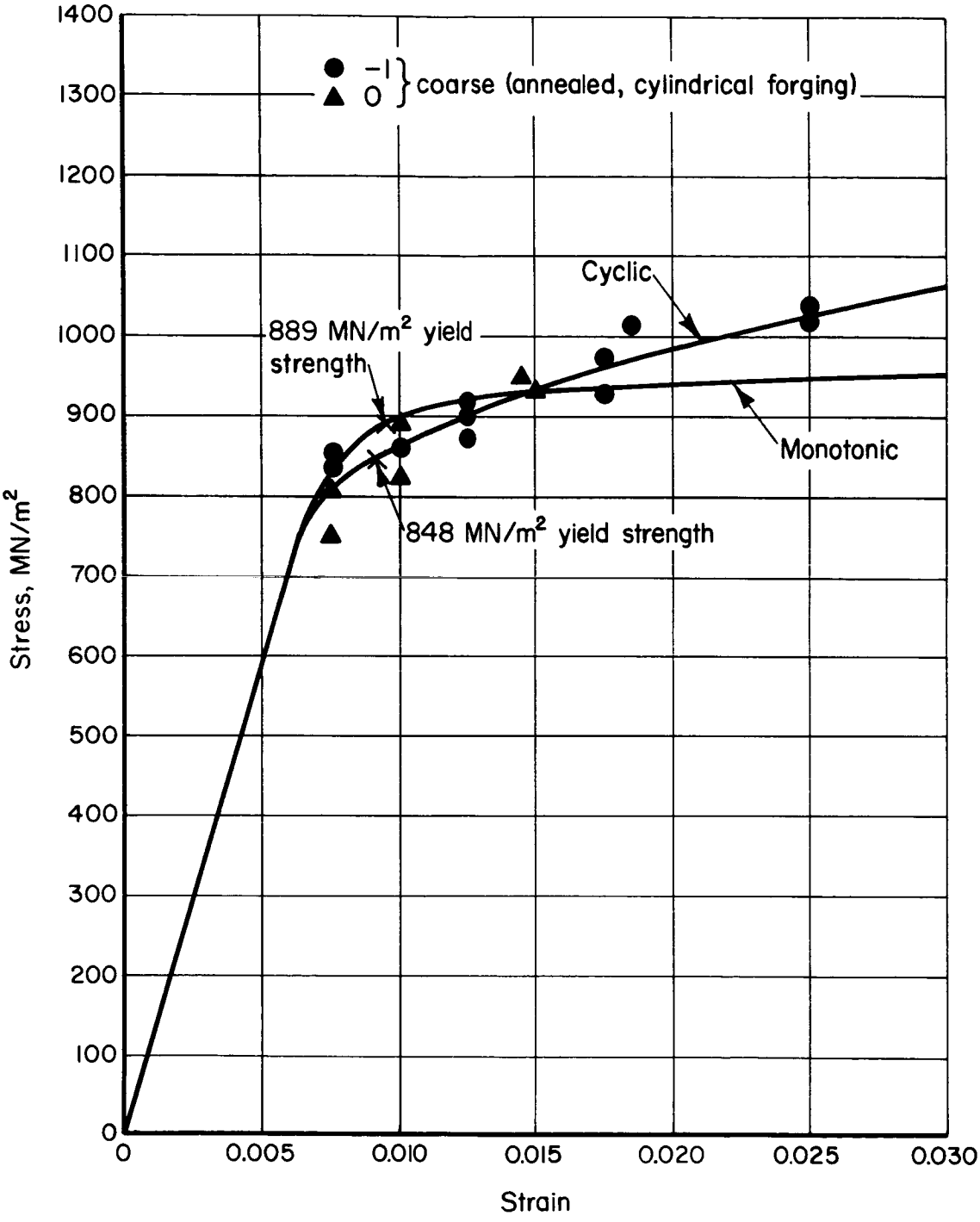

Figure B6. — Cyclic stress-strain behavior of annealed Ti-6Al-4V forging, data from Gamble (data source ref. 90).

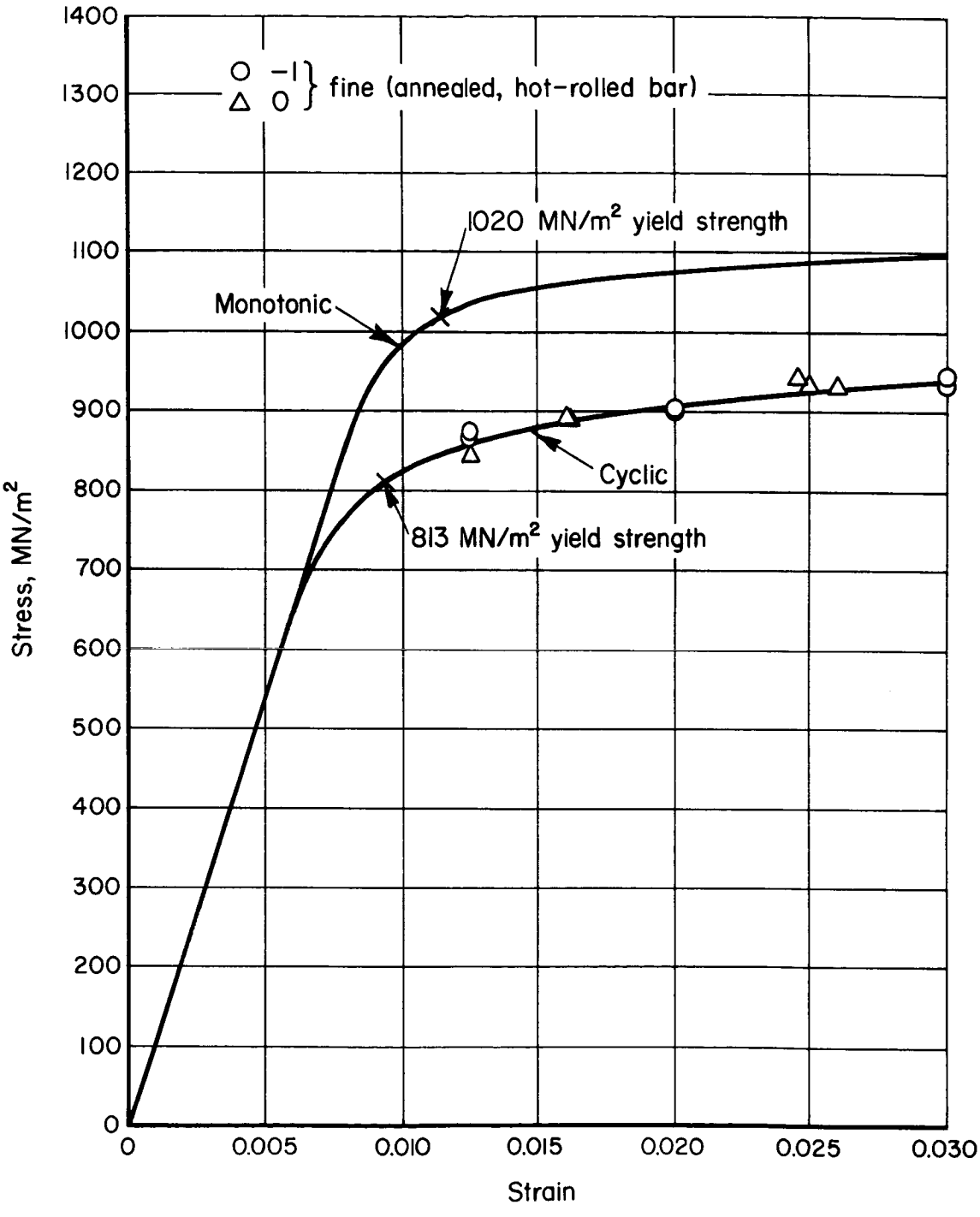

Figure B7. — Cyclic stress-strain behavior of annealed Ti-6Al-4V bar, data from Gamble (data source ref. 90).

APPENDIX C

STEP-BY-STEP APPROACH TO ANALYSIS OF FATIGUE DATA

The following outline provides an illustration of the procedure which was developed for the consolidation and analysis of fatigue data. Each part of the analysis is broken down in a step-by-step fashion so that the details of the process might be more clearly defined. Possible simplifying assumptions are also noted.

A. Material Data Acquisition

(1) Constant-amplitude smooth-specimen fatigue data (preferably obtained over a range of stress ratios or mean stress values) are required to optimize the equivalent strain m factor. If only notched data are to be analyzed, an optimum m value must be estimated.

(2) Constant-amplitude notched-specimen fatigue data make up the second part of the data file for a given material. Again, data generated at various K_t values are desirable if a reasonable value for ρ is to be determined.

(3) Monotonic and cyclic stress-strain information for the investigated material, heat treatment and product form are required for both the smooth and notched fatigue specimen analyses. In order to perform the analyses, it may be necessary, in some cases, to develop reasonable estimates of the cyclic and monotonic curves on the basis of available information. This should be done with considerable caution, however, since effectiveness of the entire analysis is based on appropriate material property definition.

B. Smooth Specimen Fatigue Data Analysis

(1) Calculate maximum nominal stress and alternating strain values for the complete data set.

(a) If the input is in terms of maximum strain and strain ratio, calculate alternating strain values

for each specimen according to the following expression:

$$e_a = \frac{e_{max}(1-R)}{2} \quad , \tag{C1}$$

and determine maximum stress values through usage of the cyclic stress-strain curve [eq. (10)].

(b) If input is in terms of maximum stress and stress ratio, calculate values of alternating stress in the same manner as shown in equation (C1), substituting values of S_a and S_{max} for values of e_a and e_{max}. Then determine alternating strain values according to the cyclic stress-strain curve [eq. (10)].

(2) Convert cycles to failure to log N_f.

(3) Set limits within which the optimum m value is likely to occur. In most cases, limits of 0.30 and 0.50 would bound the optimum m value.

(4) For a particular m value, calculate values of equivalent strain for the entire smooth data set according to equation (9b).

(5) Fit a third order polynomial [eq. (29)] to the set of calculated equivalent strain values through a least-squares regression process. (The polynomial, rather than the $\tanh^{-1}$ function, was used in computations involving an optimization on m because the quality of fit for the polynomial was related solely to the degree of data consolidation. Quality of fit for the $\tanh^{-1}$ function, however, was somewhat dependent on the specific function limits which were used, and these limits could not be appropriately determined until a specific m value was chosen.)

(6) Calculate and record the total sum of squares and the sum of squares of deviations for the regressed equation. Then calculate an R^2 value according to equation (4).

(7) Repeat steps B4 through B6 for complete range of m values and select the best m value in terms of maximum R^2. (This procedure is almost necessarily handled by a computer using an iterative process.)

(8) Using the optimum m value (or a satisfactory approximation), perform a least-squares regression to determine the best fit inverse hyperbolic tangent equation for the investigated data set. If the data cover the entire fatigue life range from 10 to 10^8 cycles, establish the range of the function according to equations (36) and (37). Otherwise reasonable values must be specified for these limits.

(9) Apply the weighting function $W(\epsilon_{eq})$, [eq. (42)], to the residuals and determine whether the modified residuals are sufficiently uniform throughout the range of data. It may be desirable to examine normality through construction of a frequency distribution plot of the residuals. This is done by plotting the frequency of occurrence versus the magnitude of deviations from the mean curve.

(10) If step B9 is completed satisfactorily, probability of survival lines can be constructed according to equation (7), and the resultant curves may then be displayed graphically along with the individual equivalent strain data values.

C. Notched Specimen Fatigue Data Analysis

(1) As in the smooth specimen fatigue analysis, nominal values of maximum stress and alternating strain must be calculated in the analysis of notched specimen data. Steps B1a and B1b are applicable. The cyclic stress-strain function [eq. (10)] is used in both cases.

(2) To calculate local mean stress values according to equations (23) and (27a), it is also necessary to calculate monotonically based values of nominal maximum and alternating stress and strain. The same stress-strain equation [eq. (10)] is used for these calculations as was used in step C1, but monotonic parameters (as in table 6) are required.

(3) Convert cycles to failure to log N_f.

(4) Set limits within which the optimum ρ value is likely to occur. (In most cases, limits of 0.00 and 0.03 would bound the optimum ρ value.)

(5) For a particular ρ value, calculate values for the fatigue concentration factor according to equation (20). Knowledge of the notch root radius is required for this calculation.

(6) Calculate an estimate of local alternating strain values according to the following expression:

$$\epsilon_a = K_f e_a \quad . \tag{C2}$$

(7) Then calculate approximate values for local maximum stress using the following relationship:

$$\sigma_{max} = \sigma_a + \sigma_m \quad . \tag{C3}$$

It is not possible to calculate σ_{max} directly because cyclic plasticity allows mean stress relaxation that decreases stable local mean stress values. Equation (C3) is an approximate means of accounting for that relaxation for constant-amplitude loading.

(a) In this equation, σ_a is calculated from equation (10) using values of local alternating strain determined in equation (C2).

(b) Values for σ_m in equation (C3) are found according to equations (23) and (27a).

(i) In equation (27a), the value, $\epsilon'_{max}/2$, is equivalent to a monotonic value of local alternating strain. This quantity can be determined by multiplying the monotonic nominal value of alternating strain, found in step C2, by the fatigue concentration factor which was found in step C5.

(ii) Similarly, the magnitude of the monotonic local maximum strain used in equation (23) can be determined by multiplying the monotonic maximum nominal strain found in step C2, by the fatigue concentration factor K_f.

(8) For a particular ρ value and for an optimum m value found in part B, calculate values of equivalent strain for the entire notched data set according to equation (9b). Values of σ_{max} and ϵ_a calcu- in steps C6 and C7 are used, however, in place of S_{max} and e_a.

(9) Fit a third order polynomial [eq. (29)] to the set of equivalent strain values in the same manner as in step B5.

(10) As in step B6, determine TSS, SSD, and R^2 values for the regressed equation.

(11) Repeat steps C5 through C10 for the complete range of ρ values and select an optimum ρ on the basis of a maximum R^2 value. (Again, the computer is almost essential for this operation.)

(12) Using optimum values for m and ρ, determine a best-fit inverse hyperbolic tangent equation in the same manner as in step B8.

(13) As in step B9, apply the weighting function, examine the residuals; and if necessary, construct a frequency distribution plot of the residuals.

(14) If step C13 is completed satisfactorily, construct probability of survival lines as in step B10.

APPENDIX D

RESULTS OF CONSTANT-AMPLITUDE FATIGUE DATA CONSOLIDATION

The collection of figures in this appendix displays results of the constant-amplitude fatigue data consolidation effort. One figure is presented on each page, and each figure consists of two related plots. The upper plot shows the consolidated data along with the regressed mean curve. Below the mean curve, are the calculated 90 and 99 percent statistical tolerance curves, respectively, which were established at a 95 percent confidence level. The lower plot illustrates the pattern of weighted residuals for the consolidated data shown in the upper plot. As explained earlier (see page 30), the abscissa is in terms of actual fatigue life. The residual plots were included to provide a visual indication of whether the statistical requirements of randomness, zero mean deviations, and uniformity of variance were satisfied for the consolidated data.

Figures D1 through D4 represent consolidated data for 2024-T3 and 2024-T4 aluminum. Figures D5 through D9 consist of consolidated data on 7075-T6 and 7075-T651 aluminum. For both series of aluminum, the data consolidation was substantial. The best collapse of data (R^2 = 99.6 percent) was obtained for the unnotched 7075-T6 clad sheet material, where all data came from a single source. In all but one case (fig. D8), consisting of both notched and unnotched aluminum data, the R^2 value was 94 percent or greater. Other than the noted exception, unnotched data were consolidated better than notched data. Nonuniformity of variance was of some concern in several cases (figs. D2 and D6), but this problem was not due to inadequacy of the weighting function; it was due to layering of data from different sources in the high cycle fatigue range. This layering made it impossible to account for data in this region as effectively as data in the lower cycle regions where no such layering was evident. The nonuniformity of variance was not considered to be severe enough, however, to make the construction of tolerance limits inappropriate.

Results for the 300M steel fatigue analysis are presented in figures D10 and D11. The R^2 values for both curves were not as high as the values determined for the aluminum alloys, but the overall data collapse was considered good since the inherent data scatter for the two data sets was quite large.

The Ti-6Al-4V alloy data, displayed in figures D12 through D23, were the most difficult to analyze and provided the poorest results. The difficulties were due

to two major factors. First, the titanium data file consisted of a large number of different product forms and heat treatments, and although an attempt was made to develop accurate monotonic and cyclic stress-strain data for each variation, only a rough approximation of these curves was possible in some cases. Secondly, the inherent scatter in most of the titanium data was very great, making a consolidation effort difficult. Despite these problems, R^2 values exceeding 80 percent were obtained in figures D12, D17, D19, D20, D22, and D23. The best results were found for the Ti-6Al-4V data in the solution-treated and aged condition. For cases where the data consolidations were not acceptable as shown in figures D13, D14, D15, D16, D18, and D21, the values of R^2 were below 80 percent. Such curves cannot be used for design applications and are included in this report only to show how poorly the analytical procedures worked in some instances. Until more experimental information is obtained upon the cyclic stress-strain and fatigue behavior of Ti-6Al-4V alloy, it will not be possible to refine the analytical procedures to account for such anomalies.

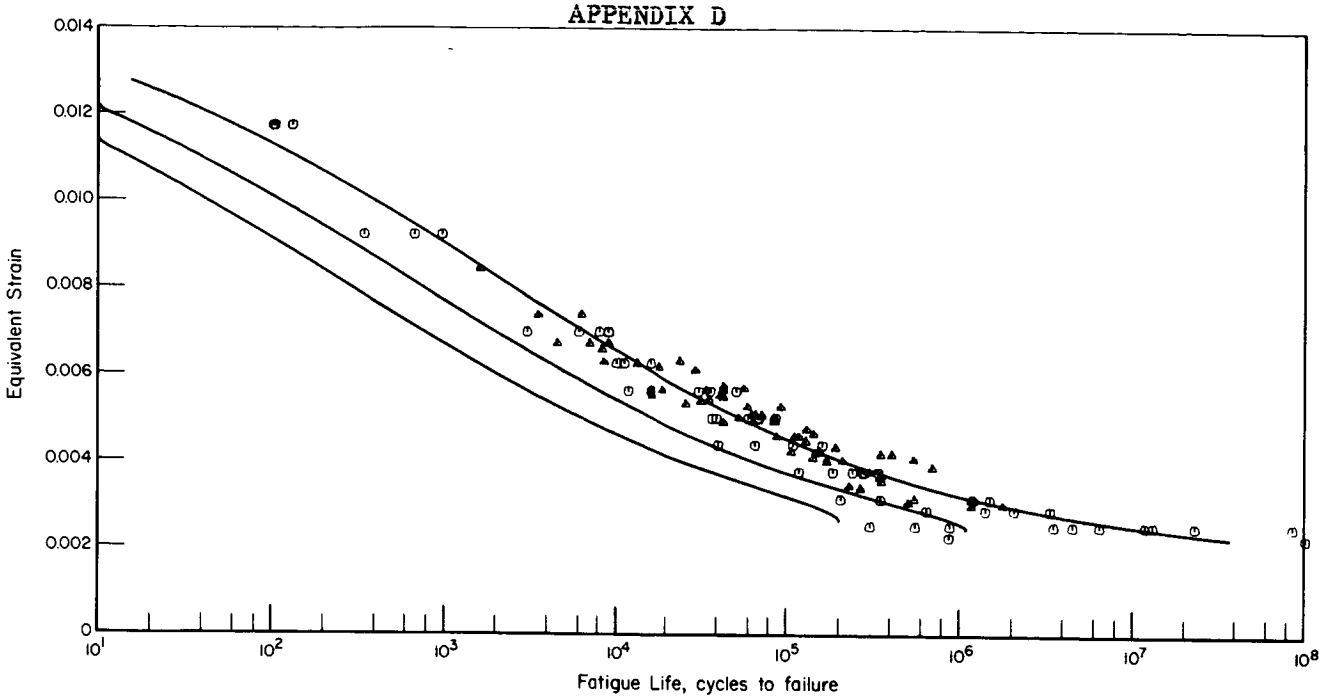

a. Consolidated fatigue data with mean curve and 90 and 99 percent survival lines.

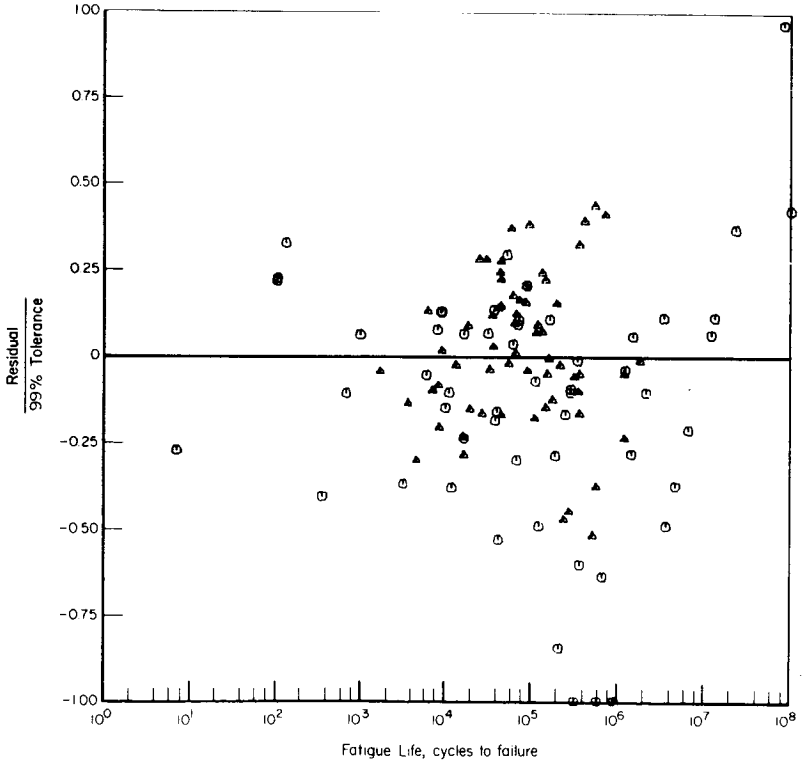

b. Distribution of weighted residuals.

Figure D1. – 2024-T3 Sheet (unnotched).

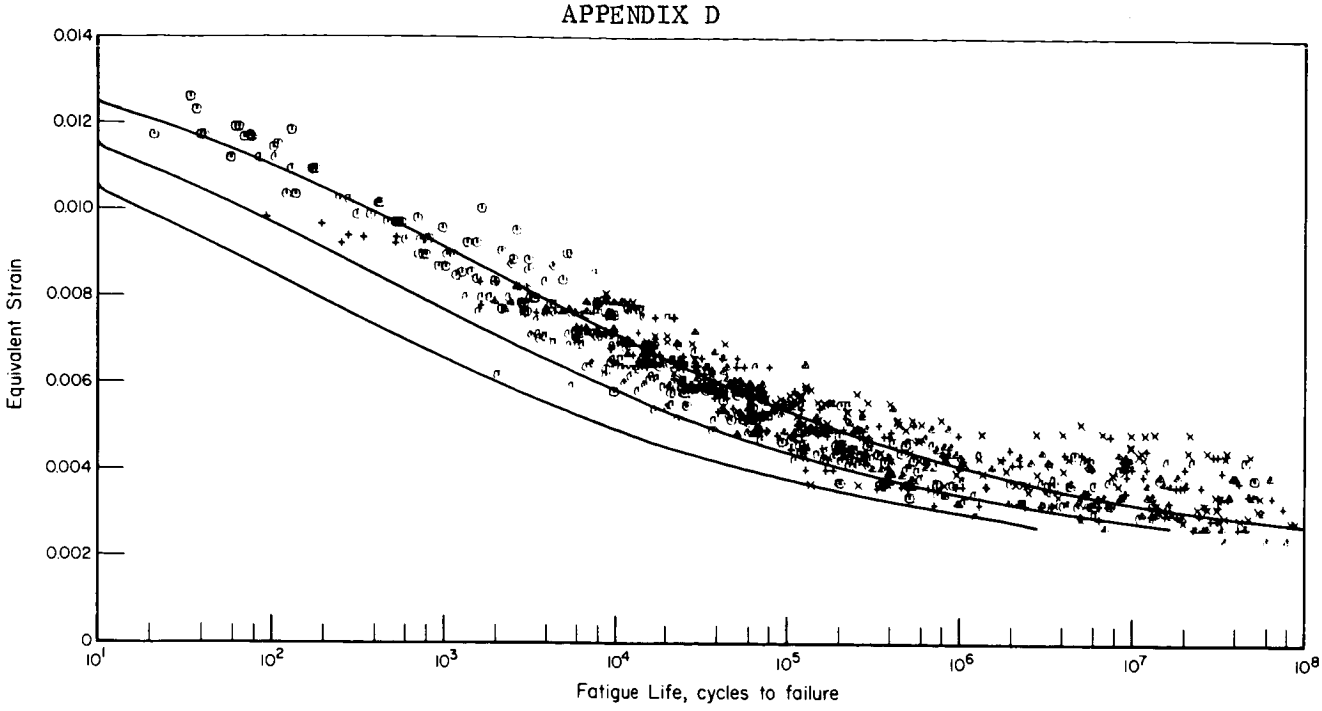

a. Consolidated fatigue data with mean curve and 90 and 99 percent survival lines.

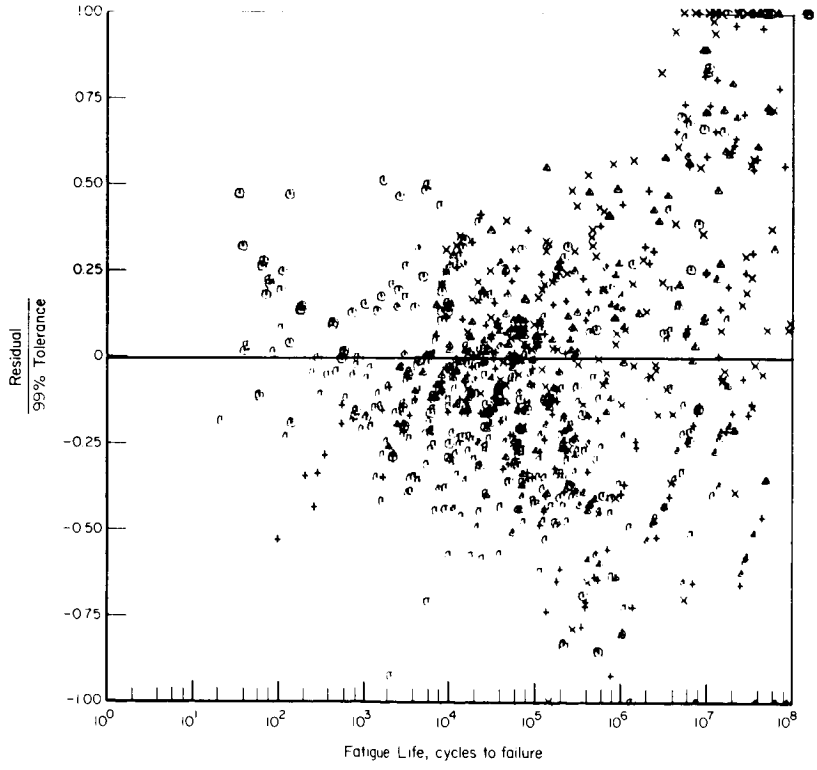

b. Distribution of weighted residuals.

Figure D2. – 2024-T3 Sheet (notched).

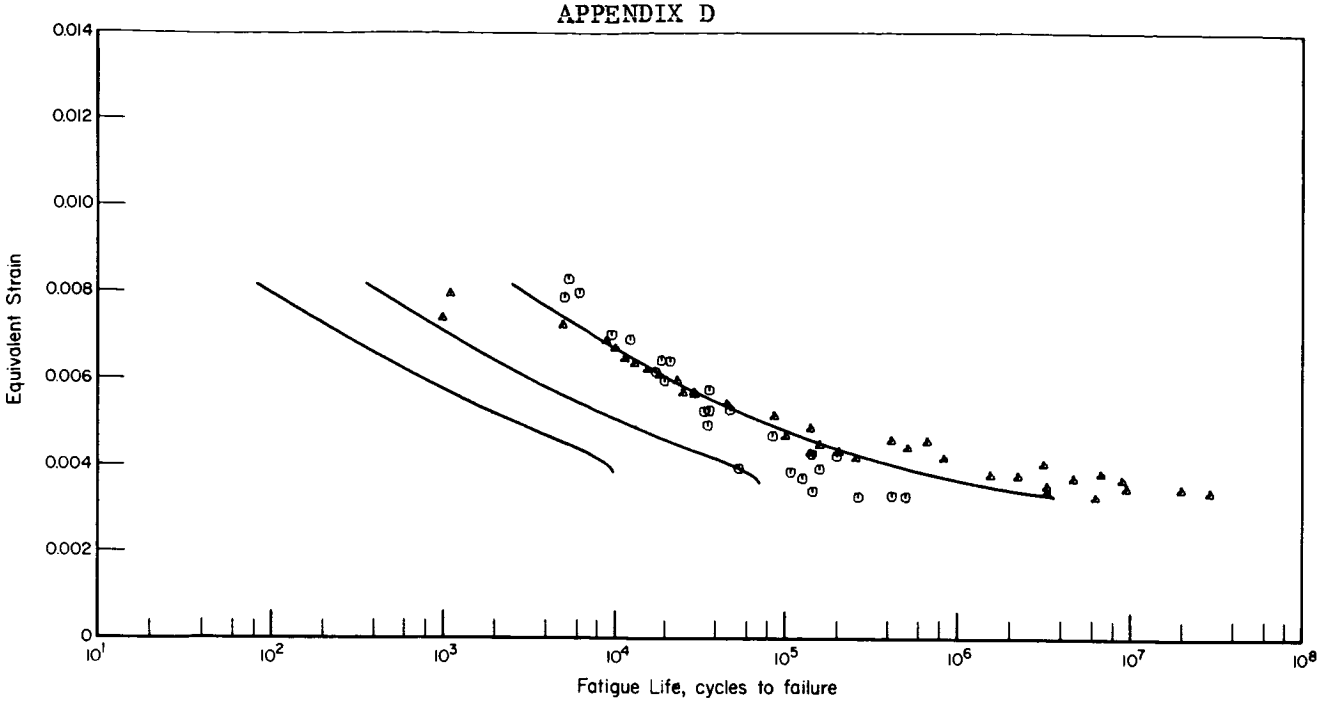

a. Consolidated fatigue data with mean curve and 90 and 99 percent survival lines.

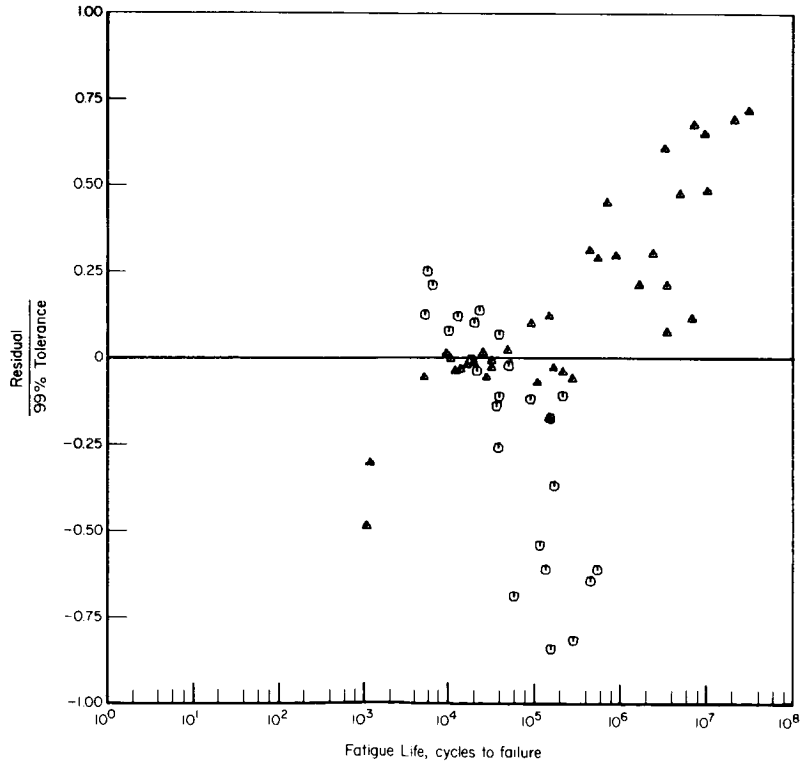

b. Distribution of weighted residuals.

Figure D3. – 2024-T4 Bar and rod (unnotched).

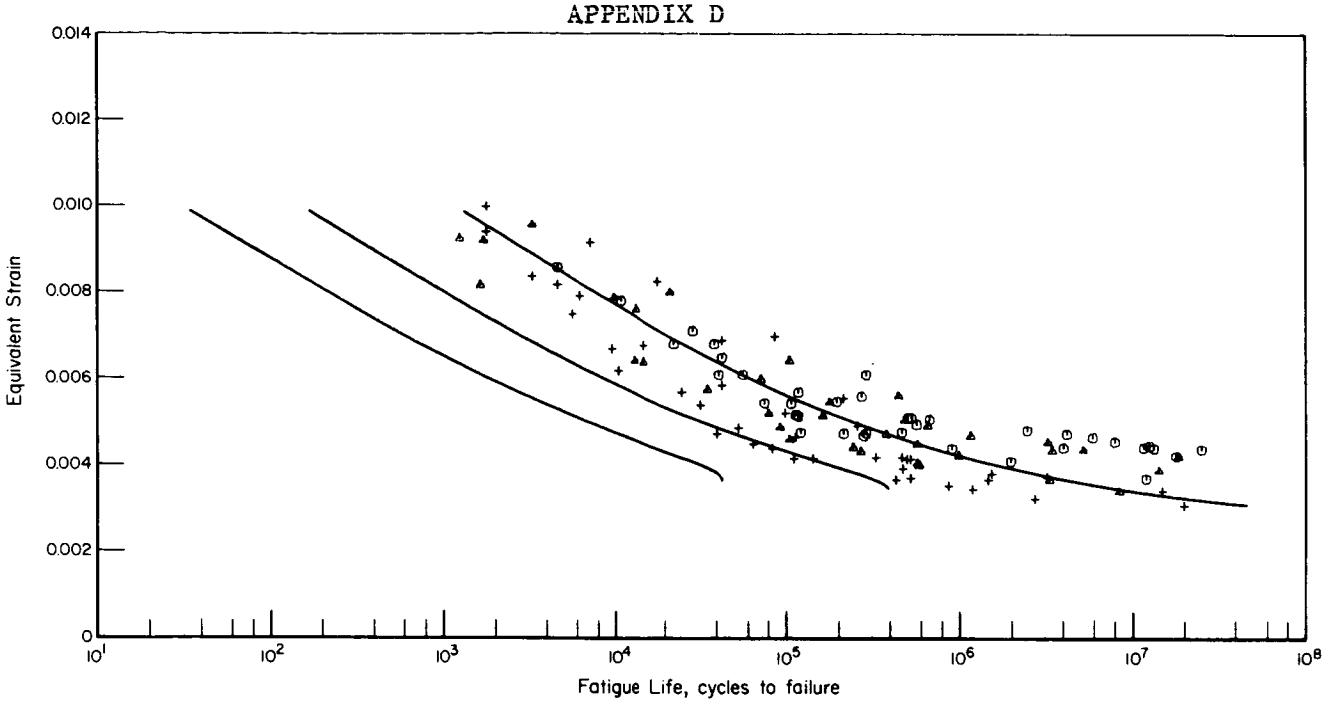

a. Consolidated fatigue data with mean curve and 90 and 99 percent survival lines.

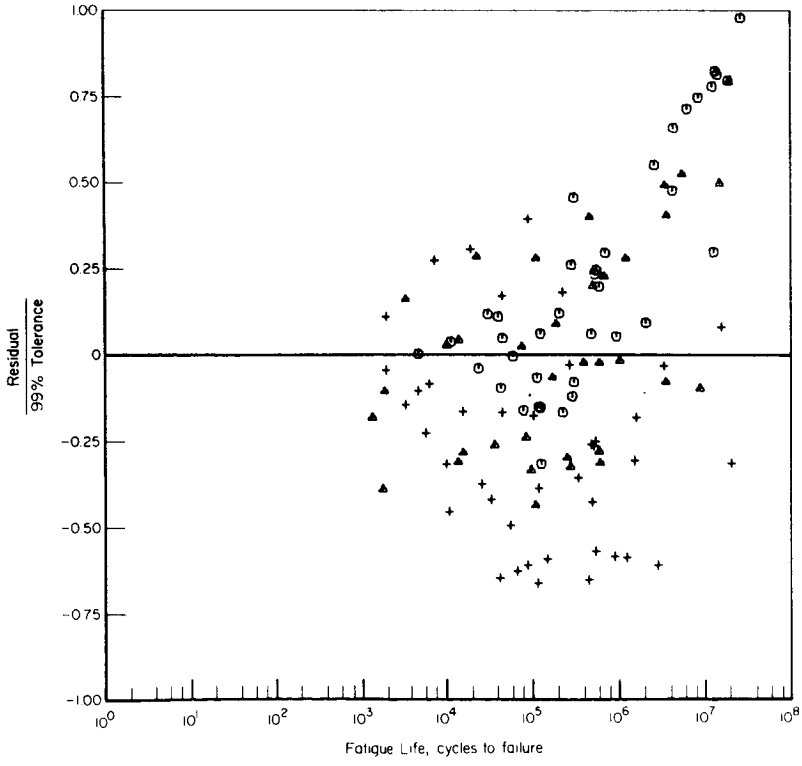

b. Distribution of weighted residuals.

Figure D4. – 2024-T4 Bar and rod (notched).

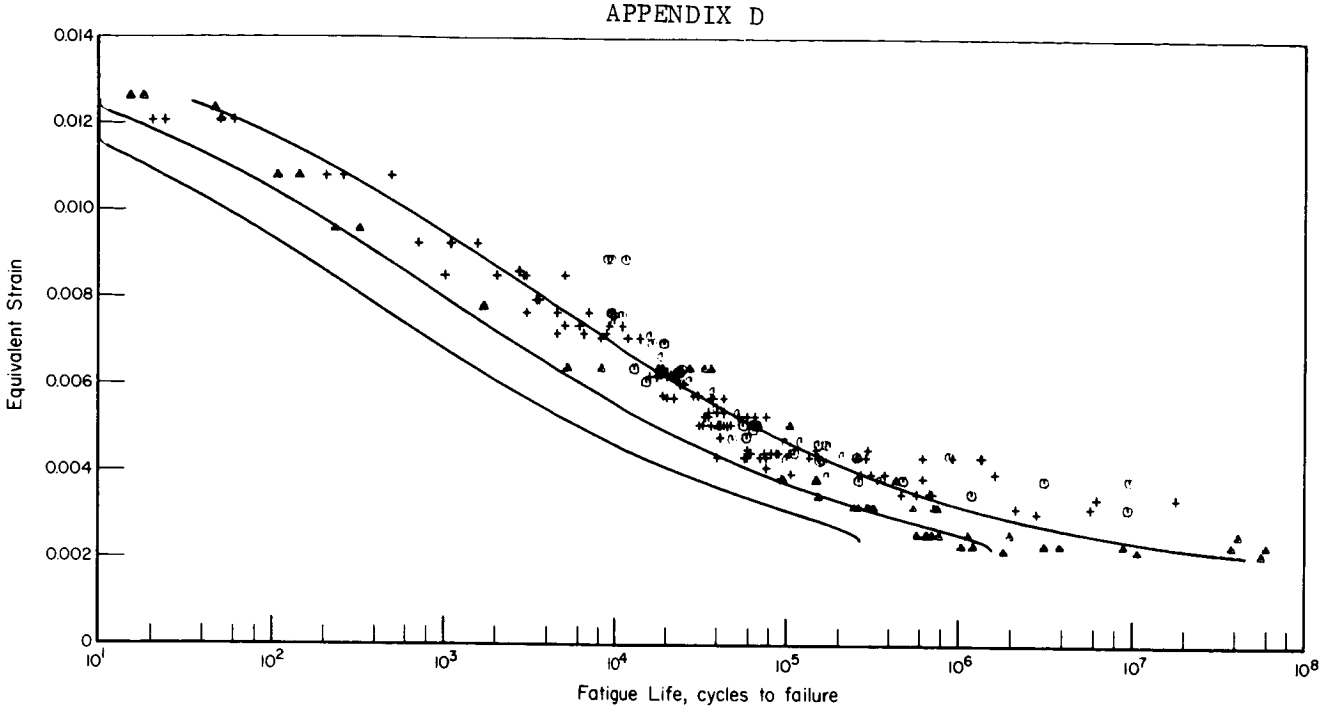

a. Consolidated fatigue data with mean curve and 90 and 99 percent survival lines.

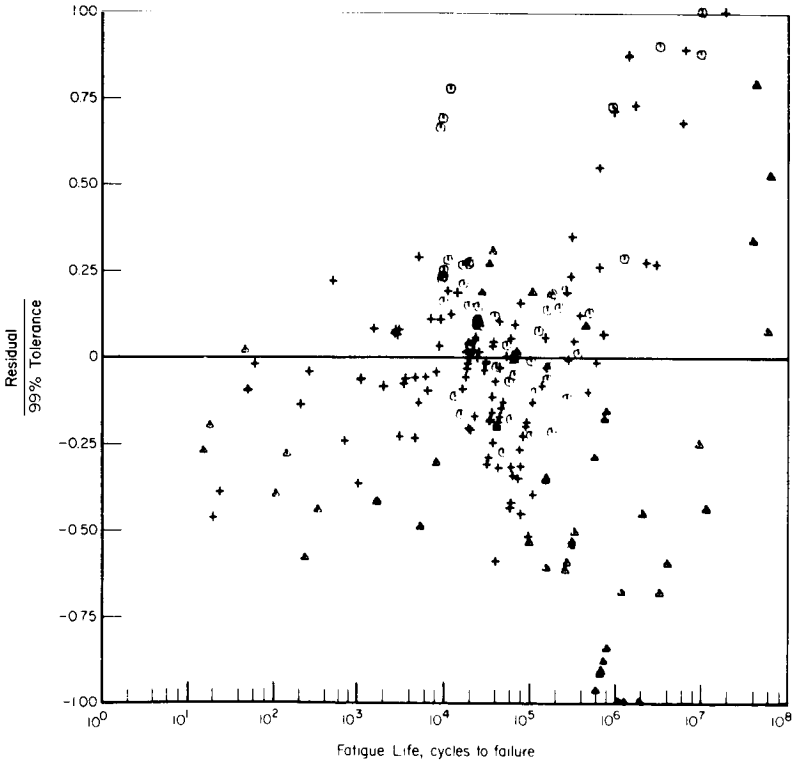

b. Distribution of weighted residuals.

Figure D5. — 7075-T6 Sheet (unnotched).

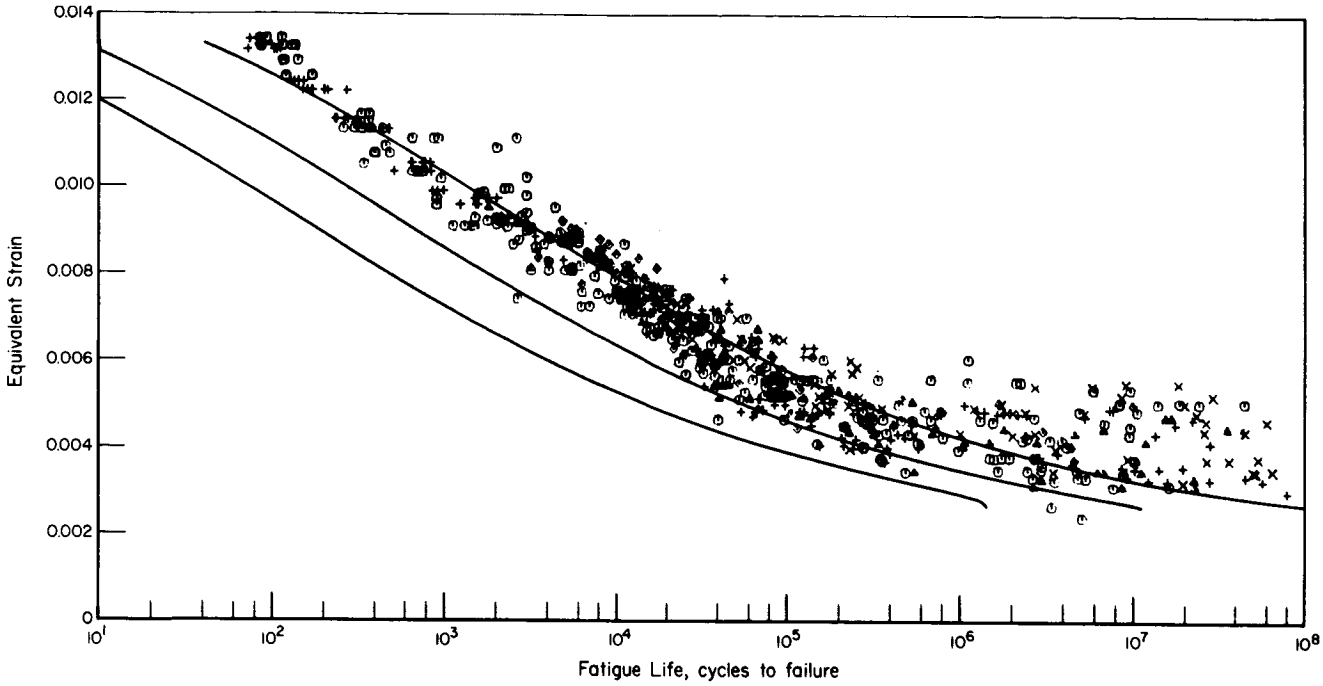

a. Consolidated fatigue data with mean curve and 90 and 99 percent survival lines.

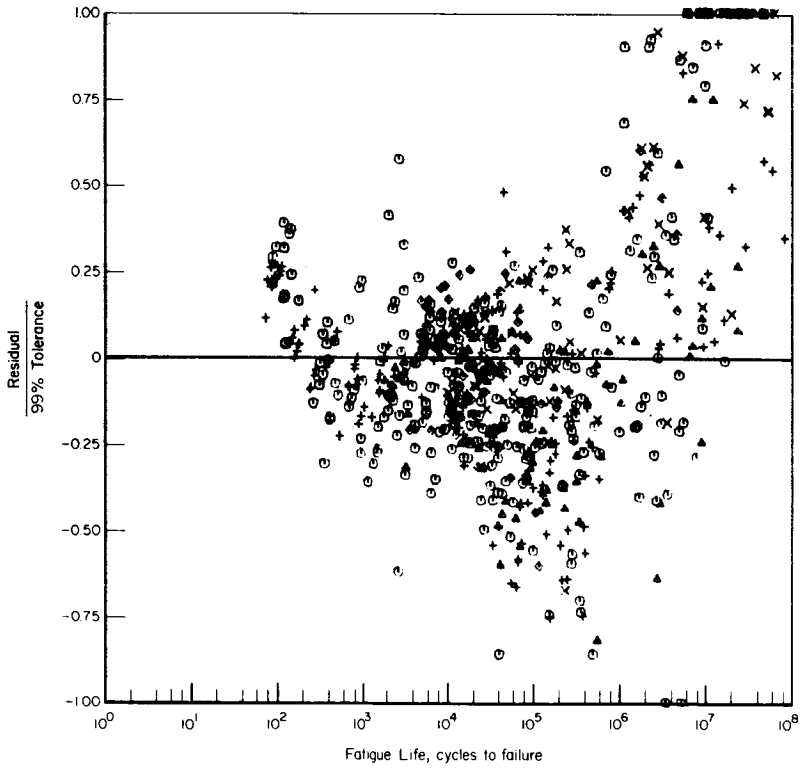

b. Distribution of weighted residuals.

Figure D6. — 7075-T6 Sheet (notched).

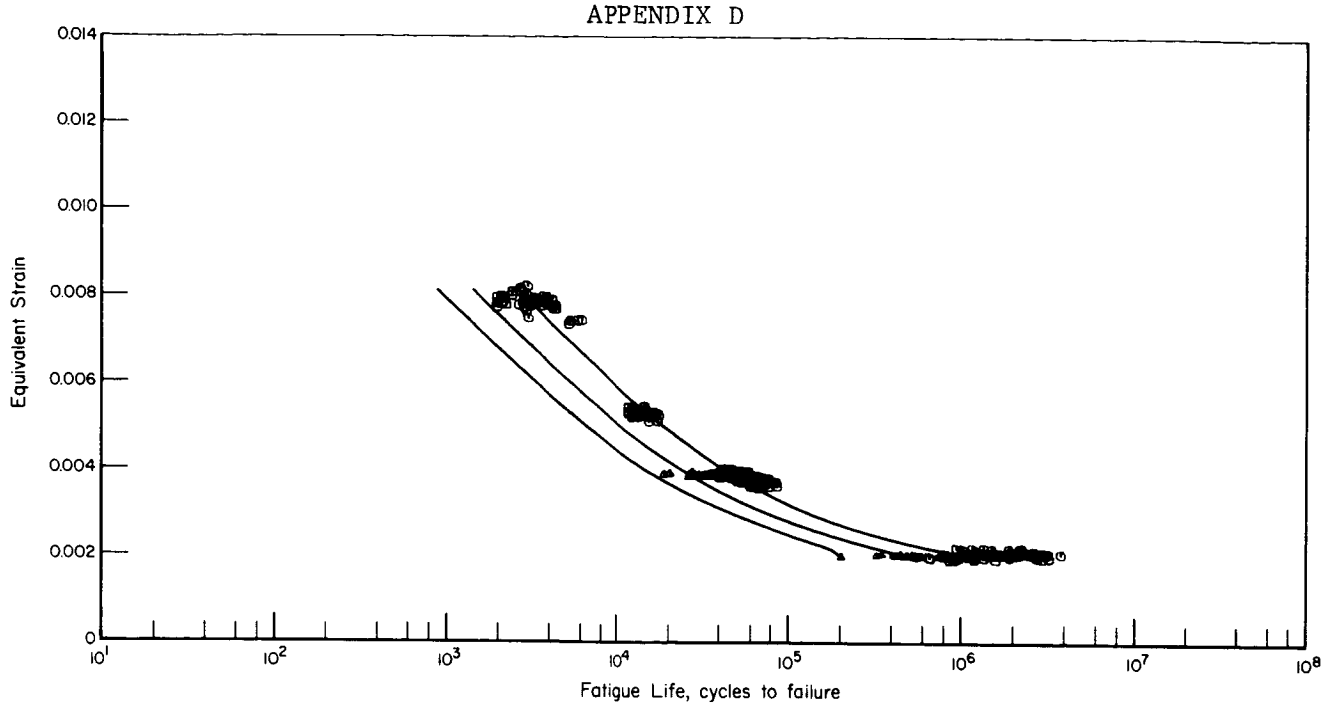

a. Consolidated fatigue data with mean curve and 90 and 99 percent survival lines.

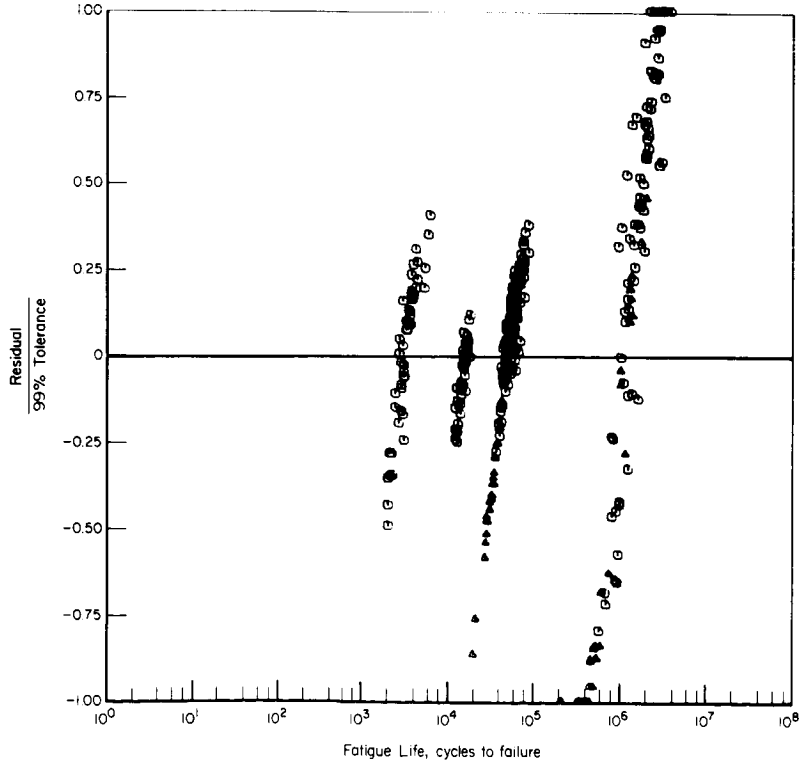

b. Distribution of weighted residuals.

Figure D7. — 7075-T6 Clad sheet (unnotched).

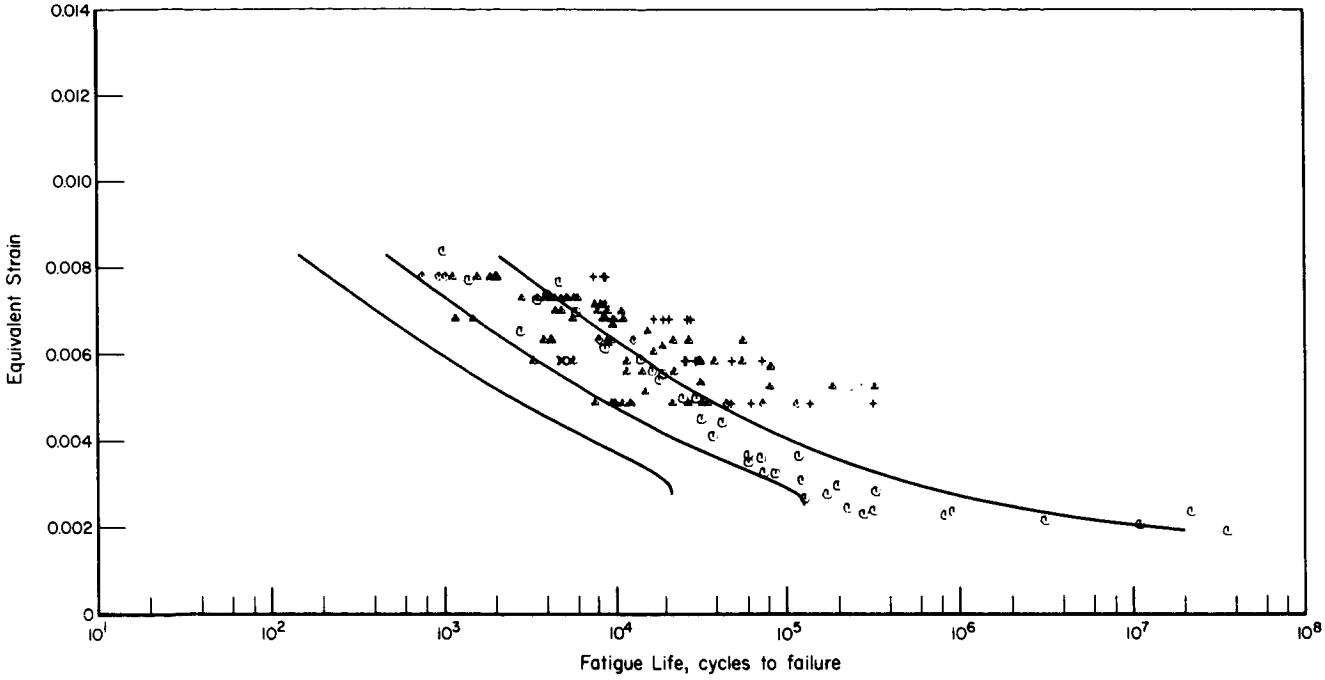

a. Consolidated fatigue data with mean curve and 90 and 99 percent survival lines.

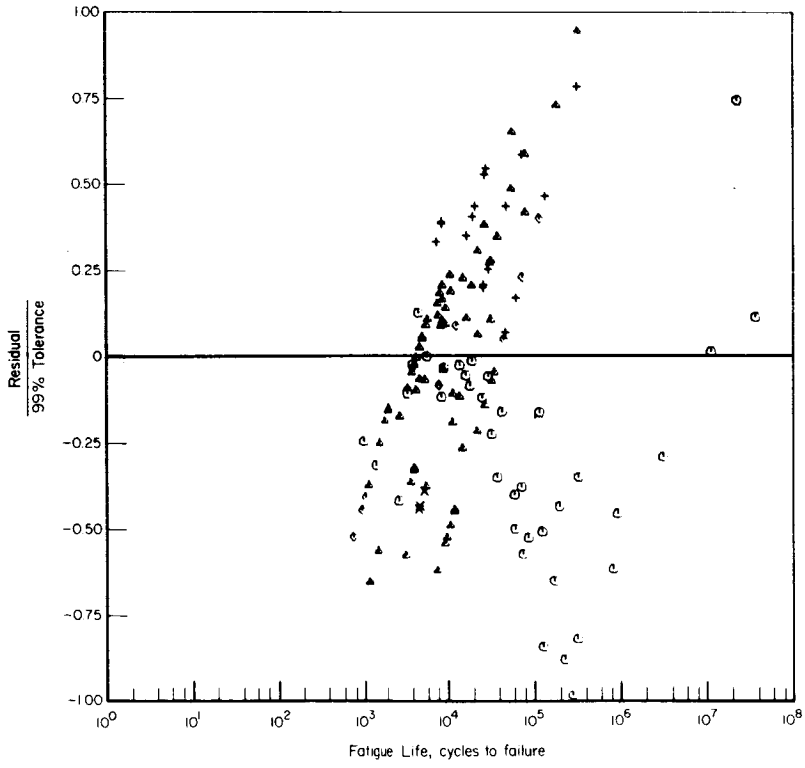

b. Distribution of weighted residuals.

Figure D8. – 7075-T6 and 7075-T651 Bar (unnotched).

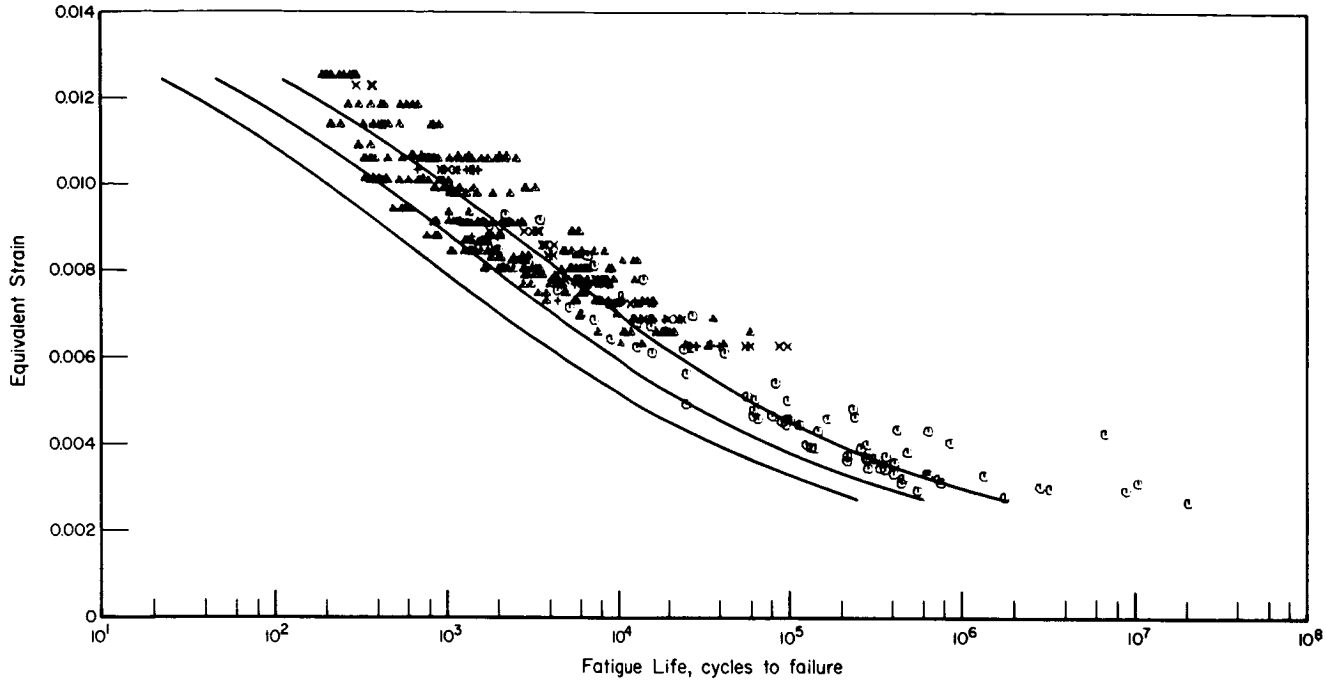

a. Consolidated fatigue data with mean curve and 90 and 99 percent survival lines.

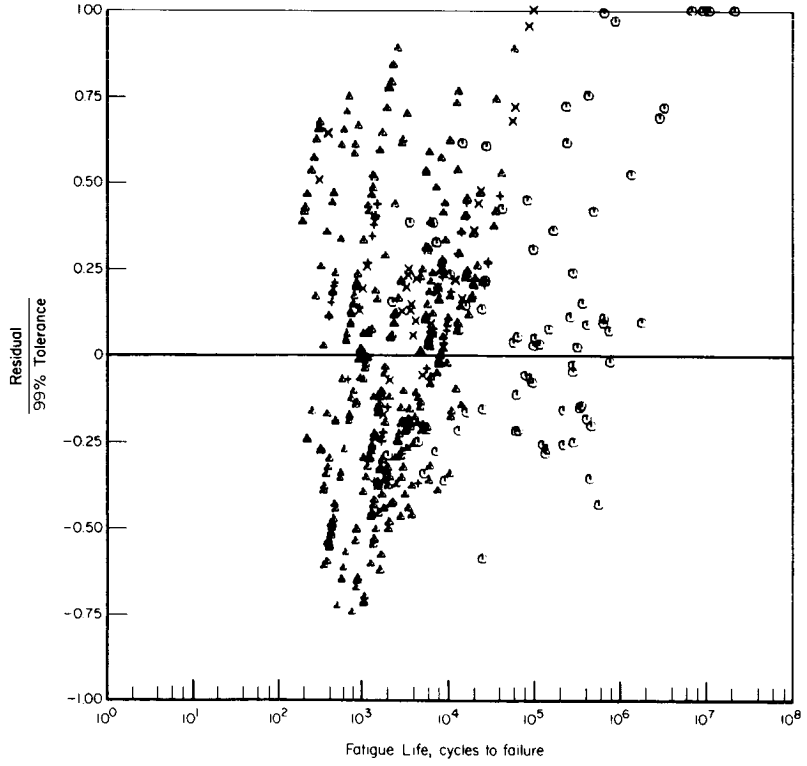

b. Distribution of weighted residuals.

Figure D9. – 7075-T6 and 7075-T651 Bar (notched).

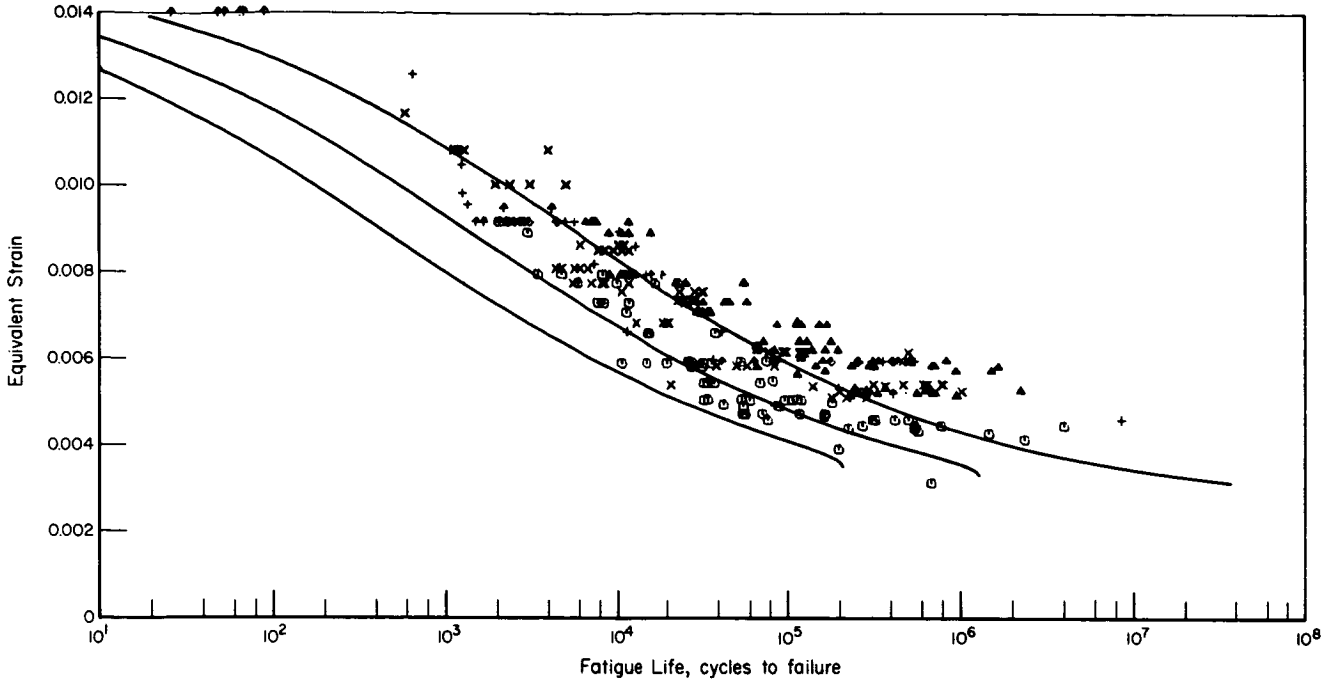

a. Consolidated fatigue data with mean curve and 90 and 99 percent survival lines.

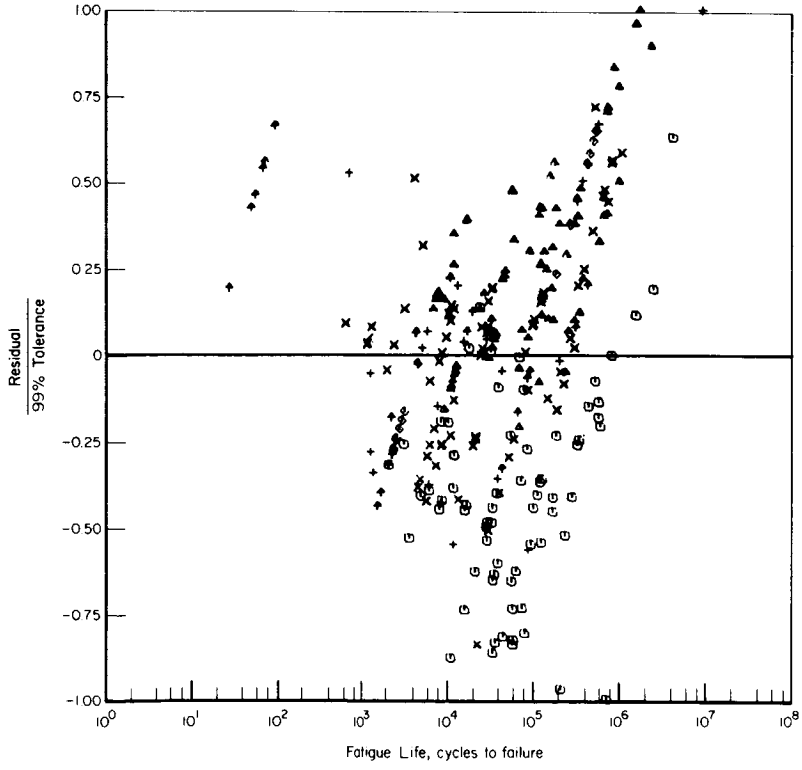

b. Distribution of weighted residuals.

Figure D10. — 300M Billet and forging (unnotched).

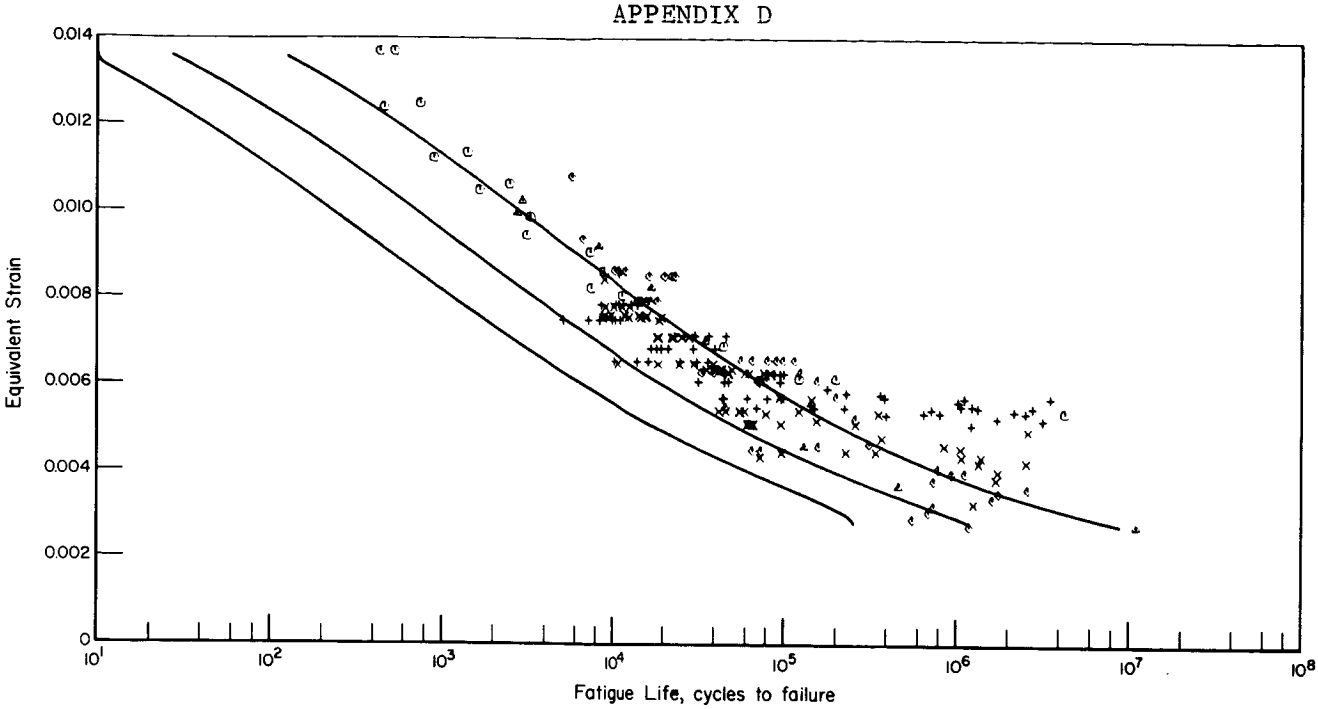

a. Consolidated fatigue data with mean curve and 90 and 99 percent survival lines.

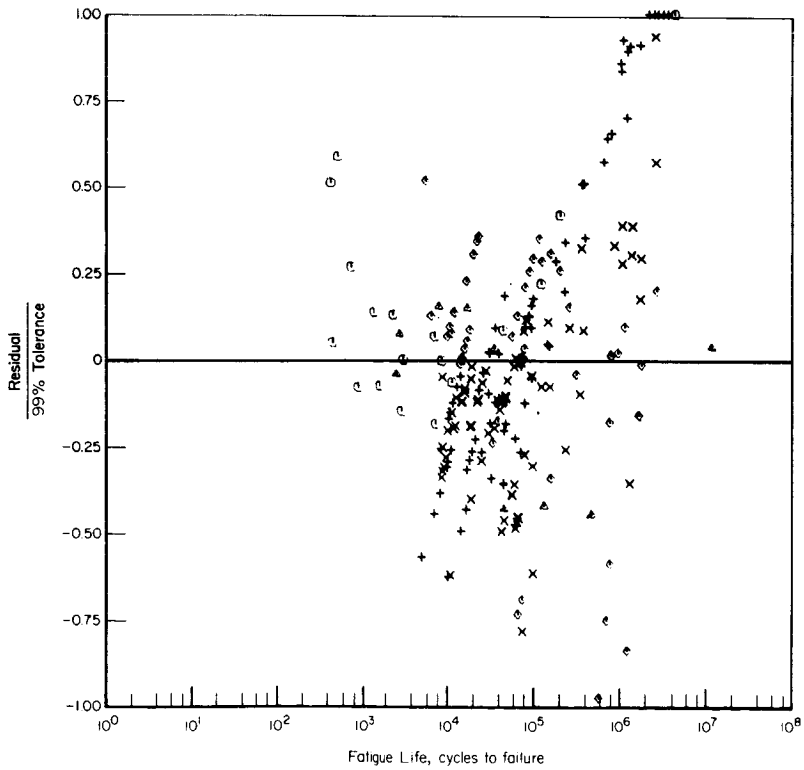

b. Distribution of weighted residuals.

Figure D11. – 300M Billet and forging (notched).

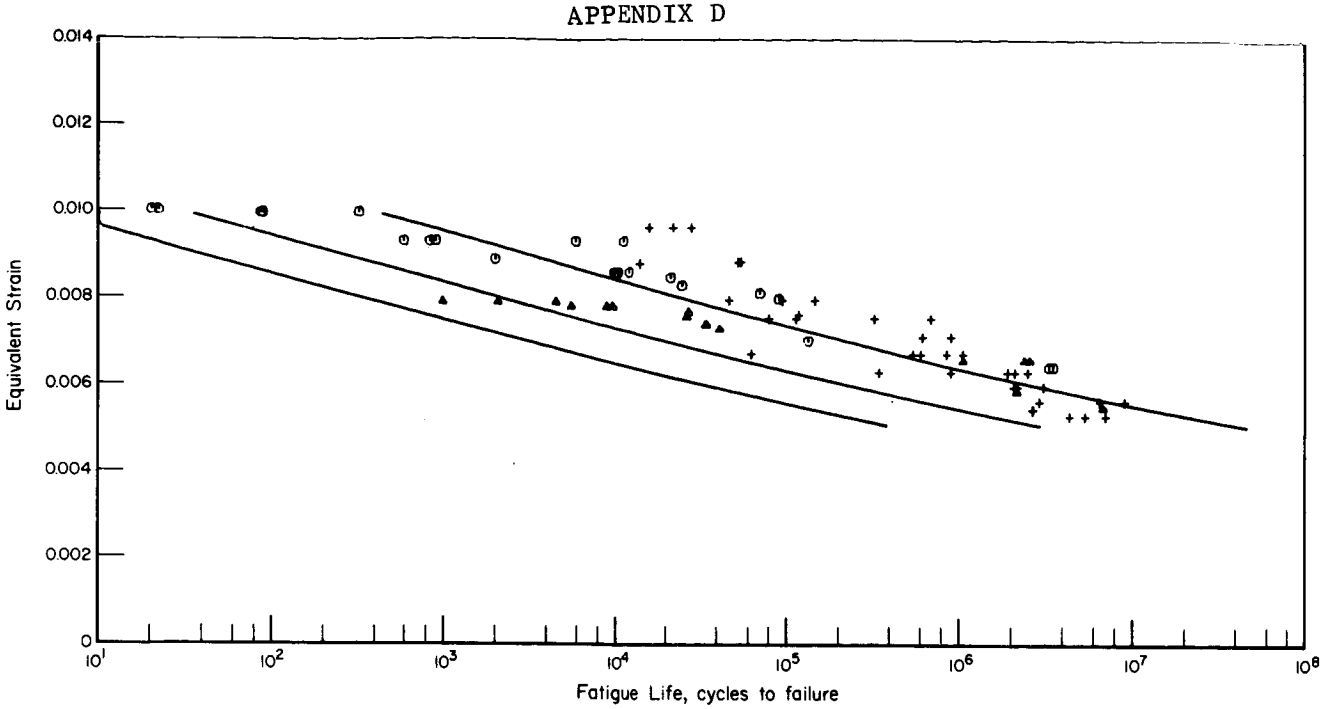

a. Consolidated fatigue data with mean curve and 90 and 99 percent survival lines.

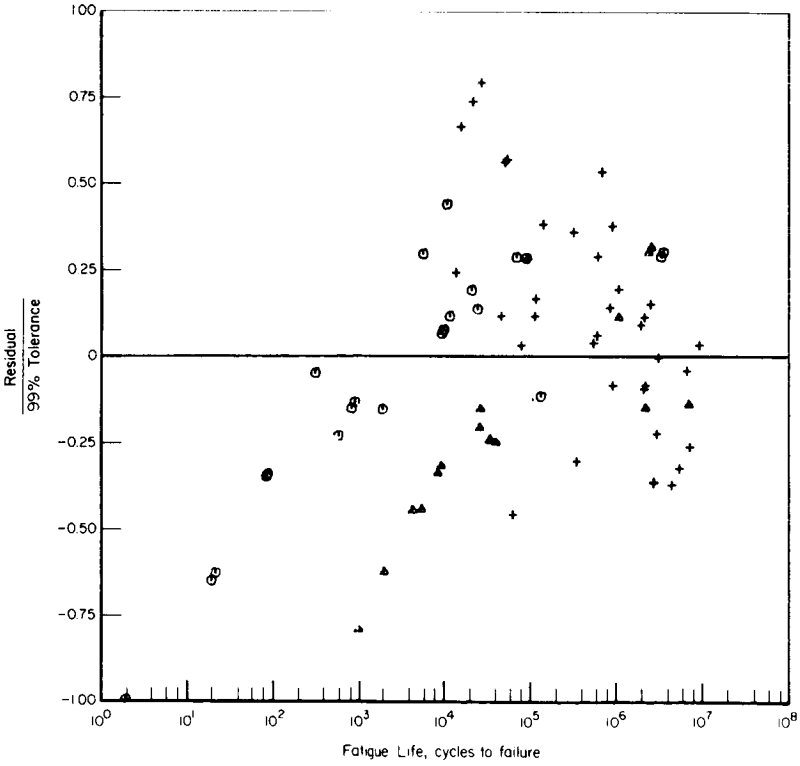

b. Distribution of weighted residuals.

Figure D12. – Annealed Ti-6Al-4V sheet (unnotched).

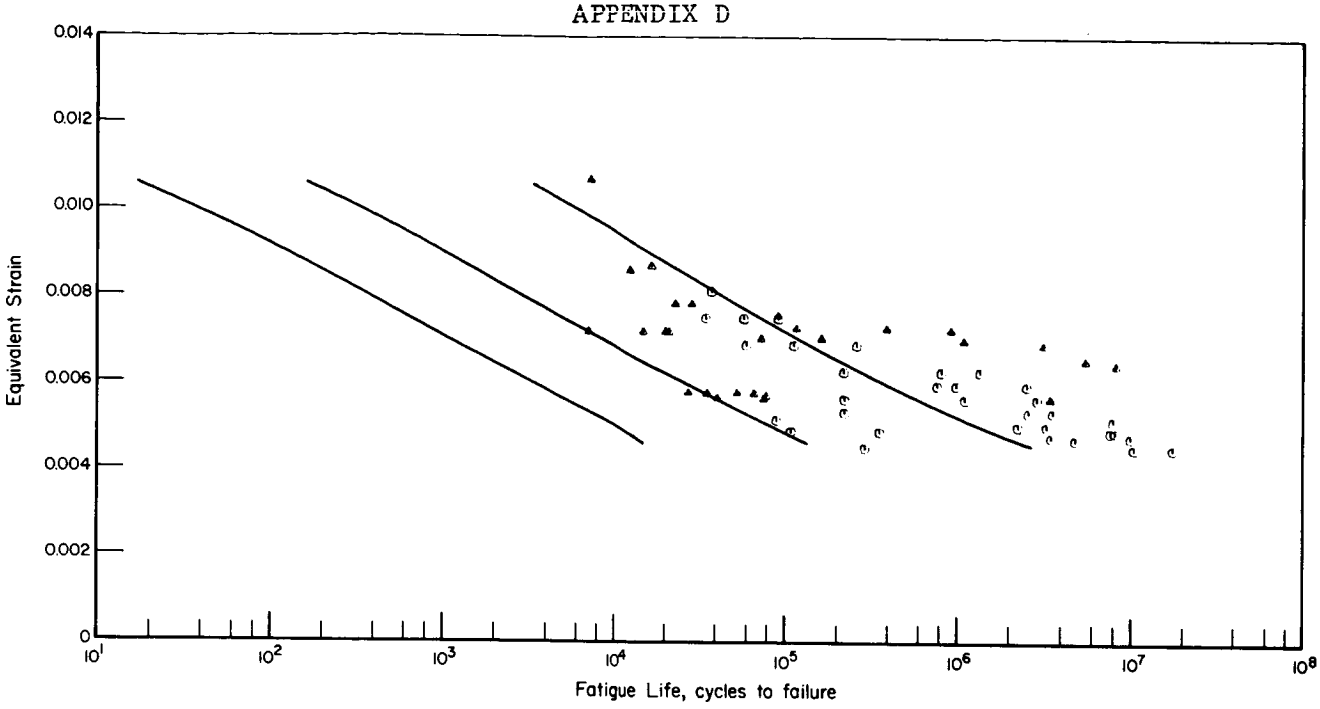

a. Consolidated fatigue data with mean curve and 90 and 99 percent survival lines.

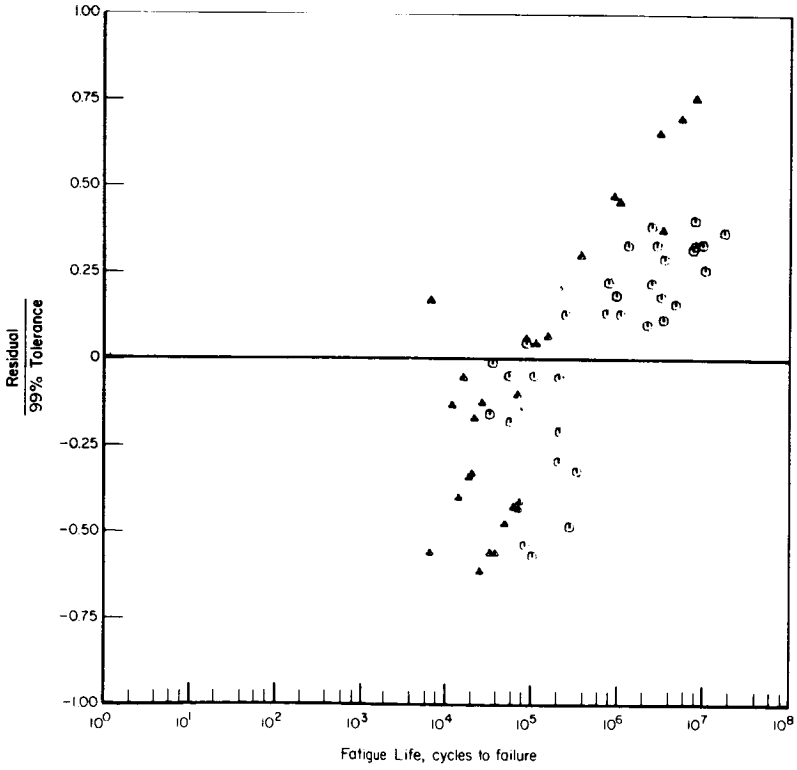

b. Distribution of weighted residuals.

Figure D13. – Annealed Ti-6Al-4V bar and extrusion [125 ksi TYS (unnotched)].

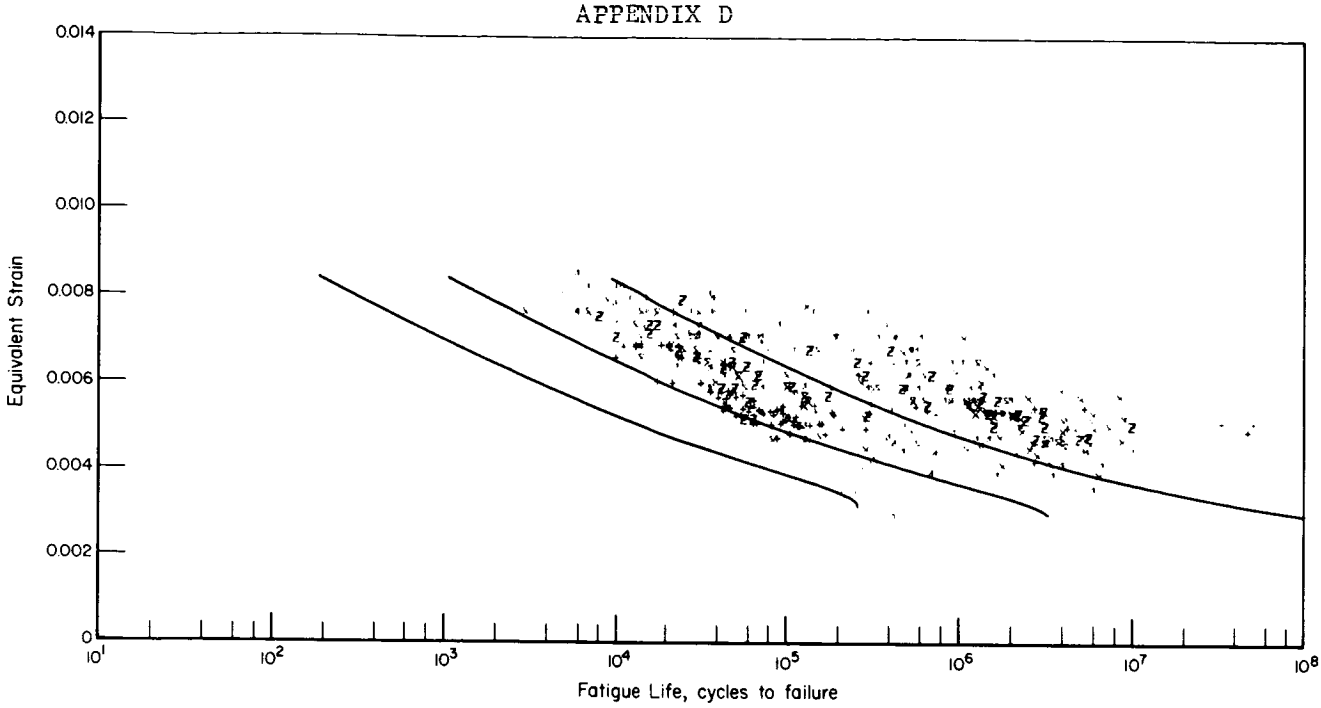

a. Consolidated fatigue data with mean curve and 90 and 99 percent survival lines.

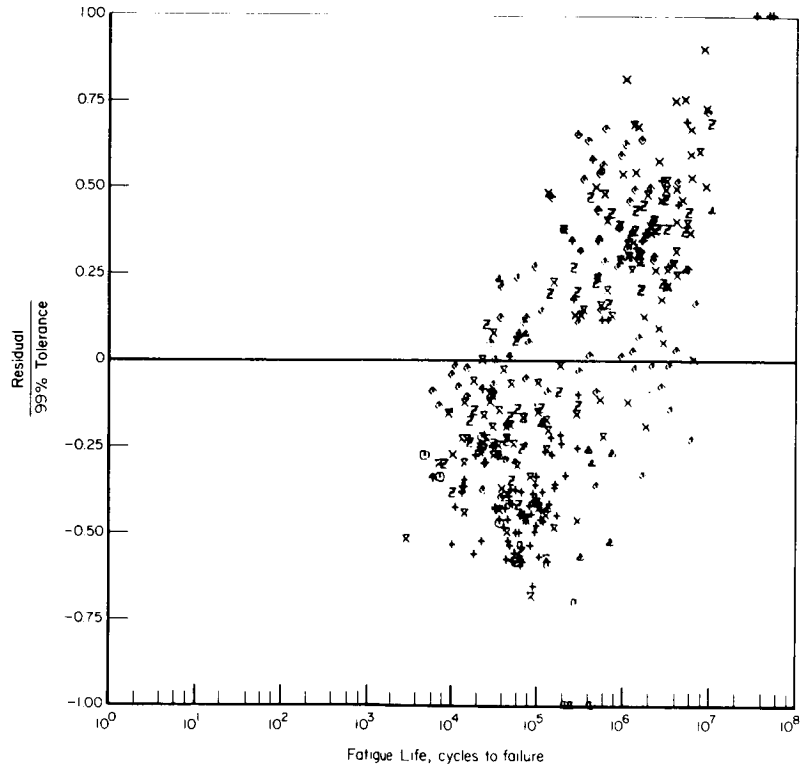

b. Distribution of weighted residuals.

Figure D14. – Annealed Ti-6Al-4V bar, extrusion, and forging [140 ksi TYS (unnotched)].

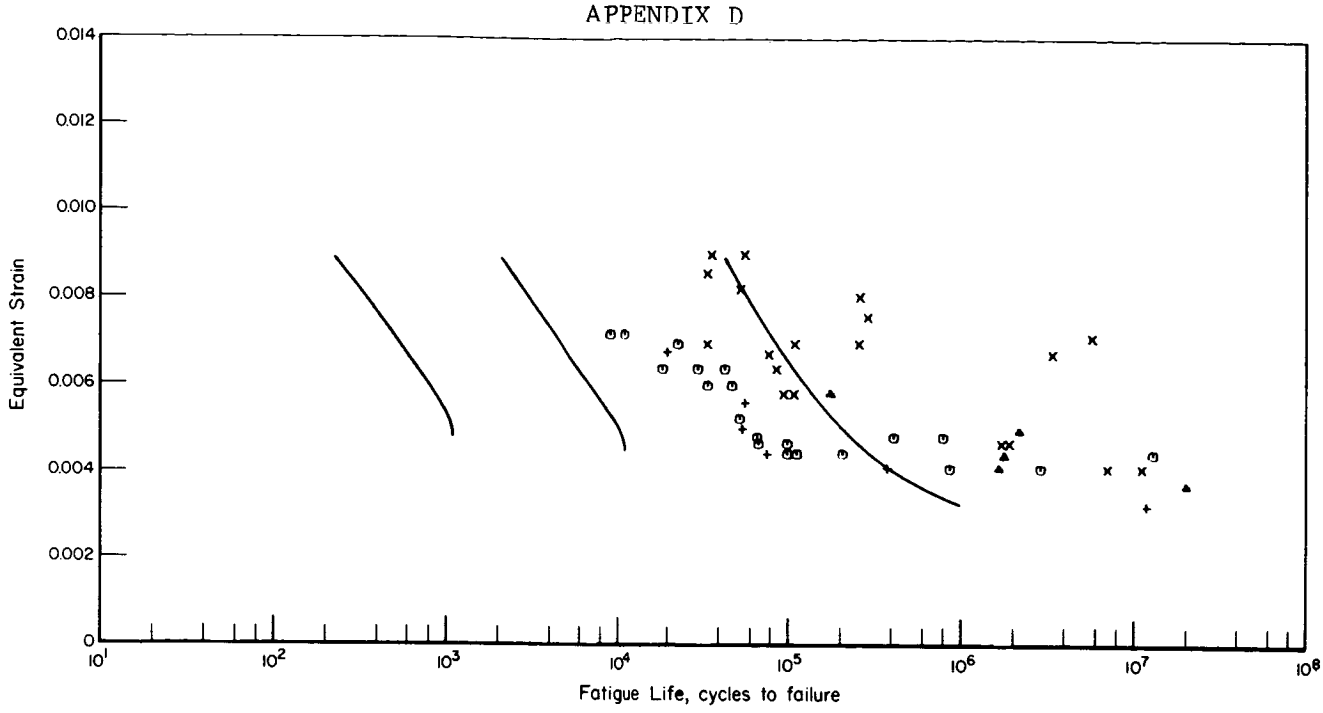

a. Consolidated fatigue data with mean curve and 90 and 99 percent survival lines.

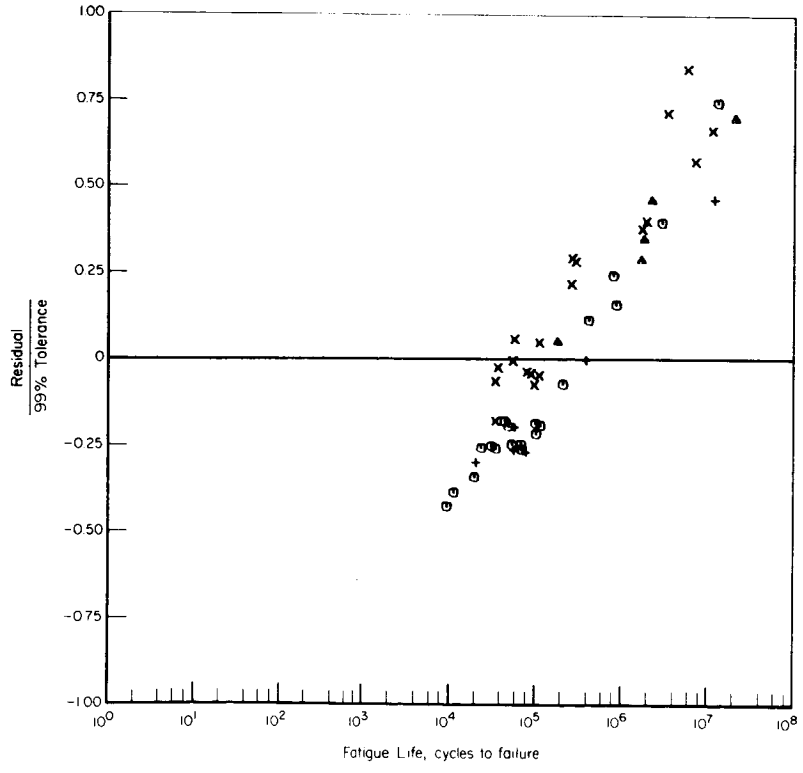

b. Distribution of weighted residuals.

Figure D15. – Annealed Ti-6Al-4V casting (unnotched).

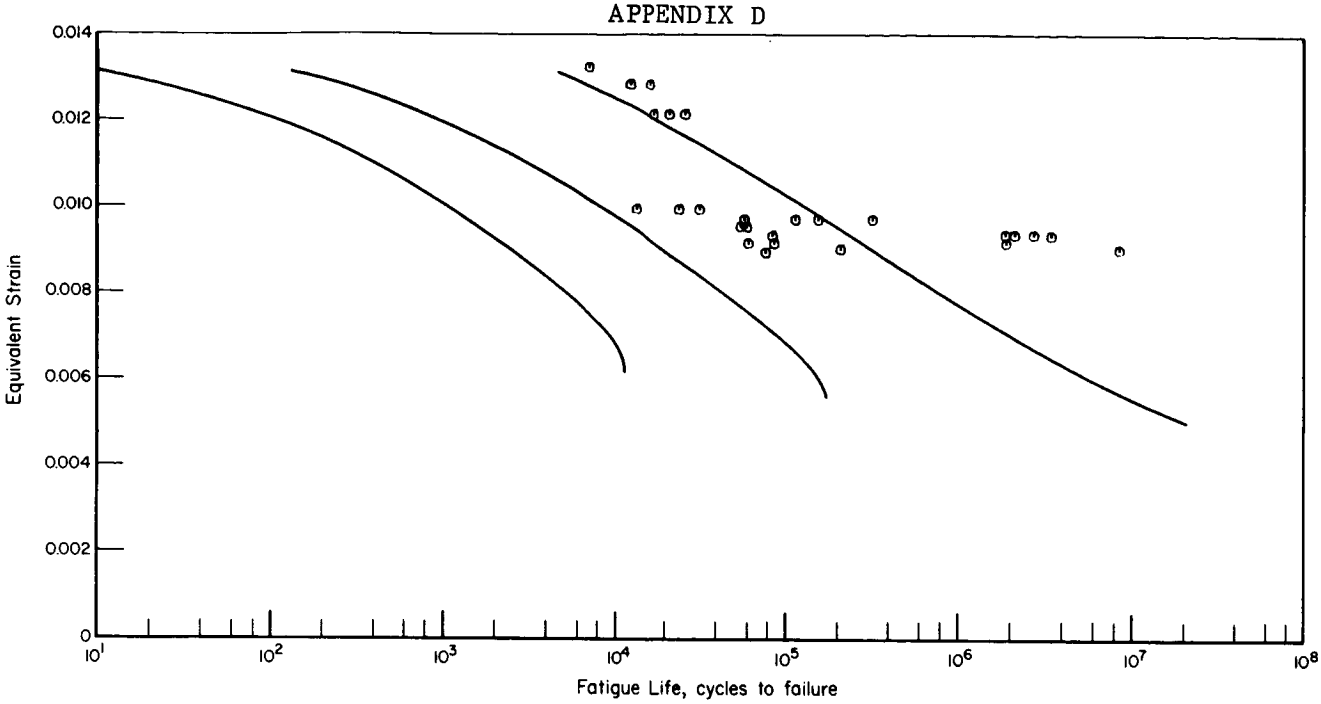

a. Consolidated fatigue data with mean curve and 90 and 99 percent survival lines.

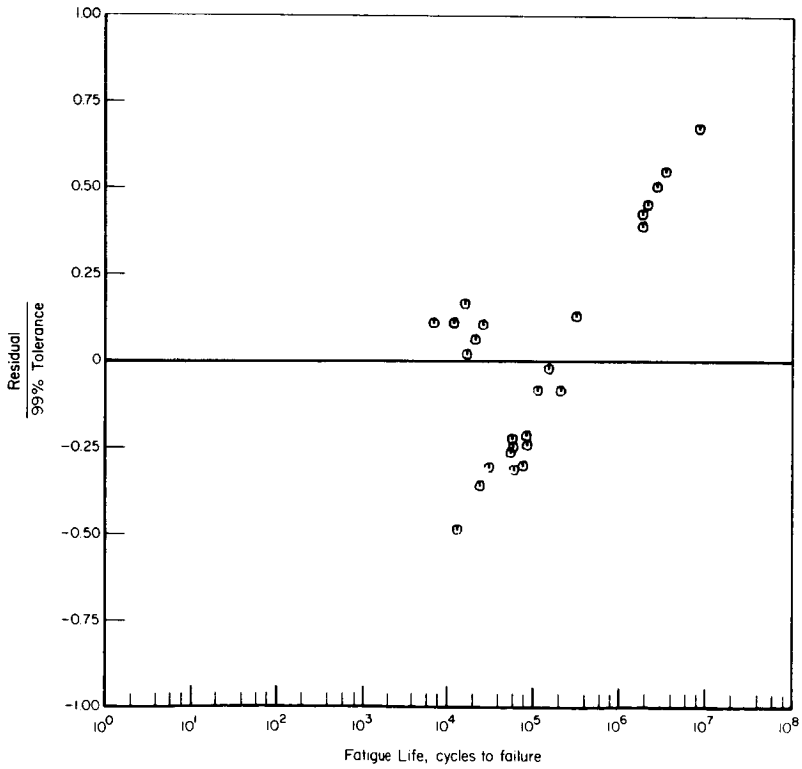

b. Distribution of weighted residuals.

Figure D16. – Annealed Ti-6Al-4V sheet (notched).

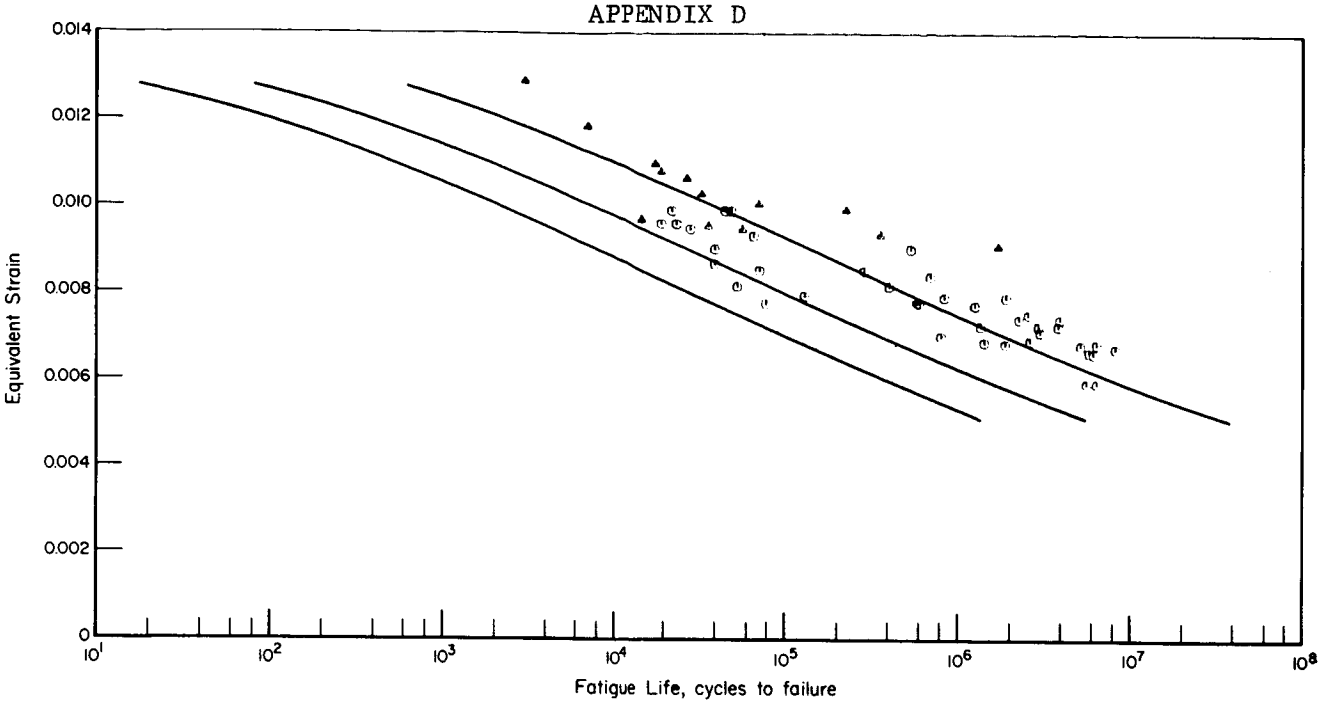

a. Consolidated fatigue data with mean curve and 90 and 99 percent survival lines.

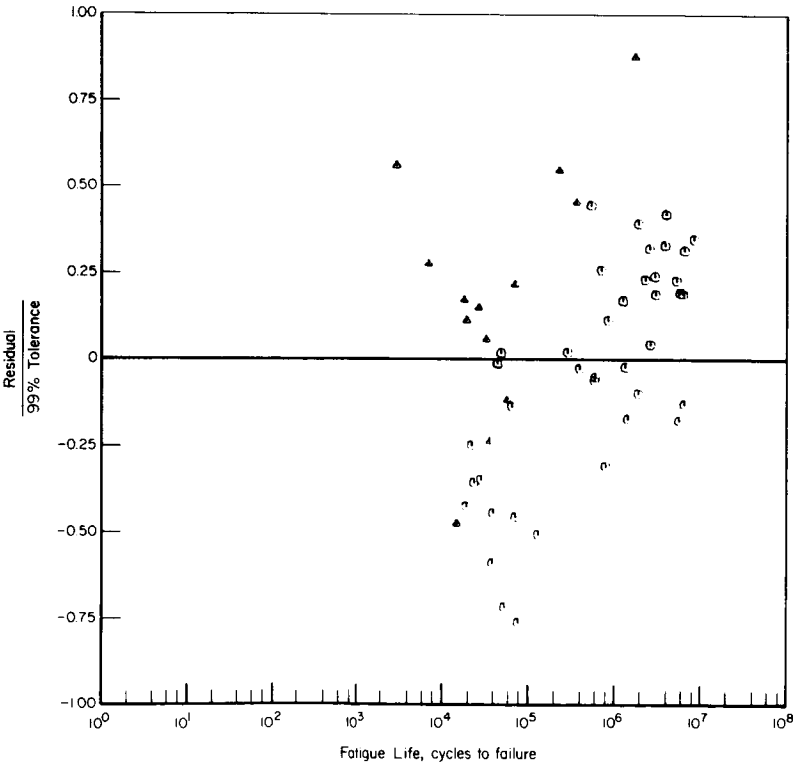

b. Distribution of weighted residuals.

Figure D17. – Annealed Ti-6Al-4V bar and extrusion [125 ksi TYS (notched)].

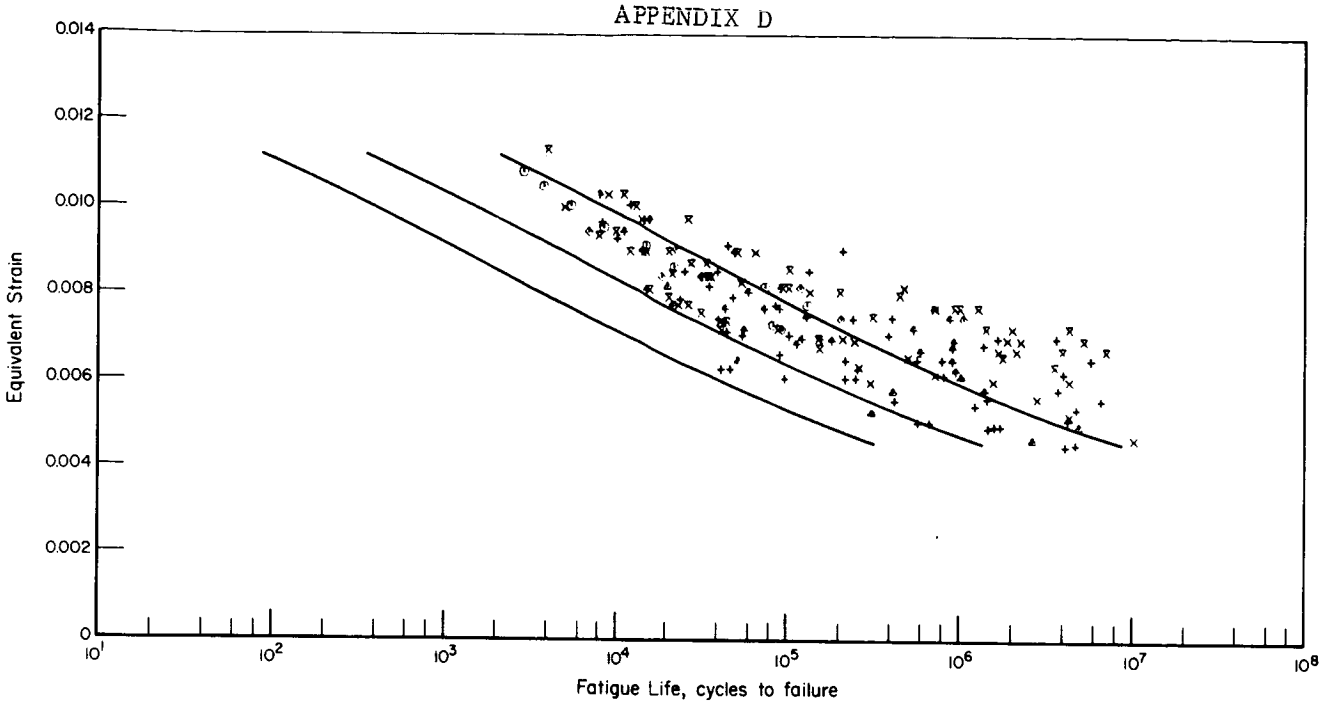

a. Consolidated fatigue data with mean curve and 90 and 99 percent survival lines.

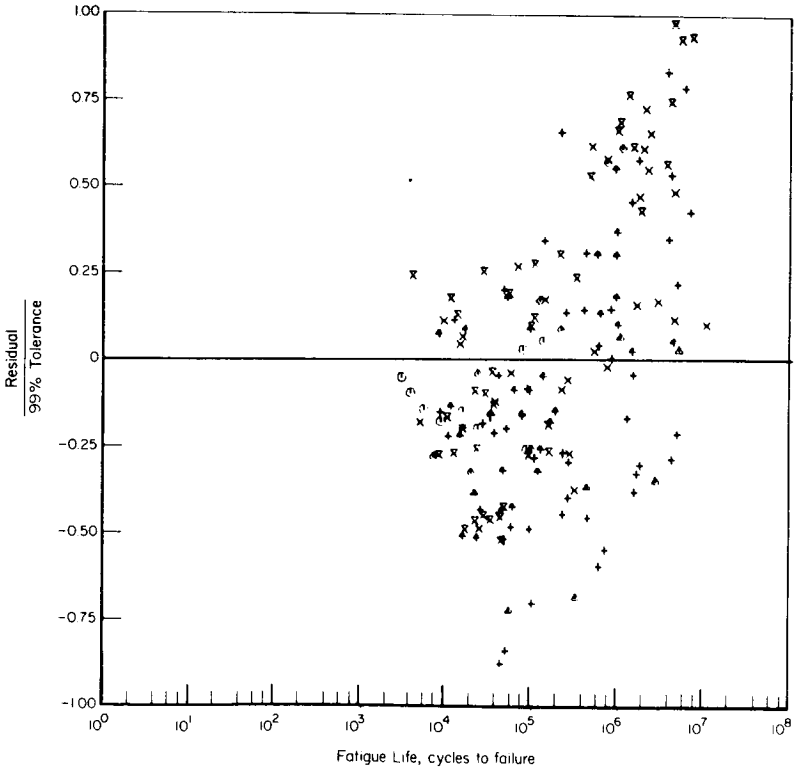

b. Distribution of weighted residuals.

Figure D18. — Annealed Ti-6Al-4V bar, extrusion, and forging [140 ksi TYS (notched)].

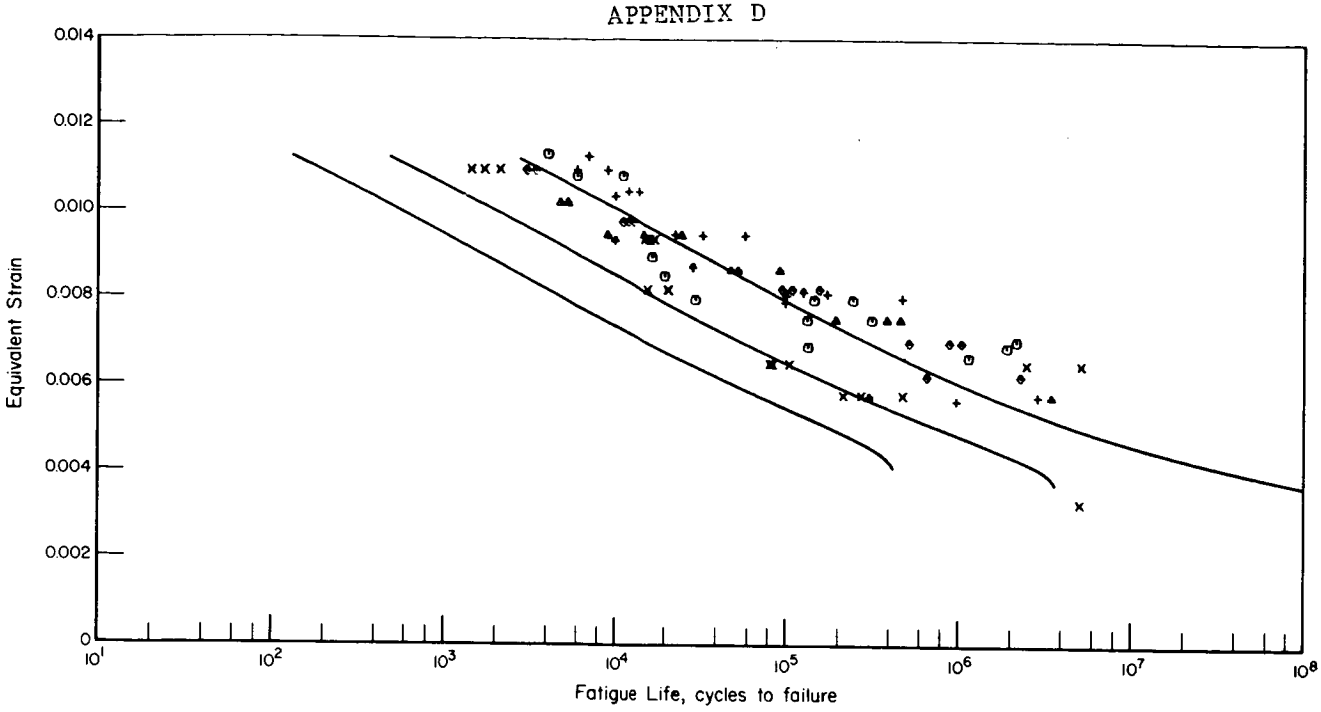

a. Consolidated fatigue data with mean curve and 90 and 99 percent survival lines.

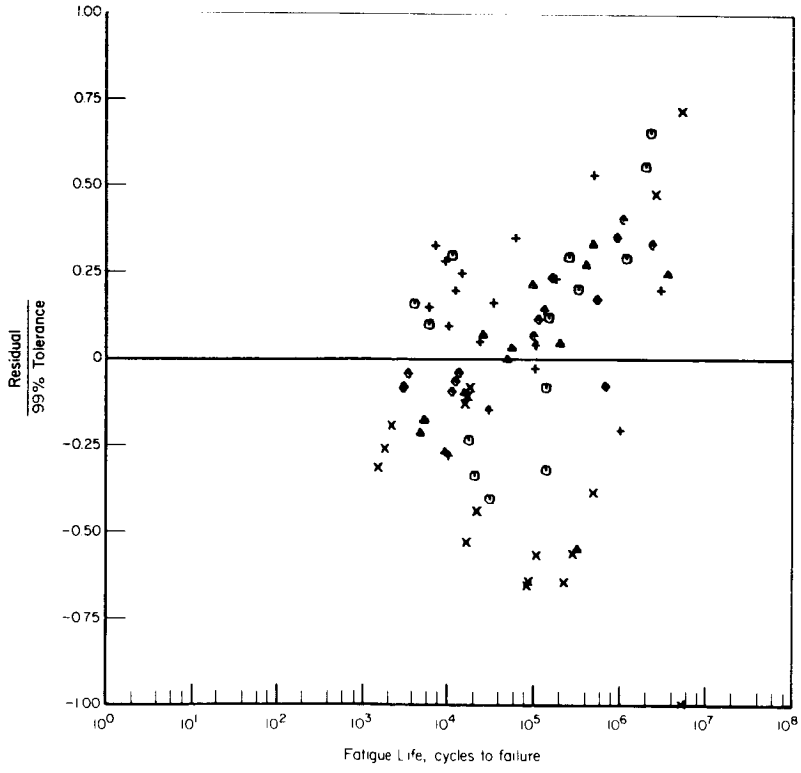

b. Distribution of weighted residuals.

Figure D19. – Annealed Ti-6Al-4V casting (notched).

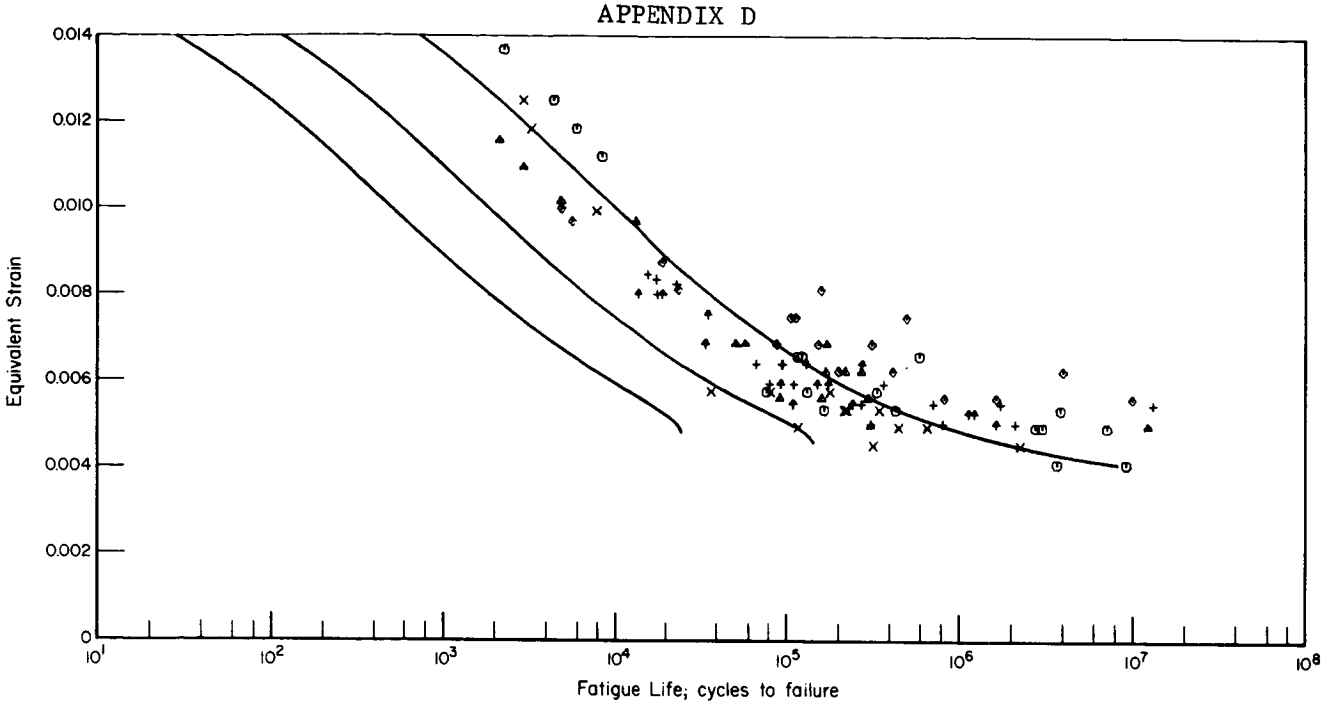

a. Consolidated fatigue data with mean curve and 90 and 99 percent survival lines.

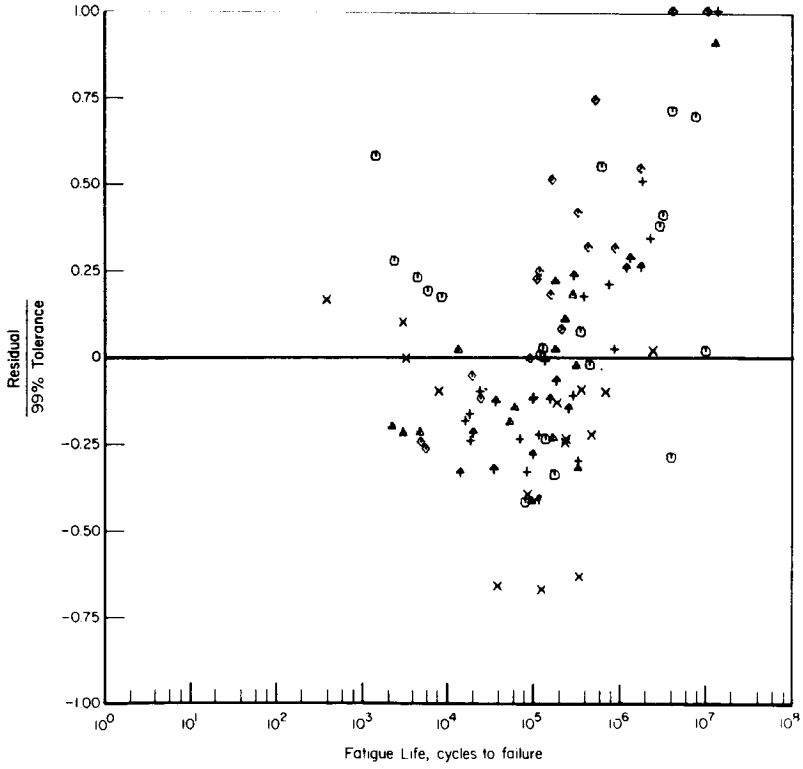

b. Distribution of weighted residuals.

Figure D20. — STA Ti-6Al-4V sheet (unnotched).

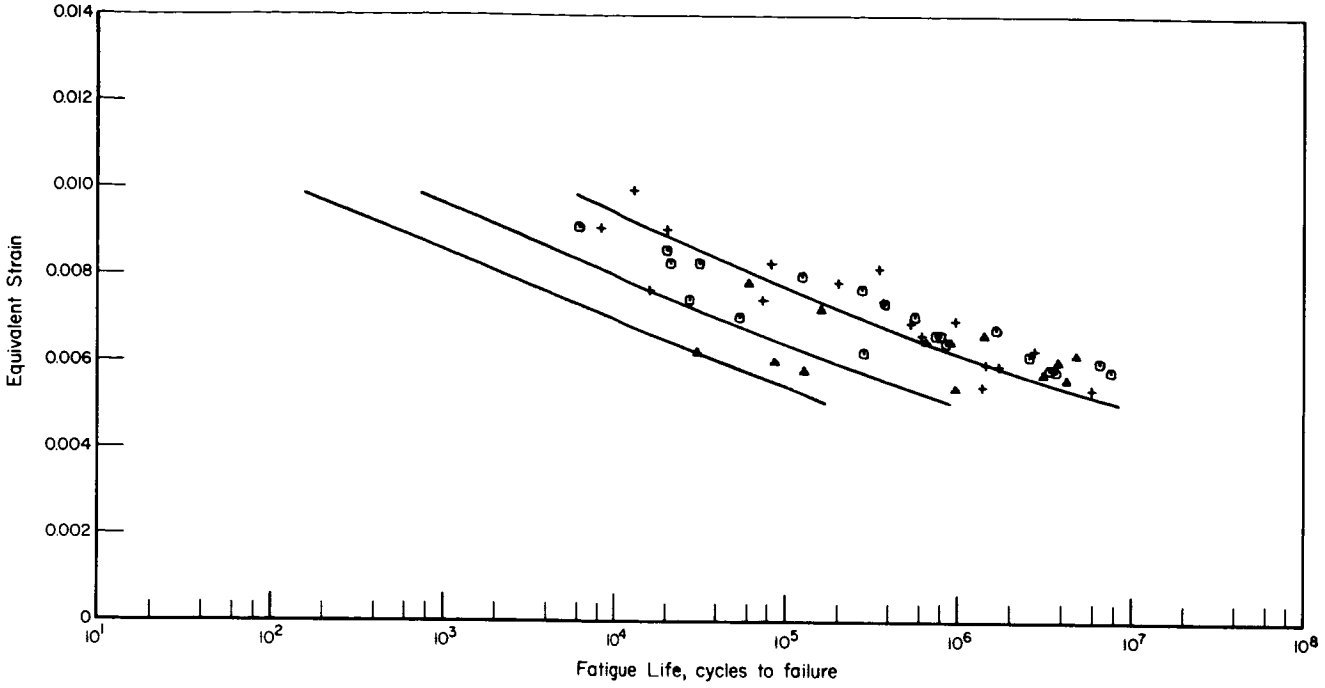

a. Consolidated fatigue data with mean curve and 90 and 99 percent survival lines.

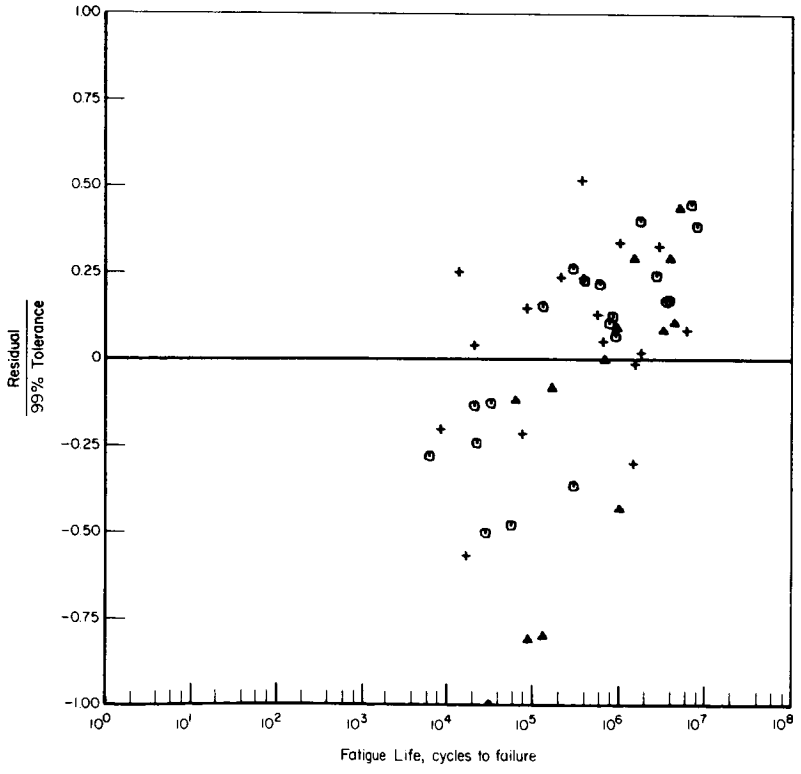

b. Distribution of weighted residuals.

Figure D21. – STA Ti-6Al-4V forging, casting, and plate (unnotched).

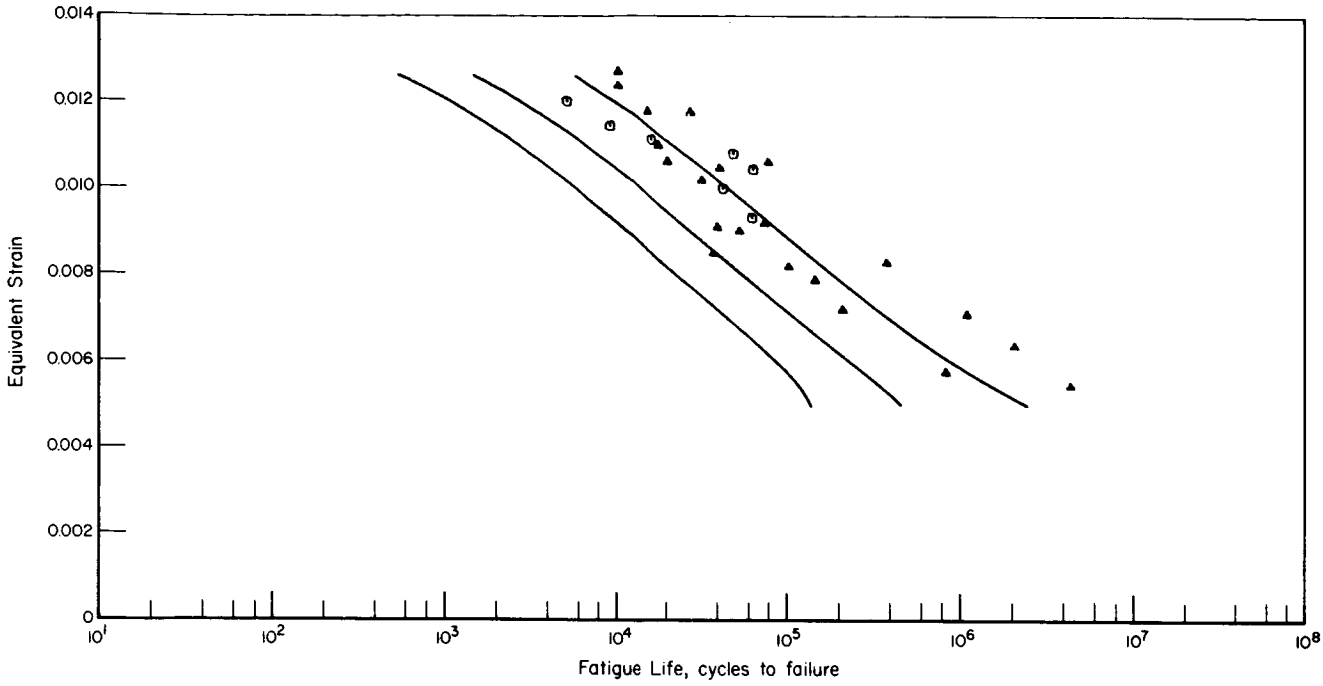

a. Consolidated fatigue data with mean curve and 90 and 99 percent survival lines.

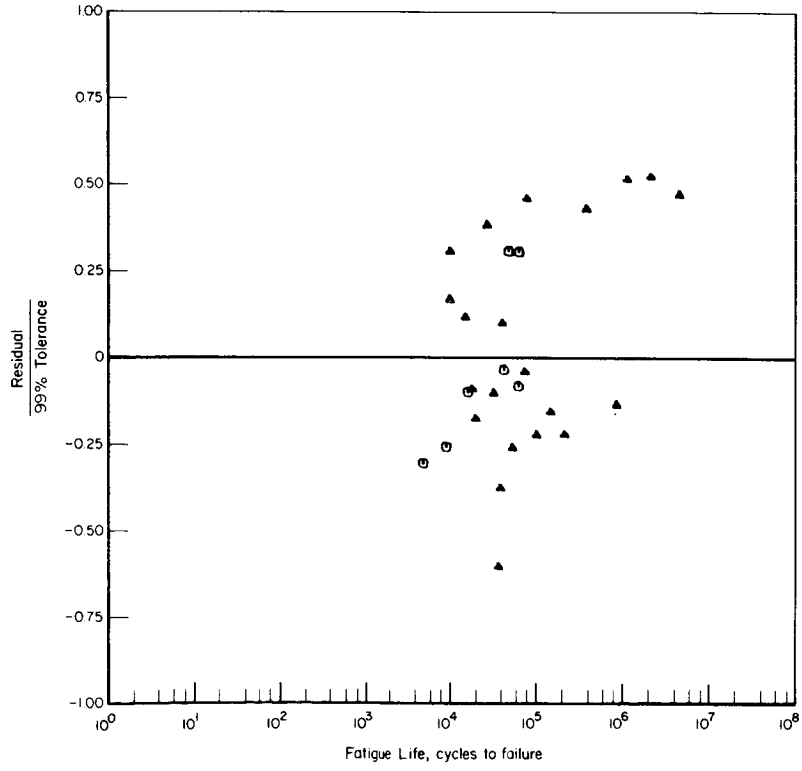

b. Distribution of weighted residuals.

Figure D22. – STA Ti-6Al-4V sheet (notched).

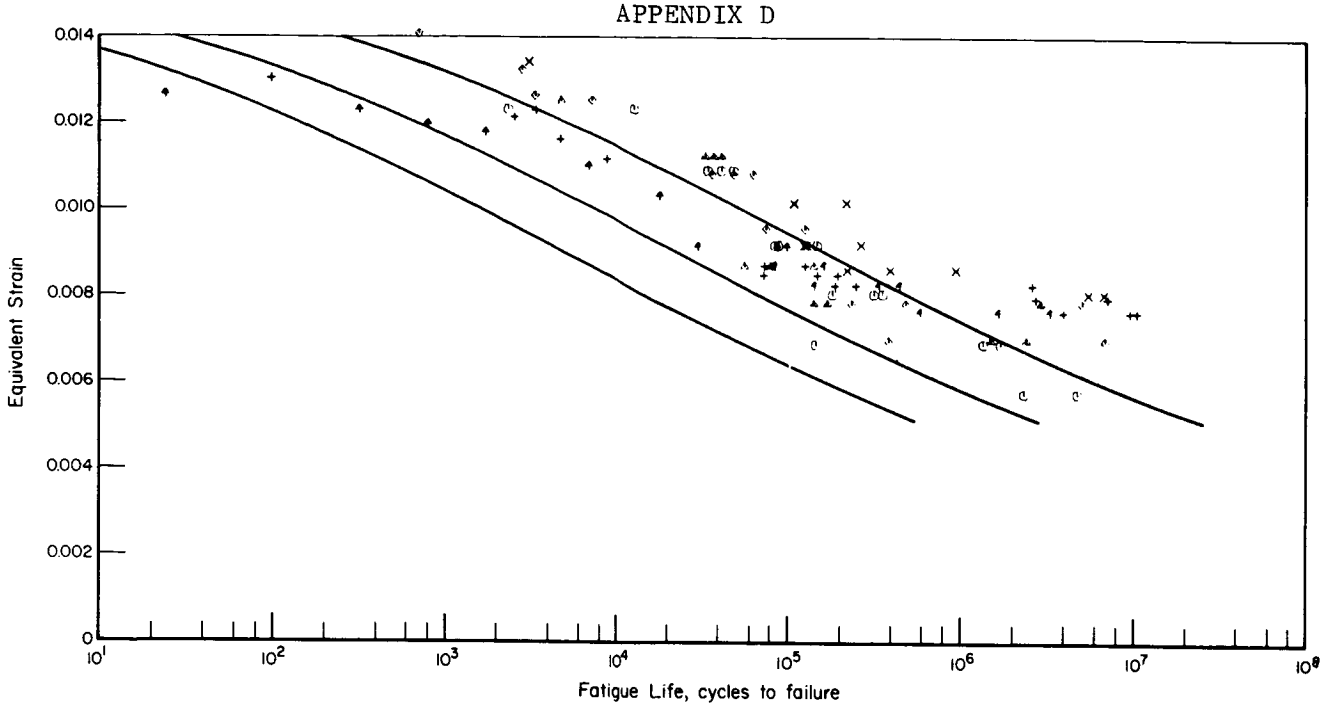

a. Consolidated fatigue data with mean curve and 90 and 99 percent survival lines.

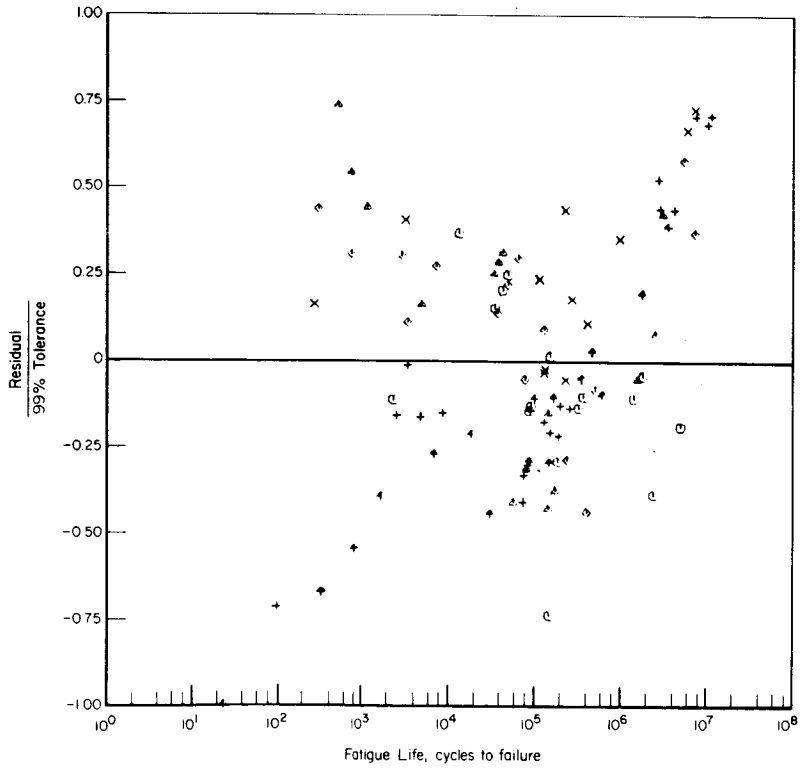

b. Distribution of weighted residuals.

Figure D23. – STA Ti-6Al-4V casting and plate (notched).

APPENDIX E

APPLICATION OF FATIGUE-CRACK-PROPAGATION RATE ANALYSIS

An actual structural element functioning in a real world environment is usually subjected to an extremely diverse loading spectrum. Large fluctuations in maximum stress, stress ratio, and frequency, not to mention temperature and environment, are likely to occur.

A crack extending in a structural element in such a loading environment will propagate in a complex manner. It is this highly complex situation that the designer must consider when structural life predictions are made. Clearly, some simplifications of the actual loading situation must be made for the purposes of analysis. Crack-growth-rate analysis is often used to predict life. Such an approach provides a model of the damage process by which cracks grow under constant-amplitude cyclic loading. Once the characteristic model for a material is obtained, it can be integrated to yield life predictions. Application of the rate analysis approach developed in the program is discussed briefly in this appendix.

Fatigue-Crack-Growth Rate Model

Previous discussions in the main body of this report have examined how crack-growth data can be converted to a crack-growth-rate format and subsequently represented by an analytical model of fatigue-crack propagation. Using this approach, data from a large number of sources, covering a wide range of parameters, can be combined to characterize a material quite thoroughly. As a result of this investigation, the inverse hyperbolic tangent model has been proposed as a suitable tool for data analyses.

Rate Integration

Once a satisfactory composition for the governing differential equation has been developed, the second part of the fatigue-crack-propagation problem, integration, becomes important. Some of the possible integration procedures are presented here in schematic form. However, implementation of these procedures was outside the scope of the present work. The general expression,

$$da/dN = f[K(a)] \quad , \tag{E1}$$

is a first order, linear differential equation. Although the fatigue-crack-propagation law is in the form of a rate equation, it is essential that the designer be able to calculate crack length for the case where a given number of cycles have been applied under specified loading conditions. This calculation can be accomplished by using the result of integrating equation (E1),

$$\int_{a_1}^{a_2} \frac{da}{f[K(a)]} = \int_{N_1}^{N_2} dN \quad . \tag{E2}$$

Mathematically speaking, this integration is representative of a class of solutions of differential equations known as "initial value problems". In other words, it is desired to find the final crack length after a certain number of cycles have elapsed, starting from initial values for crack length and cycle number.

Two general methods of solution of the initial value problem are available. The first, and most straightforward method consists of carrying out the integration indicated in equation (E2) to yield a closed-form solution. The closed-form solution has the advantage of being a concise equation from which the number of cycles required for a crack to grow to a given length is easily computed. Unfortunately, it is not always easy, or even possible, to perform the integration of the differential equation. The second method of solution involves the use of a numerical integration scheme such as the Runge-Kutta method.

Hoskin (ref. 30) gives some closed-form soltuions to the most common fatigue-crack-propagation models where the variables can be readily separated and integrated. Consider, for example, Paris' Law,

$$da/dN = C(\Delta K)^{n'} \quad . \tag{E3}$$

Assuming $K_{max} = S_{max}\sqrt{\pi a}$ for the case of center-cracks where width effects are negligible, the integration for $n' \geq 2$ is given as

$$N = \frac{\left[1 - \left(\frac{a_i}{a}\right)^{\frac{n'}{2}-1}\right]}{\left[S_{max}\,\pi^{\frac{1}{2}}(1-R)\right]^{n'}\left(\frac{n'}{2}-1\right)\left(a_i^{\frac{n'}{2}-1}\right)} \quad . \tag{E4}$$

APPENDIX E

A similar procedure may be carried out for the Forman-model differential equation,

$$da/dN = \frac{C(\Delta K)^{n'}}{(1-R)(K_c - K_{max})} \quad , \tag{E5}$$

yields for $n' > 3$

$$N = \frac{2}{C\left[S_{max}\,\pi^{\frac{1}{2}}(1-R)\right]^{n'-1}\left[a_i^{(n'-3)/2}\right]}\left[\frac{(a_c/a_i)^{\frac{1}{2}}}{(n'-2)}\left\{1-(a_i/a)^{\frac{n'}{2}-1}\right\} - \frac{1}{(n'-3)}\left\{1-\frac{a_i^{(n'-3/2)}}{a}\right\}\right] . \tag{E6}$$

When the K expression involves more complex algebraic or transcendental functions for which a closed form solution often cannot be achieved. Such is the case when width effects are not negligible. For example, when a width correction factor term is used, the expression for K_{max} becomes

$$K_{max} = S_{max}\sqrt{\pi a \sec\left(\frac{\pi a}{w}\right)} \quad , \tag{E7}$$

and the integration is much more complex.

The alternative to closed-form solution of equation (E2) is numerical integration, which necessitates the use of a digital computer. Engle (ref. 38) for example, utilized the Runge-Kutta numerical integration scheme in Program CRACKS (which, incidentally, accommodates variable-amplitude loads as well as the more elementary constant-amplitude cases). This is typical of the type of numerical solutions used today. Since the inverse hyperbolic tangent model has been based on the above form for K_{max}, equation (E7), the integration process becomes exceedingly complex. A closed-form integration of the model does not seem to be practical. However, the model may be integrated numerically. The expression may be put in the form,

$$N_2 - N_1 = 10^{-C_1} = \int_{a_1}^{a_2} 10^{-\left\{C_2 \ln\left[\frac{\log\frac{K_o}{K_c} + \log\left(\frac{K_o K_c}{(1-R)^{2m}\,S^2\,\pi a \sec \pi a/w}\right)}{\log\frac{K_o}{K_c} - \log\left(\frac{K_o K_c}{(1-R)^{2m}\,S^2\,\pi a \sec \pi a/w}\right)}\right]\right\}} da$$

which is suitable for numerical integration. Several integration schemes are directly applicable to this expression. These include iterated Gaussian quadratures as well as the Runge-Kutta method mentioned earlier.

Summary of the Life Prediction Procedure

The procedure for predicting the life of a structure, neglecting variable-amplitude loading effects is outlined below,

(1) Crack growth data on the material of interest is collected and combined.

(2) Crack growth data are converted to crack-growth-rate values by means of the five-point divided difference scheme. Values of K_{max} are calculated.

(3) The inverse hyperbolic tangent function is fitted to the data to yield regression and optimization coefficients, as well as statistical parameters.

(4) Initial and final crack lengths, the stress levels, and mean stresses for the structures to be investigated are specified. This information may be presented in the form of load spectrum.

(5) Finally, the values specified in item (4) are used to integrate the characteristic fatigue-crack-propagation model for the number of cycles required to extend the crack to the specified final crack length.

APPENDIX F

RESULTS OF FATIGUE-CRACK-PROPAGATION ANALYSIS FOR FIVE MATERIALS

Figures F1 through F10 present the results of analyses performed on 2024-T3, 7075-T6, and 7075-T7351 aluminum alloys, 300M steel, and Ti-6Al-4V alloy. The composition of these data sets was previously described in the report. (See pages 79 and 80.) Each material is characterized by a crack-growth-rate curve and an accompanying plot of the distribution of residuals as a function of actual crack propagation ate.

The crack-growth-rate curves consist of the experimental data plotted on a $K_{eff} = (1-R)^{m}K_{max}$ basis. The best-fit regression curve is represented by the solid central line through the data points. On either side of the mean curve are the 90 and 99 percent tolerance limits, with 95 percent level of confidence. Coefficients of the inverse hyperbolic tangent model and the tolerance limit formula were presented previously in Table 12.

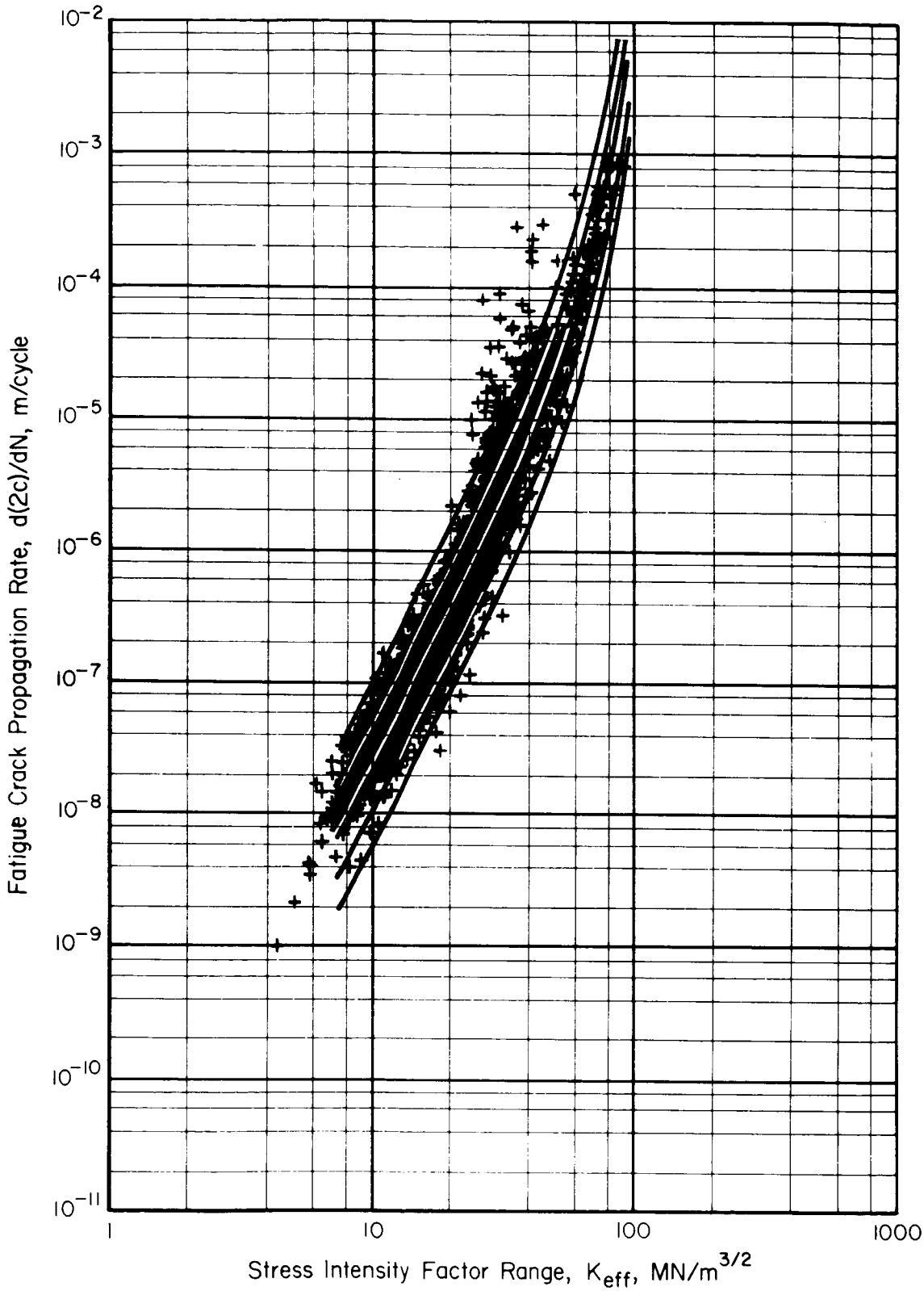

Figure F1. – Fatigue-crack-propagation-rate curve for 2024-T3 aluminum alloy

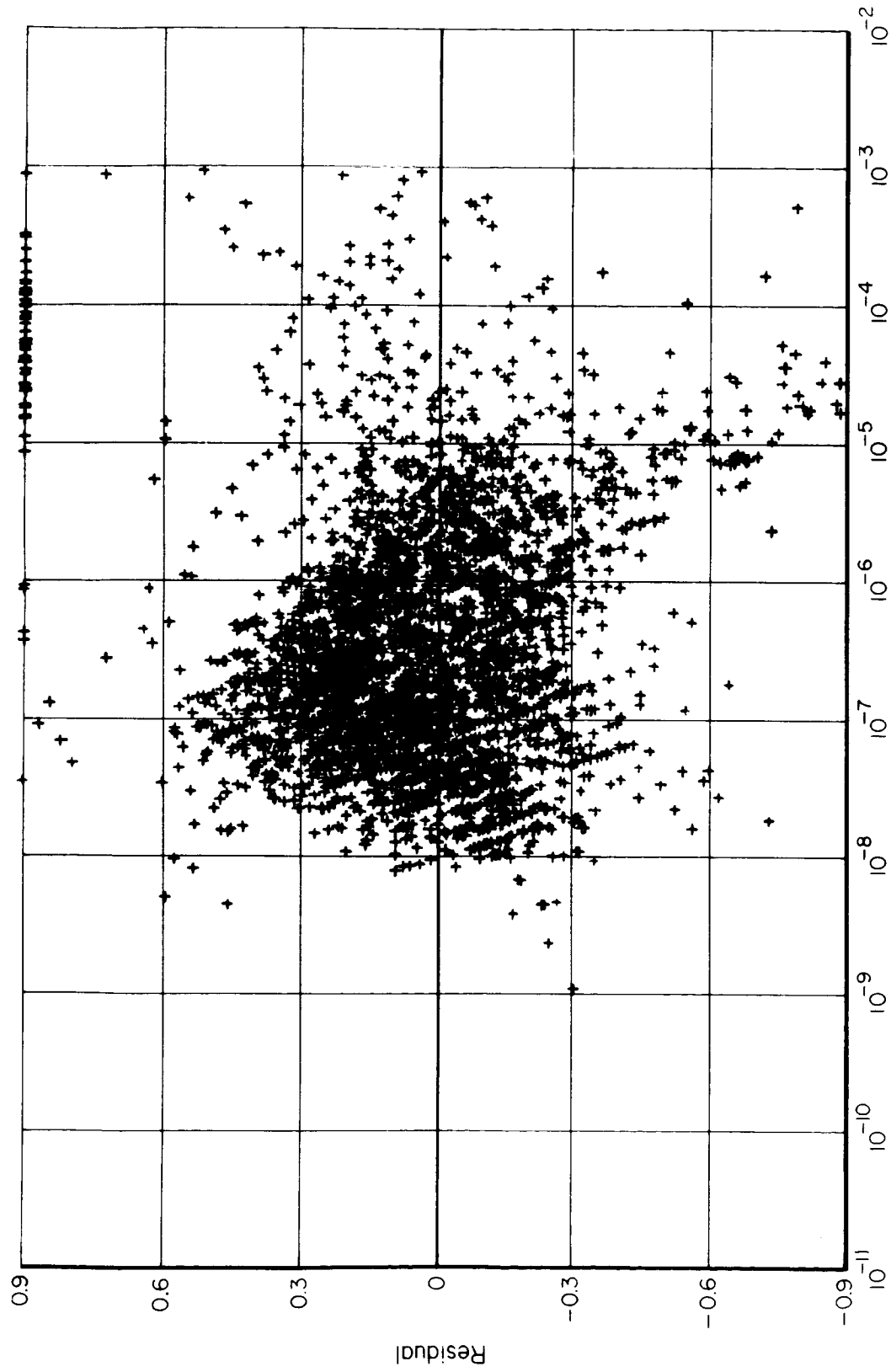

Figure F2. — Distribution of residuals for regression equation representing 2024-T3 aluminum alloy.

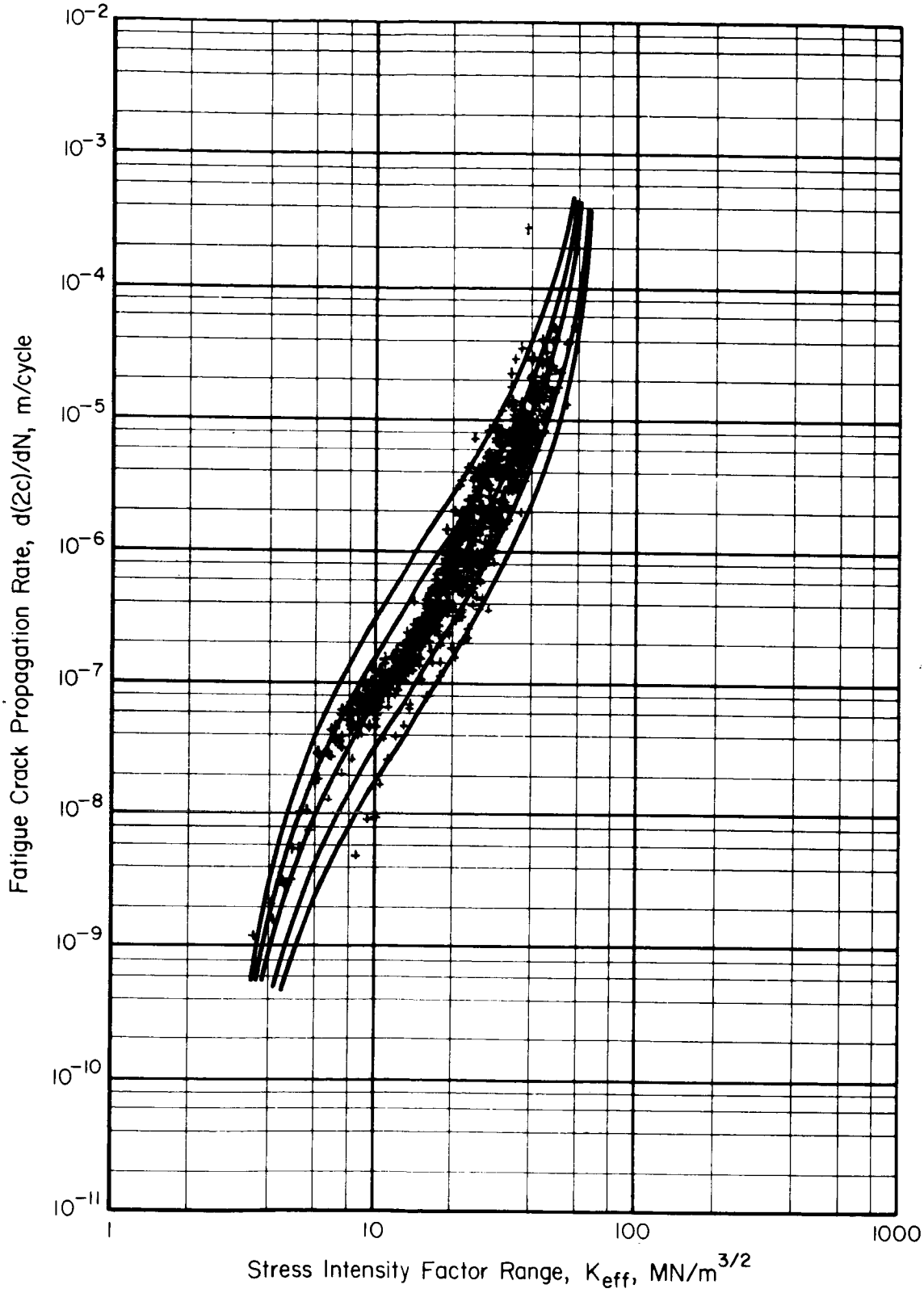

Figure F3.— Fatigue-crack-propagation-rate curve for 7075-T6 aluminum alloy.

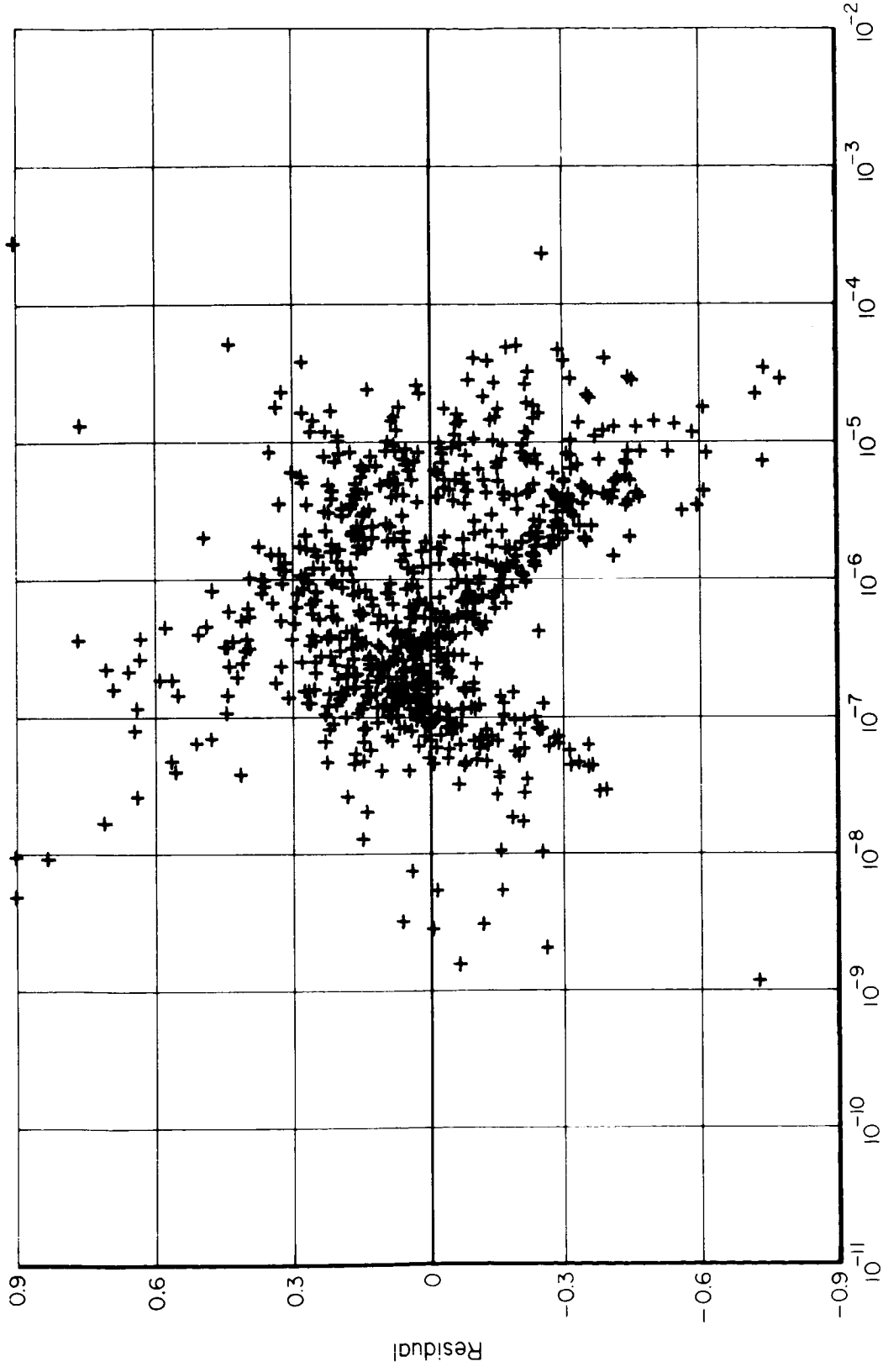

Figure F4. – Distribution of residuals for regression equation representing 7075-T6 aluminum alloy.

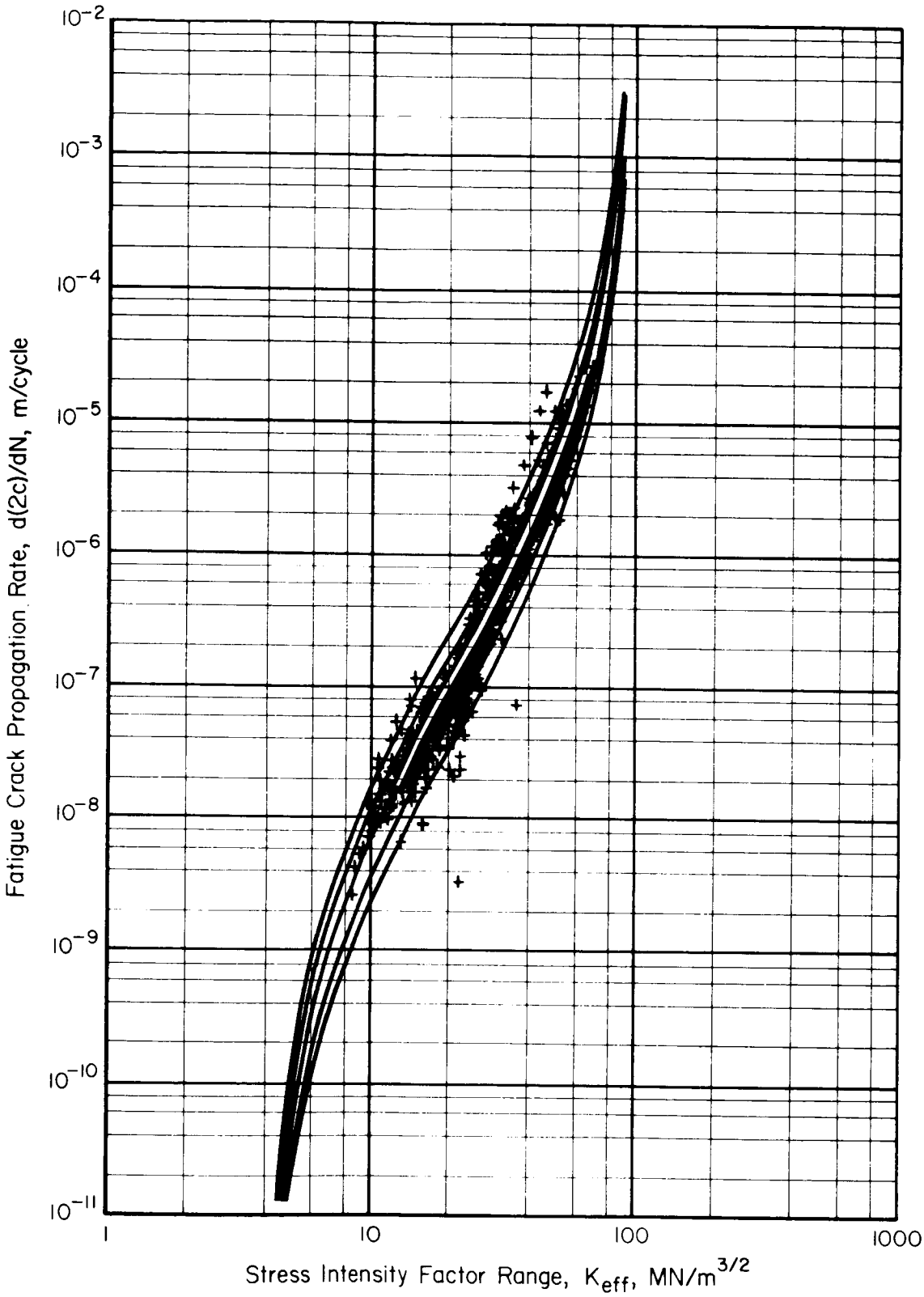

Figure F5. — Fatigue-crack-propagation-rate curve for 7075-T7351 aluminum alloy.

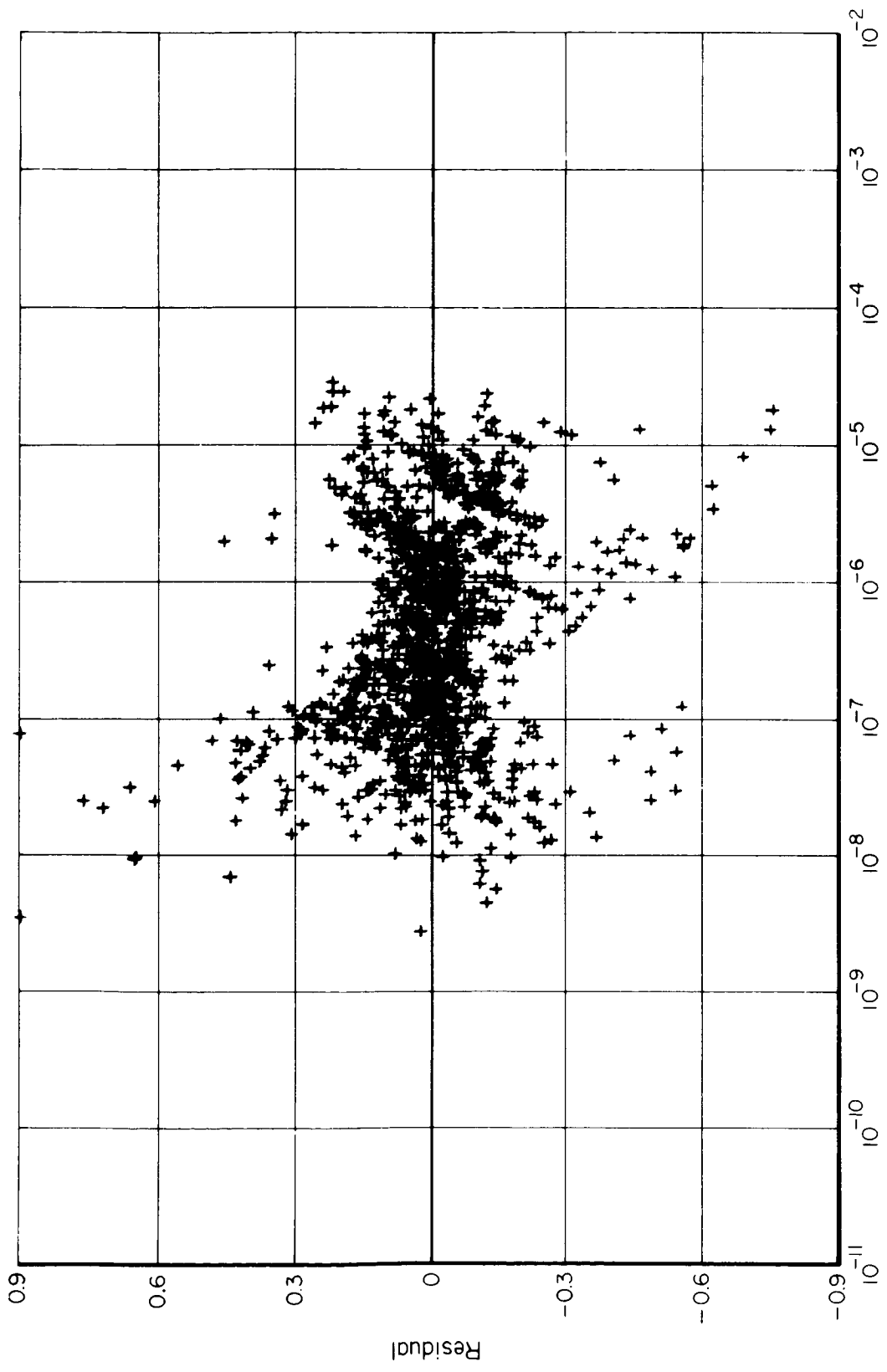

Figure F6. - Distribution of residuals for regression equation representing 7075-T7351 aluminum alloy.

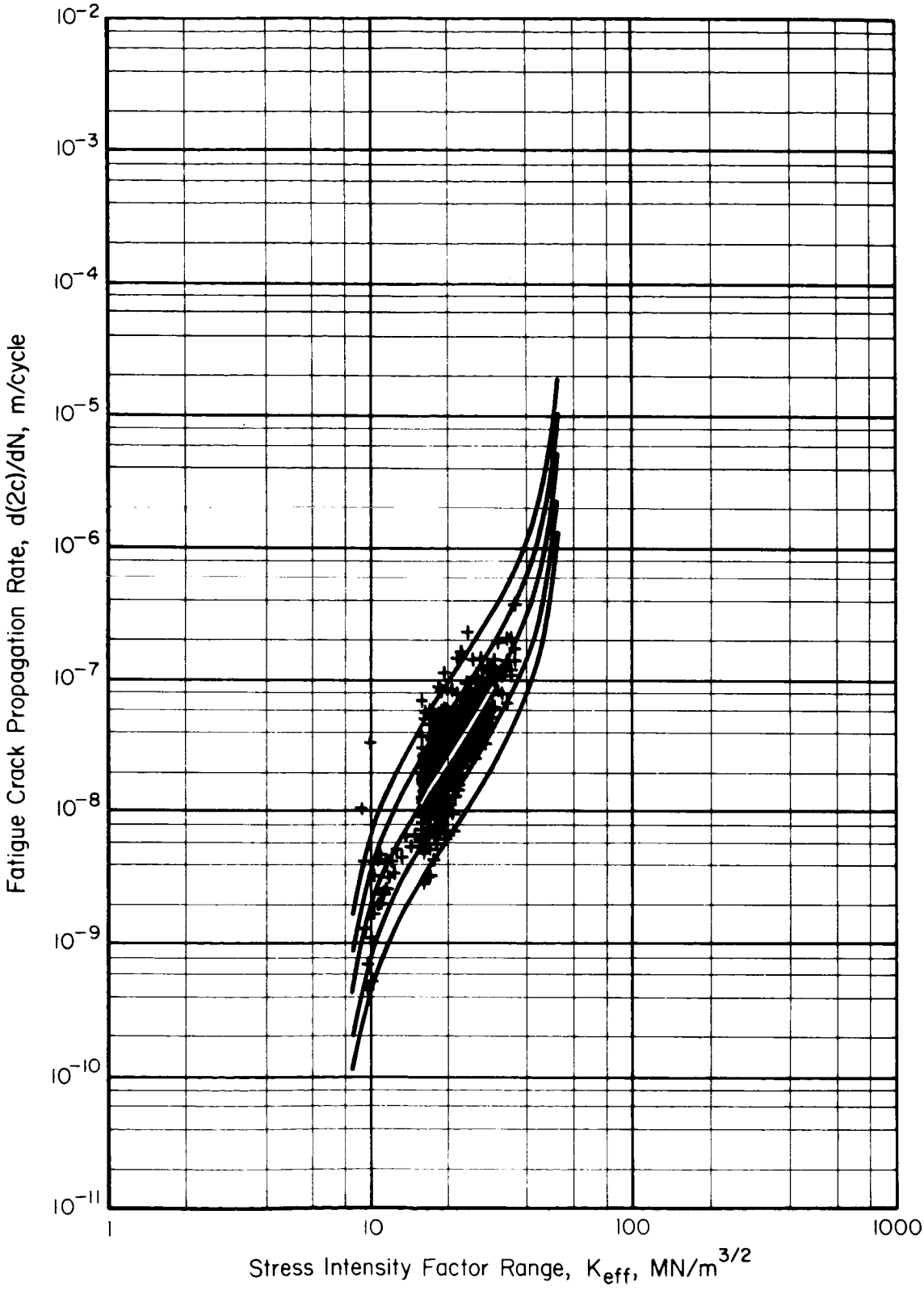

Figure F7.– Fatigue-crack-propagation-rate curve for 300M steel alloy.

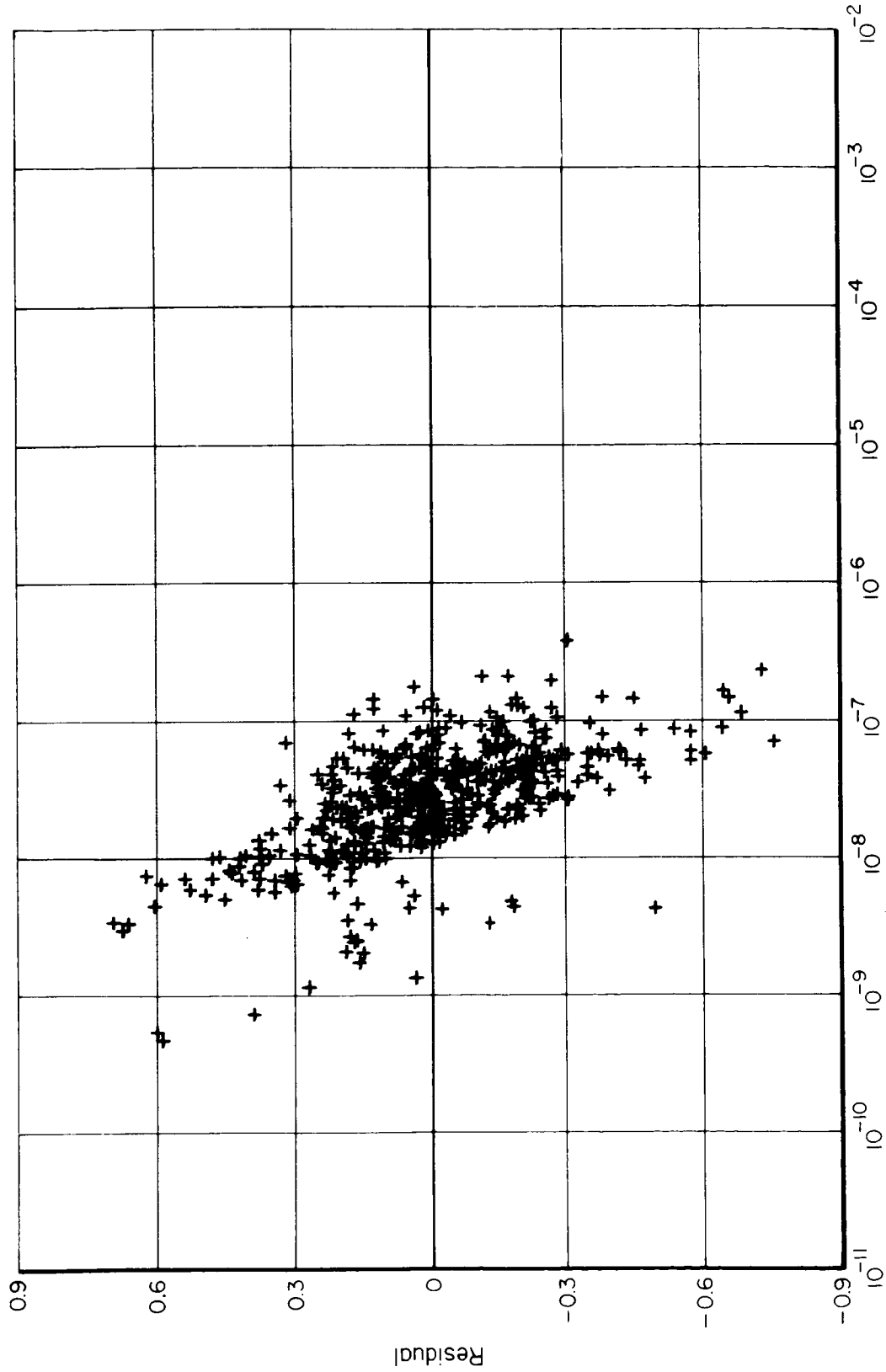

Figure F8. - Distribution of residuals for regression equation representing 300M steel alloy.

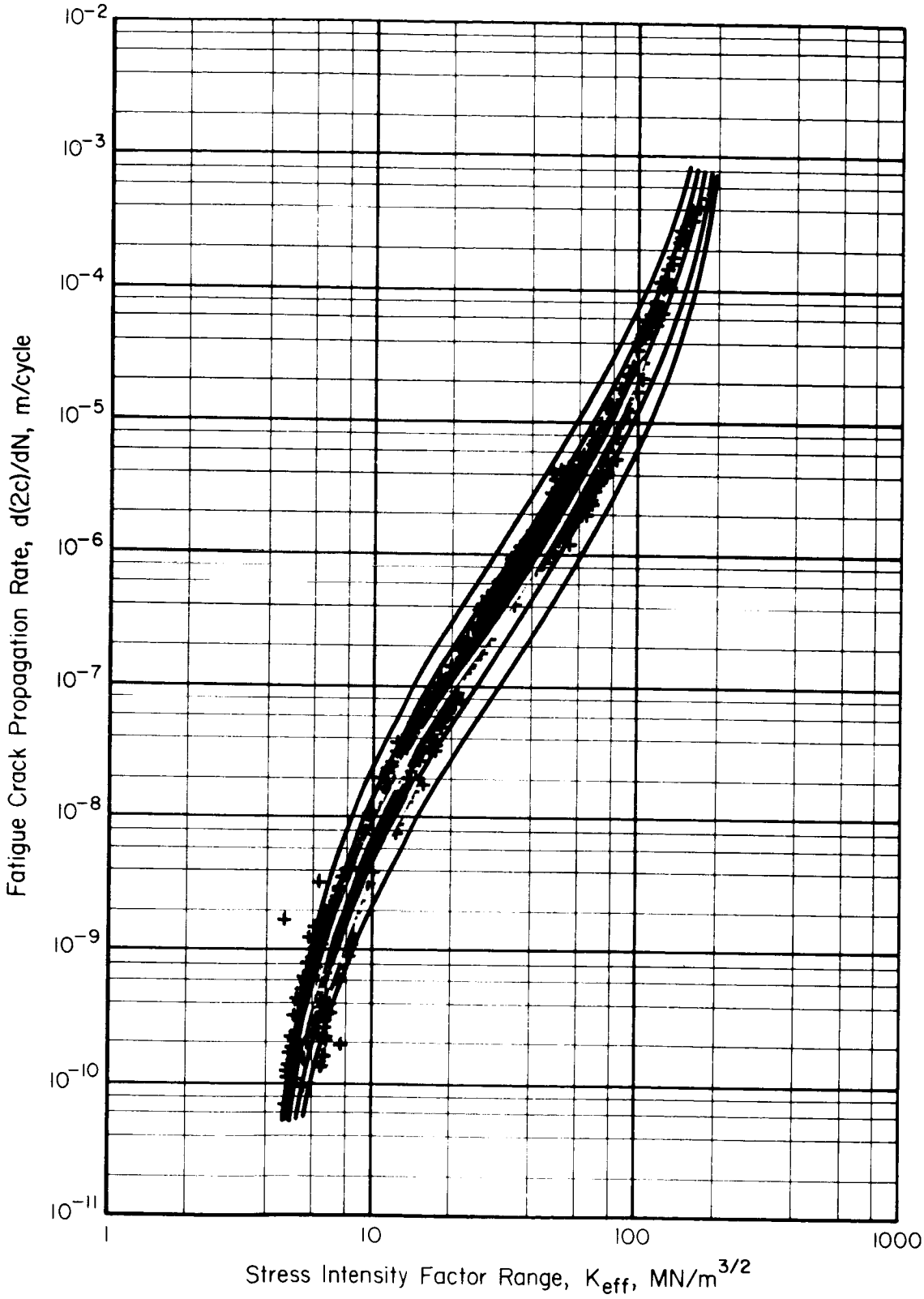

Figure F9. — Fatigue-crack-propagation-rate curve for Ti-6Al-4V alloy.

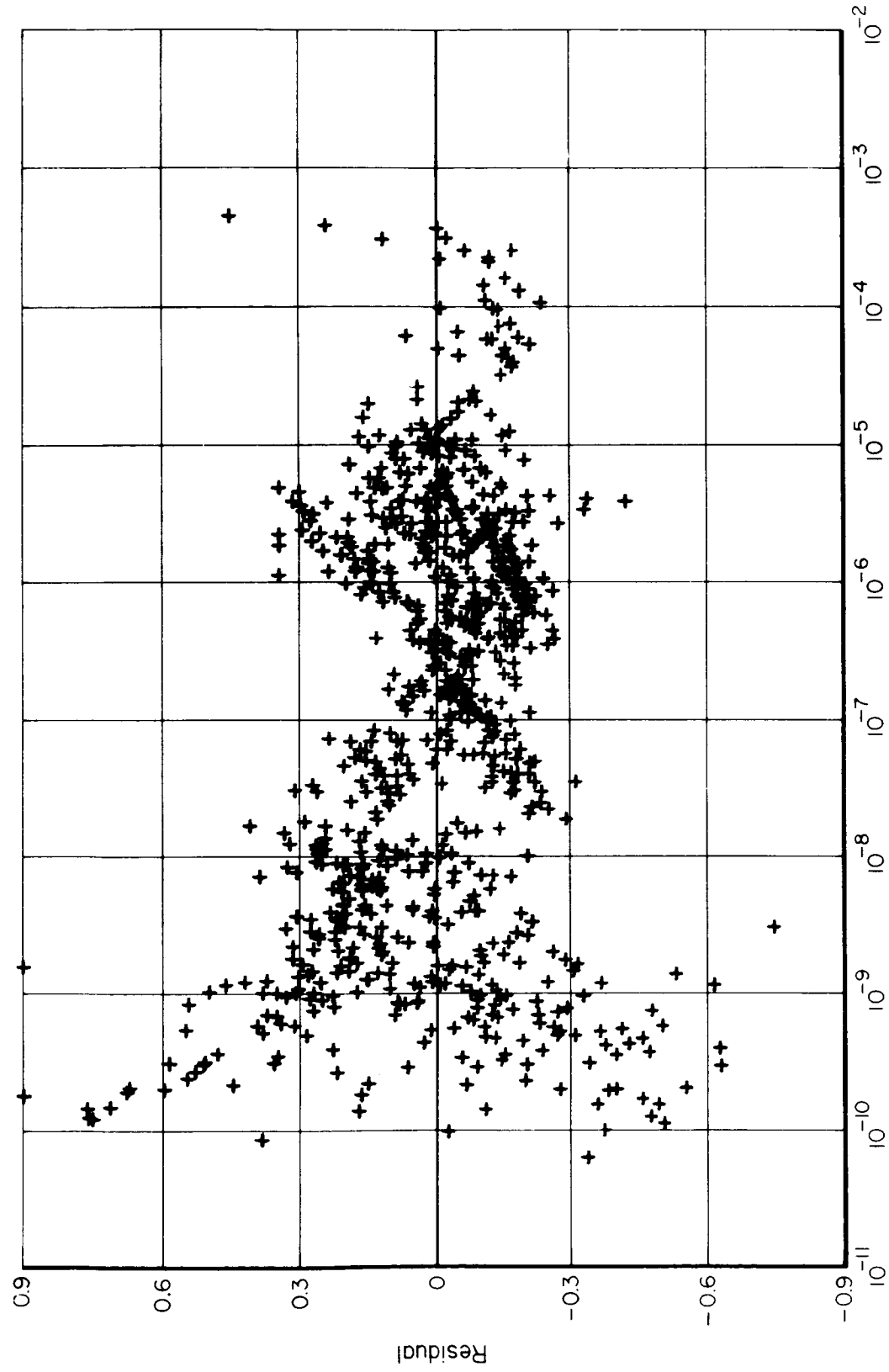

Figure F10. - Distribution of residuals for regression equation representing Ti-6Al-4V alloy.

APPENDIX G

COMPUTER PROGRAM FOR FRACTURE ANALYSIS TABULATION

A listing of the computer program, FRACTAB, for the analysis of fracture data is presented in this appendix. The data input formats for this computer routine have been presented in the subsection on Data Recording and Storage. The typical printout formats have been illustrated in figures 24, 25, and 26.

APPENDIX G

```
      C     FOR ENGLISH INPUT** PLACE SWITCH,2. CARD IN SOURCE DECK FOR      A  10
      C     ENGLISH OUTPUT, OMMIT SWITCH,2. CARD FOR METRIC OUTPUT           A  20
      C                                                                      A  30
      C     FOR METRIC INPUT** PLACE SWITCH, 2. CARD IN SOURCE DECK FOR      A  40
      C     METRIC OUTPUT, OMIT SWITCH,2. CARD FOR ENGLISH OUTPUT            A  50
      C                                                                      A  60
            PROGRAM FRACTAB(INPUT,OUTPUT,TAPE5=INPUT,TAPE6=OUTPUT)           A  70
000003      DIMENSION KODE1(50), KODE2(50), KOMENT(8), SUM(3), SSQ(3), XN(3),  A  80
           1AVG(3), DEV(3), XXVAR(3), KFLAG(3), RATIO(3), X1(2)              A  90
000003      ZO=1H*                                                           A 100
      C                                                                      A 110
      C     READ AND STORE REPLACEMENT CODE NUMBERS                          A 120
000005      DO 10 N=1,51                                                     A 130
000006      READ (5,455) KODE1(N),KODE2(N)                                   A 140
000015      IF (EOF,5) 105,100                                               A 150
000020 100  CONTINUE                                                         A 160
000022      STOP 1                                                           A 170
000024 105  CALL SSWTCH (1,ISW1)                                            A 180
000026      CALL SSWTCH (2,IMET)                                             A 190
000030      PRINT 460                                                        A 200
000034      LIM=N                                                            A 210
000035      THICX=0.                                                         A 220
      C                                                                      A 230
      C     READ AND STORE NEW TITLE, E.OF STOP RUN                          A 240
000037 110  READ (5,465) IUNIT,ITA,ITB,ITC,THICX                             A 250
000055      IF (EOF,5) 395,115                                               A 260
000060 115  READ (5,530) KOMENT                                              A 270
000066      READ (5,540) THICK,ITYPE                                         A 280
000076      IF (THICX.EQ.0.) THICX=THICK                                     A 290
000100      GO TO 325                                                        A 300
      C                                                                      A 310
      C     MOVE INPUT RECORD BACK ONE CARD                                  A 320
000101 120  BACKSPACE 5                                                      A 330
      C                                                                      A 340
      C     ZERO SUMS FOR NEXT DATA SUBSET                                   A 350
000103 125  DO 130 N=1,3                                                     A 360
000105      SUM(N)=0.                                                        A 370
000106      SSQ(N)=0.                                                        A 380
000107 130  XN(N)=0.                                                         A 390
      C                                                                      A 400
      C     READ NEXT DATA CARD                                              A 410
000112 135  READ (5,545) IDENT,THICK,WIDTH,CSUB0,SSUB2,SSUB3,VDCCL,PRCCL,STMAX  A 420
           1,TYS,TUS,SPECL,ITYPE,ISPEC,ITEMP,IREF                            A 430
000156      IF (EOF,5) 275,140                                               A 440
      C                                                                      A 450
      C     TEST FOR BLANK CARD (WIDTH=0)                                    A 460
000161 140  IF (WIDTH.EQ.0.) GO TO 275                                       A 470
      C                                                                      A 480
      C     IF SWITCH1 IS ON, REPLACE REF CODE                               A 490
000162      IF (ISW1.EQ.2) GO TO 155                                         A 500
000164      DO 145 N=1,LIM                                                   A 510
000166      IF (IREF.EQ.KODE1(N)) GO TO 150                                  A 520
000170 145  CONTINUE                                                         A 530
000172      GO TO 155                                                        A 540
000173 150  IREF=KODE2(N)                                                    A 550
```

```
000175            GO TO 155                                                  A 560
                  C                                                          A 570
                  C     CHECK FOR MISSING INPUT DATA                         A 580
000176      155   IF (TYS.LT.1.) GO TO 390                                   A 590
                  C                                                          A 600
                  C     BLANK OUT FLAG, K, & RATIO                           A 610
000201            DO 160 N=1,3                                               A 620
000202            XKVAR(N)=0.                                                A 630
000203            RATIO(N)=0.                                                A 640
000204      160   KFLAG(N)=1H                                                A 650
                  C     CHECK INPUT AND TYPE OF OUTPUT DESIRED AND MAKE ANY CHANGES  A 660
000210            IF (IUNIT.EQ.1) GO TO 165                                  A 670
000212            IF (IMET.EQ.2) GO TO 180                                   A 680
000214            GO TO 170                                                  A 690
000214      165   IF (IMET.EQ.2) GO TO 175                                   A 700
000216            GO TO 180                                                  A 710
                  C     SWITCH METRIC UNITS TO ENGLISH UNITS                 A 720
000217      170   THICK=THICK/0.0254/1000                                    A 730
000222            WIDTH=WIDTH/0.0254/1000                                    A 740
000225            CSUBC=CSUBC/0.0254/1000                                    A 750
000230            AO=6.895                                                   A 760
000231            IF (ITYPE.EQ.1) AO=4.45                                    A 770
000235            SSUB2=SSUB2/AO                                             A 780
000237            SSUB3=SSUB3/AO                                             A 790
000240            STMAX=STMAX/AO                                             A 800
000241            VOCCL=VOCCL/0.0254/1000                                    A 810
000244            PRCCL=PRCCL/0.0254/1000                                    A 820
000247            TYS=TYS/6.895                                              A 830
000250            TUS=TUS/6.895                                              A 840
000251            ITEMP=ITEMP*9./5.+32.                                      A 850
000255            SPECL=SPECL/0.0254/1000                                    A 860
000260            GO TO 180                                                  A 870
                  C     SWITCH ENGLISH UNITS TO METRIC UNITS                 A 880
000261      175   THICK=THICK*0.0254*1000                                    A 890
000264            WIDTH=WIDTH*0.0254*1000                                    A 900
000267            CSUBC=CSUBC*0.0254*1000                                    A 910
000272            AO=6.895                                                   A 920
000273            IF (ITYPE.EQ.1) AO=4.45                                    A 930
000277            SSUB2=SSUB2*AO                                             A 940
000301            SSUB3=SSUB3*AO                                             A 950
000302            STMAX=STMAX*AO                                             A 960
000303            VOCCL=VOCCL*0.0254*1000                                    A 970
000306            PRCCL=PRCCL*0.0254*1000                                    A 980
000311            TYS=TYS*6.895                                              A 990
000312            TUS=TUS*6.895                                              A1000
000313            ITEMP=(ITEMP-32.)*5./9.                                    A1010
000317            SPECL=SPECL*0.0254*1000                                    A1020
000323            GO TO 180                                                  A1030
                  C                                                          A1040
                  C     BRANCH TO APPROPRIATE EQUATION                       A1050
                  C     1  #COMPACT TENSION#                                 A1060
                  C     2  #CENTER CRACK#                                    A1070
                  C     3  #SURFACE FLAW -                                   A1080
                  C     4  #SURFACE FLAW -                                   A1090
                  C     5  #DOUBLE CANTILEVER BEAM#                          A1100
                  C     6  #NOTCH BEND#                                      A1110
```

```
                C
                C     SELECT CRITICAL STRESS AND CRACK                                  A1120
                C                                                                       A1130
000323      180       SCRIT=SSUB3                                                       A1140
000324                CCRIT=PROCL                                                       A1150
000326                IF (SCRIT.EQ.0.) SCRIT=SSUB2                                      A1160
000330                IF (CCRIT.EQ.0.) CCRIT=VDCCL                                      A1170
000332                IF (ITYPE.EQ.0) GO TO 390                                         A1180
000333                IF ((ITYPE+5)/6.NE.1) STOP                                        A1190
000342                GO TO (185,220,245,390,390,390), ITYPE                            A1200
                C                                                                       A1210
                C     COMPACT TENSION                                                   A1220
000354      185       IF (CSUB0.EQ.0.) GO TO 390                                        A1230
000355                IF (THICK.EQ.0.) GO TO 390                                        A1240
000356                X=CSUBF/WIDTH                                                     A1250
000357                XKVAR(1)=SSUB3/WIDTH/THICK**SQRT(CSUB0)*(29.6-185.5*X+655.7*X*X-101A1260
                     17.*X**3+638.9*X**4)                                             A1270
000400                XKVAR(2)=SIMAX/WIDTH/THICK**SQRT(CSUB0)*(29.6-185.5*X+655.7*X*X-101A1280
                     17.*X**3+638.9*X**4)                                             A1290
000421                X1(1)=(2.5*(XKVAR(1)/TYS)**2)                                     A1300
000424                X1(2)=(2.5*(XKVAR(2)/TYS)**2)                                     A1310
000426                IF (IMET.NE.2) GO TO 195                                          A1320
000430                DO 190 N=1,2                                                      A1330
000432                XKVAR(N)=XKVAR(N)*1000*SQRT(0.001)                                A1340
000437      190       X1(N)=(2.5*(XKVAR(N)/TYS)**2)*1000                                A1350
                C                                                                       A1360
                C     CHECK 2.5(K/TYS)**2 GE B OR CSUB0                                 A1370
000446      195       RATIO(1)=X/THICK                                                  A1380
000450                RATIO(2)=X/CSUB0                                                  A1390
                C                                                                       A1400
                C     CALCULATE NET SECTION STRESSES AND COMPARE WITH YIELD             A1410
000451                IF (SSUB3.GT.0.) SNET=SSUB3/THICK/(WIDTH-CSUB0)*(1.+3.*(WIDTH+CSUBA1420
                     10)/(WIDTH-CSUB0))                                               A1430
000465                IF (IMET.NE.2) GO TO 200                                          A1440
000467                SNET=SNET*1000                                                    A1450
000471      200       XX=SNET/TYS                                                       A1460
                C                                                                       A1470
                C     COMPARE MAX LOAD WITH 5 PERCENT OFFSET LOAD- SHOULD NOT EXCEED 1.1A1480
000473                IF (SSUB3.GT.0.) RATIO(3)=SIMAX/SSUB3                             A1490
000476                DO 215 N=1,2                                                      A1500
000500                IF (X1(N).GT.THICK) GO TO 205                                     A1510
000504                IF (X1(N).GT.CSUB0) GO TO 205                                     A1520
000507                IF (N.EQ.2) SNET=SNET*SIMAX/SSUB3                                 A1530
000513                IF (SNET.GT.TYS*.8) GO TO 205                                     A1540
000520                IF (RATIO(3).GT.1.1) GO TO 205                                    A1550
000523                GO TO 210                                                         A1560
                C                                                                       A1570
                C     INVALID                                                           A1580
000523      205       KFLAG(N)=1H*                                                      A1590
000525                NOAST=2                                                           A1600
000526                GO TO 215                                                         A1610
000527      210       XN(N)=XN(N)+1.                                                    A1620
000532                SUM(N)=SUM(N)+XKVAR(N)                                            A1630
000534                SSQ(N)=SSQ(N)+XKVAR(N)**2                                         A1640
000536      215       CONTINUE                                                          A1650
                C                                                                       A1660
000540                IT=1                                                              A1670
```

```
C     PRINT ONE LINE OF INPUT/OUTPUT DATA                                A1680
000541      WRITE (6,400) IDENT,ITEMP,TYS,TJS,THICK,WIDTH,CSUB0,SSUB3,STMAX,((  A1690
           1XKVAR(N),KFLAG(N)),N=1,2),X1(1),X1(2),RATIO(3),XX,IREF          A1700
000611      LINES=LINES1                                                    A1710
000613      GO TO 135                                                       A1720
C                                                                           A1730
C     CENTER CRACK                                                        A1740
000613 220  X=1.5708*CSUB0                                                 A1750
000615      IPCT=8                                                          A1760
C                                                                           A1770
C     COMPUTE STRESS RATIOS                                               A1780
C     1  *APPARENT*                                                       A1790
000616      IF (CSUB0.GT.0.) RATIO(2)=STMAX/TYS/(1.-CSUB0/WIDTH)            A1800
C     2  *CRITICAL*                                                       A1810
000624      IF (CCRIT.GT.0.) RATIO(3)=STMAX/TYS/(1.-CCRIT/WIDTH)            A1820
C     3  *OFFSET*                                                         A1830
000632      IF (CSUB0.GT.0.) RATIO(1)=SCRIT/TYS/(1.-CSUB0/WIDTH)            A1840
000640      IF (X.GT.0.) XKVAR(2)=STMAX*SQRT(X/COS(X/WIDTH))                A1850
000652      IF (X.GT.0.) XKVAR(1)=SCRIT*SQRT(X/COS(X/WIDTH))                A1860
000664      X=1.5708*CCRIT                                                  A1870
000666      IF (X.GT.0.) XKVAR(3)=STMAX*SQRT(X/COS(X/WIDTH))                A1880
C                                                                           A1890
000700      IF (IMET.NE.2) GO TO 230                                        A1900
000702      DO 225 N=1,3                                                    A1910
000704 225  XKVAR(N)=XKVAR(N)*SQRT(0.001)                                   A1920
C     CHECK N-S STRESS RATIO LE .8                                        A1930
000711 230  DO 240 N=1,3                                                   A1940
000713      IF (XKVAR(N).LT.1.) GO TO 240                                   A1950
000716      IF (RATIO(N).LE..8) GO TO 235                                   A1960
C                                                                           A1970
C     INVALID                                                             A1980
000720      KFLAG(N)=1H*                                                    A1990
000722      NOAST=1                                                         A2000
000723      GO TO 240                                                       A2010
C                                                                           A2020
C     VALID                                                               A2030
000723 235  XN(N)=XN(N)+1.                                                 A2040
000726      SUM(N)=SUM(N)+XKVAR(N)                                          A2050
000730      SSQ(N)=SSQ(N)+XKVAR(N)**2                                       A2060
000732 240  CONTINUE                                                        A2070
C                                                                           A2080
C     PRINT ONE LINE OF INPUT/OUTPUT DATA                                 A2090
000734      IT=2                                                            A2100
000735      WRITE (6,405) IDENT,ITEMP,TYS,TJS,THICK,WIDTH,CSUB0,CCRIT,SCRIT,ST  A2110
           1MAX,((XKVAR(N),KFLAG(N)),N=1,3),RATIO(1),RATIO(2),RATIO(3),IREF    A2120
001005      LINES=LINES+1                                                   A2130
001007      GO TO 135                                                       A2140
C                                                                           A2150
C     SURFACE FLAW                                                        A2160
001007 245  IF (SPECL.EQ.0) GO TO 390                                      A2170
001010      IF (CSUB0.EQ.0) GO TO 390                                       A2180
001011      IF (STMAX.EQ.0) GO TO 390                                       A2190
001012      IPCT=9                                                          A2200
C                                                                           A2210
C     COMPUTE ASPECT AND STRESS RATIOS                                    A2220
001013      ASPECT=SPECL/CSUB0                                              A2230
```

```
C.
      001014          X=TYS*(1.-.7854*SPECL*CSUB0/THICK/WIDTH)                  A2240
      001022          RATIO(1)=SCRIT/X                                          A2250
      001024          RATIO(2)=STMAX/X                                          A2260
                C                                                             A2270
                C     PRELIMINARY COMPUTATIONS                                  A2280
      001026          PHISQ=1.+4.6*ASPECT**1.65                                 A2290
      001034          XXXSQ=(STMAX/TYS)**2/5.656                                A2300
      001037          PHIXX=SQRT(PHISQ)                                         A2310
                C                                                             A2320
      001041          XKVAR(1)=1.1*SCRIT*SQRT(3.1416*SPECL)/SQRT(PHISQ-1.2*XXXSQ)  A2330
      001055          XKVAR(2)=1.1*STMAX*SQRT(3.1416*SPECL)/SQRT(PHISQ-1.2*XXXSQ)  A2340
      001072          XKVAR(3)=1.1*STMAX*SQRT(3.1416*SPECL)/SQRT(PHISQ-1.2*XXXSQ)  A2350
      001107          IF (IMET.NE.2) GO TO 255                                  A2360
      001112          DO 25  N=1,3                                              A2370
      001113    250   XKVAR(N)=XKVAR(N)*SQRT(0.80)                              A2380
                C                                                             A2390
                C     CHECK N-S STRESS RATIO LE .9                              A2400
      001121    255   DO 265 N=1,2                                              A2410
      001123          IF (XKVAR(N).LT.1.) GO TO 255                             A2420
      001126          IF (RATIO(N).GT..9) GO TO 260                             A2430
                C                                                             A2440
                C     VALID                                                     A2450
      001131          XN(N)=XN(N)+1.                                            A2460
      001132          SUM(N)=SUM(N)+XKVAR(N)                                    A2470
      001135          SSQ(N)=SSQ(N)+XKVAR(N)**2                                 A2480
      001137          GO TO 265                                                 A2490
                C                                                             A2500
                C     INVALID                                                   A2510
      001140    260   KFLAG(N)=1H*                                              A2520
      001142          NOAST=1                                                   A2530
      001143    265   CONTINUE                                                  A2540
                C                                                             A2550
      001145          IT=3                                                      A2560
                C     PRINT ONE LINE OF INPUT/OUTPUT DATA                       A2570
      001146          WRITE (6,425) IDENT,ITEMP,TYS,TJS,THICK,WIDTH,CSUB0,SPECL,SCRIT,ST  A2580
                     1MAX,((XKVAR(N),KFLAG(N)),N=1,2),RATIO(1),RATIO(2),ASPECT,IREF  A2590
      001216          LINES=LINES+1                                             A2600
      001220          GO TO 135                                                 A2610
                C                                                             A2620
                C     IF LAST CARD WAS BLANK SET MORE=2; IF EOF, SET MORE=1     A2630
      001220    270   MORE=2                                                    A2640
      001221          GO TO 280                                                 A2650
      001222    275   MORE=1                                                    A2660
                C                                                             A2670
                C     COMPUTE AND PRINT STATISTICS IF XN GT 1                   A2680
      001223    280   DO 285 N=1,3                                              A2690
      001225          AVG(N)=0.                                                 A2700
      001226          DEV(N)=0.                                                 A2710
      001227          IF (XN(N).LT.2.) GO TO 285                                A2720
      001232          AVG(N)=SUM(N)/XN(N)                                       A2730
      001234          DEV(N)=SQRT((SSQ(N)-SUM(N)*SUM(N)/XN(N))/(XN(N)-1.))      A2740
      001246    285   CONTINUE                                                  A2750
      001250          WRITE (6,455)                                             A2760
      001254          IF ((XN(1).LE.1.).AND.(XN(2).LE.1.).AND.(XN(3).LE.1.)) GO TO 310  A2770
                C     BRANCH TO APPROPRIATE OUTPUT FORMAT                       A2780
      001273          GO TO (295,290,300,390,390,390), IT                       A2790
```

```
001305   290    WRITE (6,415) AVG                                          A2800
001313          WRITE (6,430) DEV                                          A2810
001321          GO TO 385                                                  A2820
001322   295    WRITE (6,420) AVG(1),AVG(2)                                A2830
001332          WRITE (6,435) DEV(1),DEV(2)                                A2840
001342          GO TO 365                                                  A2850
001343   300    WRITE (6,410) AVG(1),AVG(2)                                A2860
001353          WRITE (6,440) DEV(1),DEV(2)                                A2870
001363   305    LINES=LINES+2                                              A2880
001365   310    WRITE (6,455)                                              A2890
001371          LINES=LINES+2                                              A2900
001373          GO TO (315,320), MORE                                      A2910
001401   315    IF (NOAST.EQ.1) WRITE (6,445) IPCT                         A2920
001411          IF (NOAST.EQ.2) WRITE (6,450)                              A2930
001417          GO TO 110                                                  A2940
001420   320    IF (LINES.LT.35) GO TO 125                                 A2950
001423          IF (NOAST.EQ.1) WRITE (6,445) IPCT                         A2960
001432          IF (NOAST.EQ.2) WRITE (6,450)                              A2970
001440   325    IF ((ITYPE+5)/6.NE.1) STOP                                 A2980
001447          NOAST=2                                                    A2990
001450          LINES=0                                                    A3000
         C      CHECK INPUT AND OUTPUT TYPE AND BRANCH TO APPROPIATE FORMAT A3010
001450          IF (IUNIT.EQ.1) GO TO 330                                  A3020
001453          IF (IMET.EQ.2) GO TO 350                                   A3030
001455          GO TO 340                                                  A3040
001455   330    IF (IMET.EQ.2) GO TO 335                                   A3050
001457          GO TO 345                                                  A3060
001460   335    THICX=THICX*0.0254*1000.                                   A3070
001462          GO TO 350                                                  A3080
001462   340    THICX=THICX/25.4                                           A3090
001464   345    GO TO (355,360,365,365,385,385), ITYPE                     A3100
001476   350    GO TO (370,375,380,380,385,385), ITYPE                     A3110
001510   355    WRITE (6,470) THICX,ITA,ITB,ITC                            A3120
001524          WRITE (6,535) KOMENT                                       A3130
001532          WRITE (6,500)                                              A3140
001536          GO TO 385                                                  A3150
001537   360    WRITE (6,480) THICX,ITA,ITB,ITC                            A3160
001553          WRITE (6,535) KOMENT                                       A3170
001561          WRITE (6,510)                                              A3180
001565          GO TO 385                                                  A3190
001566   365    WRITE (6,490) THICX,ITA,ITB,ITC                            A3200
001602          WRITE (6,535) KOMENT                                       A3210
001610          WRITE (6,520)                                              A3220
001614          GO TO 385                                                  A3230
001615   370    WRITE (6,475) THICX,ITA,ITB,ITC                            A3240
001631          WRITE (6,535) KOMENT                                       A3250
001637          WRITE (6,505)                                              A3260
001643          GO TO 385                                                  A3270
001644   375    WRITE (6,485) THICX,ITA,ITB,ITC                            A3280
001660          WRITE (6,535) KOMENT                                       A3290
001666          WRITE (6,515)                                              A3300
001672          GO TO 385                                                  A3310
001673   380    WRITE (6,495) THICX,ITA,ITB,ITC                            A3320
001707          WRITE (6,535) KOMENT                                       A3330
001715          WRITE (6,525)                                              A3340
001721   385    IF (MORE.EQ.2) GO TO 125                                   A3350
```

```
      GO TO 120                                                          A3360
C                                                                        A3370
C     ERROR MESSAGE - MISSING INPUT DATA                                 A3380
  390 PRINT 550                                                          A3390
      GO TO 135                                                          A3400
  395 CONTINUE                                                           A3410
C                                                                        A3420
C                                                                        A3430
C                                                                        A3440
  400 FORMAT (1X,A8,I4,4X,F5.1,3X,F5.1,2X,F6.3,3X,F6.3,3X,F6.3,3X,F6.3,2 A3450
     1X,F5.3,4X,F5.2,A1,F8.2,A1,F6.1,F6.1,F8.3,3X,F5.3,A7)               A3460
  405 FORMAT (1X,A8,I4,1X,2X,F5.1,1X,F6.1,1X,F6.3,2X,F6.2,2X,F6.2,2X,F6. A3470
     12,3X,F6.2,2X,F6.2,2X,F6.2,A1,1X,F6.2,A1,1X,F6.2,A1,1X,F6.3,2X,F6.3 A3480
     2,2X,F6.3,A7)                                                       A3490
  410 FORMAT (64X,*AVERAGE VALUE*F9.2,5X,F7.2)                           A3500
  415 FORMAT (61X,*AVERAGE VALUE*,3X,F6.2,2X,F6.2,2X,F6.2)               A3510
  420 FORMAT (59X,*AVERAGE VALUE*,4X,F6.2,3X,F6.2)                       A3520
  425 FORMAT (1X,A8,1X,I4,F8.1,F8.1,F8.3,F8.2,F8.2,F8.2,F8.2,F8.2,F8.2,A A3530
     11,4X,E7.2,A1,F6.3,F9.3,F8.3,2X,A7)                                 A3540
  430 FORMAT (61X,*STANDARD DEV.*,3X,F6.2,2X,F6.2,2X,F6.2/)              A3550
  435 FORMAT (59X,*STANDARD DEV.*,4X,F6.2,3X,F6.2)                       A3560
  440 FORMAT (64X,*STANDARD DEV.*F8.2,5X,F7.2)                           A3570
  445 FORMAT (2H0*,*NOTE- NET SECTION STRESS EXCEEDS *,I3,* PERCENT OF Y A3580
     1IELD STRENGTH.  VALUE NOT INCLUDED IN AVG. VALUE OR STD. DEV. *)   A3590
  450 FORMAT (2H0*,*NOTE- INVALID KIC VALUE, NOT INCLUDED IN AVG. VALUE  A3600
     1OR STD. DEV.*)                                                     A3610
  455 FORMAT (2A7)                                                       A3620
  460 FORMAT (*PM IF DISPOSE, PRINT UNLINED ON 512 PR*)                  A3630
  465 FORMAT (3X,I1,7X,A8,2A10,5X,2*X,F5.3)                              A3640
  470 FORMAT (*1TABLE          KC AND K1C FRACTURE TOUGHNESS VALUES FOR   A3650
     1COMPACT TYPE SPECIMENS OF *,F5.3,* INCH THICK *A9,A10,* ALLOY *,A1  A3660
     20/)                                                                A3670
  475 FORMAT (*1TABLE          FRACTURE TOUGHNESS VALUES FOR COMPACT TYPE A3680
     1SPECIMENS OF *,F5.2,* MILLIMETER THICK *A9,A10,* ALLOY *A10/)       A3690
  480 FORMAT (*1TABLE          PLANE-STRESS AND TRANSITIONAL FRACTURE TO  A3700
     1UGHNESS OF *,F5.3,* INCH THICK *A9,A10,* ALLOY *,A10/)             A3710
  485 FORMAT (*1TABLE       PLANE-STRESS AND TRANSITIONAL FRACTURE TOUGHN A3720
     1ESS OF*,F5.2,* MILLIMETER THICK *A8,A10,*ALLOY*A10/)               A3730
  490 FORMAT (*1TABLE          SURFACE-FLAW FRACTURE TOUGHNESS OF *,F5.3,  A3740
     1* INCH THICK *,A8,A10,* ALLOY *,A10/)                              A3750
  495 FORMAT (*1TABLE          SURFACE-FLAW FRACTURE TOUGHNESS OF *,F5.2,* M A3760
     1ILLIMETER THICK *,A8,A10,*ALLOY *,A10/)                            A3770
  500 FORMAT (1X,*SPECIMEN TEST    +++TENSILE+++  ++++SPECIMEN DIMENSIONS  A3780
     1+++    ++++LOAD++++  MATERIAL TOUGHNESS  SIZE REQT   LOAD    STRESS A3790
     2   REF*/2X,* IDENT  TEMP     PROPERTIES    THICK-   WIDTH    CRACK  A3800
     3     P(Q)  P(MAX)     OFFSET    APPRNT  OFF-  APP-    RATIO   RATIO* A3810
     4/34X,*NESS              LENGTH *39X,*SET  RNT */12X,*F     TYS     TU A3820
     5S      (T)       (W)        (A)*23X,*K(IC)   K(APP)  *,8X,* PQ/PMAX  S A3830
     6N/TYS  */17X,*KSI      KSI      INCH     INCH    INCH     KIPS       A3840
     7/KKPS    **KSI-SQRT(INCH)**   INCH  INCH  */)                       A3850
  505 FORMAT (1X,*SPECIMEN TEST    +++TENSILE+++  ++++SPECIMEN DIMENSIONS  A3860
     1+++    ++++LOAD++++  MATERIAL TOUGHNESS  SIZE REQT   LOAD    STRESS A3870
     2   REF*/2X,* IDENT  TEMP     PROPERTIES    THICK-   WIDTH    CRACK  A3880
     3     P(Q)  P(MAX)     OFFSET    APPRNT  OFF-  APP-    RATIO   RATIO* A3890
     4/34X,*NESS              LENGTH *39X,*SET  RNT */12X,*C     TYS     TU A3900
     5S      (T)       (W)        (A)*22X,*K(IC)   K(APP)       *5X,*PQ/P A3910
```

```
     6MAX  SU/TYS    */1/X,*++MN/SQ(M)+++  ++++++++MILLIMETER++++++  K   A3920
     7ILONENTONS++  ++++MN/(M)3/2++++  MILLIMETER  *//)                  A3930
001731  51v  FORMAT (1X,*SPECIMEN  TEST  TENSILE  +++++SPECIMEN DIMENSIONS++  A3940
     1++++  ++++STRESS++++  ++MATERIAL TOUGHNESS++  +++NET STRESS RATIO  A3950
     2++  REF */2X,*IDENT  TEMP PROPERTIES  THICK-  WIDTH + CRACK LE  A3960
     3NGTH + OFFSET  MAXI-  OFFSET  APPRNT  CRITCL  S(-)/TYS(1-2C(-)/  A3970
     4W)*/16X,* YIELD ULT  NESS  INITIAL  FINAL  MU  A3980
     5M  OFFSET  APPRNT  CRITCL*/12X,*F  STR  A3990
     6  STR  (T)  (W)  2C(O)  2C(C)  S(O)  S(C)  K(Q)  A4000
     7K(APP)  K(C)*/12X,*  KSI  KSI  INCH  INCH  INCH  INC  A4010
     8H  KSI  KSI  ++++KSI-SQRT(INCH)+++ *//)  A4020
001731  515  FORMAT (1X,*SPECIMEN  TEST  TENSILE  +++++SPECIMEN DIMENSIONS++  A4030
     1++++  ++++STRESS++++  ++MATERIAL TOUGHNESS++  +++NET STRESS RATIO  A4040
     2++  REF */2X,*IDENT  TEMP PROPERTIES  THICK-  WIDTH + CRACK LE  A4050
     3NGTH + OFFSET  MAXI-  OFFSET  APPRNT  CRITCL  S(-)/TYS(1-2C(-)/  A4060
     4W)*/16X,* YIELD ULT  NESS  INITIAL  FINAL  MU  A4070
     5M  OFFSET  APPRNT  CRITCL*/11X,* C  SR  A4080
     6  STR  (T)  (W)  2C(O)  2C(C)  S(O)  S(C)  K(Q)  A4090
     7 K(APP))  K(C)*/12X,*  MN/SQ(M)  ++++++++++MILLIMETER++++++++  A4100
     8++  +++MN/SQ(M)+++  ++++++++MN/M3/2++++++++*//)  A4110
001731  52v  FORMAT (1X,*SPECIMEN  TEST  +++TENSILE+++  ++++++SPECIMEN DIMENSIO  A4120
     1NS+++++  ++++STRESS++++  MATERIAL TOUGHNESS  +*NET STRESS+*  A/  A4130
     22C  REF*/2X,*IDENT  TEST  PROPERTIES  THICK-  WIDTH  +*CRACK  A4140
     3 SIZE+++  OFFSET  MAXI-  OFFSET  APPRNT  RATIO*/16X,* YI  A4150
     4ELD  ULT  NESS  LENGTH  DEPTH  MUM*26X,*OFF  A4160
     5SET  APPRNT*/12X,*F  STR  STR  (T)  (W)  2(C)  A(  A4170
     60)  S(O)  S(C)  K(Q)  K(APP)*/18X,*KSI  KSI  INCH  A4180
     7  INCH  INCH  INCH  KSI  KSI  **KSI-SQRT(INCH)+++*//)  A4190
001731  525  FORMAT (1X,*SPECIMEN  TEST  +++TENSILE+++  ++++++SPECIMEN DIMENSIO  A4200
     1NS+++++  ++++STRESS++++  MATERIAL TOUGHNESS  +*NET STRESS+*  A/  A4210
     22C  REF*/2X,*IDENT  TEST  PROPERTIES  THICK-  WIDTH  +*CRACK  A4220
     3 SIZE+++  OFFSET  MAXI-  OFFSET  APPRNT  RATIO*/16X,* YI  A4230
     4ELD  ULT  NESS  LENGTH  DEPTH  MUM*26X,*OFF  A4240
     5SET  APPRNT*/12X,*C  STR  STR  (T)  (W)  2(C)  A(  A4250
     60)  S(O)  S(C)  K(Q)  K(APP)*/17X,*++*MN/SQ(M)**  +++++  A4260
     7+++++MILLIMETER+++++++++  +++MN/SQ(M)**  ++++MN/(M)3/2+++++*//)  A4270
001731  53v  FORMAT (8A10)  A4280
001731  535  FORMAT (40X,8A10//)  A4290
001731  540  FORMAT (8X,F5.0,50X,I1)  A4300
001731  545  FORMAT (A8,11F5.0,I1,A2,3X,I4,A7)  A4310
001731  55v  FORMAT (* ---- THIS LINE OMITTED - MISSING TYS OR SPEC TYPE*)  A4320
001731       END  A4330
```

APPENDIX H

THE WEIGHTING FUNCTION, W(X)

In order to obtain uniformity of variance in combined sets of fatigue data, a weighting function, W(X), was applied to each data population. The following comments are included to clarify the method employed in this weighting process.

Initially, the data were analyzed without weights, and the quality of fit was based on the R^2 parameter. The process used in maximizing R^2 involved a minimization of the sum of squares of deviations or SSD. Using equations (2) and (4), the unweighted SSD can be described as

$$SSD = \sum_{i=1}^{n} (Y_i - \bar{Y})^2 = \sum_{i=1}^{n} (Y_i - A_0 - A_1\bar{X})^2 \qquad (H1)$$

where $\bar{X}$ represents the mean, or predicted value of X for a particular value of Y_i.

When the weighting function was used, the minimization was based on a modified SSD, written as follows,

$$SSD = \sum_{i=1}^{n} W_i \, (Y_i - A_0 - A_1\bar{X})^2 \quad . \qquad (H2)$$

In this way, each deviation from the mean is modified according to the magnitude of W_i. When W_i is small, the square of the residual is reduced correspondingly. If W_i is near unity, almost no modification of the residual results.

REFERENCES

1. Anon.: Military Standardization Handbook, Metallic Materials and Elements for Aerospace Vehicle Structures. MIL-HDBK-5B, 1971.

2. Anon.: Tentative Recommended Practice for Constant Amplitude Axial Fatigue Tests of Metallic Materials, ASTM Designation: E-466-72T. Annual Book of ASTM Standards, Part 31, 1973.

3. Anon.: Standard Method of Test for Plane-Strain Fracture Toughness of Metallic Materials, ASTM Designation: E-399-72. Annual Book of ASTM Standards, Part 31, 1973.

4. Walker, K.: The Effect of Stress Ratio During Crack Propagation and Fatigue for 2024-T3 and 7075-T6 Aluminum. Effects of Environment and Complex Load History on Fatigue Life. Spec. Tech. Publ. 462, ASTM, 1970, pp. 1-14.

5. Smith, K. N.; Watson, P.; and Topper, T. H.: A Stress-Strain Function for the Fatigue of Metals. J. Matl., vol. 5, no. 4, Dec. 1970, pp. 767-778.

6. Anon.: Fatigue Cracking of Aluminum and Titanium Alloys. NASA Literature Search Number 18683, 1972.

7. Anon.: Fatigue Failure of Nickel Chromium Steels. NASA Literature Search Number 18692, 1972.

8. Anon.: Fatigue Cracking of Aluminum and Titanium Alloys. DDC Literature Search Number 082157, 1972.

9. Anon.: Fatigue Cracking/AISI 4340 Steel. DDC Literature Search Number 082156, 1972.

10. Snedecor, G. W.; and Cochran, W. G.: Statistical Methods. Sixth ed., The Iowa State University Press, 1967, pp. 400-403.

11. Draper, N. R.; and Smith, H.: Applied Regression Analysis. Wiley Publications in Statistics, 1966.

12. Williams, E. J.: Regression Analysis. Wiley Publications in Statistics, 1959.

13. Mandel, J.; and Paule, R. C.: Interlaboratory Evaluation of a Material with Unequal Numbers of Replicates. Anal. Chem., vol. 42, no. 11, Sept. 1970, pp. 1194-1197. (Correction in Anal. Chem., vol. 43, no. 10, Aug. 1971, p. 1287.)

14. Stulen, F. L.: Fatigue Life Data Displayed by a Single Quantity Relating Alternating and Mean Stresses. AFML-TR-65-121, 1965.

15. Topper, T. H.; and Sandor, B. I.: Effects of Mean Stress and Prestrain on Fatigue-Damage Summation. Effects of Environment and Complex Load History on Fatigue Life. Spec. Tech. Publ. 462, ASTM, 1970, pp. 93-104.

16. Endo, T.; and Morrow, JoDean: Cyclic Stress-Strain and Fatigue Behavior of Representative Aircraft Metals. J. Matl., vol. 4, no. 1, March 1969, pp. 159-175.

17. Landgraf, R. W.; Morrow, JoDean; and Endo, T.: Determination of the Cyclic Stress-Strain Curve. J. Matl., vol. 4, no. 1, March 1969, pp. 176-188.

18. Smith, R. W.; Hirschberg, M. H.; and Manson, S. S.: Fatigue Behavior of Materials Under Strain Cycling in Low and Intermediate Life Range. NASA TN D-1574, 1963.

19. Morrow, JoDean; Wetzel, R. M.; and Topper, T. H.: Laboratory Simulation of Structural Fatigue Behavior. Effects of Environment and Complex Load History on Fatigue Life. Spec. Tech. Publ. 462, ASTM, 1970, pp. 74-91.

20. Topper, T. H.; Wetzel, R. M.; and Morrow, JoDean: Neuber's Rule Applied to Fatigue of Notched Specimens. J. Matl., vol. 4, no. 1, March 1969, pp. 200-209.

21. Neuber, H.: Theory of Stress Concentration Shear Strained Primatical Bodies with Arbitrary Nonlinear Stress Strain Law. J. Appl. Mech., Dec. 1961, pp. 544-550.

22. Peterson, R. E.: Notch-Sensitivity. Metal Fatigue. Sines, G.; and Waisman, J. L. eds., McGraw-Hill Book Co., 1959, pp. 293-306.

23. Raske, D. T.: Section and Notch Size Effects in Fatigue. T. & A. M. Report No. 360, Univ. of Illinois, 1972.

24. Morrow, JoDean: Cyclic Plastic Strain Energy and Fatigue of Metals. Internal Friction, Damping, and Cyclic Plasticity. Spec. Tech. Publ. 378, ASTM, 1965, pp. 45-87.

25. Paris, P. C.; Gomez, M. P.; and Anderson, W. E.: A Rational Analytic Theory of Fatigue. The Trend in Eng., vol. 13, no. 1, 1969, pp. 9-14.

26. Mukherjee, B.; and Burns, D. J.: Regression Models for an Effect of Stress Ratio on Fatigue Crack Growth Rate. Probabilistic Aspects of Fatigue. Spec. Tech. Publ. 511, ASTM, 1972, pp. 43-60.

27. Roberts, R.; and Erdogan, F.: The Effect of Mean Stress on Fatigue-Crack Propagation in Plates Under Extension and Bending. J. Basic Eng., ser D, vol. 89, 1967, pp. 885-892.

28. Elber, W.: The Significance of Fatigue-Crack Closure. Damage Tolerance in Aircraft Structures. Spec. Tech. Publ. 486, ASTM, 1971, pp. 230-242.

29. Erdogan, F.: Crack Propagation Theories. NASA CR-901, Oct. 1967.

30. Hoskin, B. C.: Simple Theoretical Studies of Fatigue-Crack Propagation Using a Fracture Mechanics Approach. NTIS N72-28897, Dec. 1971.

31. Coffin, L. F.: Fatigue, Annual Review Material Science, vol. 2, 1972, pp. 313-348.

32. Paris, P. C.: The Growth of Cracks Due to Variations in Loads. Ph.D. Thesis, Lehigh University, 1962.

33. Forman, R. G.; Kearney, V. E.; and Engle, R. M.: Numerical Analyses of Crack Propagation in Cyclic-Loaded Structures. J. Basic Eng., vol. 89, 1967, pp. 459-464.

34. Collipriest, J. E.: An Experimentalist's View of the Surface Flaw Problem. The Surface Crack: Physical Problems and Computational Solutions. ASME, 1972, pp. 43-62.

35. Donahue, R. J.; Clark, H. McI.; Atanmo, P.; Kumble, R.; and McEvily, A. J.: Crack Opening Displacement and the Rate of Fatigue-Crack Growth. Int. J. Fracture Mech., vol. 8, no. 2, 1972, pp. 209-219.

36. Campbell, J. E.; Berry, W. E.; and Feddersen, C. E.: Damage Tolerant Design Handbook. MCIC HB-01, Battelle's Columbus Laboratories, 1972.

37. Jaske, C. E.; Mindlin, H.; and Perrin, J. S.: Cyclic Stress-Strain Behavior of Two Alloys at High Temperature. Cyclic Stress-Strain Behavior – Analysis, Experimentation, and Failure Prediction. Spec. Tech. Publ. 519, ASTM, 1973, pp. 13-27.

38. Engle, R. M.: Cracks, A Fortran IV Digital Computer Program for Crack Propagation Analyses. AFFDL-TR-70-107, 1970.

DISTRIBUTION LIST

	No. Copies
NASA Langley Research Center Hampton, VA 23665	
Attn: Report & Manuscript Control Office, Mail Stop 180A	1
Raymond L. Zavasky, Mail Stop 115	1
C. Michael Hudson, Mail Stop 465	10
NASA Ames Research Center Moffett Field, CA 94035	
Attn: Library, Mail Stop 202-3	1
Dell P. Williams III, Mail Stop 240-1	1
NASA Flight Research Center P. O. Box 273 Edwards, CA 93523	
Attn: Library	1
NASA Goddard Space Flight Center Greenbelt, MD 20771	
Attn: Library	1
NASA Lyndon B. Johnson Space Center 2101 Webster Seabrook Road Houston, TX 77058	
Attn: Library, JM6	1
NASA Marshall Space Flight Center Huntsville, AL 35812	
Attn: Library	1
Margaret W. Brennecke, S&E-ASTN-MM	1
Jet Propulsion Laboratory 4800 Oak Grove Drive Pasadena, CA 91103	
Attn: Library, Mail 111-113	1
NASA Lewis Research Center 21000 Brookpark Road Cleveland, OH 44135	
Attn: Library, Mail Stop 60-3	1
Samuel S. Manson, Mail Stop 49-1	1
Marvin H. Hirschberg, Mail Stop 49-1	1
NASA John F. Kennedy Space Center Kennedy Space Center, FL 32899	
Attn: Library, IS-DOC-1L	1
National Aeronautics & Space Administration Washington, DC 20546	
Attn: KSS-10/Library	1
RW/NASA Headquarters	1

DISTRIBUTION LIST (Continued)

	No. Copies
Naval Air Development Center Warminster, PA 18974 Attn: Frank F. Borriello M. S. Rosenfeld	 1 1
U. S. Naval Research Laboratory Metallurgy Division, Code 6381 Washington, DC 20390 Attn: J. Goode T. W. Crooker	 1 1
U. S. Department of Commerce National Bureau of Standards Washington, DC 20234 Attn: L. Mordfin, EM219	 1
Air Force Materials Laboratory Wright-Patterson Air Force Base, OH 45433 Attn: T. J. Reinhart/MBC C. L. Harmsworth, Materials Support Division (LAE) D. A. Shinn, Chief, Aeronautical Systems Support Branch (MX)	 1 1 1
Air Force Flight Dynamics Laboratory Wright-Patterson Air Force Base, OH 45433 Attn: H. A. Wood/FBR	 1
Mr. Walter J. Trapp 9131 Shawhan Drive Centerville, OH 45499	 1
Army Materials & Mechanics Research Center Watertown, MA 02172 Attn: J. I. Bluhm, AMXMR-T	 1
U. S. Army Air Mobility Research & Development Laboratory Eustis Directorate Ft. Eustis, VA 23604 Attn: Robert Berrisford, Chief Ward Figge, Project Engineer	 1 1
McDonnell Douglas Corporation Douglas Aircraft Company 3855 Lakewood Boulevard Long Beach, CA 90801 Attn: P. R. Abelkis, Mail Stop 35-42 Fred C. Allen, Mail Stop 35-42	 1 1
Northrop Corporation 3901 West Broadway Hawthorne, CA 90250 Attn: D. R. Apodaca, Department 3495/32, Aircraft Division D. P. Wilhem, 3761/62, Aircraft Division	 1 1

DISTRIBUTION LIST (Continued)

	No. Copies
Kaiser Aluminum & Chemical Corporation Center for Technology P. O. Box 870 Pleasanton, CA 94566 Attn: Larry J. Barker	1
TRW Inc. 23555 Euclid Avenue Cleveland, OH 44117 Attn: E. Barrett, T/M 3417	1
Lockheed Aircraft Corporation Lockheed-Georgia Company 86 South Cobb Drive Marietta, GA 30060 Attn: Eddie J. Bateh, Department 72-26, Zone 459 L. W. Lassiter, Department 72-26, Div. Engr. Adv. Struct.	1 1
Belfour Stulen Incorporated Mechanical Properties Data Center 13919 West Bay Shore Drive Traverse City, MI 49684 Attn: Technical Information Systems Division	1
McDonnell Douglas Corporation 5301 Bolsa Avenue Huntington Beach, CA 92647 Attn: George E. Bockrath, Dept. A3-250, MS 11 AB00	1
Rockwell International Corporation 12214 Lakewood Boulevard Downey, CA 90241 Attn: Curtis D. Brownfield, Dept. 191, Mail Code AD88	1
General Dynamics Corporation P. O. Box 748 Fort Worth, TX 76101 Attn: W. T. Burtin, Mail Zone 2863 Oscar N. Thompson, Mail Zone 2863	1 1
General Electric Company Metallurgy and Ceramics Research Department P. O. Box 1088 Schenectady, NY 12301 Attn: L. F. Coffin, Jr., Metals Studies Section	1
A. O. Smith Corporation P. O. Box 584 Milwaukee, WI 53201 Attn: Ben E. Coursin, Product Engineering, Building 83	1

DISTRIBUTION LIST (Continued)

	No. Copies
Rockwell International Corporation International Airport Los Angeles, CA 90009	
Attn: Cecil L. Davis, Department 56-034 AD28	1
G. E. Fitch, Jr., Department 56-034 AD28	1
Ford Motor Company Scientific Laboratory 20000 Rotunda Drive Dearborn, MI 48121	
Attn: C. E. Feltner	1
R. W. Landgraf	1
Materials Science Corporation 1777 Walton Road Bluebell, PA 19422	
Attn: B. J. Fleischer	1
Deere and Company Moline, IL 61265	
Attn: James A. Graham, Materials Engineering Department	1
Federal Aviation Administration Washington, DC 20590	
Attn: Bernie Grochal, FS-120, Airframe Branch	1
Titanium Metals Corporation of America 195 Clinton Road West Caldwell, NJ 07006	
Attn: W. H. Heil, Mgr., Application Development Engineering	1
Grumman Aerospace Corporation Oyster Point Road Bethpage, Long Island, NY 11714	
Attn: Ronald Heitzmann, F-14M. and P. Department, Plant 1	1
R. E. Hooson, Structural Mechanics, Plant 35	1
RMI Company Niles, OH 44446	
Attn: Walter Herman, Manager, Customer Technical Service	1
Lockheed Aircraft Corporation Lockheed-California Company P. O. Box 551 Burbank, CA 91503	
Attn: D. W. Hoeppner, D/78-25 B/243 P/2	1
Virgil D. Moss, D/74-41 B167 P/B1	1
E. K. Walker	1
Rex Chainbelt, Inc. 5101 West Beloit Road West Milwaukee, WI 53101	
Attn: William F. Hoffmeister	1

DISTRIBUTION LIST (Continued)

	No. Copies
Rockwell International Corporation 2445 West Maple Road Troy, MI 48084 Attn: Louis Hrusovsky	1
McDonnell Douglas Corporation McDonnell Aircraft Company P. O. Box 516 St. Louis, MO 63166	
Attn: L. F. Impellizzeri, Dept. 237, Building 32, Level 2	1
Dan L. Rich, Department 237, Building 32, Level 2	1
General Motors Proving Ground Hickory Ridge & GM Road Milford, MI 48042 Attn: Raymond Isaacson	1
Aluminum Company of America Alcoa Research Laboratories Freeport Road New Kensington, PA 15068 Attn: J. G. Kaufman	1
The Boeing Company P. O. Box 3999 Seattle, WA 98124 Attn: K. J. Kenworthy, Military Aircraft Systems Division	1
The Boeing Company Commercial Airplane Group P. O. Box 3707 Seattle, WA 98124	
Attn: Cecil E. Parsons, Org. 6-8733, Mail Stop 77-18	1
U. G. Goransson	1
Bell Aerospace Company Buffalo, NY 14240	
Attn: Alexander Krivetsky, Chief, Advanced Structural Techn.	1
J. Padlog	1
United Aircraft Corporation Sikorsky Aircraft North Main Street Stratford, CT 06602 Attn: Glenn E. Lattin	1
University of Connecticut Storrs, CT 06268 Attn: A. J. McEvily, Jr., Metallurgy Department	1

DISTRIBUTION LIST (Continued)

	No. Copies
Bethlehem Steel Corporation Homer Research Laboratories Bethlehem, PA 18016 Attn: H. S. Reemsnyder	1
Aerospace Industries Association of America Aerospace Technical Council 1725 DeSales Street, N. W. Washington, DC 20036 Attn: J. P. Reese, Executive Secretary Materials & Structures Committee	1
Marion Power Shovel Company 617 West Center Street Marion, OH 43302 Attn: George J. Thompson	1
The Boeing Company Vertol Division P. O. Box 16858 Philadelphia, PA 19142 Attn: Main Library, Boeing Center	1
LTV Aerospace Corporation Vought Aerospace Corporation P. O. Box 5907 Dallas, TX 75222 Attn: Wesley B. Vorhes, Unit 2-53443	1
United Aircraft Corporation Hamilton Standard Division Windsor Locks, CT 06096 Attn: T. Zajac, Heat of Materials & Standards	1
Reynolds Metals Company Metallurgical Research Division 4th & Canal Streets Richmond, VA 23218 Attn: R. E. Zinkham	1
General Electric Company Material & Process Technology Laboratory Evendale, OH 45215 Attn: G. Best, K60	1
Teledyne Allvac P. O. Box 759 Monroe, NC 28110 Attn: W. M. Bancom, Librarian	1
NASA Scientific & Technical Information Facility P. O. Box 33 College Park, MD 20740	10 plus reproducible copy